LF 47b

UNIVERSITY OF LEICESTER

Author ....DANLADI, Reuben.....

Title INTEGRATED MAGNETOTELLURIC (MT) AND TRANSIENT ELECTROMAGNETIC (TEM) STUDIES OF STRUCTURAL CONTROL ON MASSIVE SULPHIDE MINERALISATION IN PART OF NORTHEASTERN...

Degree .....Ph.D.....Date ....1997....

DECLARATION TO BE SIGNED BY EACH READER CONSULTING THIS THESIS

I recognise that the copyright of the above-described thesis rests with the author or the university to which it was submitted, and that no quotation from it or information derived from it may be published without the prior written consent of the author or university (as may be appropriate).

NAME AND ADDRESS (BLOCK LETTERS PLEASE)	SIGNATURE	DATE

ABSTRACT

Integrated Magnetotelluric (MT) and Transient Electromagnetic (TEM) Studies of Structural Control on Massive Sulphide Mineralisation in part of Northeastern Troodos Ophiolite Complex, Cyprus

Reuben Danladi

The massive Fe- and Cu-sulphide mineralisation is the most valuable economic resource in the Troodos and has been explored and exploited mainly through exploratory drilling around ancient slags, gossans and old workings. The exhaustion of these superficial guides has meant a shift to locating orebodies at depth. Direct detection of orebodies by traditional geophysical methods has been difficult. Structures parallel and perpendicular to the spreading axes in the region are thought to control the localisation of the sulphide deposits. Their identification should aid indirect detection of mineralisations.

Prior to speculating on possible geological meanings of data from an area not known for sulphide mineralisation, 33 MT and 48 TEM soundings were perfomed at Klirou, a known area of buried massive sulphide mineralisation. The joint MT/TEM methods identified the low resistivity lithological unit that hosts the mineralisation and the bounding faults, demonstrating their usefulness in mapping the lithological units and structures that host and control these mineralisations. Coincident IP and geological or geochemical anomalies could then be used to locate the orebodies.

In Ayia Marina area, 37 MT and 68 TEM soundings were undertaken. Some ENE structures corresponding to the western flank of Mitsero graben, where the extrusion of the Troodos sulphide-bearing lavas is envisaged to have taken place, have been confirmed by ground MT/TEM surveys. The occurrence of olivine-bearing rocks north of Ayia Marina and the existence of an andesite plug 2 km north-northwest of Ayia Marina suggest that the interpreted low resistivity zone in the area may correspond to a prospective zone for massive sulphide occurrence.

A 24.5 km 2-D interpretive geoelectric section across part of NE Troodos, the first at such a scale, has been produced revealing resistivity zones corresponding to lithological units and reliable estimates of depth to resistivity boundaries comparable to borehole depths.

INTEGRATED MAGNETOTELLURIC (MT) AND TRANSIENT ELECTROMAGNETIC (TEM) STUDIES OF STRUCTURAL CONTROL ON MASSIVE SULPHIDE MINERALISATION IN PART OF NORTHEASTERN TROODOS OPHIOLITE COMPLEX, CYPRUS

Thesis submitted for the degree of

Doctor of Philosophy

at the University of Leicester

by

Reuben Danladi BSc, MSc (Zaria)

Department of Geology

University of Leicester

September, 1997.

ProQuest LLC
789 East Eisenhower Parkway
P.O. Box 1346
Ann Arbor, MI 48106-1346

DEDICATION

This research work is dedicated to my ever loving wife and God given help-meet Hajaratu Lynn and our beloved children Jemima Cetosnami and Jamin Shekwoduza, who by the grace of God managed to put up with me throughout this research period. For this, I want to say thank you and God's abundant blessings upon you all according to His wonderful and ever faithful promises. We give God all the glory, now and always, amen.

ACKNOWLEDGEMENTS

I thank Almighty God for enabling me to undertake this research work. Many thanks to the Commonwealth Scholarship Commission London for funding this research, without which the work would not have been completed. The assistance of the Geololgical Survey Department Cyprus and Hellenic Mining Company Ltd. Cyprus in the provision of accomodation, field personnel and logistic support is gratefully acknowledged. Thank you Mum for bringing me up the way you did and for your support and that of late Dad (R.I.P.).

My Special thanks go to my supervisor Dr. Max A. Meju for all his support. The enthusiasm shown throughout the work, the advice at various stages of the work and all the effort put in the fieldwork arrangements to ensure a successful research program are gratefully acknowledged.

I acknowledge the help offered at different stages of the work by Dr. S. Kramvis, Dr. G. Maliotis, Prof. M. A. Khan, Dr. P. Maguire, Dr. J. Ibohon and Mr. A. Parker. I also thank Andreas and Loizus of the Geological Survey Department Cyprus for all their care and assistance. The help of all the field staff of the Geological Survey Department Cyprus, who in one way or the other contributed towards the completion of this work is thankfully acknowledged.

Many thanks to my colleagues Christopher, Emin, Vivi, Matt, Vassilis, Mat, and all the research students in Geology Department. I can never forget the support of Messr C. Becket, P. Denton and D. York . Thank you Ron, Lila and Mike for all your help and support. A big thank you to all the members of Melbourne Hall Evangelical Free Church for all your prayer and support, especially to our Pastor Rev. P. Bassett. Thank you all for making life in Leicester exciting.

To Mrs. E. Walker, you have been a mother to me and my family. May God truly bless you and reward you according to His riches in glory through Christ Jesus our Lord. To all those whose names do not appear above especially members of the Leicestershire branch of Oversees Fellowship of Nigerian Christians, your contribution was not too small to deserve being mentioned, it's just that I am only human very capable of forgetting and making errors. A very big "thank you" to all of you. God bless you all.

INTEGRATED MAGNETOTELLURIC (MT) AND TRANSIENT ELECTROMAGNETIC (TEM) STUDIES OF STRUCTURAL CONTROL ON MASSIVE SULPHIDE MINERALISATION IN PART OF NORTHEASTERN TROODOS OPHIOLITE COMPLEX, CYPRUS

LIST OF CONTENTS

LIST OF FIGURES

CHAPTER FOUR

CHAPTER FIVE

CHAPTER SIX

LIST OF TABLES

CHAPTER 1

INTRODUCTION

1.1 Research Objectives

Nearly all the known economical massive sulphide deposits in the Troodos ophiolite complex of Cyprus have been explored and extensively exploited. Essentially all the known deposits and prospects are surface or near surface mineralisations that have been identified through exploratory drilling in the vicinity of ancient slags and over gossans, and in the environments of known deposits. With the exhaustion of these apparent surface indicators of the presence of massive sulphide mineralisation, attention has moved to locating massive sulphide deposits buried at depth employing various geophysical techniques. Traditional geophysical exploration for massive sulphide deposits in the Troodos have been useful in the evaluation of the gossans and environments of known ore deposits, but have not been helpful in the direct detection of deposits that are buried at depth with no apparent surface indication.

Searle (1972) and Adamides (1984) have suggested that the massive sulphide deposits of Troodos ophiolite in Cyprus must have been genetically associated with major fracture zones which provided the pathways for the mineralising fluids. The fractures have been revealed from regional studies of data from aeromagnetic surveys and satellite imagery (Hunting, 1969; Cooper, 1993). Although the deposits themselves may be difficult to detect directly (Busby et al., 1983), other phenomena such as the major tectonic structures associated with the spreading centres and intrusive bodies that produced the hydrothermal systems which sustained the deposits could be identified. This study explores the proposed genetic relationship of the sulphide ores with major fracture zones that are thought

to have controlled the movement and deposition of the mineralising fluids that formed the ores. The study therefore aims at investigating the applicability of joint MT/TEM methods in the study of the stratigraphy and the identification of the structures in the Ayia Marina area of northeastern Troodos and in assessing the controls imposed by these structures on the sulphide mineralisation in the area using high resolution (100 m spacing) measurements. The presence or otherwise, and the locations of these structures where present may become apparent at the end of the study.

1.2 Previous Geophysical Exploration for Mineral Prospects in Cyprus

Gravity anomalies in Cyprus were revealed as early as 1939 by Mace (1939). The first comprehensive account of the geology and geophysical setting of the Troodos by Gass & Masson-Smith (1963) concluded that it formed as a volcanic pile affected by extensional stresses within an oceanic setting located between Africa and Eurasia. This aroused a lot of interest on the Troodos within the academic community. After the discovery of the sea-floor spreading by F. Vine and D. Matthews in 1963, Gass (1968) proposed that the Troodos was a fragment of ocean floor generated by sea-floor spreading at an ocean ridge (see also Vine and Moores, 1969). This conclusion was a milestone that was to influence much of later research in Cyprus.

Most of the geophysical investigations of the Troodos ophiolite have been mainly for industrial exploration for the identification of massive sulphide ore bodies and academic exploration for the quantification of ophiolitic structures and comparison with modern oceanic crust, and for testing the potentials of various geophysical research equipment. The United Nations Development Program (UNDP) initiated a coordinated program of regional- and prospect-scale exploration

across Troodos in 1962, after the Cypriot independence. The regional study constituted airborne electromagnetic, aeromagnetic and localised gravity surveys over 1,500 km of the Troodos flanks and was aimed at optimising mineral and hydrological exploration within Cyprus and at delineating structural lineations related to mineralisation. The ground survey assessed the applicability of gravity, electromagnetics, resistivity and self potential methods for direct sulphide detection in the complex ophiolitic stratigraphy.

Political and economic factors in the late 1970s led to a decline in mineral exploration in Cyprus. However, the Hellenic Mining company of Cyprus in conjunction with Leicester University sustained IP studies from 1970-1984 (Maliotis and Khan, 1980). The recognition of Troodos as a potential spreading centre led to subsequent geological re-evaluation of the massif through further gravity, high level aeromagnetic and seismic refraction projects to constrain the new models proposed (eg. Khan et al.,1972; Vine et al., 1973). The Cyprus Crustal Study Project (CCSP) from 1980-1986, an integrated field and research drilling program produced a three dimensional stratigraphic model of Troodos for the complete ophiolitic succession, with a comprehensive geophysical logging suite from the sediments to basal tectonised ultramafics. Allerton and Vine (1987) refined the extensional spreading structure model proposed by Varga and Moores (1985). Cooper (1993) undertook an integrated geophysical exploration of the northeast Troodos ophiolite.

A considerable range of ground geophysical methods have been assessed to determine the optimum approach to mineralisation detection in the Troodos. Since experimentation by Helenic Mining Company (HMC) in 1947, the gravity method has found wide usage in mapping 'basement' depths. The Cyprus-type mineralisation cannot be detected in a complex environment like the Troodos by the gravity method because of its high porosity and lack of appreciable density contrast

with its host extrusives. It could probably be used to reveal the high density intrusives within the extrusive sequence which source the mineralisation concentrations. Drilling of positive Bouguer anomalies over high density intrusives however, failed to relate the anomalies to mineralisation. The gravity method was therefore abandoned for the purposes of direct mineral detection but served as a useful tool for correlation with airborne data. It was thus used by the UNDP to verify specific aeromagnetic anomalies. Whereas mineralisation should be detectable as a magnetic low, high frequency noise in the observed magnetic field limits detection at depth and/or within near-vertical fault zones (Allerton and Vine, 1987; Cooper, 1993).

During the 1960's, the HMC tested the frequency domain electromagnetics (FEM) employing the McPhar's 70 and McPhar's 300 systems, but transmitter to receiver alignment errors which increase the primary field noise (McCracken et al, 1980) reduced the definition of the faint target to host contrasts (Cooper, 1993). The UNDP revisited the method in later years with the Turam and Minigun systems. Massive mineralisation is usually very conductive (3-5 Ωm) but silicic alteration increases bulk resistivities. Similarly, the disseminated mineralisation bear higher bulk resistivities often to a point where they are indistinguishable from the low resistivity Lower Pillow Lava (LPL) host (8-15 Ωm). Results have shown that concentrated electrolytic conductors caused by increased porosity, fracturing, argillaceous alteration and/or salinity of the interstitial fluids will produce responses indistinguishable from mineralisation by the frequency domain electromagnetic methods (Cooper, 1993; Cooper and Swift, 1996).

The first field testing of the pulse electromagnetic time domain (PEM) system was undertaken in the Skouriotissa prospect area, Cyprus by Newmont Exploration for Cyprus Mines Corporation using a ground system designed by McLaughlin in

1962 (Crone, 1977). Inspite of the 90 auto batteries used to power the system, initial results were disappointing. In 1978 Noranda Exploration (Cyprus) Ltd. decided to use the PEM method again but instead of massive sulphides, they preferentially located fault zones. The time domain electromagnetic (TEM) instrumentation and methodology saw great advancement in the 1980's providing enhanced sounding data resolution, this led to the re-evaluation of the method for the Cypriot mining environment. The HMC was able to discriminate certain shallow mineralisation occurrences after extensive testing but the geological complexity remains a big constraint for the system resolution (Swift, 1990). The conductive mineralisation and associated resistive, silicified halo in the Troodos produce an "averaged" response indistinguishable from the barren host for realistic transmitter and receiver loop dimensions of 50-100 m. The method nevertheless offers efficient coverage for structural mapping at a lithological resolution comparable to any other, and has infact been shown to be a powerful tool for reconnaissance structural mapping and identification of mineralisation targets in homogeneous environments (McNeill, 1980; Cooper, 1993; Meju, 1994). The TEM method can be used to resolve major lithological boundaries and for the mapping of structures even in geologically complex areas like the Cypriot environment.

The DC resistivity method is limited by indistinguishable mineralised and non-mineralised unit resistivities for sulphide concentrations of less than 30% (Cooper, 1993). In theory, the coincidence of positive IP and negative DC anomalies is indicative of massive mineralisation while coincident positive IP and DC anomalies indicate low grade disseminated mineralisation. The DC method cannot contribute to direct mineralisation detection in isolation, but apparently compliments EM and IP studies. IP exploration has proved to be the most successful geophysical method in the ophiolite environment since its adoption in

1970 (Maliotis, 1978; Maliotis & Khan, 1980; Busby et al., 1983). McPhar tried using the frequency-domain IP for Cyprus Mines Corporation in 1962 and were followed later by Hunting Geology and Geophysics Ltd. for Limni Mines in 1967. Although results of the early surveys are not in the public domain, the subsequent rejection of the method by both companies would suggest unsatisfactory results. The UNDP in their study concluded that the IP was distorted by argillaceous alteration of the conductive host.

The HMC started using a 7.50 kW time domain Huntec system for extensive exploration of the Mathiatis, Klirou, Kokkinovounaros, Vrechia, Petra and Kambia prospects. For reconnaissance surveys, a dipole-dipole configuration with receiver separation of 50 m and reading out to at least n=4 was used while the pole-dipole array with its enhanced target to host ratios because of the negligible effect of the second current electrode (the infinite electrode-located very far away) to the measurement (Griffiths and King, 1981; Sheriff, 1991) was preferred for detailed surveys. The targets were more readily discernable in barren homogeneous hosts than within heterogenous environments. It has succeeded in defining mineralisation in prospect areas and identified new mineralisation at Klirou and New Sha. Results have shown its suitability for imaging extensive, intermediate bodies down to depths of 250 m (Maliotis, 1978; Maliotis & Khan, 1980; Busby et al., 1983). The IP method is, however, constrained by its time and labour intensive nature which makes it unsuitable for rapid recconnaisance survey, its limitated depths of investigation and its blindness to near-vertical mineralised fault zones.

The Magnetotelluric (MT) method has been used to obtain information on deep structures in the northeast Troodos ophiolite complex. Preliminary MT and TEM surveys were conducted in 1991 along a 17 km long NE-SW profile across part of NE Troodos. The results show a resistivity structure with similar depth range and

vertical resolution to the seismic interpretation of the same line (Cooper, 1993; Meju, 1994). The MT method has however, not been used for the direct detection of minerals. The Audiofrequency Magnetotelluric (AMT) method is an audio- or high-frequency (over 1Hz) application of the MT method which has made it applicable to mineral prospecting (Lakanen, 1986). The MT method is good in terms of sophistication and ease of interpretation, suitability in locating vertical structures/boundaries and study of deep structures, and can be used in resistive environments and areas hampered by surface volcanics (Meju, 1988, 1994).

1.3 Electromagnetic (EM) Methods in Mineral Exploration

The earth science literature is rich with case histories describing exploration for a variety of mineral resources employing Electrical and Electromagnetic (EM) methods of geophysics. The EM methods that have been used include Frequency Domain Electromagnetics (FDEM), Time-Domain Electromagnetics (TDEM) or Transient Electromagnetics (TEM), Airborne Electromagnetics (AEM), Audiofrequency Magnetotellurics (AMT) and Controlled Source Audio frequency Magnetotellurics (CSAMT). These tools or methods have been employed successfully in the exploration for massive and non-massive sulphide deposits, vein deposits, iron, uranium and kimberlite deposits.

Most of the massive sulphide deposits that have been discovered with the EM methods are associated with submarine volcanic rocks and are of volcanogenic origin. A smaller number of deposits are associated with other types of rocks and have been formed by a variety of processes. Metallic sulphide minerals such as pyrite and pyrrhotite form the primary constituents of most massive sulphide deposits and their conductivity depends largely on these minerals. Chalcopyrite and galena are conductive and sometimes contribute significantly to the overall

conductivity of a deposit, but sphalerite is generally a poor conductor. In small samples, pyrite, pyrrhotite and many other sulphide minerals are conductive, but the bulk conductivity of a deposit depends mostly on how well individual grains and the deposit as a whole are connected electrically.

Often, surface EM exploration is used to pinpoint the location and help to characterise conductors that have been detected by airborne EM surveys. In other cases, surface EM surveys are used as primary exploration tools, particularly where the area of interest is relatively small. Electromagnetic methods are not yet capable of distinguishing between economic and barren sulphide deposits as are other geophysical methods, as such the location of any economic sulphide deposit is regarded as a technical success. Although many more prospects than ore bodies are found, EM exploration has been instrumental in the location of many important ore bodies.

In many areas the explorationist must take into consideration the possibility that sulphide orebodies occur within more extensive conductive zones of non economic sulphides or carbonaceous or graphitic material. There is no single strategy that is optimal for locating economic deposits within otherwise barren sulphide or graphitic zones. In some cases economic deposits may have a higher conductance than the surrounding rocks. Two of the primary criteria used in the evaluation of airborne and ground electromagnetic data to select conductors for further study are short strike length and relatively high conductivity. Thickness is an important criteria as volcanogenic massive sulphides are not likely to exceed 50 m in width (Boldy, 1981), whereas some formational conductors are much thicker. Graphitic or carbonaceous conductors are much more likely to be highly anisotropic than massive sulphide orebodies due to the laminated fabric of the rock where highly conductive carbonaceous lamina may alternate with resistive lamina. The

adverse effect of a conductive overburden in areas where they occur by limiting the penetration and distorting the measured EM response is another factor the explorationist has to contend with.

1.4 Present Study Outline

The limited successes achieved in the search for massive sulphide mineralisation in the Troodos ophiolite complex by traditional geophysical methods, in particular the Induced Polarisation (IP) method, have been attributed more to exploratory drilling over gossans and environments of known deposits than to geophysical methodology. Except for one or two examples, even the IP method has not been able to locate sulphide deposits that are buried at depth. This difficulty stems from the lack of appreciable resistivity contrast between the variably altered (silicified) sulphide ore deposits and the conductive host volcanic rocks, the lateral and vertical inhomogeneity of the host pillow lavas and their associated fractures and dykes, and the relatively small size of the deposits which combine to produce complex, inconsistent target-to-host contrasts that make the mineralised bodies difficult geophysical targets.

The interpretation of aeromagnetic and satellite imagery data by Hunting (1969) and Cooper (1993) has revealed near north-south trending structural lineaments along with crosscutting almost east-west trending structures in the Ayia Marina area. Known massive sulphide deposits in the northeastern part of Troodos appear to be related to structures parallel (NNW) and perpendicular (transcurrent) to the graben axes (Searle, 1972; Adamides, 1984). Wisdom seems to suggest that further exploration for new deposits should be concentrated in environments with such structural features and hence the choice of Ayia Marina area. In addition, mineralisation occurrence shows that massive sulphide deposits and prospects in

the northeastern part of Troodos occur and are distributed along a zone that trends northwest to southeast with the Ayia Marina area right at the western end of the zone. These factors clearly suggest that Ayia Marina area could be a prospective area for massive sulphide mineralisation.

The TEM method has been used in northeastern Troodos and has been found to offer efficient coverage and yield reliable depth estimates for structural and lithological mapping in such an area to depths of up to 250 m (Swift, 1990; Cooper, 1993). MT surveys have also been carried out in northeastern Troodos and preliminary results have yielded valuable information at greater depths (Cooper, 1993; Meju, 1994c). A combination of the two EM methods should therefore yield resistivity, structural and lithological information at shallow and great depths in the area of study. This was the approach undertaken in this study. Following this introductory chapter, chapter 2 reviews the general geology of Cyprus with emphasis on the Troodos ophiolite complex. Chapters 3 and 4 give overviews of the MT and TEM theories respectively highlighting their potential usefulness in this type of study. Chapter 5 describes how the fieldwork was undertaken and the factors that were taken into account before, during and after the fieldwork including the simple data processing techniques employed to retrieve useful information from the raw field data. Chapter 6 looks at the one dimensional data interpretation carried out while chapter 7 describes the two dimensional modelling and inversion of data from Ayia Marina area. Chapter 8 discusses the results obtained and intercorrelates them with pre-existing models while chapter 9 lists the conclusions that have been drawn from this study.

CHAPTER 2

THE GEOLOGY AND STRUCTURE OF TROODOS OPHIOLITE

2.1 Introduction

Current geological and structural knowledge and understanding of the Troodos ophiolite complex, Cyprus and the surrounding region of eastern Mediterranean is reviewed in this chapter. The tectonic setting of Troodos ophiolite in the light of its main structural features and the concept of its formation within a Tethyan ocean environment from regional reconstruction is briefly discussed. The main geological terrains of Cyprus are highlighted while the various lithological units of the Troodos are discussed in terms of their mineralogical composition and stratigraphical relationships. A section lists the main mineralisations and host rocks within the Troodos ophiolites with emphasis on the utility and mode of occurrence of the massive sulphide mineralisation. A fairly detailed description of the geology of the geophysical survey areas is given at the end.

2.2 General Geology of Cyprus

The Island of Cyprus in the Middle East lies in the northeastern part of the Mediterranean sea between the lattitudes 34°33′ and 35°43′ N and between the longitudes 32°16′ and 34°36′ E (fig.2.1). It is the third largest island in the Mediterranean sea after Scicily and Sardinia which lie in the western part. It is located between and close to the continents of Europe, Asia and Africa about 64 km south of Turkey, 97 km west of Syria and 300 km north of Egypt such that it claims to be a stepping stone to the three continents. It has a somewhat east-northeast elongation stretching for about 240 km from the west coast to its easternmost tip and about 96 km from north to south. It also has a total surface area of about 9,250

sq.km.

The general geomorphology of Cyprus consists of a central plain with Kyrenia mountain range to the north and the Troodos massif to the south. The central plain rises to just over 200 m above sea level with gentle slopes to the

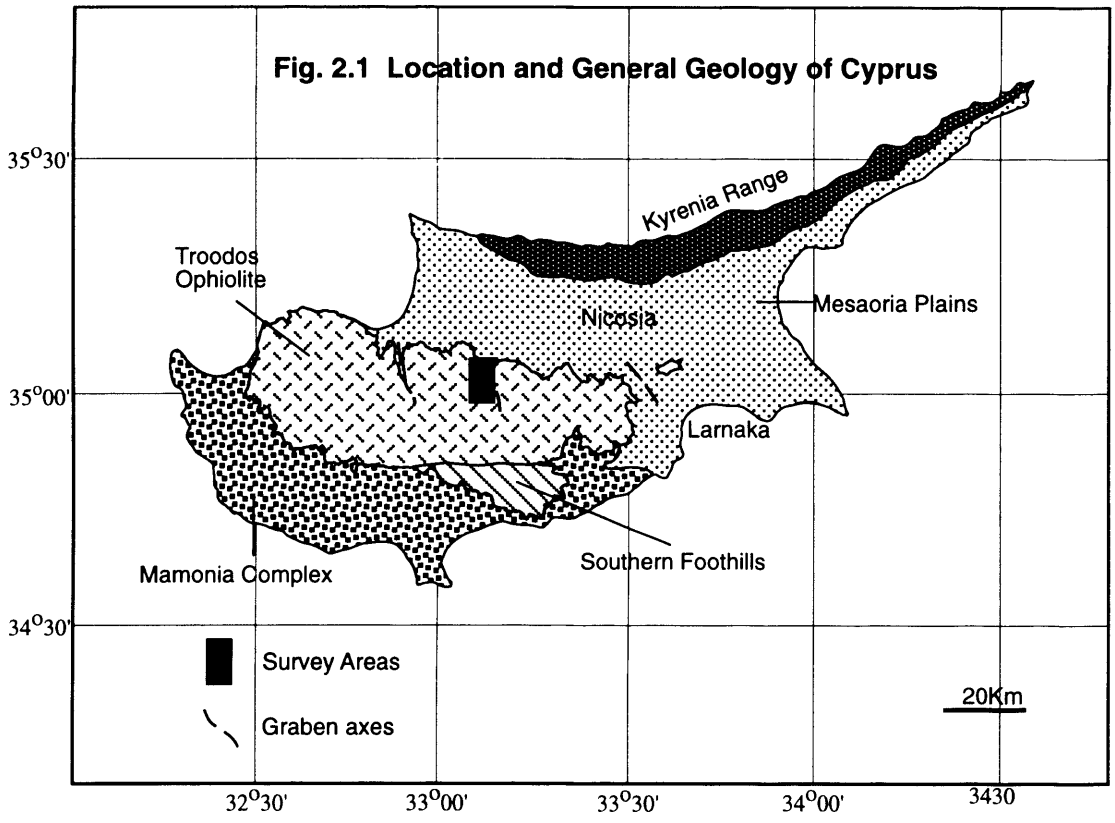

east and west toward the sea. The mountain ranges to the north and south generally exhibit an undulating topography ranging from over 200 m above sea level at the foot of the hills to about 1951 m at the peak of Mount Olympus which is right at the centre of the Troodos.

The Troodos ophiolite complex is one of the five distinct, slightly arcuate, E-W trending terranes that make up the island of Cyprus. In very broad terms, the other terranes are to the north, the Kyrenia mountain range considered to be the most southern expression of the Tauro-Dinaric alpine belt of Greece, Crete and southern Turkey (Panayiotou, 1979); the Mesaoria plain, a broad valley south of the

Kyrenia range underlain by a series of sedimentary rocks and shows a hummocky topography in its highly folded Kythrea flysch northern belt and a generally undeformed sequence of the Circum-Troodos sedimentary succession in it's southern half; the southern Foothills consisting of the Limassol forest area to the southeast; and the highly deformed sequence of Triassic-Cretaceous rocks to the southwest of Cyprus known as the Mamonia complex.

2.3 Troodos Ophiolite

Of all the component terranes of Cyprus, the Troodos ophiolite is the most prominent and striking structural feature standing out as an uplifted dome that has survived weathering and erosion producing an annular outcrop pattern with oblique exposure of the complete ophiolite stratigraphy (fig.2.2). The first fully integrated account of the geology and geophysical setting of the Troodos was given by Gass and Mason-Smith (1963) concluding that it formed as a volcanic pile affected by extensional stresses within an oceanic setting, located between Africa and Eurasia. It occurs as an elongate exposure lying parallel to a spreading direction occupying about 3,000 sq.km of the southwestern part of Cyprus (Gass, 1968; Vine and Moores, 1969). It is the westernmost member of a discontinuous ophiolite belt that stretches along the northern margin of the Afro-Arabian platform (Fig.2.3). The Troodos which has been dated from radiometric and inter-laval fossil studies (Thy and Moores, 1988; Dilek and Eddy, 1992) to be a late Cretaceous, Campanian terrane (about 85 my) consists of a typical ophiolite suite starting from the topmost upper pillow lavas, through a gradational basal group to a massive sheeted dyke complex down to a plutonic core and intermediate ultramafics (Moores and Vine, 1971; Gass and Smewing, 1973; Panayiotou, 1979).

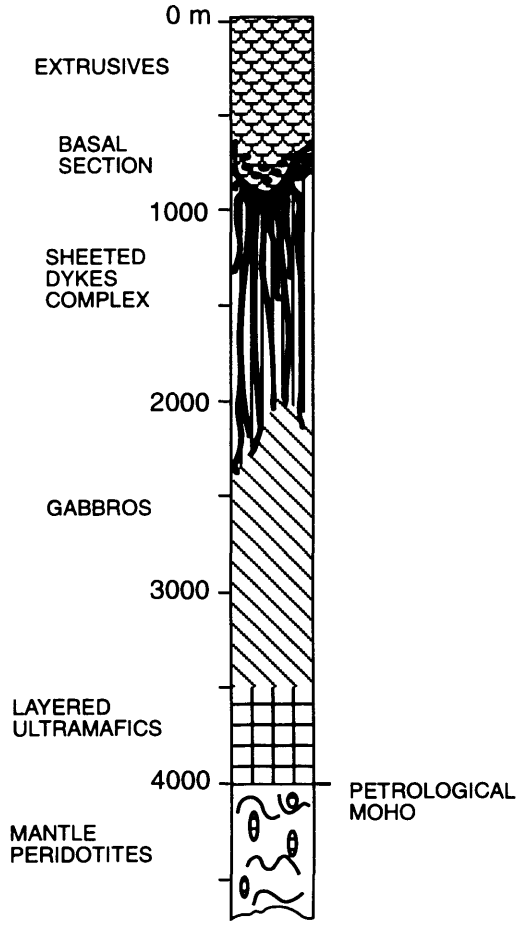

Fig. 2.2 Troodos ophiolite stratigraphy (after Malpas et al, 1989)

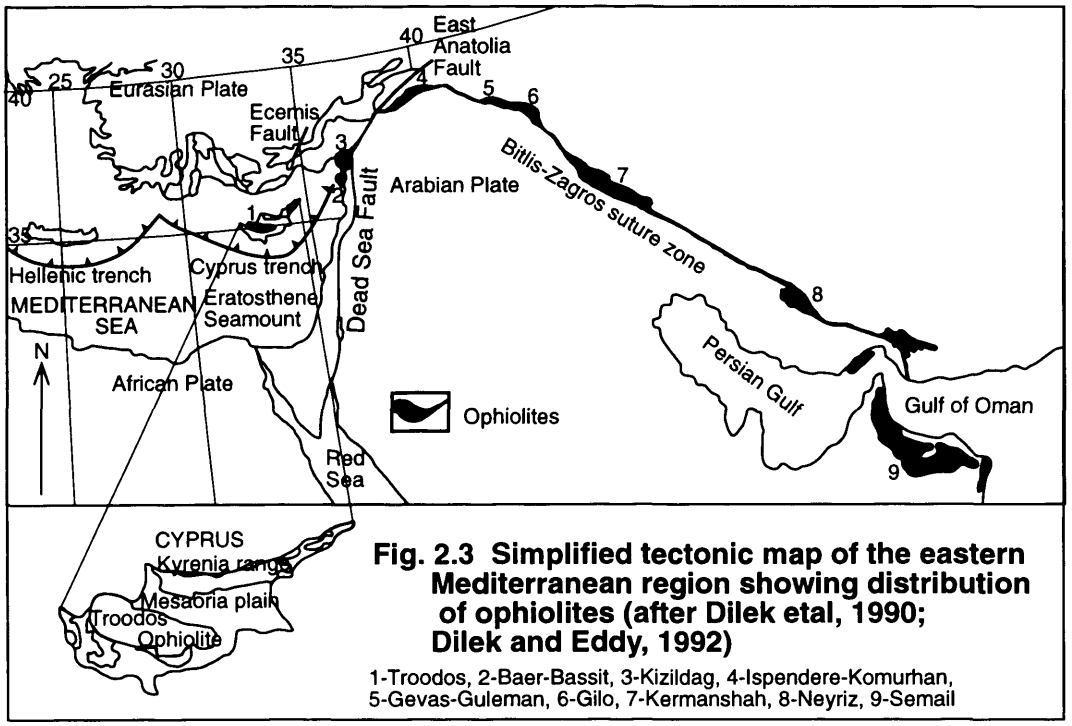

Fig. 2.3 Simplified tectonic map of the eastern Mediterranean region showing distribution of ophiolites (after Dilek etal, 1990; Dilek and Eddy, 1992)

1-Troodos, 2-Baer-Bassit, 3-Kizildag, 4-Ispendere-Komurhan, 5-Gevas-Guleman, 6-Gilo, 7-Kermanshah, 8-Neyriz, 9-Semail

2.4 Lithological units of Troodos

Geological studies of the Troodos ophiolite complex indicate a succession from plutonic igneous rocks at the core through to extrusive pillow lavas at the periphery (fig. 2.4). The succession grades from uppermost pillow lavas which have traditionally been divided into Upper Pillow Lava (UPL) and Lower Pillow Lava (LPL) units (Wilson, 1959; Gass, 1960). The UPL can be defined by the presence of olivine phenocrysts, and are locally differentiated by semi-continuous layers of metalliferous mudstones and volcanogenic sediments (Thy and Moores, 1988; Boyle and Robertson, 1984). They are pillowed, porphyritic, olivine-rich basaltic andesites with low TiO_2 and high SiO_2 compositions (Pantazis, 1979; Thy and Moores, 1988). They form predominantly vesicular flattened pillows in outcroop, with sparse brecciation and up to 10% feeder dykes. Olivine phenocryst alteration to brown iddingsite lends the UPL a pinkish hue relative to the grey brown LPL unit.

The next unit, the LPL rocks are pillowed, rhyodacite to andesite lavas with high TiO_2 and a predominance of non-vesicular massive flows and sheeted dykes (Schminke and Bednarz, 1990). They show a rarity of pyroclastics, ponded lava flows and perpendicular transcurrent faults. Geochemical and petrological data for the LPL show oceanic arc affinities. The Basal Group (BG) lies beneath the LPL (Bear, 1960) and is a gradational feature between the extrusive LPL and the intrusive sheeted dyke horizons. The BG unit is marked by a rapid increase in the proportion of dykes, and is said to grade into 100% diabasic dyke screens at the top of the sheeted dyke complex (SDC).

The sheeted dyke complex (SDC) exhibits compositional variance from basaltic to andesitic (and locally rhyodacitic) dykes due to high-level fractionation of discrete magma sources (Thy and Moores, 1988). Individual dykes are typically 0.1

Fig. 2.4 Geology of Troodos Ophiolite

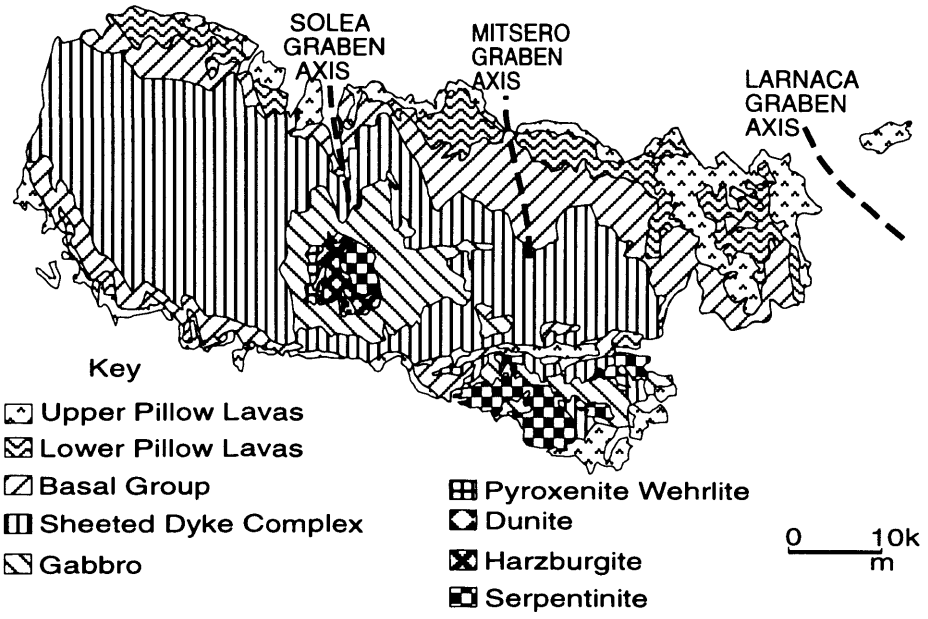

to 5.0m wide, fine grained, non-vesicular and metamorphosed to greenschist- and amphibolite-facies. Lower levels show 30 to 50% epidosite composition due to maximum hydrothermal interaction and fluid enrichment (Richardson et.al, 1987), and the base is marked by rapid vertical and irregular lateral transition to gabbroic composition apparently due to multiple intrusions (Allerton and Vine, 1987).

A thick series of coarse to fine grained gabbros collectively named the high level intrusives (Gass, 1980) lie beneath the SDC. The gabbros show phase layering and a downward increase in mafic content. They are broadly divisible on petrological and geochemical criteria into an upper and lower series (Thy & Moores, 1988). The upper cummulates are plagioclase enriched and are characterised by frequent compositional reversals towards progressively more Mg-rich phases. The lower cummulates are plagioclase free, show one compositional reversal and are genetically related to LPL, BG and SDC.

A pyroxinite unit underlies the gabbroic high-level intrusives. The base of the whole ophiolite complex is olivine-rich and composed mainly of tectonised

harzburgite (80% vol.), with localised wehrlite and dunite pods (Allerton & Vine, 1987). In the field, it is difficult to differentiate the harzburgite host from inter-layered dunitic lenses, but the latter contain economic chromite concentrations and isoclinal folding (Gass, 1980). A serpentinite unit is thought to underlie the mainly harzburgite unit.

2.5 Tectonic Setting of Troodos

Diverse structural and intrusive contact relationships between the SDC and the underlying plutonic sequence including Arakapas transform fault, the arclike chemistry of sheeted dykes and related extrusive rocks, and the inferred highly depleted and hydrous nature of the mantle source of the late stage intrusive and extrusive rocks, suggest the formation of Troodos ophiolite complex within a Tethyan ocean system (Robertson and Woodcock, 1980; Dilek et al, 1990) or one of a number of small ocean basins (Gass, 1980; Robertson et al, 1991) formed by rifting and spreading of the north margin of the Gondwana over a subduction zone initially during the Triassic (fig.2.5). The exact orientation or location of this subduction zone and the direction in which it dipped is, however, yet to be substantiated by direct evidence (Robertson and Dixon, 1984; Dilek et al, 1990, 1992; Macleod et al, 1992; Robertson and Xenophontos, 1993). A popular view is that the Troodos formed above a northward dipping subduction zone similar in some respect to the origin of the SW Pacific forearcs, essentially based on the inference for other late Cretaceous ophiolites in the Mediterranean including Oman (Lippard et al, 1986; Macleod et al, 1992). Regional reconstruction has however, led others to believe that rifting and spreading during the Triassic-Jurassic led to the formation of a marginal basin in Cyprus area either of the Red sea type (Robertson and Dixon, 1984) or of a marginal basin type developed over an active or recently

Fig. 2.5 Tethyan ocean system during rifting and spreading in the Jurassic depicting evolving Neotethyan ocean and Paleotethys along with major plate boundaries (after Dilek et al, 1990)

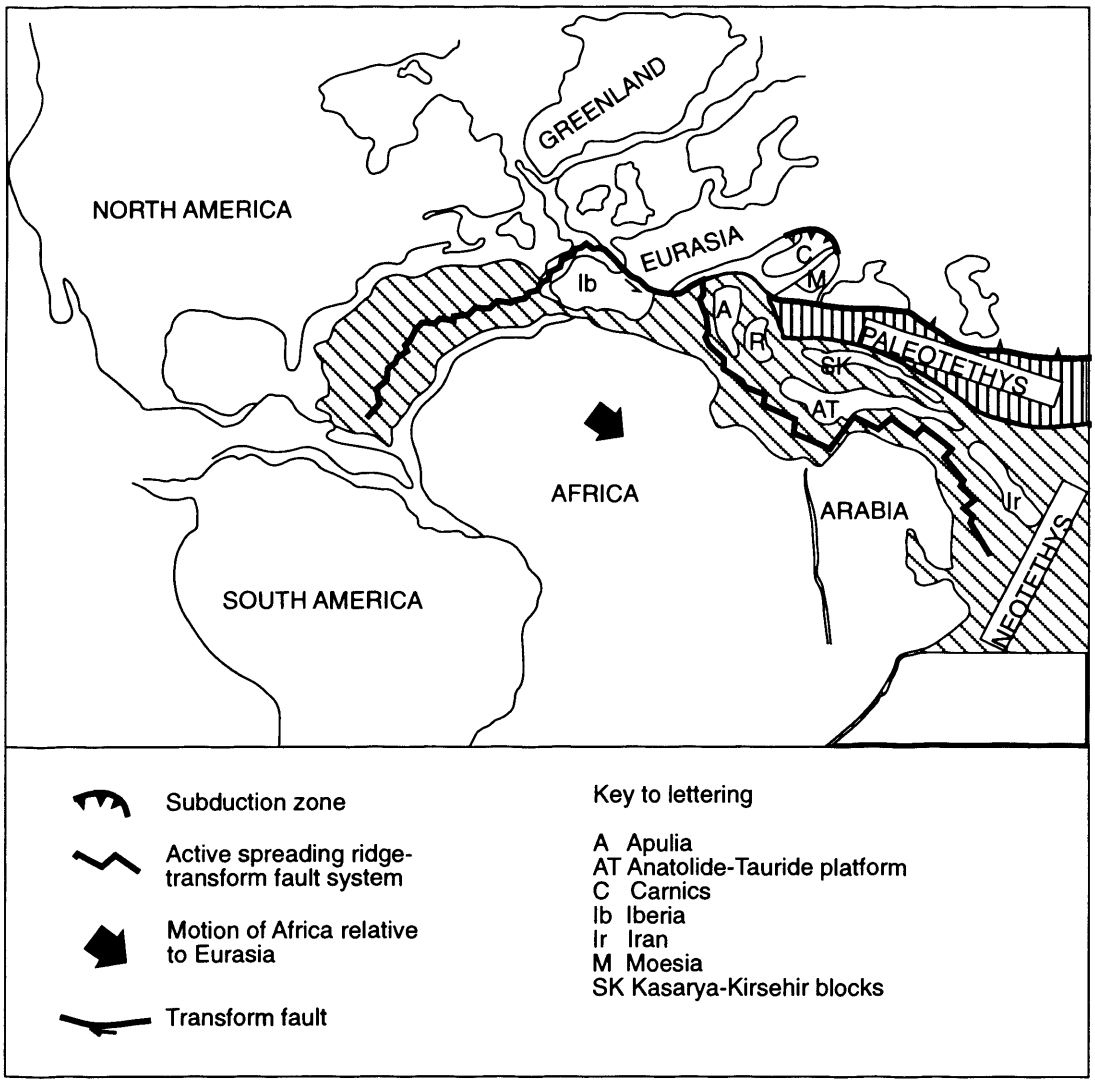

active southward dipping subduction zone (Dewey et al, 1973; Leith, 1982; Sengor et al, 1984; Dilek and Moores, 1990; Dilek et al, 1990, 1992; Dilek and Eddy, 1992).

The Troodos ophiolite was formed and then deformed, rotated 90° while remaining at oceanic depths (Moores and Vine, 1971; Clube and Robertson, 1986; Robinson and Malpas, 1987; Dilek et al, 1990) before being juxtaposed with the Mamonia complex of southwest Cyprus during the late Cretaceous-early Tertiary period. The emplacement of the Kyrenia mountain range near its present position is thought to have occured during the late Eocene (Baroz, 1980; Robertson and Woodcock, 1986; Searle and Panayiotou, 1980; Swarbrick, 1980). The final phase

essentially involved the northward underthrusting of the African plate beneath Cyprus (Ben-Avraham, 1978; Innocenti et al, 1976; Dilek et al, 1990, 1992; Robertson and Xenophontos, 1993).

The relative thinness of the Troodos oceanic crust, the absence of pyroclastic rocks interbedded with extrusive rocks, the existence of overlying Cretaceous-Paleogene pelagic sedimentary sequence and the extensively developed sheeted dyke complex in Troodos appear to be in major conflict with a conventional island arc origin of the ophiolites (Dilek et al, 1990). Also there is no geological evidence displayed by the Troodos ophiolite for frontal and/or remnant arcs, suggesting a rifted volcanic arc origin. In the light of the foregoing, an alternative interpretation to an island arc or backarc proposes a fore-arc tectonic setting of the ophiolite during initial stages of a subduction (Pearce et al, 1984). This is based on the presence of boninitic lavas that are interpreted to have formed prior to the generation of arc tholeiites (Hickey and Frey, 1982; Bloomer and Hawkins, 1987). The fact that boninitic lavas can also form in the late stages of volcanic activity in an arc setting as indicated by magma chemistry and stratigraphic relationships of backarc tholeiite, arc tholeiite and boninite in the western Pacific (Crawford et al, 1981; Wood et al, 1980; Sharashkin et al, 1981) implies that the spatial and temporal relationships of boninitic erruptions to volcanic arc activities are not yet well defined and understood and should be used with care in the case of Troodos. In addition the mineralogy and major element chemistry of the Troodos boninitic rocks are somewhat dissimilar to those of western Pacific fore-arc boninites (Thy and Moores, 1988).

Gass (1968) and Vine and Moores (1969) first proposed that the Troodos massif was a fragment of oceanic lithosphere. Major extensional detachment faults like the "Kakopetria detachment" (fig.2.6) have since been identified within and

particularly near the base of the sheeted dyke complex (Verosub and Moores, 1981). Later mapping and palaeomagnetic work indicated the existence of a number of discrete sea-floor grabens described as fossil extensional block structures analogous to those of modern ridges and have since been called Solea, Mitsero and Larnaca grabens (Varga and Moores,1985, 1990; Allerton and Vine, 1987, 1991; Varga, 1991; Macleod et al, 1990, 1992; Hurst et al, 1994). Sophisticated palaeomagnetic technique showed the Troodos spreading fabric in terms of discrete half-grabens and grabens that developed off-axis in response to amagmatic stretching (Allerton and Vine, 1987, 1990; Allerton, 1988; Allerton, 1989).

Fig. 2.6 Main structural features of Troodos ophiolite

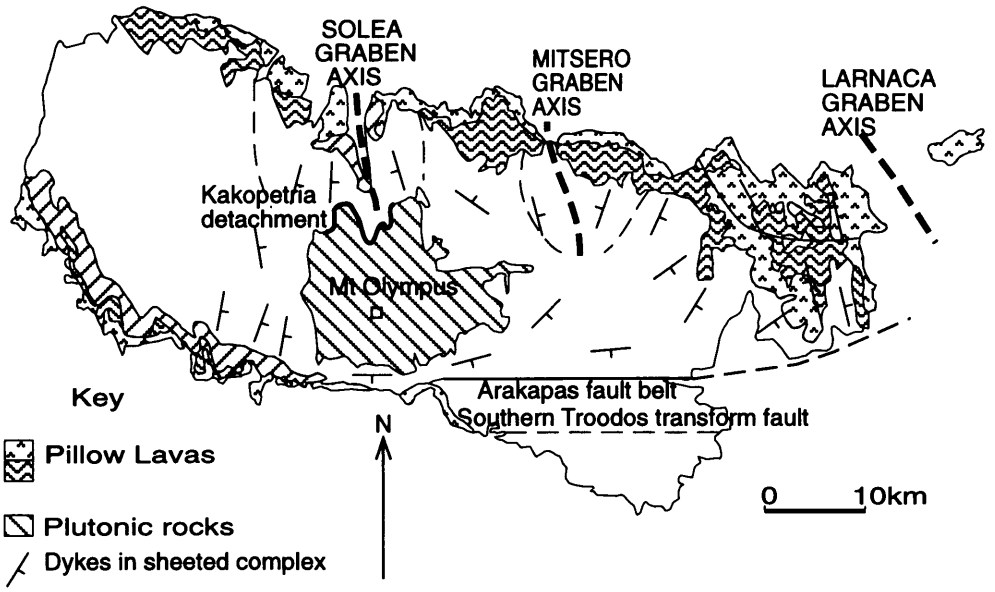

Interpretation of the sense of ridge offset across the Arakapas transform fault and symmetry of dyke domains on either side of the Solea and Mitsero grabens led Varga and Moores (1985) to propose a structural model for the Troodos complex involving eastward migration of a slow-spreading mid-ocean ridge north of a right-

offset (dextral) transform fault (Arakapas fault zone) and preserved by ridge jumping. The absence of serpentinised faults in the extrusive section of the Troodos and the comparatively subdued sediment-subsediment surface have caused Allerton and Vine (1987) to conclude that in general the Troodos does not appear to have the tectonic structures of a slow spreading ridge. On the basis of field observations and the above, they believe the graben structures were generated by normal axial tectonic processes at the Troodos axis, which, applying a simple mid-ocean ridge analogy, formed at an intermediate to fast spreading centre (see also Allerton and Vine, 1991). Varga (1991) has defined three primary fault sets: NW directed faults which relate to the graben bounding faults and typically dip toward their respective graben axis; NE faults which are orthogonal to the structural strike of the grabens and represent transcurrent or tear features formed either syn- or immediately post-extension; and E-W features which post date extension and are generally thrust faults that resulted from the N-S directed compression uplift.

Several faults with dominantly down-dip slickensides cut the Solea graben and are responsible for structural rotations (Varga and Moores, 1985). Many large normal faults contain higher temperature metamorphic mineral assemblages than surrounding rocks and appear to have channelled ascending hydrothermal fluids (Varga and Moores, 1985). Dykes of more than one generation occur together at several outcrops with the most steeply dipping dykes cutting shallower dipping dykes and related normal faults. Kakopetria detachment is cut by undeformed gabbroic dykes in at least one area south of Kakopetria, suggesting formation close to an active spreading centre during magmatic or tectonic extension (Varga and Moores, 1985). The occurrence of three of the largest massive sulphide deposits in the Troodos ophiolite within the Solea graben only add to its essential characteristic elements of axial valleys on modern spreading centres.

The Mitsero graben axis lies 25 km to the east of the Solea axis and is also defined by a north-northwest trending axis of symmetry across which dykes dip toward each other. It is considerably less deformed than the Solea graben, and Allerton and Vine, 1987 have proposed formation through normal magmatic extension. Westward dipping dykes of the Mitsero graben crosscut the gabbroic base of the Solea structure and indicate that the grabens young to the east. The Larnaca graben is the least known of the three and it's axis lies about 55 km east of Solea axis and it's western flank occupies the northeastern extremity of the Troodos outcrop. The graben is defined based on northeast-dipping dykes of the eastern end of the main Troodos massif and southwest-dipping dykes of the Troulli inlier. Moores et al. (1987) have further recognised three oriented dyke domains to the west of Solea graben. These are the NNE trending Stavros, NW trending Polis and NE trending Pomos domains which exhibit similar cross-cutting relations to the major grabens and young eastwards. The Polis structure which correlates with the Limni mineralisation is thought to be a fourth fossil ridge axis.

2.6 Mineralisation

Mineralisation in the Troodos Ophiolite complex is essentially of three types, viz: the massive sulphides within the extrusive pillow lavas, the chromite within the harzburgite-hosted dunite pods, and the serpentine asbestos within the basal plutonics. The massive Fe- and Cu-sulphide mineralisation is the most valuable economic resource, ranging in quantity from 15,000 tonnes to over 15,000,000 tonnes and average Cu content of less than 0.5 to 4.5% with additional disseminated pyrites and chalcopyrites (Bear, 1963; Adamides, 1984). They were first considered to be of volcanic exhalative origin by Hutchinson (1965) and belong to a major class of volcanogenic massive sulphide deposits known as the Cyprus-

type (Adamides, 1984) occuring in clusters defining five major mining districts (Bear, 1963). Geochemically, the massive and disseminated pyrites are composed of Fe, S, and minor Cu and Zn concentrations. A number of small gossans and zones of hydrothermal alteration also occur within the extrusive sequence of the Troodos ophiolite.

The Troodos sulphide deposits mostly consist of a lenticular upper zone of massive sulphide ore, predominantly of pyrite with lesser amounts of chalcopyrite, which represents the exhalative part of the mineralisation. This is underlain by a pipe shaped stockwork zone consisting of veined silica and pyrite in brecciated, altered and silicified rock and surrounded by a broad alteration halo which passes into chloritic lavas impregnated by sulphides (Contantinou, 1979; Adamides, 1984, 1990). Sphalerite is another common constituent of both the massive ore and the stockwork zone, but generally exists in minor amounts (Bear, 1963; Constantinou and Govett, 1973). Most of the deposits follow, to a large extent, this model (fig.2.7) and are thought to have been structurally controlled by faults associated with the major grabens and are hence located along old spreading axes. They are usualy stratigraphically located at the LPL-UPL boundary, in the LPL sequence and at the LPL-BG boundary. Only disseminated sulphide ore mineralisation has been reported in the rocks of the BG and SDC (Robinson et al, 1987).

It is believed that the massive sulphides were precipitated on the original surface of the lavas where the ore bearing fluids were exhaled on the sea floor through the fractured, sulphide impregnated zone represented by the stockworks. The concordance of the massive sulphide deposits with their overlying unaltered lavas, the high purity of the sulphide ores (Table 2.1) and the absence of titanium in the pyrite of the massive ore in contrast to the pyrites from the stockwork zone are all in support of the inference above (Hutchinson and Searle, 1971; Constantinou

Fig. 2.7 Idealised Cyprus sulphide deposit (after Hutchinson and Searle, 1972)

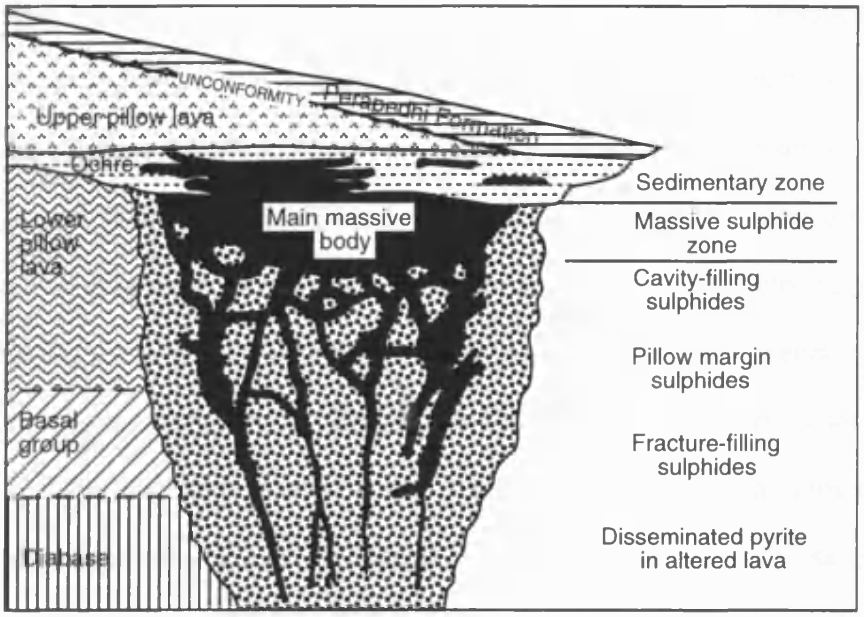

Table 2.1 Composite sample of Skouriotissa ore, example of high purity of Cyprus sulphide ores (after Cullis and Edge, 1927 in Adamides, 1984)

Element/Oxide	Percentage content
Fe	44.47
S	50.90
Cu	1.36
SiO_2	0.81
Al_2O_3	0.71
CaO	0.22
MgO	0.16
As	0.02
Mn	0.01
Pb	Trace
Zn	Trace
Cd	Nil
Undetermined	1.342

and Govett, 1972). Some mineralisations have apparently resulted from the secondary alteration and the local reconcentration, perhaps through new convection cells initiated about minor off-axis magma chambers (Robinson et al., 1987).

Adamides (1984) has suggested that the Cyprus massive sulphide lavas must have been genetically related to the UPL and were both (sulphide and UPL lavas) extruded at the flanks of the spreading axis. The absence of well defined structural or stratigraphic break between these lavas and the older members of the Troodos ophiolites, the continuity of alteration mineralogy and the presence of interdigitation relationships between the two suites suggest close environmental relationship. Available geochemical data seem to favour a model whereby both suites are related by fractional crystallisation (Adamides, 1984). These presuppose a diapiric rise of magma identical to those that generated the Diabase-Lower Pillow Lavas, resulting from the off-axis regime of extrusion. Intrusion of high level magma chambers responsible for the chemically primitive lavas is thought to have caused intense fluid circulation, leaching of ore metals from the SDC and the formation of the sulphide deposits (Adamides, 1984). Geochemical patterns of enrichment and depletion of various elements in the SDC are consistent with a model of seawater-rock interaction in the derivation of the hydrothermal fluids.

The patterns above are seen by Adamides (1984) to be consistent with a model whereby seawater that was originally trapped within the rocks by secondary mineral formation is gradually heated under the influence of the geothermal gradient. Hydrothermal metamorphism results in the enrichment of these fluids in elements originally contained in the component minerals of the lava. The intrusion of magma at high levels creates a low pressure, high temperature regime and causes the movement of metal enriched fluids to higher levels. These chambers

are thought to have been oriented parallel to the spreading axes. The proposed hydrothermal model suggests that all the deposits in a single mining district are genetically related and of contemporaneous formation precluding earlier suggestions (Spooner, 1977) which necessitated the existence of a specific circulation cell for each deposit.

The initial movement of the hydrothermal fluids is thought to have been aided by deep major fractures, either related to the spreading axis regime or to the intrusion of the main chamber, which provided the channelways for the mineralising fluids. The localisation of the deposits within the mining districts has been found to be mostly controlled by the local structure. Indeed graben bounding faults are often characterised by disseminated mineralisation and silicification and massive sulphide occurences tend to cluster about the fossil axes (Lydon, 1983; Adamides, 1984; Richardson et al., 1987; Lydon & Galley, 1988). Although fractures were instrumental in the formation and localisation of strongly focused rich deposits during one period of mineralisation, they were not themselves the cause of movement of the hydrothermal fluids. The circulation of the hydrothermal fluids was triggered off by deep seated causes such as the presence of heat source to promote circulation during the earliest phase of UPL vulcanicity (Adamides, 1984).

The hydrothermal fluids, which at the beginning of their ascent were essentially seawater enriched in S, Si, Cu, Zn, Ca, Ba, Fe, Mn and strongly depleted in Mg relative to unreacted water, ascended to higher levels along pipe-like structures created by the fractures, and deposited massive mineralisation in the form of extensive lenses directly above the pipes (Adamides, 1984). Stratigraphic relationships have been interpreted as implying that a very small time interval separated hydrothermal ore deposition, UPL lava vulcanicity and umber deposition, and that the massive sulphide lenses may be overlain by genetically related umber

or simply by rocks of the UPL (Adamides, 1984). It is thought that rapid extrusion of later flows of lavas was responsible for the preservation of the orebodies and their spatial seperation from the genetically related umbers. The orebodies are preserved under a cover of umber where little or no lavas were deposited as at Skouriotissa and Kinousa. Some of the sulphide ore mineralisations like the Agrokipia 'B' orebody are localised within the LPL sequence and are deduced to have been formed by the replacement of favourable horizons (Adamides, 1984).

The paragenetic relationships of the minerals of the massive sulphides are thought to suggest early precipitation of pyrite, followed by copper and finally zinc sulphide (Adamides, 1984). Wall rock alteration by hydrothermal fluids is considered contemporaneous with the mineralisation, and the term 'propylitisation' has been used in the field to describe the action on hydrothermally altered rocks. Although the hydrothermal action is mainly represented by chloritisation and silicification which makes the term 'propylitisation' a misnomer as it also includes albite, epidote and carbonates (Meyer and Hemley, 1967; Bates and Jackson, 1987), it's usage still persists.

Constantinou and Govett (1972) have suggested that an understanding of the genesis of the sulphides depends on a correct interpretation of the origin of the ochre that occurs conformably overlying the sulphide ore. Ochre is a manganese poor, iron-rich bedded deposit with varying proportions of interbedded chert, tuffaceous material and sometime limestone. It characteristically contains bands or fragments of sulphides and is enriched in Cu and Zn. Its stratigraphic position immediately above the sulphide ore and its geographical restriction essentially within the boundaries of the sulphide deposits is believed to suggest a close genetic relation between ochre and the ore. The ochre has been interpreted as being directly derived from submarine leaching of the sulphides (Constantinou and Govett,

1972). It usually occurs between the sulphides and the umber where it occurs overlying the sulphides or just below the pillow lavas that sometime separate it from the umber. Identification of ochre on the surface of the pillow lavas should therefore suggest the presence of ore mineralisation below.

2.7 Geology of the Geophysical Survey sites

2.7.1 The Klirou Test Site

The Klirou massive sulphide mineralisation is located in an area about 3 km east of Klirou town and occurs in three different parts of the area within the Lower Pillow Lava section of the extrusive Pillow Lava sequence. The first ore mineralisation is the exposed Kokkinorotsos ridge to the northwest of the Klirou area which forms a colourful gossan in places; the second is the small and shallow seated mineralisation located in the southwestern part of the area; and the third mineralisation which is the main mineralisation and the focus of the survey in the area occurs as a deep seated lenticular massive copper sulphide ore body about 10m thick, northeast of the shallow and small mineralisation in the southwest, and east of the gossans (fig.2.8). The main ore body occurs as a massive Cu ore at the centre, above a stockwork, surrounded by a zone of gradually decreasing concentration of Zn mineralisation. The zinc mineralisation overlies and flanks the central copper ore and can be traced laterally to 20-50 m from the copper ores. The mineralisation has undergone silicic alteration and is underlain by a columnar stockwork zone rich in Cu-ores (Maliotis and Khan, 1980). The body shows a NW orientation and is structurally defined by NW and NE striking faults. The LPL is the main outcropping rock in the area with some occurrences of rocks of the Upper Pillow Lava (UPL) to the north of the area and gossans to the north and east along with some weathered soil cover. The LPL is underlain by rocks of the basal group

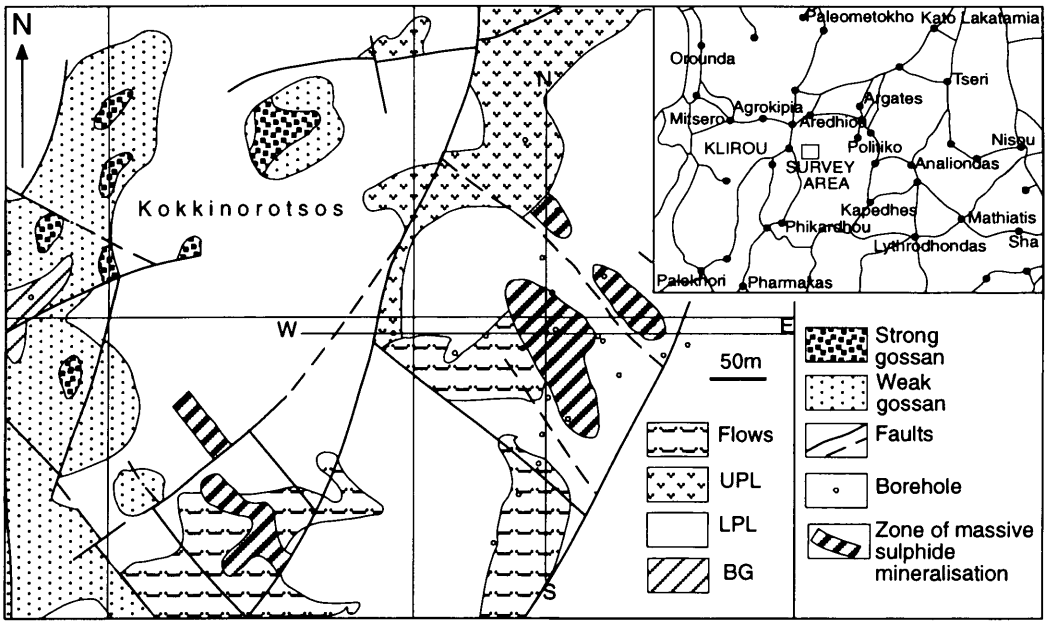

Fig. 2.8 Location and geology of Klirou area

which outcrop in a very small part to the west of the area. The area is strongly fractured with two dominant northeast striking faults and other faults mostly alligned to the northwest direction. The system of faults appear to break up the whole area into northwest trending blocks with the major one hosting the main ore body.

2.7.2 Ayia Marina Area (Main Prospect)

The Ayia Marina area is situated on part of the northern slopes of the Troodos mountain range. It is immediately underlain by rocks of the Pillow Lava series, mostly the Lower Pillow Lava (LPL) rocks which cover most of the area (fig.2.9). The rocks of the Pillow Lava series in this area consist principally of pillow lavas, dykes and sill-like sheets and are generally divided into Upper Pillow Lavas (UPL), Lower Pillow Lavas (LPL) and Basal Groups (BG) mostly on the basis of changing field appearance (Carr and Bear, 1960). These rocks are underlain by rocks of the Diabase which is a fine-grained sheeted complex. Below the Diabase comes the Gabbros and granophyres, rocks of the plutonic complex. The maximum exposed thickness of the rocks of the Pillow Lava series observed was between 80

and 100 m, but exposures of more than 250 m thickness have been reported. The proportion of extrusive rocks in the Basal Group increases from the Diabase contact with more lava than intrusives around the Lower Pillow Lava contact. The high lava proportion remains constant in the succeeding Lower Pillow lava but the Upper Pillow lava remains relatively free of intrusives, especially dykes. All the rocks show variable degree of propylitic alteration which is most widespread near the diabase. The diabase grades into the Pillow Lava series consisting predominantly of sheeted diabase and quartz-diabase. The plutonic complex represented by gabbro and granophyre are cut by propylitised basic dykes and are emplaced mainly in the diabase but also the basal group.

Fig. 2.9 Geology of Ayia Marina area showing the survey traverse and representative sounding sites for clarity

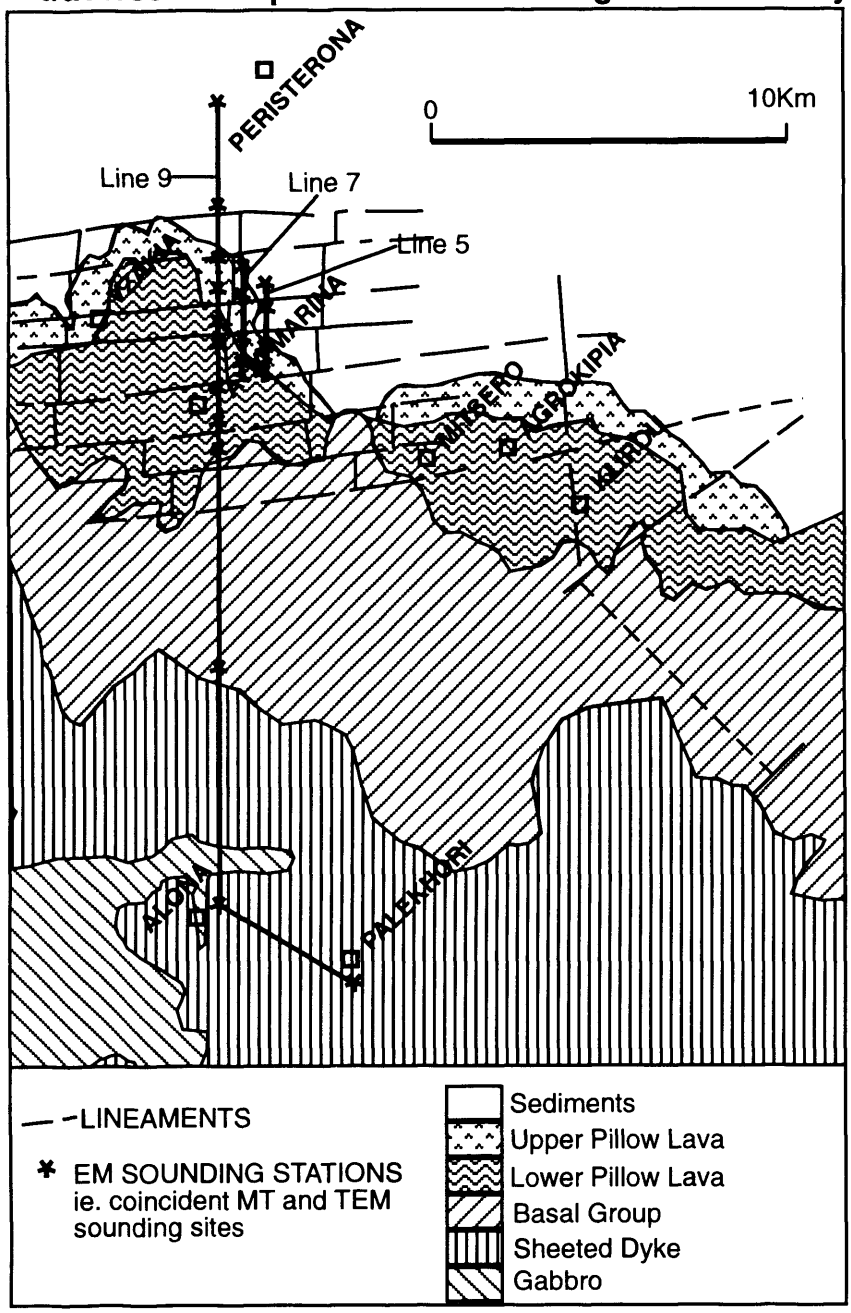

CHAPTER 3

THEORY OF THE MAGNETOTELLURIC (MT) METHOD

3.1 Introduction

Studies of the time variations of the earth's magnetic field over the years have shown that the time variations of any magnetic field are associated with an electric field which induces electric currents in conducting media. Although the existence of such currents could have been inferred in the past, this was proved experimentally by Barlow in 1847 through measurements made using telegraph lines. The concept of using natural electromagnetic (EM) energy to determine the electrical characteristics of the crust was first proposed in 1950 by Tikhonov in the USSR and Kato, Kikuchi and Rikitake in Japan. A comprehensive work on the basic theory of the magnetotelluric (MT) method of geophysical prospecting was later published by Cagniard (1953). The following years of theoretical and experimental work saw the emergence of the method in the early 1960's as a viable exploration technique. Commercial exploration using MT began in the United States in 1967. The method has experienced a slow but steady growth to the point where since 1988 several service companies both in the United States and elsewhere offer contract data acquisition and processing services and many oil and gas companies include MT in their arsenal of geophysical tools (Orange, 1989).

3.2 Electrical Properties of Rocks

The propagation of natural EM waves through the earth is dependent on the electrical characteristics of the earth materials (rocks) through which they travel. EM methods are mainly concerned with the detection of resistivity (or conductivity) variations beneath the surface as determined by the geoelectric section. An

understanding and subsequent interpretation of MT and TEM data therefore requires familiarity with the relationship between the resistivities that are determined from EM data and rock types, and the processes involved in the conduction of currents through rocks. The conduction of current in most rocks is controlled by the fluids (mostly water and dissolved salts) contained within the rocks because the dry rock matrix is a virtual insulator (Griffiths and King, 1981). The main factors that determine the resistivity of the pore fluid are the salinity followed by the temperature. Also, total rock porosity including fracture, intergranular and vuggy porosity, and permeability affect the insitu bulk resistivity of subsurface formations.

Conduction in rocks usually takes place through ionic or electronic conduction. In ionic conduction, charges move in an ordered manner due to the displacement of ions in the crystal lattice under the influence of an external field. This is usually the most common and dominant process of conduction in earth rocks. Electronic conduction on the other hand involves the ordered movement of electrons under the influence of external electric field. Because most rocks act as semiconductors, electronic conduction in them is due to a limited number of free electrons. Metals are good conductors as they have many more free electrons, but conduction in them reduces with increasing temperature because thermally induced electron activity inhibits current flow. However, temperature increase in semiconductors leads to increase in conduction as more electrons are made free to act as charge carriers. Metallic sulphides and some other metallic ores are semiconductors, but have lower resistivities than the common rock forming minerals (Griffiths and King, 1981) and electronic conduction predominates in them over ionic conduction.

The resistivity of subsurface formations is one of the physical properties usually determined through logging in boreholes. Though there is a correlation

between the rock resistivities obtained from well logging and those obtained from MT investigations, it should be noted that the log is used to investigate properties only in the immediate vicinity of the borehole while MT gives information on bulk properties averaged over a considerable volume of rock. In most porous rocks, faulting or fracturing has little or no effect on the bulk formation resistivity. In very tightly compacted/crystalline rocks such as igneous, metamorphic and nonporous carbonate rocks however, the conductivity is usually controlled by fluids present in joints, cracks and fault zones, and on how well connected they are. Small concentrations of such minerals as magnetite, specular haematite, graphite, pyrite and pyrrhotite can significantly reduce bulk resistivity in rocks where they are well connected (Keller and Frischknecht, 1966). The water table, that is, the highest level at which cracks and pores are fully saturated with water, can be very important in near surface resistivity variations. The water that percolates down to the water table is usually meteoric (or surface) with resistivity range of 10-1000 ohm.m while connate water has a resistivity range of 10-100 ohm.m (Ward and Fraser, 1987). Where clays are present, conduction takes place through them by way of the weakly bonded surface ions. Clay conduction can be important as pore fluids become more resistive.

Archie (1942 and 1947) first developed an empirical relationship between the water content of a rock and the resistivity where ionic conduction is dominant and assuming that pores are filled with water as

$$\rho_r = \rho_w \phi^{-n}$$

where ρ_r is the bulk resistivity of the rock, ρ_w is the resistivity of the pore water, and ϕ is the rock porosity and the exponent *n* is an empirically derived parameter that varies from about 1.3 to 2.2 (Parkhomenko, 1967). A modified version of Archie's law has been suggested by some workers as

$$\rho_r = a\rho_w\phi^{-n}$$

where a second factor *a* is added to provide a better fit to observations (Orange, 1989). The factor *a* has a wide range of 0.6 to 3.5 (Parkhomenko 1967).

The effect of measurement frequencies where membrane polarisation restricts ion mobility especially at low frequencies resulting in a decrease in conductivity is very important. The problem is said to be greatest in rocks with low pore fluid ionic concentrations (Ward and Fraser, 1967). Subsurface rocks are seldon isotropic and usually exhibit one form of anisotropy or another. Anisotropy in rocks can be intrinsic/granular occurring at molecular/granular level or structural occurring on a larger scale as a result of layering, oriented fractures and formation from a number of different constituents with different properties. These types of anisotropy could lead to resistivity anisotropy within subsurface formations.

It will be realised from the discussion above that formation resistivities vary widely, not only from one rock formation to another formation, but even within a particular formation especially in near surface unconsolidated materials. Whereas changes in lithology may not necessarily lead to significant changes in resistivity, variations in porosity/permeability and degree of saturation/pore fluid composition may lead to considerable change in resistivity over a very short distance within the same formation. There is therefore no precise correlation of lithology with resistivity (Griffiths and King, 1981) and this should be borne in mind in interpreting EM results. Nonetheless, certain generalisations are possible where the order of increasing resistivity for water saturated rocks tends to be clay-sand and gravel-limestone-crystalline rocks (whose values are higher still). Table 3.1 shows the range of resistivities for some rocks, minerals and water where the high end of some of the rocks represent the resistivities of relatively unfractured and contaminant free rock masses.

Table 3.1 (a) Common rock resistivities (after Telford et al., 1990)

Rock	Resistivity (ohm.m)	Rock	Resistivity (ohm.m)
Granite	300-1000000	Tuff	2000-60000000
Diorite	104-100000	Slate	600-40000000
Dacite	20000(wet)	Marble	100-200000000
Andesite	45000-1700	Shale	20-2000
Dolerite	20-50000000	Conglomerate	2000-10000
Lava	100-50000	Sandstone	1-600000000
Gabbro	1000-1000000	Limestone	50-10000000
Basalt	10-13000000	Dolomite	350-5000
Schist	20-10000	Clay	100

(b) Common mineral and ground water resistivities (after Telford et al., 1990)

Mineral	Range (ohm.m)	Average (ohm.m)
Chalcopyrite	0.000012-0.3	0.004
Pyrite(100%)	0.000029-1.3	0.3
Pyrite(95%)	/	7
Pyrite(40%)	/	130
Pyrite(18%)	/	300
Pyrrhotite	0.0000065-0.05	0.0001
Galena	0.000035-300	0.002
Sphalerite	1.5-10000000	100
Bauxite	200-6000	/
Haematite	0.0035-10000000	/
Magnetite	0.00005-5700	/
Water (igneous)	0.5-150	9
Water (sedimentary)	1-100	3
Sea water	/	0.2
Brine (3%)	/	0.15
Brine (20%)	/	0.05

3.3 Magnetotelluric Energy Source

The MT method employs the transient portion of the earth's magnetic field as its source field. The study of natural EM fields has shown that the amplitude of the electric field component (E) is strongly dependent on local geology and can vary by a factor of 20 over a distance of about 1 km. On the other hand, the magnetic field component (H) is very much less dependent on local geology and seldon varies by more than a factor of 1.5 within the distance of a few kilometres (Vozoff,1972). In geophysical exploration therefore, E is of more diagnostic importance than H as opposed to the custom of considering only H in the study of the worldwide characteristics of natural EM fields. The role of H is primarily to provide the normalisation for E. The main source of the time variations at frequencies below 1 Hz is the energy that originates in the upper ionosphere and magnetosphere. It results from the interaction of the solar wind (charged particles emanating from the sun) and the plasma layers that form the magnetosphere and the ionosphere. This category includes the secular fields, ionospherics and a large proportion of the micropulsations. The main sources of fields at frequencies above 1 Hz include magnetic storms, the ever-present worldwide thunderstorm activity (sferics) and direct radiation of EM waves from the Sun or stellar fields (fig.3.1). Only the micropulsations and sferics which are of practical use in mineral exploration and shallow structural mapping are discussed here.

3.3.1 Micropulsations

Micropulsations have a frequency range of 0.00167 to 5 Hz (i.e. periods of 0.2 to 600 seconds) and belong to the exospherics which result from the interaction of the ionised gas clouds that originate from the sun (solar wind) with the earth's main magnetic field and the atmosphere. Micropulsations occur almost

Fig. 3.1 Magnetotelluric signals

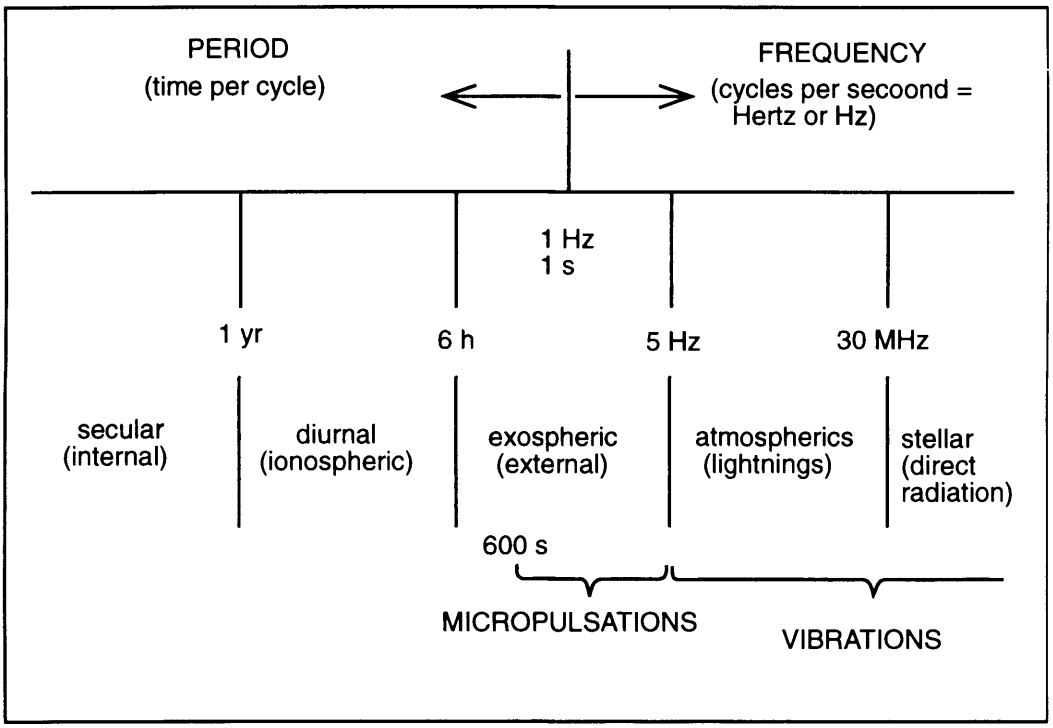

continuously as background noise and their amplitudes depend on solar activity, latitude, frequency, season, local and universal times, and local geology. They can be grouped into continuous and irregular pulsations generally based on the time of the day during which they occur. Continuous pulsations occur mostly during the day time forming wave trains that last for tens of minutes. Their amplitudes tend to peak in the early afternoon (local mean time). Irregular pulsations occur mostly during the night time with wave trains that are of limited duration and a period range of about 40 to 120 seconds (i.e. frequency range of between 0.025 to 0.00833 Hz). In areas where industrial electromagnetic noise is too high for any meaningful exploration during day light hours, irregular pulsations are very useful.

3.3.2 Sferics

The sferics or atmospherics belong to the vibrations and have a frequency range of 1 Hz to 30 MHz. The major cause of the atmospherics is the worldwide

thunderstorm activities which are concentrated in the tropics occurring almost continuously in the Amazon region, Central Africa and Indonesia (the three storm centres) with an average of 100 storm days per year. They are distributed in such a way that during any hour of the day there is perhaps a storm in progress in one of the centres (Telford et al, 1990). These atmospherics occur mostly in the audiofrequency range and are very important in mineral exploration. The earth-ionosphere cavity resonance called the Schumann resonance which has a fundamental frequency of about 8 Hz is usually present in this group and is useful in exploration.

3.4 The Magnetotelluric Theory

The magnetotelluric (MT) method makes use of the propagation properties of electromagnetic waves in conducting media to measure the resistivity of the earth as a function of depth. The electromagnetic field in non-linear media is extremely complicated, and in linear but anisotropic media it is very complicated. Earth materials are fairly linear and in geophysical work the media are assumed to be linear and isotropic so that inhomogeneity is dealt with separately. Under such circumstances, Maxwell's macroscopic field equations in the case of a material medium (matter) are given by

$$\nabla x\mathbf{E} = -\frac{\partial \mathbf{B}}{\partial t} \qquad 3.1$$

$$\nabla x\mathbf{H} = \mathbf{J} + \frac{\partial \mathbf{D}}{\partial t} \qquad 3.2$$

where $\mathbf{H}$ (A/m) = magnetic field vector, $\mathbf{E}$ (V/m) = electric field vector, $\mathbf{J}$ (A/m^2) = current density vector, $\mathbf{D}$ (C/m^2) = electric displacement vector, $\mathbf{B}$ (T) = magnetic induction vector.

The constitutive or auxiliary relations of Maxwell for a linear homogeneous

isotropic medium (half space) relate the physical equations or laws to the subsurface physical properties. The constitutive equations are

$$\mathbf{J} = \sigma\mathbf{E} \qquad 3.3$$

$$\mathbf{D} = \varepsilon\mathbf{E} \qquad 3.4$$

$$\mathbf{B} = \mu\mathbf{H} \qquad 3.5$$

where σ (S/m) = electrical conductivity of the medium (earth), ε (F/m) = dielectric constant (or permittivity) of the medium and μ (H/m) = magnetic permeability or inductive capacity of the medium. The physical quantities defined by the constitutive equations above combine as a single characteristic of the medium referred to as the wave number to determine the behaviour of the electromagnetic field. Substituting the constitutive equations 3.3 to 3.5 into the field equations 3.1 and 3.2 gives

$$\nabla x\mathbf{E} = -\mu\frac{\partial\mathbf{H}}{\partial t} \qquad 3.6$$

and $$\nabla x\mathbf{H} = \sigma\mathbf{E} + \varepsilon\frac{\partial\mathbf{E}}{\partial t} \qquad 3.7$$

In the frequency domain assuming a time dependence of the form $e^{\iota\omega\tau}$ (one-dimensional Fourier transformation leads to the replacement of $\partial/\partial t$ by $\iota\omega$ where $\omega = 2\pi f$ which implies that $f = \omega/2\pi$), equations 3.6 and 3.7 then become

$$\nabla \times \mathbf{E} = -\iota\omega\mu\mathbf{H} \qquad 3.8$$

and $$\nabla \times \mathbf{H} = (\sigma + \iota\omega\varepsilon)\mathbf{E} \qquad 3.9$$

(ω is the angular frequency of the source field in radian per second).

3.4.1 Uniform Homogeneous Half-space

A homogeneous conducting half-space model with air above is the simplest earth model to consider (figure 3.2). If the current field induced by a time-varying EM

field flows parallel to the earth's surface along the x-axis, that is,

$$\mathbf{E} = \mathbf{E}_x \mathbf{i}, \quad \frac{\partial \mathbf{E}_x}{\partial x} = \frac{\partial \mathbf{E}_x}{\partial y} = 0$$

then, for perpendicular **E** and **H** fields in a uniform isotropic conductor, taking the curl on both sides of equations 3.8 and 3.9 will give (Wait, 1962; Vozoff, 1972)

$\nabla \times \nabla \times \mathbf{E} = -\iota\mu\omega(\sigma + \iota\varepsilon\omega)\mathbf{E} = (\mu\varepsilon\omega^2 - \iota\mu\sigma\omega)\mathbf{E}$ for the E field and,

$\nabla \times \nabla \times \mathbf{H} = (\sigma + \iota\varepsilon\omega)(-\iota\mu\omega)\mathbf{H} = (\mu\varepsilon\omega^2 - \iota\mu\sigma\omega)\mathbf{H}$ for the H field.

Using the identity $\nabla \times \nabla \times \mathbf{F} = \nabla(\nabla.\mathbf{F}) - \nabla^2\mathbf{F}$ and remembering that for a homogeneous medium $\nabla.\mathbf{F} = 0$, where **F** stands for either **H** or **E**, we have that

$$\nabla^2 \mathbf{E} = (\iota\mu\sigma\omega - \mu\varepsilon\omega^2)\mathbf{E} \qquad 3.10$$

$$\nabla^2 \mathbf{H} = (\iota\mu\sigma\omega - \mu\varepsilon\omega^2)\mathbf{H} \qquad 3.11$$

Fig. 3.2 Homogeneous half space

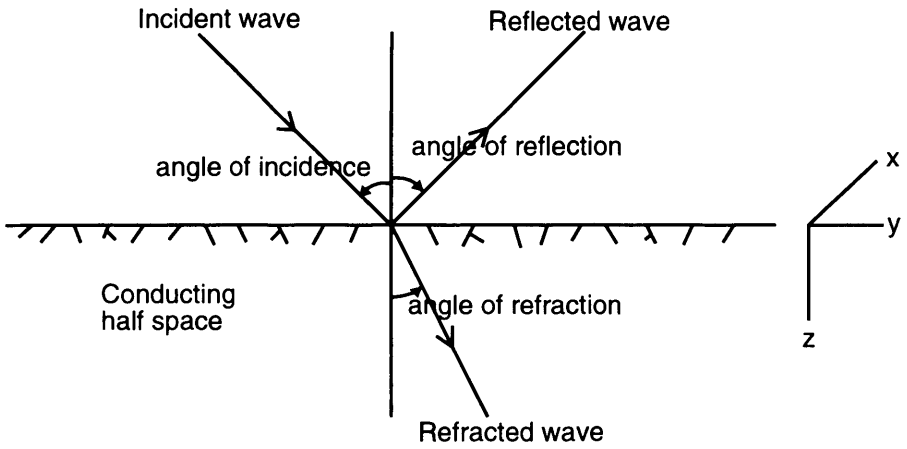

These are the wave equations for the magnetic and electric fields in the frequency domain also known as the Helmholtz equations in H and E. Equations 3.10 and 3.11 could be written simply as

$$\nabla^2\mathbf{E} = k^2\mathbf{E} \qquad 3.12$$

and $$\nabla^2\mathbf{H} = k^2\mathbf{H} \qquad 3.13$$

where $k^2 = (\iota\mu\sigma\omega - \mu\varepsilon\omega^2)$. Here the **H** and **E** fields have been separated from the

earth properties (μ,σ,ε) and the frequency which are now all included in k = the wave number or propagation constant. The components of a field can be treated separately and combined at the end. From Maxwell's equations it can be shown that E_x is associated only with H_y. For a harmonically time-varying field, the elementary solution of equations 3.12 and 3.13 are in this case given as (Yungul, 1996)

$$E_x = Ae^{kz} + Be^{-kz} \quad \text{and} \quad H_y = -\frac{k}{i\omega\mu}\left[Ae^{kz} - Be^{-kz}\right]$$

where E_x and H_y are evidently out of phase or the only solution would be the trivial one which is the values of the amplitudes of the electric and magnetic fields at the surface being equal to zero (Thomas and Meadows, 1985). The time variations of all alternating quantities is given by the factor $e^{i\omega t}$ from which we have a general solution of the form:

$$E_x = Ae^{(i\omega t+kz)} + Be^{(i\omega t-kz)} \qquad 3.14$$

$$H_y = -\frac{k}{i\omega\mu}\left[Ae^{(i\omega t+kz)} - Be^{(i\omega t-kz)}\right] \qquad 3.15$$

where $k = \pm (\iota\mu\sigma\omega - \mu\varepsilon\omega^2)^{1/2}$ and A and B are arbitrary constants evaluated by applying the boundary conditions. These equations are for an unbounded homogeneous medium. For earth materials at frequencies less than 10^5 Hertz which is the frequency range relevant in MT method, $\mu\varepsilon\omega^2 << \mu\sigma\omega$ because σ is more dominant and several orders of magnitude more than ε so that the term containing ε may be neglected (that is the conduction currents predominate over the displacement currents which become negligible). In this case the dependence of k on ε then disappears and equations 3.10 and 3.11 simplify to

$$\nabla^2\mathbf{H} = \iota\mu\sigma\omega\mathbf{H} \text{ and } \nabla^2\mathbf{E} = \iota\mu\sigma\omega\mathbf{E}$$

where $k^2 = (\iota\mu\sigma\omega)$ and $\pm k = (\mu\sigma\omega/2)^{1/2} + \iota(\mu\sigma\omega/2)^{1/2}$

(eg. Keller & Frischknecht, 1966).

Removing the term containing ε means that the propagation is no longer a real wave but rather diffusion just like the flow of heat and the field equations then represent a quasi-static electromagnetic field. For earth materials, μ is approximately the same as that for free space which is $\mu_0 = 4\pi \times 10^{-7}$ H/m. Using $T = 2\pi/\omega$, $\omega = 2\pi/T$, noting that $\sigma = 1/\rho$ and putting them in α = real k gives $\alpha = \frac{2\pi}{10^4}(10/\rho T)^{1/2}$. For a harmonic plane wave normally incident on the surface of the earth (fig.3.2), the equations 3.14 and 3.15 represent the downward transmitted part of the wave. As $z \rightarrow \infty$, E_x cannot be infinite therefore A must be equal to zero (no reflected wave). Using $e^{i\omega\tau} = \cos\omega t + i \sin\omega t$, also remembering that $\sqrt{i} = e^{i\pi/4}$, equations 3.14 and 3.15 become (Yungul, 1996)

$$E_x = Be^{-\alpha z}\left[\cos(\omega t - \alpha z) + i\sin(\omega t - \alpha z)\right]$$

and $$H_y = \left(\frac{1}{\omega\rho\mu_0}\right)^{1/2} Be^{-\alpha z}\left[\cos(\omega t - \alpha z - \pi/4) + i\sin(\omega t - \alpha z - \pi/4)\right]$$

and taking only the real parts, the equations then reduce to

$$E_x = Be^{-\alpha z}\left[\cos(\omega t - \alpha z)\right] \qquad 3.16$$

and $$H_y = \left(\frac{1}{\omega\rho\mu_0}\right)^{1/2} Be^{-\alpha z}\left[\cos(\omega t - \alpha z - \pi/4)\right] \qquad 3.17$$

where $\alpha + \iota\alpha = \pm k = (\iota\mu\sigma\omega)^{1/2} = (\mu\sigma\omega/2)^{1/2} + \iota(\mu\sigma\omega/2)^{1/2}$. As can be seen from the equations there is a phase lag of 45° in H_y which comes from the fact that $\sqrt{i} = e^{i\pi/4}$.

The ratio of the amplitudes of E_x and H_y on the surface (i.e. where $z = 0$) is given by $\left|\frac{E_x}{H_y}\right| = |Z|$ where Z is Cagniard or wave impedance measured in ohm.

$$|Z| = \left|\frac{E_x}{H_y}\right| = (\rho\mu_0\omega)^{1/2} = \frac{2\pi}{10^3}\left(\frac{\rho}{5T}\right)^{1/2} \qquad 3.18$$

It follows from the above that the resistivity of the subsurface can be obtained from

$$|Z|^2 = \left|\frac{E_x}{H_y}\right|^2 = \rho\mu_0\omega \text{ ie, } \rho = \frac{1}{\sigma} = \frac{|Z|^2}{\mu_0\omega} = \frac{1}{\mu_0\omega}\left|\frac{E_x}{H_y}\right|^2 = \frac{5x10^6}{4\pi^2}T\left|\frac{E_x}{H_y}\right|^2 \quad 3.19$$

where ρ is the resistivity, the inverse of conductivity. Measuring this ratio, is how the MT method determines the resistivity of the subsurface. For practical purposes, E is measured in mV/km, H in gamma or nanotesla (nT) and resistivity in ohm.m (Ω.m)

so that equation 3.19 becomes $\rho = 0.2T\left|\frac{E_x}{H_y}\right|^2$.

From equation 3.16, the amplitude of E_x at the surface where $z = 0$ is B, at $z = 1/\alpha$ the amplitude is B/e which is about $0.37B$ and at $z = n/\alpha$ the amplitude is B/e^n. The phase of E_x at $z = 1/\alpha$ lags by 1 radian with respect to E_x at $z = 0$ while that of E_x at $z = n/\alpha$ lags by n radians. This indicates an exponential decay of amplitude along the travel path. The depth $z = 1/\alpha$ is called the radian wave length or the skin depth (the depth at which the amplitude of the field has been attenuated by $1/e$ or 0.37 of its value at the surface) given by $\delta = 1/\text{real } k = \left(\frac{2\rho}{\mu\omega}\right)^{1/2} \cong 503\,(\rho T)^{1/2}$ (m) 3.20

where $\alpha = \left(\frac{\mu\omega}{2\rho}\right)^{1/2}$ from $k = (\iota\mu\sigma\omega)^{1/2} = \left(\frac{\mu\omega}{2\rho}\right)^{1/2} + \iota\left(\frac{\mu\omega}{2\rho}\right)^{1/2} = \alpha + \iota\alpha$

Longer period waves therefore penetrate deeper into the earth, thus allowing different depths to be probed by different frequency waves using equation 3.20 above. The phase lag at a depth $z = 2\pi/\alpha$ is 2π radian from which the wave length can be derived as $\lambda = 2\pi\delta = 2\pi\left(\frac{2\rho}{\mu\omega}\right)^{1/2} = 10^4\left(\frac{\rho T}{10}\right)^{1/2}$ $10^4(\rho T/10)^{1/2}$ metres.

α is called the attenuation constant because when the depth is increased by $\delta = 1/\alpha$ the amplitude is attenuated by 1/e and the phase lags by 1 radian. The velocity of a downward transmitted wave will be the product of the wave length and the

frequency given as $V = f\lambda = \left(\frac{\omega}{2\pi}\right) 2\pi\delta = \omega\delta = \omega/\alpha = 10^4\left(\frac{\rho}{10T}\right)^{1/2}$

3.4.2 One-Dimensional Environment

In this case, the conductivity is a function of depth only where the subsurface consists of *n*-1 horizontal homogeneous and isotropic layers underlain by a half-space (the *n*th layer) of resistivity ρ_n (fig.3.3). Although in reality the earth is never one-dimensional the representation of the earth by *n* horizontal layers is an important approximation in MT, and with appropriate care can be used as a reasonable approximation to depth under a measurement site in many cases. Except in the air, the general equations for a plane wave propagating in the positive z direction would be as given in 3.14 and 3.15, these are

$$E_x = Ae^{(i\omega t+kz)} + Be^{(i\omega t-kz)} \qquad 3.21$$

$$H_y = -\frac{k}{i\omega\mu}\left[Ae^{(i\omega t+kz)} - Be^{(i\omega t-kz)}\right] \qquad 3.22$$

where $k^2 = i\sigma\mu\omega - \varepsilon\mu\omega^2$ and A and B are arbitrary constants. Now each layer has a different k and different constants A and B. Also, apart from the nth layer, there will be both upward and downward propagating waves which affect (distort) the measured impedances and hence the calculated resistivities of the layers. Equation 3.1 is however used to measure resistivities for the layers the values of which could be very close to the true resistivties of the layers and are called apparent resistivities given by

$$\rho_a = \frac{1}{\mu\omega}\left|\frac{E_x}{H_y}\right|^2 = 0.2T\left|\frac{E_x}{H_y}\right|^2 \qquad 3.23$$

In the *n*th layer there are no reflected waves and so $A_n = 0$ as $z \rightarrow \infty$. The propagation in an *n*-layer earth is completely determined through constants

Fig. 3.3 One dimensional model

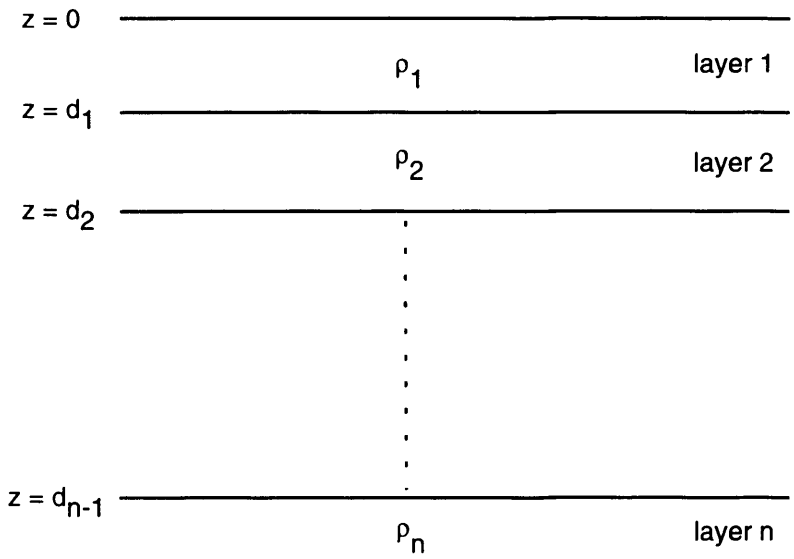

$A_1,\ldots,A_{n-1}$, $B_1,\ldots,B_n$ and the set of *2n* linear equations derived from the continuity at the layer boundaries. Starting from the top of the *n*th layer (see figure 3.3) which now appears like a homogeneous half-space, the impedance is given by (Orange, 1989) $Z_{(zn-1)} = \dfrac{E_{x(zn-1)}}{H_{y(zn-1)}} = \dfrac{-i\mu\omega}{k_n} = (-i\mu\omega\rho_n)^{1/2}$

$$= \left(\frac{\mu\omega\rho_n}{2}\right)^{1/2} - i\left(\frac{\mu\omega\rho_n}{2}\right)^{1/2} = (1-i)\left(\frac{\mu\omega\rho_n}{2}\right)^{1/2} = e^{-i\pi/4}\left(\frac{\mu\omega\rho_n}{2}\right)^{1/2}$$

For any layer of depth z_m then notice that $Z_{zm} = \dfrac{-i\mu\omega}{k_n}\dfrac{(A_m/B_m)e^{i\omega t+kz} + e^{i\omega t-kz}}{(A_m/B_m)e^{i\omega t+kz} - e^{i\omega t-kz}}$

Generally the theoretical impedance is $Z = |Z|e^{i\Phi} = \left|\dfrac{E_x}{H_y}\right|\dfrac{e^{i\phi_x}}{e^{i\phi_y}} = \left|\dfrac{E_x}{H_y}\right|e^{i(\phi_x-\phi_y)}$ 3.24

The phase of Z is the phase difference between E_x and H_y.

3.4.3 Two-Dimensional Case

Experimental models have shown that the earth is laterally inhomogeneous where the ground resistivity varies horizontally and with depth $\rho(x,y,z)$ where

$\frac{1}{\mu_0\omega}\left|\frac{E_x}{H_y}\right|^2$ is now no longer constant but depends on the directions chosen for *x* and y, and the incoming signal. The expression becomes (O'Brien and Morrison, 1967; Orange, 1989) $\frac{1}{\mu_0\omega}\left|\frac{E_x}{H_y}\right|^2 \neq \frac{1}{\mu_0\omega}\left|\frac{E_y}{H_x}\right|^2$

For an invariant expression therefore, a tensor impedance is required (Cantwell, 1960; Orange, 1989) such that ***E=ZH*** now becomes

$$E_x = Z_{xx}H_x + Z_{xy}H_y \quad \text{or} \quad \begin{bmatrix} E_x \\ E_y \end{bmatrix} = \begin{bmatrix} Z_{xx} & Z_{xy} \\ Z_{yx} & Z_{yy} \end{bmatrix}\begin{bmatrix} H_x \\ H_y \end{bmatrix}$$
$$E_y = Z_{yx}H_x + Z_{yy}H_y$$

where the tensor impedance Z has been written in the matrix form $Z = \begin{bmatrix} Z_{xx} & Z_{xy} \\ Z_{yx} & Zyy \end{bmatrix}$

Z_{xy} and Z_{yx} are the principal impedances, and Z_{xx} and Z_{yy} are the subsidiary impedances due to contributions from parallel components of the magnetic fields.

In general the measurement axes in the field may not be aligned with the strike such that Z_{xx} and $Z_{yy} \neq 0$, $Z_{xy} \neq -Z_{yx}$ and the elements of Z vary as the co-ordinate axes are rotated (Orange, 1989). However, when the axes are aligned with the structural strike *(x)*, $Z_{xx} = Z_{yy} = 0$. Also on the surface of the earth, T (the tipper) is defined by the equation $H_z = T_xH_x + T_yH_y$ where H_z is totally a secondary vertical field and is zero in the case of a horizontally layered (one-dimensional) earth. T is zero in one-dimensional cases, but nonzero in two-dimensional cases. From the discussion of the one-dimensional case, $Z_{xx} = Z_{yy} = Tx = Ty = 0$ and from Maxwell's equations $Zxy = -Zyx$. For a two-dimensional environment, the axis of symmetry will be taken as x-axis (fig.3.4). An electromagnetic wave whose electric field E is along the strike direction is said to be E-polarised (that is, the TE or transverse electric mode) while one whose magnetic field intensity H is along the strike direction is referred to as being H-polarised (that is, TM or transverse magnetic mode). Primary

waves that are E-polarised usually generate only secondary waves that are E-polarised and primary waves that are H-polarised generate only H-polarised secondary waves.

The preservation of polarisation type is equivalent to saying that in the special co-ordinate system where one axis *(x)* is along the strike, $Z_{xx} = 0$ and $Z_{yy} = 0$. These axes are actually known as the primary axes of Z. In field practice, measurement axes (x, y) are hardly aligned to the strike direction so that

$$Z_{xx} \neq 0 \text{ and } Z_{yy} \neq 0 \qquad 3.25$$

However, since in practice the trace of Z, *tr (Z)* from matrix algebra is a scalar, tr $(Z) = Z_{xx} + Z_{yy} = 0$ where the local subsurface structure is electrically two-dimensional. Equation 3.25 is a necessary but not sufficient condition for two-dimensionality. Also the quantity $Z_{xy} - Z_{yx}$ is a constant under rotation of orthogonal coordinate axes. Where the coordinate axes are aligned to the strike direction, noise-free data should yield $Z_{xx} = Z_{yy} = 0$. Mathematical rotation of the measurement axes during data analysis until $|Z_{xx}(\theta)|^2 + |Z_{yy}(\theta)|^2$ is a minimum will determine the strike direction within a 90° ambiguity. When *x* is chosen along strike direction, $T_x = 0$, $T_y \neq 0$ and $Z_{xx} = Z_{yy} = 0$. A difference between the principal axes that have been found from Z and T is one indicator of a three-dimensional structure. The apparent resistivity as in equation (3.23) is computed using the square of the electric field and as such a deviation is observed across a resistivity boundary in the H-polarisation mode from what it would ordinarily be in a one-dimensional earth. The apparent resistivity data ρ_{xy} is often inverted to yield an approximate resistivity layering beneath the site of measurement.

3.4.4 The Three-dimensional case

The conductivity distribution in MT problems is in reality three-dimensional

Fig. 3.4 Simple two-dimensional model

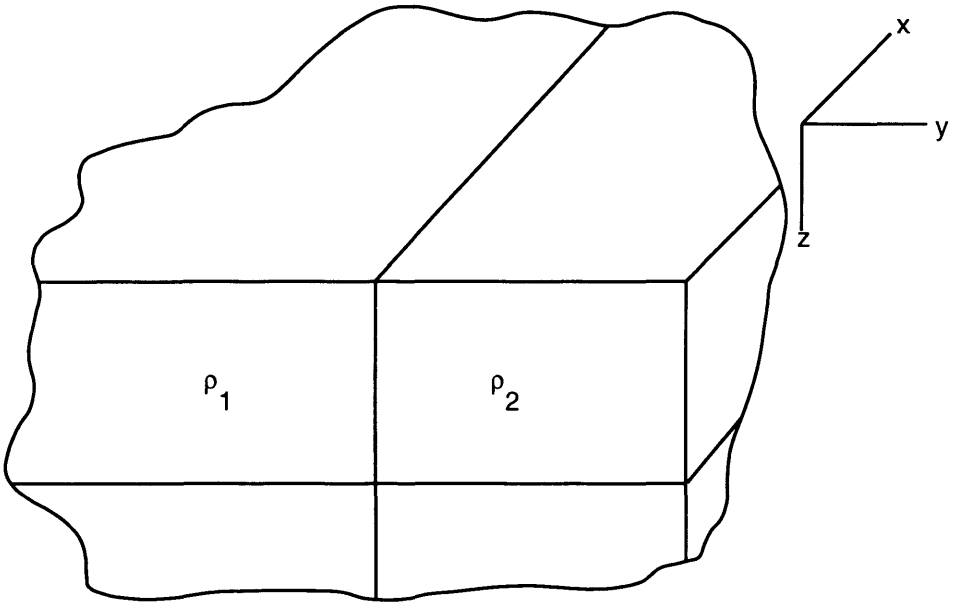

where the conductivity σ is a function of all three co-ordinate axes x, y and z such that $\sigma = \sigma(x,y,z)$ (Fig.3.5). Throughout the MT literature the terminology of transverse electric (TE) and transverse magnetic (TM) modes is used even though there are no true TE and TM modes in the three-dimensional problem. In real data, the skew which is defined as the ratio $\frac{tr(Z)}{Z_{xy}-Z_{yx}} = \frac{Z_{xx}+Z_{yy}}{Z_{xy}-Z_{yx}}$ is one common measure of deviation from the two-dimensional case. For the one- and two-dimensional cases the skew is zero. Analytical solutions to Maxwell's equations in three-dimensions are difficult where the generic three-dimensional case Z_{xx} and Z_{yy} cannot be made to vanish by a choice of axes thereby requiring consideration of the complete tensor.

As in the two-dimensional case, $\boldsymbol{E=ZH}$ now becomes (Cantwell, 1960) $E_x = Z_{xx}H_x + Z_{xy}H_y$ and $E_y = Z_{yx}Hx + Z_{yy}H_y$ giving four apparent resistivity curves from the four components of the surface impedance tensor *Zij*, and four phase curves. In addition, the vertical magnetic component Hz(T) which can be defined as the ratios *Hz/Hx* vs *T* and *Hz/Hy* vs *T* along with their phases yield another four

curves leading to twelve in all at a measurement site. Finding a model to fit all these data for each frequency at every station in order to interpret the subsurface is an extremely complicated problem (Orange, 1989; Yungul, 1996). In many cases the two-dimensional transverse magnetic mode behaves approximately like the three-dimensional case. The behaviour of the TE mode has less analogy in the three-dimensional case, and in particular, the tipper which is a TE mode effect is suppressed in three-dimensional cases (Orange, 1989). Most three-dimensional MT problems are solved by approximate two-dimensional techniques. A better understanding of three-dimensional effects is however being achieved with improvements in three-dimensional modelling techniques.

Fig. 3.5 Simple three dimensional earth model showing conductivity variation in three orthogonal directions

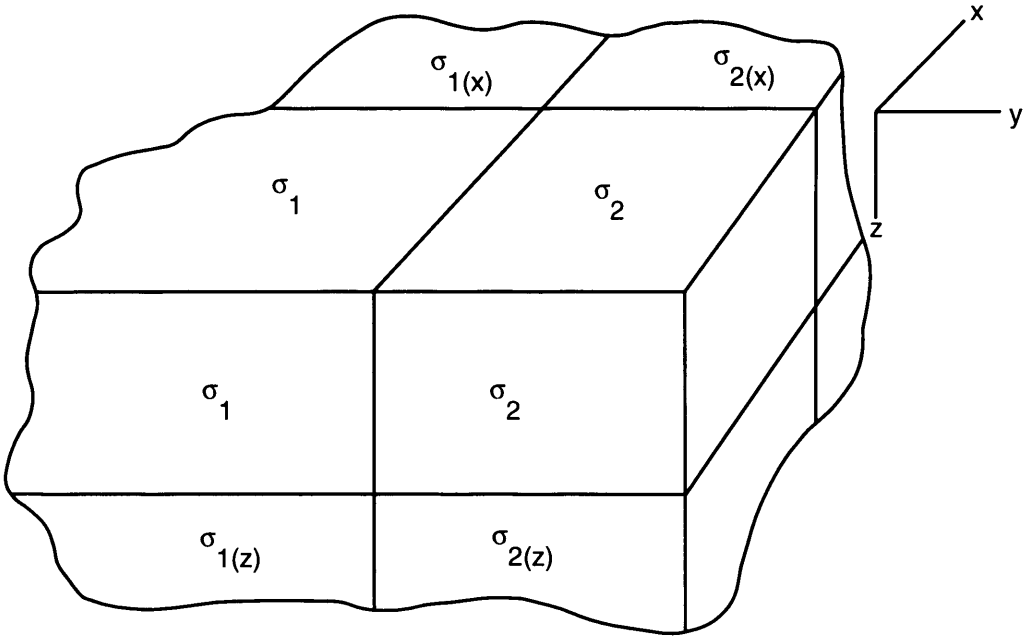

3.5 Interaction with the Earth

The expression (3.23) would suffice for the relationship between the natural electric and magnetic fields and the MT analysis would be straight forward if the earth were homogeneous or plane layered. However, the earth and the electromagnetic field relationship are more complex.

Fig. 3.6 Near isotropic and statically shifted Magnetotelluric data

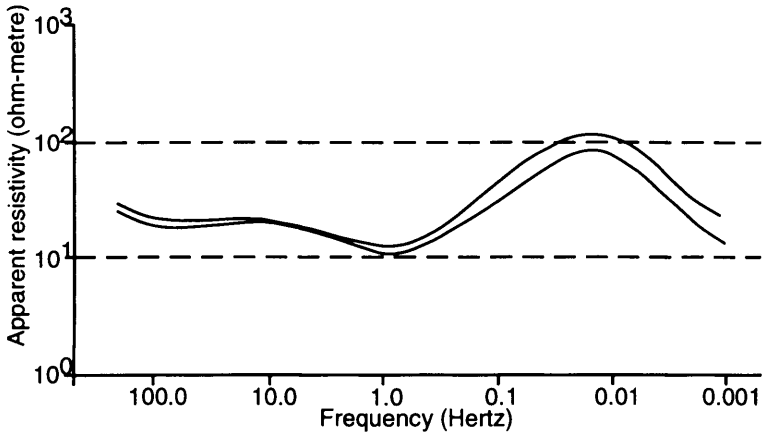

(a) Near isotropic data

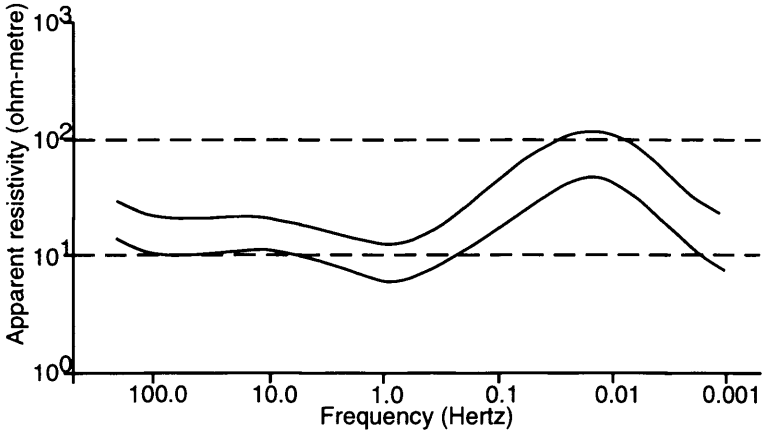

(b) Statically shifted data

3.5.1 Static effects: Statics in MT may be revealed by a parallel or near parallel separation (frequency independent) of the two resistivity curves obtained from equation 3.18 with one or both curves shifted from the "correct position" (figs.3.6a and b). Unless steps are taken to apply appropriate corrections, static shift will lead to errors in estimated depths and resistivities because normal analysis of MT resistivity-depth relationship requires knowledge of the apparent resistivity function. The distorted data may be satisfactorily corrected by simply shifting one or both curves to the appropriate level determined either through examination of near by sites or independent measurement of the near surface resistivity (Orange, 1989; Meju, 1996).

3.5.2 Geologic Structural effect: Geologic structural features such as variations in rock resistivities and fractures result in a non-uniform EM field because the induced currents are channelled by them. Unlike the statics effect above, the structurally caused anisotropy is strongly frequency dependent (fig.3.7). For a two dimensional structure the impedance tensor is rotated such that the two components Z_{xy} and Z_{yx} are parallel and perpendicular to the electrical strike. The extent to which $Z_{xx} \neq Z_{yy}$ after the tensor has been rotated is one indication of the extent to which the subsurface is not two dimensional.

Fig. 3.7 Frequency dependent structural anisotropy in Magnetotelluric data

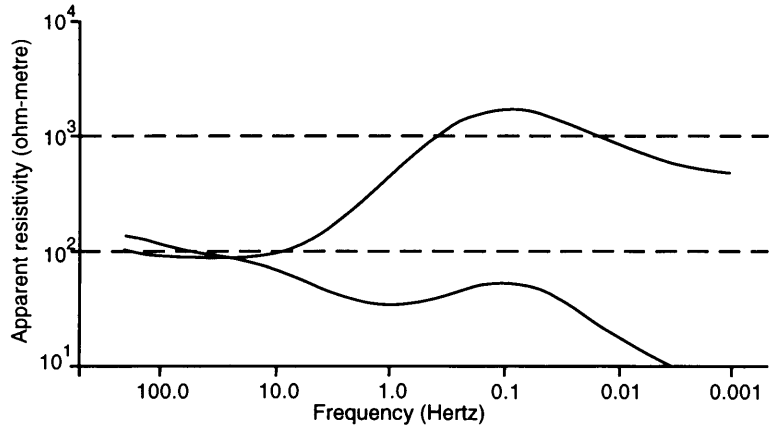

3.5.3 Distant Regional Structural effect: The effect of distant regional structures on MT fields can extend to several hundred kilometres away from the structure causing it (Ranganayaki and Madden, 1980; Park et al, 1983). A common effect is a depression of the apparent resistivity at low frequencies on one or both apparent resistivity curves which is the result of subsurface current levels being perturbed from their one dimensional values by one or more lateral resistivity boundaries.

3.6 Data Processing

3.6.1 Basic Principles:

The main objective in the analysis of MT field data is to obtain the smoothed

amplitude and phase spectra of the real time series from the measured data so that the apparent resistivity tensor can be determined and presented in a form convenient for interpretation. These earth response functions are extracted from the field records mostly by either the fast Fourier transform (FFT) or cascade decimation (CD) techniques (Orange, 1989) after manual editing as for example in Sims and Bostick (1969), Sims et al., (1971), Vozoff (1972) and Wight and Bostick (1980).

Auto and cross power estimates are computed using the fast Fourier algorithm. The tensor apparent resistivity and associated functions are computed after obtaining the constant percentage bandwidth "windows" by averaging and removal or deconvolution of the sensor and instrument transfer functions (Bostick, 1977). The fast Fourier transforms of individual segments may be added together, or "stacked" to improve the signal-to-noise ratio by suppressing uncorrelated noise. The FFT and MT function computations may be done after the survey using a large digital computer, or in the field using a dedicated mini computer.

The cascade decimation technique originally developed by Wight and Bostick, (1980) is used for computing power spectra estimates for single or multi-channel time series data. The technique is particularly well suited to applications where it is desirable to reject intervals of bad data or those that are naturally expressed on a log-frequency scale (as are MT data). In practice the cascade decimation technique is continuous, with data being "stacked" as time progresses. Recording continues until data quality is acceptable, or until a decision is made to terminate, and possibly initiate another sequence. The electric and magnetic field power spectra produced by the cascade decimation process are manipulated to produce the MT functions in a manner similar to that described for FFT.

3.6.2 Signal to Noise characteristics

Appropriate steps are usually taken in selecting and installing equipment to ensure that the best possible data are obtained under the constraints of survey objectives. Noise in the MT data can consist of internal instrument noise, sensor and cable noise especially as a result of wind effect, spurious electromagnetic radiation, spurious currents flowing in the earth, and moving metallic objects that are detected by the magnetometers. Several methods are used to improve signal-to-noise characteristics of processed data among which are editing, stacking and the use of remote reference:

Editing MT data involves the removal of sections that are obviously contaminated by noise. Because many of the serious noise problems are caused by impulsive or "burst" type noise which are often easily recognised by the eye using the record of the time series or by computer, editing is clearly feasible. Where noise contamination is suspected, the segment of data is discarded.

Stacking involves the summing up or "stacking" of the power spectra from several independent data segments usually FFT's of short 512-1024 point data samples. This acts to improve the signal to noise ratio by enhancing correlated signal at the expense of the more random noise.

Remote reference MT makes use of data acquired simultaneously at two localities separated by up to 25 km (Gamble et al, 1978, 1979). The data at each site is then analysed using the magnetic field at the other site as a "remote reference". This entails the multiplication of the equations relating the Fourier components of the electric and magnetic fields by a component of the magnetic field of the remote reference.

3.6.3 In-field Processing and Analysis

The ability to undertake initial processing of acquired field data right there in the field in order to evaluate the field data quality to ensure that data of the desired quality has been recorded before moving from a site, is a good and important feature of MT exploration surveys. In-field data processing as it is called also involves preliminary interpretation of the processed data in the field and the results then used to make important decisions in the field regarding the conduct of the survey as a whole. The same computer used for data acquisition may be used for in-field data processing or a separate computer installed with the recording instruments may be dedicated to processing data in the field. In real-time processing using remote reference, data from the base and reference sites are made available to the computer either by hard wire or radio telemetry links.

3.7 Interpretation

The computed MT earth response functions can be represented in several different ways such as plots of apparent resistivity, phase, skew, etc. against frequency in the form of graphs for single sites or pseudosections for several stations. These can be used for initial qualitative interpretation. The apparent resistivity data are then transformed to effective resistivity and depth for plotting resistivity-depth sections using techniques like the popular Niblett-Bostick transformation technique. In trying to retrieve the subsurface resistivity distribution from MT data, note that an infinite number of resistivity structures exist that can satisfy a finite set of data. Optimisation routines are used to obtain optimal solutions which may not be mathematically unique. A common approach is to incorporate a priori information.

3.7.1 Niblett-Bostick (N-B) Transformation

This is a simple semi-continuous mapping of MT data into resistivity-depth information using an algorithm based on the asymptotic response of impedance data in a horizontally layered model with infinitely conducting or resistive substrata (Niblett and Seyn-Wittgenstein, 1960; Bostick, 1977; Jones, 1983). The technique provides parameters for a single layer for each resistivity and phase point so that a continuous resistivity-depth curve may be obtained for the resistivity and depth independently. The penetration depth h and resistivity at depth h, ρ_h, incorporating the phase (in radians) information are given by (Bostick, 1977; Goldberg and Rotstein, 1982)

$$h = \left[\frac{\rho_a(\omega)}{\mu_0 \omega}\right]^{1/2} \quad \text{and} \quad \rho_h = \rho_a(\omega)\left[\frac{\pi}{2\phi(\omega)} - 1\right]$$

where ω is angular frequency and ρ_a is the observed apparent resistivity value.

3.7.2 The a priori Information Approach

A priori information refers to already known values of some parameters which can be incorporated into the optimisation scheme right from the beginning to yield a unique solution (Jackson, 1979; Meju, 1988). For example, the resistivity values or thicknesses of certain layers could be known from borehole logs or other geophysical or geological observations. These values may be retained in the final results especially if they are thought to be reliable and come from the area of interest. In addition, where an MT site x has sparse or biased data set, the resistivity distribution at a neighbouring site y, with good quality data, could be used if thought to be of similar geology.

CHAPTER 4
THE TRANSIENT ELECTROMAGNETIC (TEM) METHOD

4.1 Introduction

The Transient Electromagnetic (TEM) or Time-domain Electromagnetic method of geophysical exploration is an inductive EM method that utilises direct current in an ungrounded wire loop (figure 4.1) to generate secondary EM fields due to induced eddy currents in the earth, which is measured in the absence of the primary field. The steady (primary) current in the wire loop is abruptly terminated. This generates a time-varying (primary) magnetic field which induces eddy currents in conductive targets in the subsurface. The induced currents diffuse relatively slowly in more conductive strata than in the resistive members of the substrata and decay in a manner characteristic of the properties of the subsurface targets (mainly conductivity, shape and size). The secondary magnetic field associated with these decaying eddy currents can be measured by a receiver and the data analysed and interpreted to give the conductivity distribution and the structure of the subsurface. Subsequent treatment of the TEM principles and theory in this chapter relies heavily on McNeill (1980) and Nabighian and Macnae (1991).

The need to properly and simply separate the primary from the secondary parts of the total EM field measured in the frequency-domain EM, requirements for greater depths of exploration, improved rejection of conductive overburden or host-rock response and enhanced definition of potential ore-bearing structures all led to the idea of using transient or time-domain EM measurements. In addition, the transient electromagnetic techniques lend themselves very well to general geological mapping (McNeill, 1980). Wait (1951) first disclosed an inductive transient technique to determine the parameters of massive sulphide ore-bodies and also disclosed a patent application on behalf of Newmont Exploration Ltd. By 1962, the first version of the Newmont EMP system as part of a joint Newmont-

Cyprus Mines development program had been developed. Barringer developed the first airborne TEM system, INPUT, in 1958 (Barringer, 1962). 1960 saw the

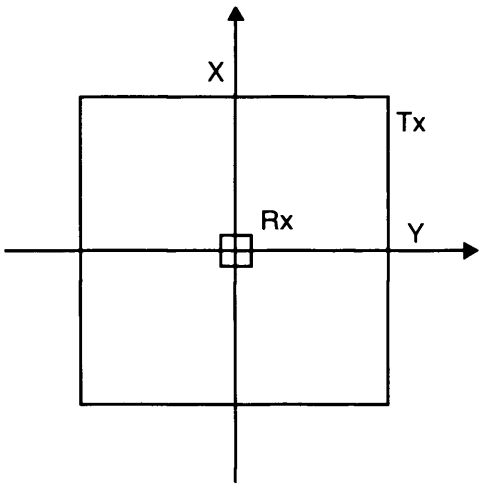

Square or rectangular transmitter loop

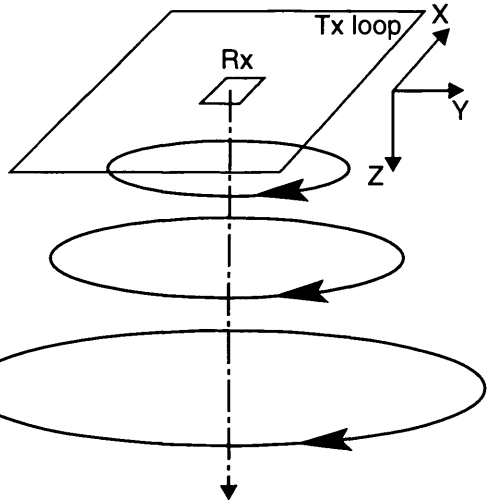

With equivalent current filaments at various times after current termination

Fig. 4.1 TEM setup with ungrounded wire loop

development in the Soviet Union of the single-loop version of the transient techniques (MPPO-1) in which the same loop is used both as transmitter and receiver (i.e., the one-loop version). With the advent of computer technology in the 1970s, the first fully digital TEM system was introduced by Newmont Exploration Limited in 1974 for in-house use together with the required software package for data processing, presentation and interpretation. CSIRO introduced SIROTEM in 1977 as the first microprocessor TEM unit operating on the single-loop. Crone PEM

and UTEM1 were introduced in 1972. Geonics EM-37 was produced in 1980. The Russian helicopter TEM, the GEOTEM and PROSPECT airborne systems were developed in 1978, 1986 and 1988 respectively. As of 1988, all manufacturers were offering fully digital systems.

4.2 Basic Transient Electromagnetic principles

As shown in figure 4.1, the loop is energised by passing a strong current through it. This is then abruptly interrupted (step function excitation) such that by Faraday's law of induction, eddy currents are induced in a neighbouring conductive sphere. Under the quasi-static approximation (Grant & West, 1965), the induced currents will be independent of the conductivity of the sphere and initially (i.e. at time t = 0) be confined to the surface of the conductor in such a way as to preserve the normal component of the pre-existing primary magnetic field at the surface S of the conductor (Weaver, 1970). This is the early time stage of the transient process (figure 4.2a) and is the high frequency limit since the current distribution is that

Fig. 4.2 Stages of transient decay process after McNeill (1980). (Sphere current flow at various times after Tx current turn-off)

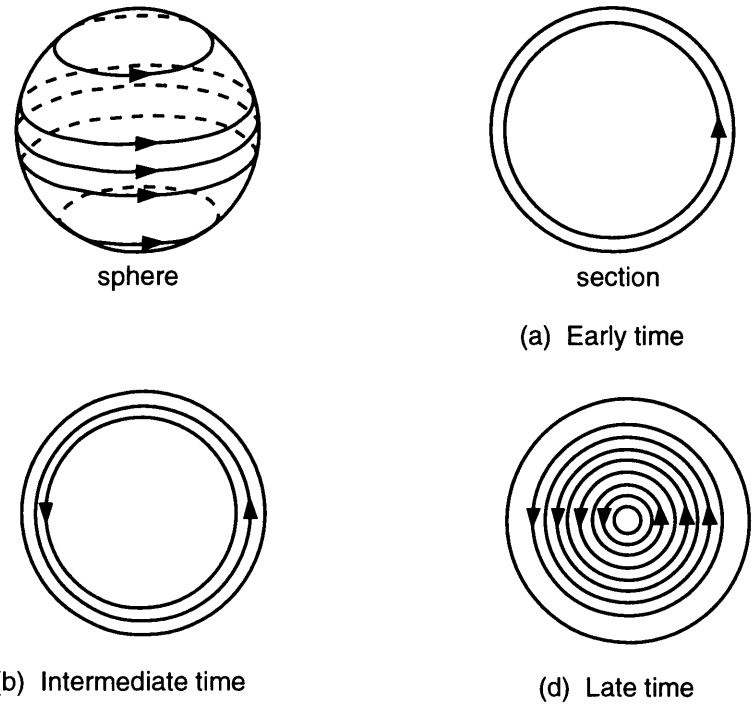

which will flow if the sphere were located in a very high frequency alternating (uniform) magnetic field. The definition of high frequency here is such that the electrical skin depth in the sphere material (McNeill, 1980) $\delta = \left(\frac{2}{\mu\sigma\omega}\right)^{1/2}$ is much less than the radius of the sphere where $\mu = 4\pi x10^{-7}$ H/m, $\omega = 2\pi f$ and f= frequency (Hz).

An inward diffusion of the current pattern later occurs as a result of ohmic losses which leads to the region immediately inside the conductor seeing a decreasing magnetic field and an induced emf that causes new current to flow. This is the intermediate-time stage of the transient process (fig.4.2b). The process continues until a stage is reached when the induced current distribution becomes more or less invariant with time. The inductance and resistance of each current ring have reached asymptotic values (stabilized) and both the currents and their associated external magnetic fields begin to decay with a time constant given by $\tau = \frac{\sigma\mu a^2}{\pi^2}$ (figure 4.2c). This is the late-time stage of the transient process.

Measurement of the transient decay or its derivative yields useful diagnostic information about the conductivity, radius and depth of the conductive sphere. The late stage of the decay commences at a value of $t/\tau \cong 0.5$ (characteristic of a sphere) and determination of τ gives a value for σa^2.

4.3 TEM Theory

A drawback of EM methods in general is that many prospective users have difficulty visualising the physics of the phenomena partly due to inability to routinely calculate realistic three dimensional electromagnetic induction models as yet (Nabighian and Macnae, 1991). This forces reliance on the intuitive approach which is greatly helped by the fact that the EM induction process, at the low frequencies commonly used in exploration, obeys primarily the diffusion equation, so wave propagation effects can be neglected. This is so for TEM, because for typical delay times of interest and distances between transmitting and receiving circuits we are

well within the quasi-static zone where time delays due to propagation at the speed of light can be ignored (Grant and West, 1965).

4.3.1 Uniform Conducting Medium

Under quasi-static approximation, the EM field components in a homogeneous region satisfy Maxwell's equations

$$\nabla^2\mathbf{E} - \mu\sigma\frac{\partial\mathbf{E}}{\partial t} = 0$$
$$\nabla^2\mathbf{H} - \mu\sigma\frac{\partial\mathbf{H}}{\partial t} = 0 \qquad 4.1$$

For the simplest case involving spatially one dimensional fields, the above equations become

$$\frac{\partial^2\mathbf{E}}{\partial z^2} - \mu\sigma\frac{\partial\mathbf{E}}{\partial t} = 0$$
$$\frac{\partial^2\mathbf{H}}{\partial z^2} - \mu\sigma\frac{\partial\mathbf{H}}{\partial t} = 0 \qquad 4.2$$

The following solution is obtained

$$E_x(z,t) = E_0 e^{-iz/\delta e - z/\delta e i\omega t}$$
$$H_y(z,t) = E_0\sqrt{\frac{\sigma}{\mu\omega}}\, e^{-i\pi/4 e - iz/\delta e - z/\delta e i\omega t} \qquad 4.3$$

where $\delta = \sqrt{2/\mu\sigma\omega}$ is the skin depth. From equation 4.3, we see that at depth $z = \delta$ the EM field is reduced in amplitude by 1/e while its phase changes by 1 radian.

For a step function excitation of magnitude H_0 established at time $t = 0$, the transient fields are given by $e_x(z,t) = \frac{2H_0}{\sigma}(1/\sqrt{2\pi})(\mu\sigma/2t)^{1/2} e^{-(\mu\sigma 2t)(z^2/2)}$

and $$h_y(z,t) = H_0 erfc(\mu\sigma/2t)^{1/2}(z/\sqrt{2}) \qquad 4.4$$

where $erfc(z)$ is the complementary error function with respect to t. If z is kept constant in equation 4.4 and the derivative of $e_x(z,t)$ is equated to zero the transient electric field reaches a maximum when $t = \frac{\sigma\mu z^2}{2}$ and $z = (2t/\mu\sigma)^{1/2} = d$ 4.5

where d = diffusion length and represents the depth at which the local electric field (or current) reaches its maximum value for a given time (i.e. the electrical skin depth). The local maximum then travels down with velocity $V = 1/(2\mu\sigma t)^{1/2}$. Often,

the diffusion distance $d = 2\pi\delta = 2\pi(2/\mu\sigma\omega)^{1/2}$ is used in analogy with the frequency domain relation between wave length and skin depth $(\lambda = 2\pi\delta)$. In frequency domain, penetration is proportional to $1/\sqrt{\omega}$ while in time domain it is proportional to $\sqrt{t}$.

4.3.2 Homogeneous Half-space

At time t = 0, just as the inducing current is abruptly terminated, a surface current flows distributed in such a manner as to maintain the magnetic field everywhere at the value just before turn-off. At time $t = 0^+$, near the transmitter the surface current starts to diffuse into the homogeneous half-space. With time the current appears to have moved out and down as a diffusing ring as described by Nabighian (1979) (see figure 4.2). The radial position of the surface current maximum at any point in time is proportional to $d = 2\pi\delta$. Since location of current maximum increases as $t^{1/2}$, the apparent velocity varies as $t^{-1/2}$. The wave initially expands rapidly but the velocity decreases to a small value as time passes and the ring diameter becomes practically self-limiting. This shows that in conductive materials, diffusion is a slow process. The late-stage occurs when the current has moved out an appreciable distance from the transmitter location producing a large region where the vertical magnetic field is not a function of position. This time is a function of transmitter-receiver spacing and is considered to have commenced when $d/r > 10$ where $r = T_x$-R_x spacing. At such late-times, the magnetic field components are simplified to

$$B_r \cong (\mu M/4\pi r^3)(r^4/32t^2)(\mu\sigma)^2$$
$$B_z \cong (\mu M/4\pi r^3)(2r^3/15\pi^{1/2})\frac{(\mu\sigma)^{3/2}}{t^{3/2}} \qquad 4.6$$

where M = transmitter dipole moment. These equations are the basis of TEM sounding (McNeill, 1980). Measurement of either B_r or B_z will allow the determination of σ. B_z is preferred because it is larger, does not depend on r, decreases slowly along it's derivative and offers adequate resolution of small

changes of terrain conductivity. Since measurements are made with a coil, it is the derivatives of B that are of significance as they are what are measured: they are given by (McNeill, 1980) $\frac{\partial B_z}{\partial t} = (\mu M/20\pi^{3/2})\frac{(\mu\sigma)^{3/2}}{t^{5/2}}$ 4.7

Unlike in the case of the isolated conductor, no insulating barrier exists here to contain the currents, they diffuse without limit, and decay as $t^{5/2}$ no longer exponential. Re-arranging by inversion, we have $\rho_a(t) = (\mu/4\pi t)(2\ \mu M/5t\beta_z)^{2/3}$ where $\beta_z = \partial Bz/\partial t$ and ρ_a = apparent resistivity of the ground.

4.3.3 The Layered Earth Model

In a two-layer earth model, it is clear that at sufficiently early time the diffusing current will be situated entirely in the upper layer and measurements of the field components will be diagnostic of that layer. At much later times the currents will be predominantly in the second layer (substratum) and measurements of the magnetic field components will be mostly diagnostic of that layer (McNeill, 1980). At intermediate times, the behaviour of the diffusing currents will be diagnostic of the thickness of the upper-layer. Yungul (1961) and Hoversten and Morrison (1982) have published computational results for the induced electric field inside some two- and three-layered geoelectric sections.

For an n-layered earth (figure 4.3), consider the TEM response measured in the field, that is, the mutual impedance Z between a large circular transmitter (*Tx* of radius *a*) located above the ground surface at z^1 and a smaller concentric receiver (*Rx* of radius *b*) loops. Morrison et al. (1969) have formulated an expression for the electric field over a layered ground from a sine wave source which has been used to produce equations for the layered earth problem with a step source. Among others, Knight and Raiche (1982) have shown that for an $e^{-\iota\omega t}$ excitation (exponential amplitude decay with time) and neglecting displacement currents, the induced electric field in the *Rx* is given by (Knight and Raiche, 1982)

$$E(\omega) = \frac{1}{2}\iota\mu\omega aI\int_0^\infty \left\{A_0(P,\omega,\lambda)e^{s_0(z+z^1)} + B_0(P,\omega,\lambda)e^{-s_0(z-z^1)}\right\}J_1(\lambda a)J_1(\lambda\rho)d\lambda \quad 4.8$$

and in the *jth* layer

$$E(\omega) = \frac{1}{2}\iota\mu\omega aI\int_0^\infty \left\{A_j(P,\omega,\lambda)e^{(s_j z)} + B_j(P,\omega,\lambda)e^{-(s_j z)}\right\}J_1(\lambda a)J_1(\lambda\rho)d\lambda \qquad 4.9$$

where $s_o = \lambda$, $s_j = (\lambda^2 - i\mu\omega\sigma_j)^{1/2}$, $\mu = 4\pi 10^{-7}$, I = *Tx* current,

σ_j = conductivity of layer j, ω = angular frequency

ρ = *Tx-Rx* distance parameter

a = *Tx* loop parameter

P = earth parameter (conductivities and thicknesses)

λ = integration variable for inverse Hankel transform.

$A(P,\omega,\lambda)$ = the layered earth response function (or the earth model kernel)

J_1 = Bessel function of the first kind of order one

For *Tx* and *Rx* location on the ground surface, $z = z^1 = 0$ in equation 4.8.

Since it is the transient or initial value problem that is being investigated, the Laplace rather than the Fourier transform is required. This is applied formally by replacing $-\iota\omega$ with p the Laplace transform variable and choosing A_0 and B_0 to satisfy the appropriate initial boundary conditions. For a step function excitation, we measure Z = V/I in the field and we have for the Laplace's transform of the appropriate quantity (Knight and Raiche, 1982)

$$Z(p) = \pi\mu ab\int_0^\infty A_0(P,p,\lambda)J_1(\lambda a)J_1(\lambda b)d\lambda \qquad 4.10$$

where p = Laplace's transform variable. To calculate the solution in time domain, the inverse Laplace transform (operator L^{-1}) is applied to the above solution noting that the ρ-dependence is now entirely contained in A_0. Applying the inverse Laplace transform operator L^{-1} then, we have for time t > 0

$$Z(t) = \pi\mu ab\int_0^\infty L^{-1}A_0(P,p,\lambda)J_1(\lambda a)J_1(\lambda b)d\lambda \qquad 4.11$$

$A_0(P,\omega,\lambda)$ can be determined by applying the boundary conditions that the tangential components of the electric and magnetic fields must be continuous at each layer boundary, $z=d_j$, *that is,* $E_j=E_{j+1}$, $\partial E_j/\partial z = \partial E_{j+1}/\partial z$

Going back to equation (4.9), the following corresponding relations are obtained

Fig. 4.3 An n-layered earth model

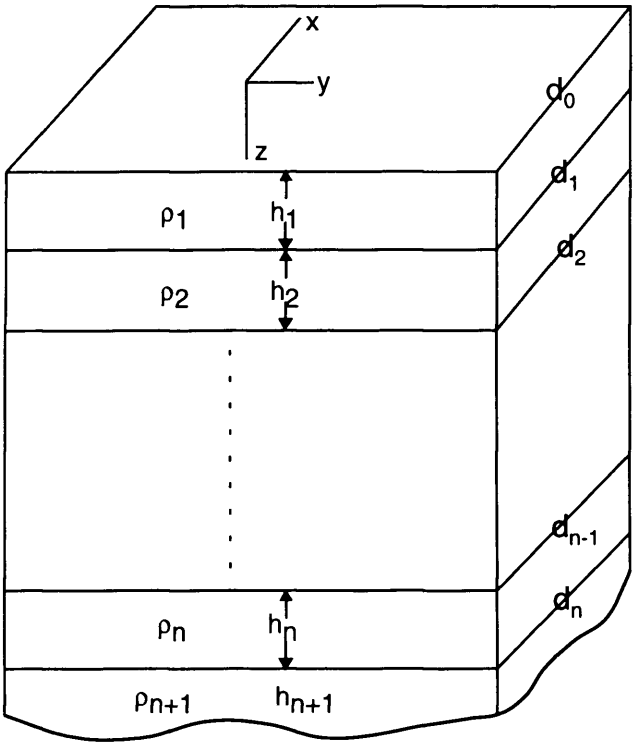

$$A_j e^{s_j d_j} + B_j e^{-s_j d_j} = A_{j+1} e^{s_{j+1} d_j} + B_{j+1} e^{-s_{j+1} d_j}$$

and $$s_j (A_j e^{s_j d_j} - B_j e^{-s_j d_j}) = s_{j+1} (A_{j+1} e^{s_{j+1} d_j} - B_{j+1} e^{-s_{j+1} d_j})$$

At $z = \infty$, the field must tend to zero so that A_{n+1}=0 and B_0=1, A_0 can thus be evaluated recursively.

4.4 Various Effects on TEM

4.4.1 Effects of Conductive Overburden

When a target under a conducting overburden is within a resistive host, there is a smoothening and a delay of the target response which is proportional to the conductivity-thickness product of the overburden and overall dimension of the measuring system. A shielding of the target occurs initially as induced surface currents flow on overburden surface, but the primary field later penetrates the overburden and the target response may be identified. When the target dyke is in contact with the overburden, currents are channelled through the more conducting dyke. Channelling is initially restricted to the upper edge of the dyke but later the

response of the dyke is recognised once the overburden currents have migrated away(Lowrie and West, 1965; Lamontagne, 1975; Lajoie and West, 1976). However, inhomogeneities in the overburden may produce current channels that can be easily confused with those of underlying targets.

4.4.2 IP Effects

IP effect is attributed to electrical polarisation induced by current flow in polarisable materials and might be measurable by an inductive sensor (Nabighian and Macnae, 1991). The polarisation current is usually in the opposite direction (negative) acting to depress the fundamental inductive current which is positive. The amount of distortion can be modelled with polarisable conductivity (Smith and West, 1988). Even when the polarisation current is very small, IP effects may seriously affect the results of conductivity modelling.

4.4.3 Magnetic Permeability variations

Except for some iron-rich minerals, magnetic permeability varies at most by a few percent from that of free space. Local variations on magnetic permeability will cause detectable TEM effects which are commonly mapped by the use of static field magnetometers such as proton precession devices (Nabighian and Macnae, 1991). Where near-surface permeability variations cause for example 600 nT or 1 percent positive anomaly in a background of 60000 nT due to earth's magnetic field, any time varying magnetic field such as the total TEM response would be slightly enhanced by about 1 percent. The enhancement is usually only detected in transmitter on time measurements (Lamontagne, 1975).

4.4.4 Super-paramagnetic Effects

Some practical results (Buselli, 1981) and theoretical work (Lee, 1984) have shown anomalous transient responses characterised by $1/t$ time dependence that lead to incorrect apparent resistivity determinations with time. They are shown to be

caused by near-surface super-paramagnetic materials that have frequency-dependent magnetic permeability. These effects are generally localised to within 3 m of the transmitter loop which has to be in close proximity to the receiver loop and the ground.

4.5 Sources of Error

The errors that affect TEM measurements consist of errors caused by geometric, cultural and electromagnetic noise effects. The geometric errors in terms of primary field noise resulting from transmitter to receiver alignment inaccuracies in FEM measurements (McCracken, 1980) have a negligible direct effect on TEM data since measurements are taken during transmitter off time. For topography, the smoke rings soon behave as if the earth were flat with no residual anomalies left behind. Cultural effects include TEM responses from currents induced in metallic conductors such as power and telephone lines, pipelines, fences, etc. whose time constants of direct induction is usually negligible because of their small cross-section. Symmetrical distribution of transmitter loops over the cultural features ensures little current is channeled into them minimizing their response. Sources of EM noise include geomagnetic signals below 1 Hz and sferics above 1 Hz. Man made noise include power distribution grid (50 and 60 Hz) and high frequency noise of VLF radio stations (10 and 25 kHz). Wind noise is another form of EM noise. TEM systems use a form of synchronous detection and stacking (averaging) to enhance signal to noise ratio.

4.6 Data Processing

TEM data processing involves editing field data, checking for accuracy (repeatability), normalising for transmitter current or calculated primary field and receiver coil moment, and correcting for transmitter turn-off time. Various graphs can then be plotted to aid interpretation. The presentations include transient decay plots of voltage with time, measured voltage response profiles at a selected time

along points of a profile, contours of measured voltage at a selected time at all stations in the survey area, and apparent resistivity plots, profiles or contours.

4.7 Interpretation

TEM data interpretation will usually involve the determination of the location and possible shape of the conducting target from profiles and contours of field measurements at various times, determination of possible conductor quality from it's time constant, and determination of effective subsurface resistivity structure at approximate exploration depths from field apparent resistivity data. 1-D interpretation schemes can be used to retrieve interpretive subsurface models from TEM data in some typical field environments where the gross subsurface structure can be approximated to 1-D. Rigorous 1-D inversion of TEM data is difficult and as such the ability to effect a first-pass interpretation prior to sophisticated inversion is very useful (Meju, 1997). Novel schemes exist for direct or approximate analysis of TEM data (e.g., Nekut, 1987; Eaton and Hohmann, 1989; Fullagar, 1989; Fullagar and Reid, 1992; Smith et al, 1994), but they require considerable numerical skill to implement (Meju, 1997). Simple approximate schemes for EM data analysis have been proposed by Meju (1995, 1996) including the Meju transformation (Meju, 1997).

4.7.1 Meju Transformation

Generally, recorded TEM apparent resistivity data are transformed to an effective subsurface resistivity at an approximate exploration depth yielding an almost continuous picture of the resistivity-depth distribution of the subsurface (Meju, 1995). It has been shown that operationally, an "equivalent phase" curve can be derived from TEM apparent resistivity curve and used to effect resistivity-depth transformation akin to the popular Niblett-Bostick transformation (Niblett and Seyn-Wittgenstein, 1960; Bostick, 1977) for MT data (Meju, 1996). That is for each apparent resistivity datum ρ_a, the effective depth of probe is approximated by

$\delta_{eff}=(3.9\rho_a t/2\pi\mu_0)^{1/2}$ and the effective resistivity is approximated by $\rho_{eff}=\rho_a\{(90/\phi)-1\}$ where t is the transient decay time in seconds, μ_0 is the magnetic permeability of free space and ϕ is the approximate equivalent phase determined from the derivative of the apparent resistivity curve (in logarithmic space). If the equivalent MT period (T in seconds) to the transient decay time is defined as $T=3.9t$ (Meju, 1995, 1997) then

$$\delta_{eff}=(\rho_a T/2\pi\mu_0)^{1/2} \text{ and } \rho_{eff}=\rho_a\frac{\left(1+\frac{\partial \log \rho_a}{\partial \log T}\right)}{\left(1-\frac{\partial \log \rho_a}{\partial \log T}\right)}.$$

The scheme now referred to as Meju transformation, is therefore equivalent to the Niblett-Bostick transformation scheme used in MT data analysis (see Jones, 1983) with the TEM late time definition (Kaufman and Keller, 1983) used and TEM field data adjusted for transmitter turn off effects (Raiche, 1984; Weidelt, 1984) before applying the procedure. Meju (1997) has shown that there is preferential enhancement of resistive and conductive parts using Meju transformation than when using the effective resistivity and depth relationship obtained from "diffusion depth" which are $\rho_{eff}=k\rho_a e^{-(1-\alpha)}$ and $\delta_{eff}=\frac{(2t\rho_a/\mu_0)^{1/2}}{k}$ where α=0.15 and k=2.3. This very similar to work of such people as Sternberg et al. (1988) who equated the frequency domain skin depth $\delta=\sqrt{2/(\mu\sigma\omega)}$ to the time domain skin depth $\delta=1.28\sqrt{t/\mu\sigma}$ to obtain the relationship between MT frequency and TEM transient time as $194/f=t$ where f is in Hz and t in ms and the factor 194 is remarkably close to the factor 200 found based on a comparison of a large number of layered earth model calculations.

CHAPTER 5

DATA ACQUISITION AND PROCESSING

5.1 Introduction

A description of the essential ingredients that were involved in the detailed formulation, planning and execution of the field data acquisition and processing in this study is presented in this chapter. Previous knowledge of the parameters sought and the problems that were encountered trying to acquire such parameters in the past were taken into consideration with a view to selecting electromagnetic methods capable of adequately retrieving the parameters. The specifications of the instrumentations used and the precautionary measures taken in their deployment in the field in order to obtain the best possible data are discussed. The infield processing techniques and further laboratory processing procedures employed on the acquired field data are also presented.

5.2 Survey Design

The current study took into consideration the general depth of occurrence of the known massive sulphide deposits in the area which is known to be from less than 40 m to about 200 m. The resistivity of the massive sulphide mineralisation has been found by the United Nations Development Program (UNDP, 1987) to be between 2 and 5 ohm.m while that of disseminated sulphides was found be as high as 8 to 15 ohm.m. The linkage that has been proposed between the massive sulphide mineralisation and the structural lineaments asociated with the regions spreading development meant trying to map out some of the structures along our traverses especially those within the lavas. The choice of an EM method for this study therefore meant using methods capable of penetrating to the known depths of

the mineralisation and far beyond especially in the light of the fact that more massive mineralisation might be present at greater depths of up to 500 m or more. It also meant the use of a system with enhanced definition of potential ore-bearing structures and one that lends itself to general geological/structural mapping.

The depth of penetration of the MT method is linked to the measurement frequencies and the average conductivity of the subsurface. With a sufficiently large range of frequencies, electrical crystalline basement or sedimentary subsoil of great thicknesses can be explored. To obtain the resistivity distribution across part of north-northeast Troodos to depths of up to 3000 m we used the resistivity information given above and the skin depth formula to get the frequency range required. For resistivity values as low as 2 ohm.m and conservative depths of 100 to 3000 m, a frequency range of 50.6 to 0.056 Hz is required while for resistivity value of 400 ohm.m at conservative depths of 500 to 3000 m, a frequency range of 404.8 to 11.2 Hz will be required.

For practical purposes, the depth of investigation for the TEM method is determined by the time it takes the signal to decay to the noise level, the source moment and the average resistivity of subsurface earth material. The minimum depth at which individual conductivity variations can be resolved by the TEM method is determined by the earliest sampling time of the measuring system and can be calculated from (see Spies, 1989)

$$d \approx \sqrt{\frac{2t}{\sigma\mu_0}}$$

where t is the sampling time, σ is the conductivity and μ_0 is the magnetic permeability of free space. Using the earliest sampling time of 50 μs found in many systems, the shallowest depth that can be mapped will be about 13 m for a resistivity of 2 ohm.m for the overlying section and about 178 m for an overlying

section resistivity of 400 ohm.m. The maximum depth d of investigation is given as (Spies,1989)

$$d \approx 40\left(\frac{IA}{\sigma}\right)^{1/5}$$

for typical noise level of 0.5 nV/m^2 where I is transmitted current and A is the area of loop. For the same resistivity conditions as above using typical 100 m loop configuration and 3.5 Amp current (from practical field experience with available loop wire), depths of up to 372 m (for 2 ohm.m overlying section) and 1075 m (for 400 ohm.m overlying section) can be mapped. The ability of the TEM method to explore shallower depths than the MT method of exploration makes it a good complementary method to the MT for filling in the shallow depth information that would otherwise not be available to the MT. In addition, the TEM data is used for the correction of statically shifted MT data. It has also been shown that the time domain EM is well suited for mineral investigations because of high magnetic moments and sensitivities compared to the frequency domain EM (FEM). TEM does not require the relative receiver-transmitter alignment accuracies that FEM require for comparative results and has the ability to measure small signals in the absence of large primary fields (McNeill, 1980).

5.3 Site Selection

The Troodos massif is a mountain range with a fairly rugged topography and restricted intervening flat lying areas. MT method of exploration requires setting up in open flat lying areas far removed from all sources of noise and distortion. Although it is rarely possible to find an ideal site, effort was made to find accessible flat or nearly flat lying sites as far away as possible from major topographic features. The sites were sometimes within farmlands or wooded areas, beside roads or across minor roads and tracks. Knowing that site selection is the first step to

acquiring high quality data, populated areas were avoided as much as possible. Even in remote rural areas one kept away from high voltage transmission lines, surface and underground metal pipes, metal fences, telephone lines and other sources of spurious electromagnetic energy. The TEM sites were mostly located on the chosen MT stations.

5.4 Instrumentation

5.4.1 MT Instrumentation

The Short Period Automatic Magnetotelluric (SPAM) MkII real-time data acquisition and analysis system developed in Edingburgh by Dawes (1984) was used. The system has a frequency range of 0.016-128 Hz divided into four overlapping bands to prevent channel saturation by large amplitude signals and obliteration of weak signals by background noise, which was considered adequate. The system is portable, battery operated, records data digitally on cartridge tapes/diskettes and incorporates full tensorial analysis and one dimensional inversion to resistivity as a function of depth.

The SPAM MkII MT system basically consists of the signal detecting part (magnetic and electric sensors) and the data recording part. The signal detecting part is made up essentially of three magnetic sensors for measuring the three orthogonal magnetic fields and two orthogonal electric sensors. The magnetic sensors used in the study were a set of three ECA EM11 induction coils that are simply multiturn fine copper wound on a core of high magnetic permeability and preamplifier with low noise connections and components all wrapped up in a waterproof casing. They have a sensitivity of 50nV/γ. The electric sensors were made up of two pairs of copper-copper sulphate porous pots connected by 50 or 25 m cable aligned in two orthogonal directions with one being parallel to regional

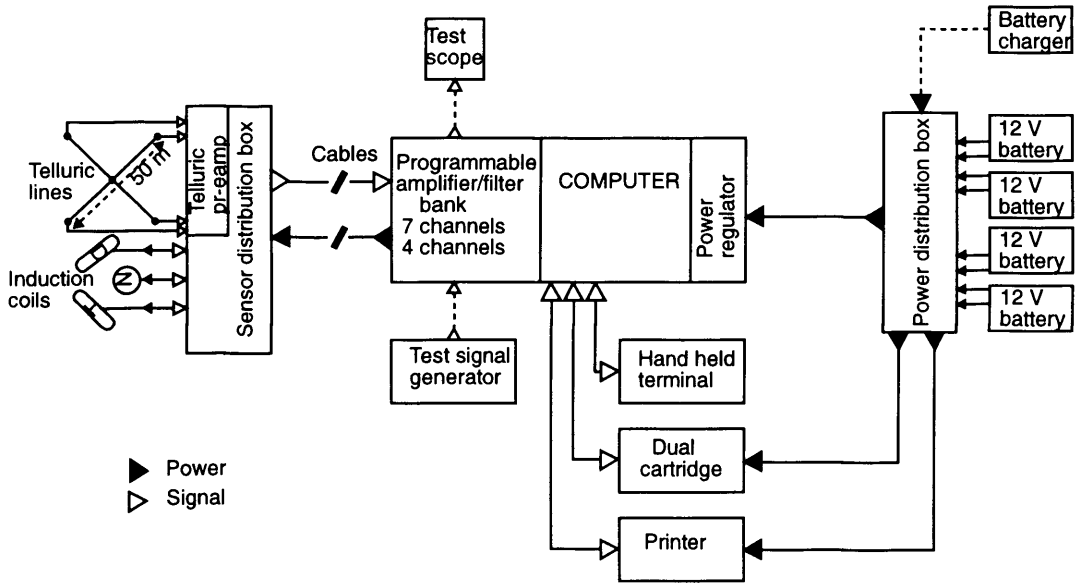

Fig. 5.1 Block diagram of the complete in-field MT System (after Dawes, 1984)

geologic strike. Two versions of the data recording system (MkIIa and IIb) were used and in general each can be further divided into six units (fig. 5.1) (i) a microcomputer, a programmable amplifier/ filter bank and a power regulator, (ii) twin cartridge/diskettes (programs and data) storage deck, (iii) alpha-numeric pocket VDU and keyboard, (iv) 40 column miniature electrosensitive printer for listing and plotting results, (v) sensor distribution box and, (vi) a power distribution box. Hutton et al (1984) has given a detailed description of the SPAM Mk II system. The computer first reads off the program tape and writes necessary information in the other tape/diskette. The main program facilities include: software band selection, instrument response corrections, automatic gain adjustment and signal selection with manual override, alteration of signal selection criteria and continuous or switchable display of results (which can be listed on the printer and/or stored on tape).

The recording system has seven signal channels for recording signals from the two electrode pairs and three magnetic coils. The extra two channels are

available for two horizontally orthogonal electrode pairs at a remote station. Each channel has switchable 50 and 150 Hz notch filters to eliminate noise from power transmission lines. The signal from each electrode pair is sent to a telluric preamplifier in the sensor distribution box, while the signals from the induction coils are brought to the sensor distribution box all through cables. The signals then go to the multiplexer-analogue to digital converter (ADC) unit through the amplifier/filter bank, where the channels are sequentially sampled and digitized. The sampling

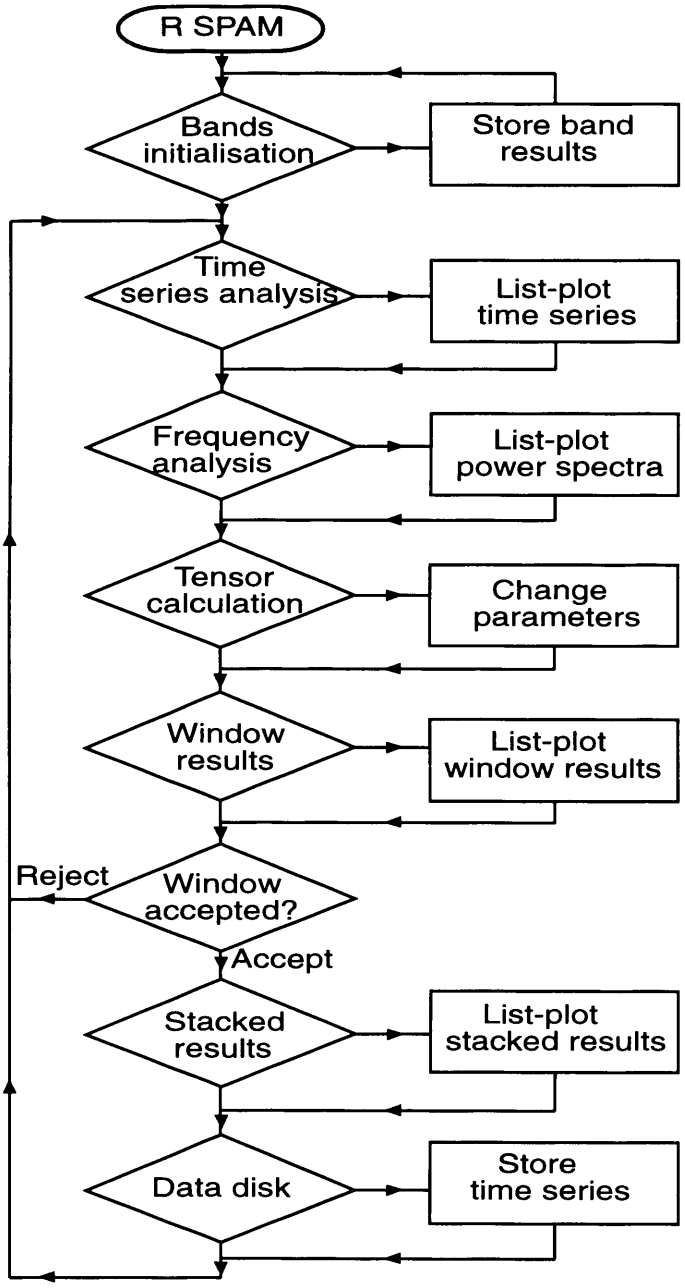

Fig. 5.2 Simplified SPAM II main analysis program flowchart

frequency is different for each frequency band, and each data set which is called an 'event' or 'window' consists of 256 samples for each of the seven channels. The data window is then passed in real-time into the computer memory for infield analysis and stored after satisfying certain preset criteria. Depending on data quality, between 24 and 30 data windows are considered adequate for any frequency band. Fig. 5.2 shows a simplified infield flowchart.

5.4.2 TEM Instrumentation

The SIROTEM Mk II SE Transient electromagnetic system developed in Australia by CSIRO (Buselli and O'Neill, 1977) was used in this study. The system is capable of discretely sampling the decaying voltage that is induced by decaying target secondary magnetic fields at specified times across a recording time span of 0.049-161 msec after pulse termination. This time span is divided into two overlapping time-bases known as 'early' and 'standard' times and was considered adequate for this study. Each of the time-bases is divided into 32 delay-time windows or channels (Table 5.1) with varying time channel widths which are contiguous in order that the maximum signal to noise ratio may be extracted from each transient (Buselli and O'Neill, 1977). The channels run on a quasi-log scale for early time and an approximately linear scale for standard time, and as the time gates for each channel suggest, the higher density early time channels give better resolution where the time-bases overlap (Table 5.1). The respective mean channel time resolutions for early and standard times are given as 0.049 and 0.161 msec, and sensitivities as less than 12 nV and less than 6 nV (Buselli et al, 1985). The transmitter frequency is proportional to the total number of channels required to record the transient down to noise level for each time-base, but is in the range of 1.4-250 Hz.

Table. 5.1 TEM (SIROTEM) delay time windows (After Buselli et al, 1985)

SIROTEM MkII Channel Times

"Early Time" Window			"Standard Time" Window		
Channel	Start (msec)	End (msec)	Channel	Start (msec)	End (msec)
01	0.025	0.074			
02	0.074	0.123			
03	0.123	0.172			
04	0.172	0.221			
05	0.221	0.278			
06	0.278	0.368			
07	0.368	0.466			
08	0.466	0.564	01	0.315	0.659
09	0.564	0.662	02	0.707	1.051
10	0.662	0.760	03	1.099	1.443
11	0.760	0.956	04	1.491	1.835
12	0.956	1.152	05	1.883	2.227
13	1.152	1.348	06	2.275	3.011
14	1.348	1.544	07	3.059	3.795
15	1.544	1.740	08	3.843	4.579
16	1.740	2.132	09	4.627	5.363
17	2.132	2.524	10	5.411	6.147
18	2.524	2.916	11	6.195	7.715
19	2.916	3.308	12	7.763	9.283
20	3.308	3.700	13	9.331	10.851
21	3.700	4.484	14	10.899	12.419
22	4.484	5.268	15	12.467	13.987
23	5.268	6.052	16	14.035	17.123
24	6.052	6.836	17	17.171	20.259
25	6.836	7.628	18	20.307	23.395
26	7.628	9.188	19	23.443	26.531
27	9.188	10.756	20	26.579	29.667
28	10.756	12.324	21	29.715	35.939
29	12.324	13.892	22	35.987	42.211
30	13.892	15.460			
31	15.460	18.596			
32	18.596	21.732			

The SIROTEM Mk II SE system consists of transmitter and receiver components housed in the same unit, two twelve volt batteries, an available central receiver box, external transmitter synchronisation and dual time-base facilities powered by a SATX-1 high power transmitter for certain configurations are also available with the necessary connecting cables and loop wire. The transmitter sends a pulse in the form of a discrete, bipolar, square wave current into a wire loop (fig. 5.3) which rises exponentially to produce a constant current before it goes down linearly after turn off producing a ramp. The excitation pulse repeats with an off-time equal to the on-time for optimum rejection of power line frequency which is 50 Hz in Cyprus. The maximum transmitter current is a function of the loop wire resistance and is rated at 10 amps for the Mk II SE, and 20 amps for the SATX-1. Voltage decays are stacked up by an internal microprocessor which normalises them with the mean current amplitude. Stacking n records means that the signal to noise ratio is improved according to $1/n^{1/2}$ and in practice the number of stacks

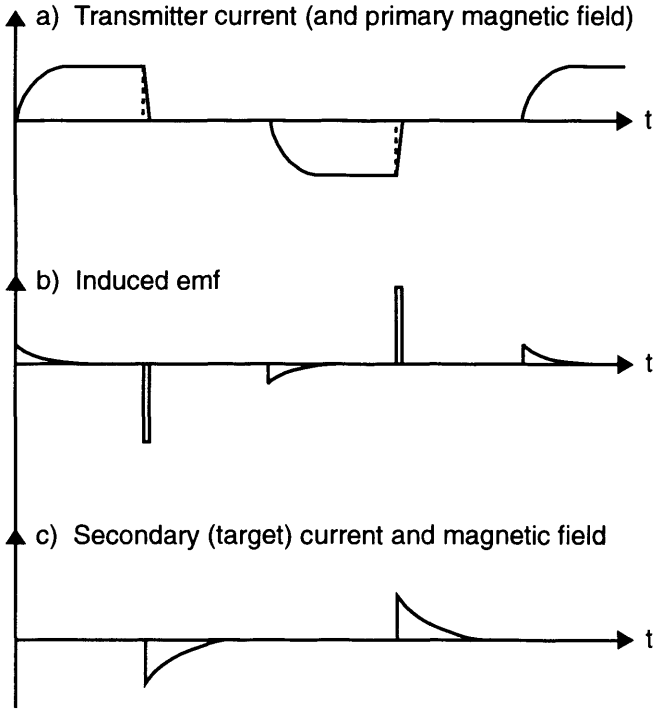

Fig. 5.3 System (bipolar) waveforms

varies as a multiple of 2 between 256 and 2048. Additional facilities include a gain function for three decade expansion of system dynamic range, sferics rejection facility set for precaution against bias from lightning effect, and a printer. The system output is printed on paper and recorded on magnetic tape which is downloaded unto a computer. Fig. 5.4 is a simplified block diagram of SIROTEM.

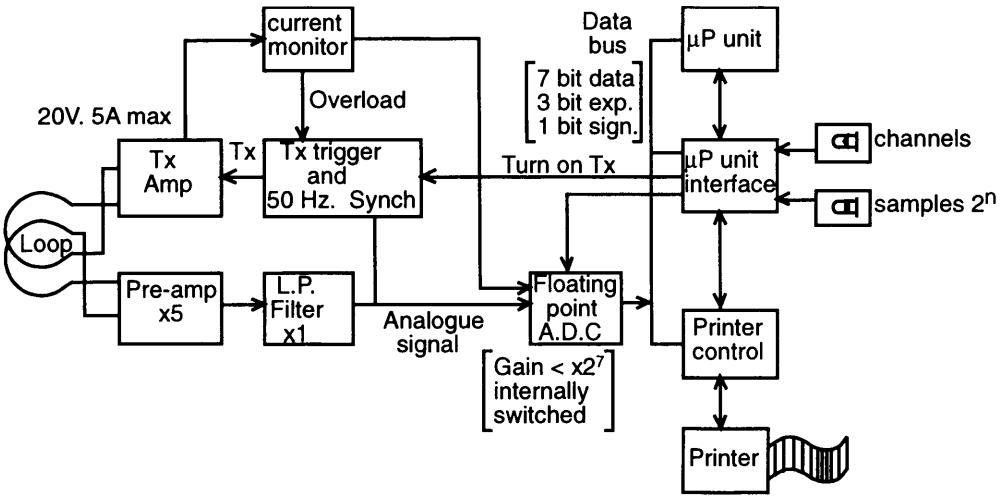

Fig. 5.4 Simplified block diagram of SIROTEM (after Buselli and O'Neill, 1977)

5.5 Site Layout

5.5.1 MT Site Layout

Two sites (main and remote) were sounded simultaneously for efficiency (see fig.5.5). The main site had both telluric and magnetic sensors alligned in two orthogonal directions (N-S and E-W with the N-S bit perpendicular to the main E-W structural trend) and centred on the sounding station. The telluric sensors consisted of two 25 or 50m electric wires grounded via porous pots for maximum ground contact. The two horizontal induction coils were laid in shallow trenches (to eliminate the effect of wind vibration on the system) also in the N-S and E-W directions. The vertical coil was placed in a deep hole again to eliminate the effect

Fig. 5.5 Magnetotelluric survey site setup

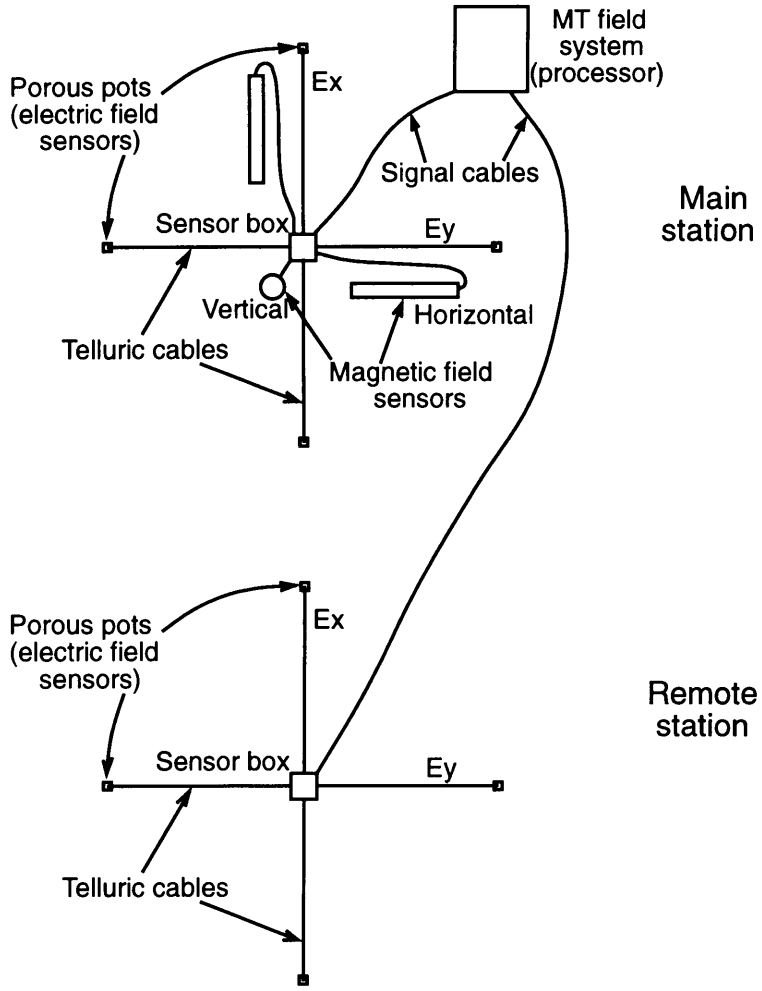

of wind vibration on the system. As a precaution, the same coil is used for the same magnetic element throughout the field campaign. Both the telluric and magnetic sensors were then connected to a sensor box situated over the sounding location. The remote site consisted only of telluric sensors in the two orthogonal directions firmly grounded through porous pots and connected to a sensor distribution box at the centre. Contact resistance between an electrode pair should not exceed 5k Ω (between 2 and 5k Ω).

With the above setup, the five components of the vector electromagnetic field required for the solution of the general equation (3.23) were measured. The three magnetic field components of adjacent main sites were used for remote sites where only the electric field components were acquired. To ensure the maximisation of the signal to noise ratio across the frequency band used for recording, dipole holes were prepared in good time to allow for stabilisation and porous pots buried and covered to provide insulation and minimise temperature related drift. Dipole wires and all connecting cables were weighed down to minimise the noise that results from wind caused movement of conductors in the earths magnetic field. The magnetic coil sensor sites were selected so as to minimise ground motion as much as possible, for example, they were away from large tree roots which transmit low frequency wind-induced motions to their surrounding ground. The coils were also partially buried and covered in shallow trenches or otherwise protected from wind effect.

5.5.2 TEM Site Layout

The TEM soundings utilised nearly square ungrounded wire loops as transmitter with side lengths of 50 or 100 m. Two configurations were used (fig.5.6) namely:

1) Coincident transmitter-receiver loop method: This configuration utilises a single loop both as transmitter and receiver (figure 5.6a). The loop acts as transmitter while current is in the loop and as receiver once the current is switched off.

2) Central loop (or in-loop) method: In this method, a dipole multiturn receiver is located at the centre of the transmitter loop (figure 5.6b).

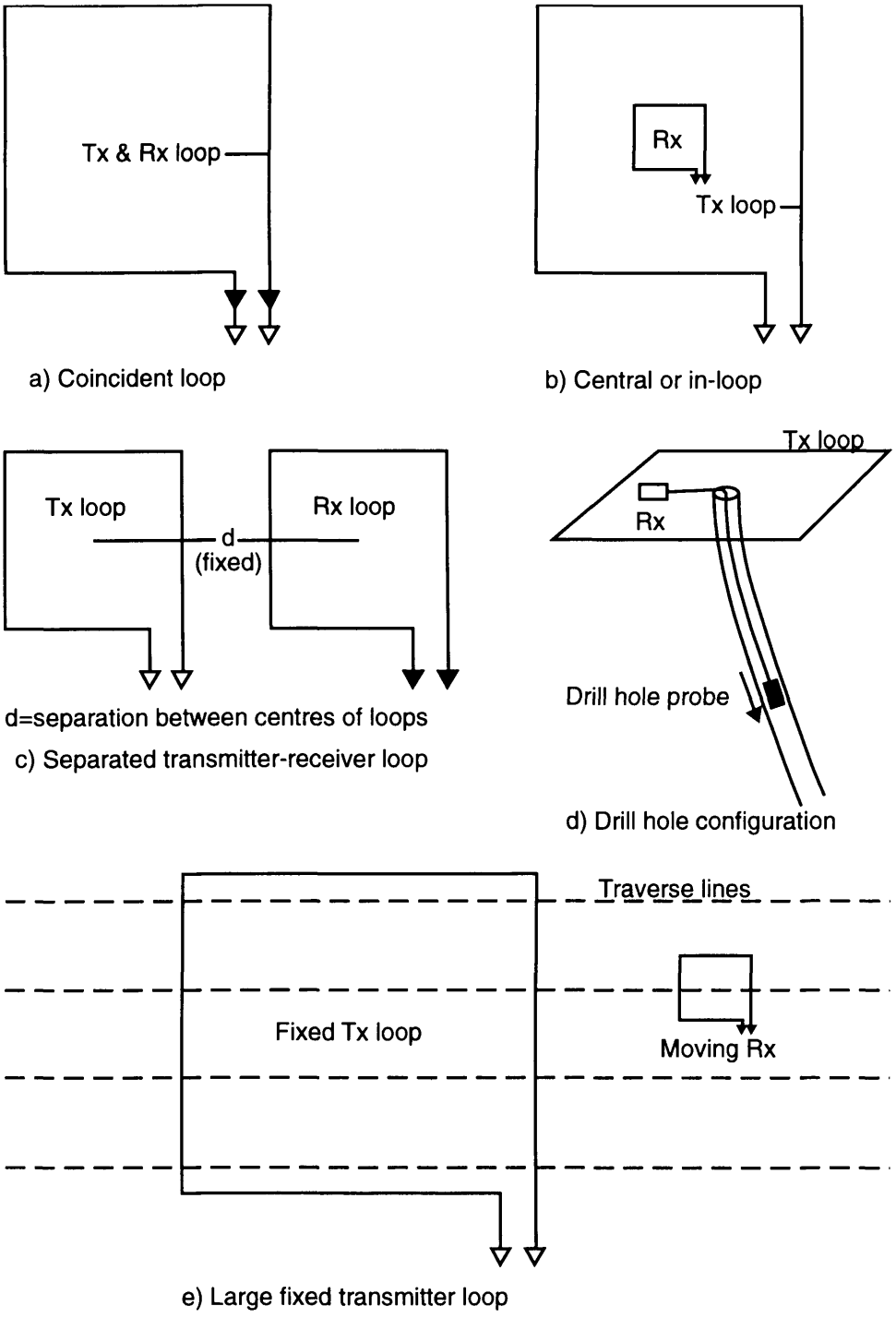

Fig. 5.6 TEM Loop Configurations

5.6 Field Measurements

5.6.1 MT Surveys

Two field trips were undertaken during the summers of 1994 and 1995 during which a total of 70 MT sounding measurements were performed. Although

the main area of study is the Ayia Marina prospect, it was deemed instructive to deploy the TEM/MT systems to the known mineralised area near Klirou. Consequently, 37 soundings were performed in the Ayia Marina area while 33 were undertaken in the Klirou area. Field MT data were acquired from one major N-S line and two minor ones in the Ayia Marina area using a station spacing of 100 m and more, and from a star shaped grid in the Klirou area using a station spacing of 25m for dense sampling (fig.5.7 and 5.8). 400m long N-S, E-W, NE-SW and NW-SE grid lines were pegged out near a borehole for control and measurements made along them. A station spacing of 100 m was employed in the gridded area around Ayia Marina increasing gradually to 4 or 5 km at the farthest station from Ayia Marina. The station spacing at Klirou area was between 25 and 50 m along 4 star shaped grid lines. The SPAM system was first calibrated at the beginning of every field campaign using a frequency analyser. The frequency analyser has an internal signal generator that produces the instruments response functions for a range of frequencies. Only data which satisfy certain preset coherency and signal to noise ratio criteria were accepted by the measuring instrument.

Once recording had started, data quality was monitored continuously by examining the electric and magnetic field data. The computed MT response functions were also checked and monitored as they were printed on paper. The recording and processing parameters were modified where necessary to obtain the highest quality of data possible from the site. The in-built in-field data processing capability enabled preliminary interpretation as survey progressed. This allowed the adaptation of the field survey by making necessary modifications to the recording parameters and/or survey geometry and number and distribution of sites as the interpretation unfolded.

Fig. 5.7 Ayia Marina measurement grid showing representative sounding sites for clarity

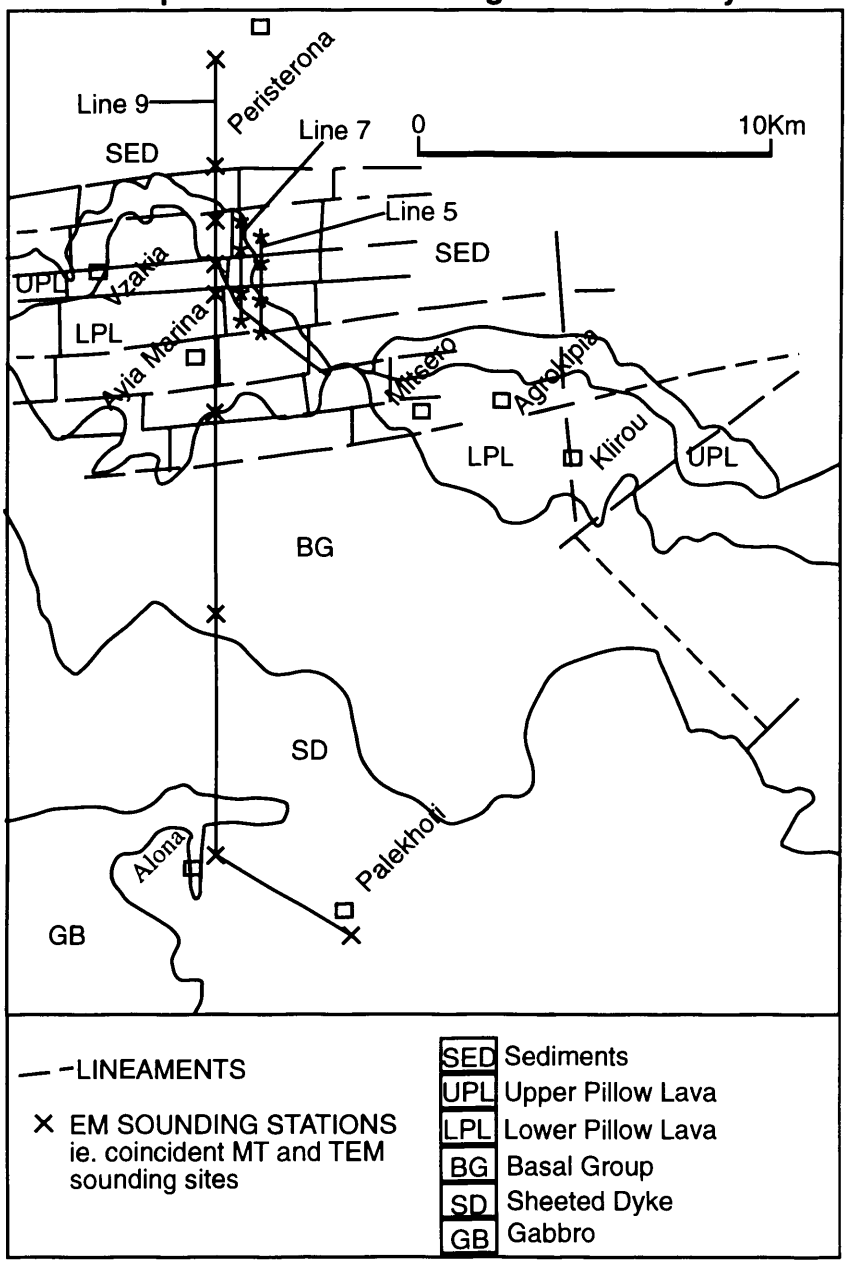

5.6.2 TEM Surveys

TEM measurements were made during the two field campaigns mentioned at all the MT sites at Ayia Marina and Klirou, and more. A total 68 sites were occupied at Ayia Marina on which central and coincident loop measurements were made using 100 m × 100 m loop size. At Klirou, 48 soundings mostly employing the central loop configuration were undertaken using 50 m × 50 m loop size. At Ayia Marina the station spacing was equal to the loop size while at Klirou the station

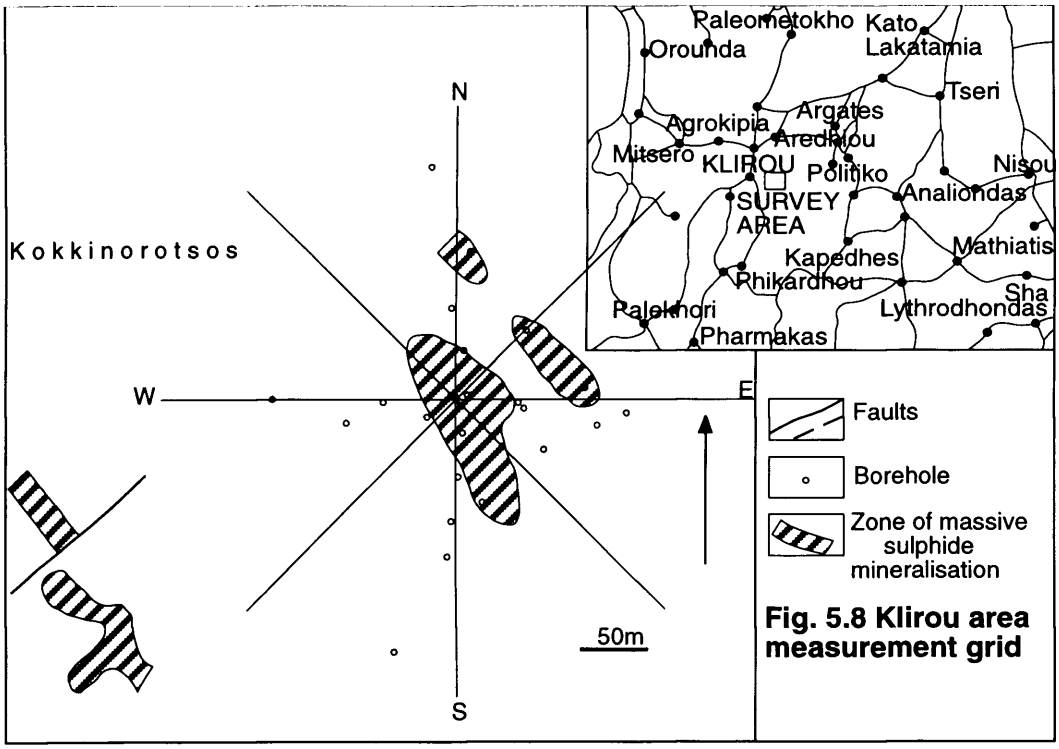

Fig. 5.8 Klirou area measurement grid

spacing was half the loop size on the N-S and E-W lines but equal to the loop size on the other two lines. The wires of the transmitting loop, the cable of the central receiver box and the cables that connect the loop to the transmitter box were all weighted down especially near the transmitter and receiver boxes to minimise the effect of the wind. The transmitter box was always offset from the transmitting loop by a 1 to 2 m long connecting cable.

5.7 Environmental Concern

Perhaps one of the great appeals of the use of MT and TEM in many frontier areas is the minimum environmental impact when compared with seismic operations. In most areas site preparation was usually straight forward involving little or no impact at all on the environment. The very shallow MT dipole ground holes and magnetic coil location pits were very easily filled and graded such that they were frequently very difficult to locate a few days after data acquisition for siting

TEM measurements. The cable runs were routed to avoid disturbing vegetation and the recording instrument shelters were positioned at a minimum impact site.

5.8 Data Processing

5.8.1 MT Data Processing

Detailed data processing techniques used prior to the extraction of the apparent resistivity tensor and associated frequency domain functions from the measured fluctuations of the natural electric and magnetic fields are given in Appendix 1. The extracted apparent resistivities were then plotted against frequency on a log-log scale. Most of the curves showed static effects as manifested by the near parallel separation of the two resistivity curves for two polarisations. The complementary central loop TEM apparent resistivity measurements from each MT site was used to shift either one or the two curves to the levels determined by the TEM data as proposed by Sternberg et al (1988) and Pellerin and Hohman (1990).

5.8.2 TEM Data Processing

TEM transient voltage data were checked in the field for accuracy (repeatability). They were then normalised with respect to transmitter current in instrument and the transmitter turn-off time corrected for (Raiche, 1984) before selected channels were then plotted to establish local noise level and identify erroneous soundings. The voltage output was then converted to apparent resistivity-frequency domain and to apparent resistivity-depth domain via the algorithm by Meju (1992a, 1995). This afforded a quick qualitative view of the gross structure and allowed some interpretation of the geoelectric section at the sounding location.

CHAPTER SIX
ONE DIMENSIONAL DATA INTERPRETATION

6.1 Introduction

One dimensional forward modelling and inversion is best suited for horizontally stratified environments which the Troodos ophiolite is certainly not. However, it has been shown that representative one dimensional sections can be recovered from complex environments like the Troodos using simple, effective one dimensional transformation schemes. In this chapter, the basic principles of one dimensional forward modelling and inversion of MT and TEM data are given along with the procedure employed in the correction of static shift in MT data. The one dimensional program used and the resulting interpretive geoelectric sections for the areas of study are discussed. The geoelectric sections are compared with borehole geological sections and IP data to assess their usefulness.

6.2 Forward Modelling

One dimensional modelling and interpretation of MT and TEM field data traditionally involves comparing MT apparent resistivity curves with theoretical master curves (Cagniard, 1953; Yungul, 1961; Wait, 1962; Srivastava, 1967; Anderson, 1982; Sandberg, 1988) generated by the application of equation (3.25) based on the assumption of a horizontally homogeneous model with one dimensional resistivity distribution. In this case we are given a set of parameters (here the number of layers and their resistivities and thicknesses) and a theoretical relationship is used to derive the values of some measurable quantities (here apparent resistivities and phases). This constitutes the forward model (Meju, 1994c). Forward modelling by interactive computing is a more versatile extension of the original curve matching technique. The theoretical curves generated for an initial model are displayed together with the field curves on an interactive terminal.

The model parameters are adjusted and the operations repeated until an acceptable visual fit between the measured field and theoretical curves is obtained.

6.3 One Dimensional Inversion

The inverse problem is a procedure in which the conductivity structure of an area is directly derived from the measured data - given some information on the values of some measured quantities (in this case the field data), a theoretical relationship is used to derive the values of a set of parameters that best explains the field observations.

The problem of retrieving a subsurface resistivity distribution from MT data is that it is a nonunique and nonlinear process. It is nonunique in the sense that an infinite number of completely different resistivity structures exist that satisfy a finite collection of MT data (Meju, 1988; Meju, 1992). Additional sources of nonuniqueness in the inversion of MT data include errors from the data themselves, the bias effects due to lateral variations in the earth's resistivity structure and cultural noise, the limited bandwidth of observations, and the fact that electromagnetic sounding data cannot resolve sharp boundaries or thin layers clearly (since the real earth structure is "smeared out" as the propagating energy becomes diffused) (Meju, 1988). Different methods of MT inversion now exist with the commonest technique being the layered earth (or parametric) inversion in which a succession of layer resistivities and thicknesses that explain or reproduce the observations is sought (eg. Wu, 1968; Nabetani and Rankin, 1969; Laird and Bostick, 1970; Jupp and Vozoff, 1975; Jones and Hutton, 1979; Larsen, 1981; Meju, 1992). A reasonable initial guess model to the resistivity strucrure is required in this method if the algorithm is to converge rapidly. Parker (1980) and Parker and Whaler (1981) have all developed schemes that do not require initial guess models while Parker (1970, 1977), Oldenburg (1979), Hobbs (1982) and others have developed inversion schemes that produce a resistivity structure that is a continuous function of depth. Techniques for obtaining a continuous resistivity function that

approximately reproduces the data have been developed by Niblett and Sayn-Wittgenstein (1960), Becher and Sharpe (1969) and Bostick (1977), for MT data and Meju (1995, 1997) for TEM data.

It is obvious that no single model will be expected to satisfy the recorded data uniquely in the absence of a priori information taking cognisance of the nature of MT data. Attempts have been made at partial remediation of this problem by the random search or Monte Carlo method (e.g., Jones and Hutton, 1979) and linear (Backus-Gilbert, 1968) methods. However the Monte Carlo method consumes too much computing time and the random search is never exhaustive. The problem of the Backus-Gilbert method is that the unique averages do not illuminate the true variability of model space (Oldenburg,1983) and the "averaged parameters" may not have physical significance (e.g., Jackson, 1979). Oldenberg et al (1984) have suggested the use of a variety of interpretation algorithms to explore the range of acceptable models as a means of appraising the nonuniqueness problem. Constable et al (1987) developed an algorithm for generating smooth models which do not have the sharp discontinuities that are typical of conventional least squares inversion. The preceding shows that there is no unequivocal method as yet for resolving nonuniqeness in MT inversion. One way of minimising the problem is to jointly invert TEM and MT data.

An effective program MTEMINV (Meju, 1992) for inverting resistivity data by ridge regression was used in this study for inverting the MT and TEM data. Meju (1992, 1996) has applied the program to MT and TEM data and has demonstrated its effectiveness and general applicability to inverting geoelectrical sounding data for subsurface resistivity structure. The inversion procedure uses a line search in a two stage least squares minimisation process resulting in a stable and rapidly converging algorithm. However, before rigorous inversion, it is instructive to carry out a first pass interpretation using the Bostick (1977) - Meju (1995, 1997) transformations.

6.3.1 Simple Depth Imaging of TEM-MT data

The one dimensional geoelectric sections along the N-S and E-W grid lines in Klirou area (earlier shown in fig.5.8) derived from above are discussed. Only the central loop TEM data measured along these lines are used because they are less sensitive to lateral variations than other TEM configurations and therefore best

Fig. 6.1 TEM early channels profiles

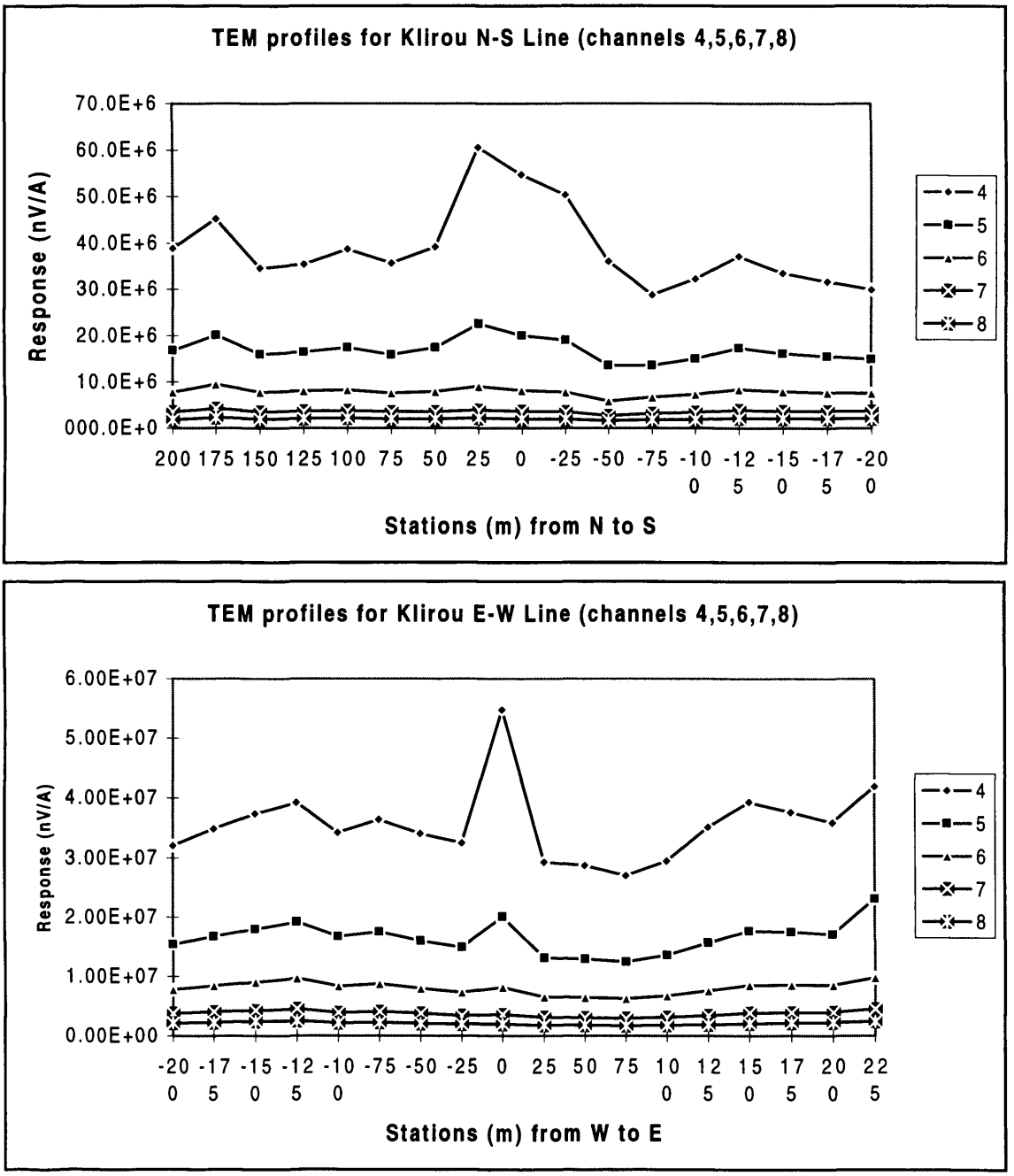

suited for MT static shift correction (Pellerin and Hohmann, 1990), and they measure the maximum field which is usually concentrated at the centre of the loop. For a first pass interpretation, useable TEM early time voltage decay data commonly available at all stations were plotted in the form of profiles. These revealed an anomaly centred on the point of intersection between the two grid lines which coincides with the position of the block faulted and upthrust, altered and conductive LPL rock that hosts the massive ore body (fig.6.1). The transformed apparent

Fig. 6.2 TEM Resistivity-Depth sections for Klirou survey site

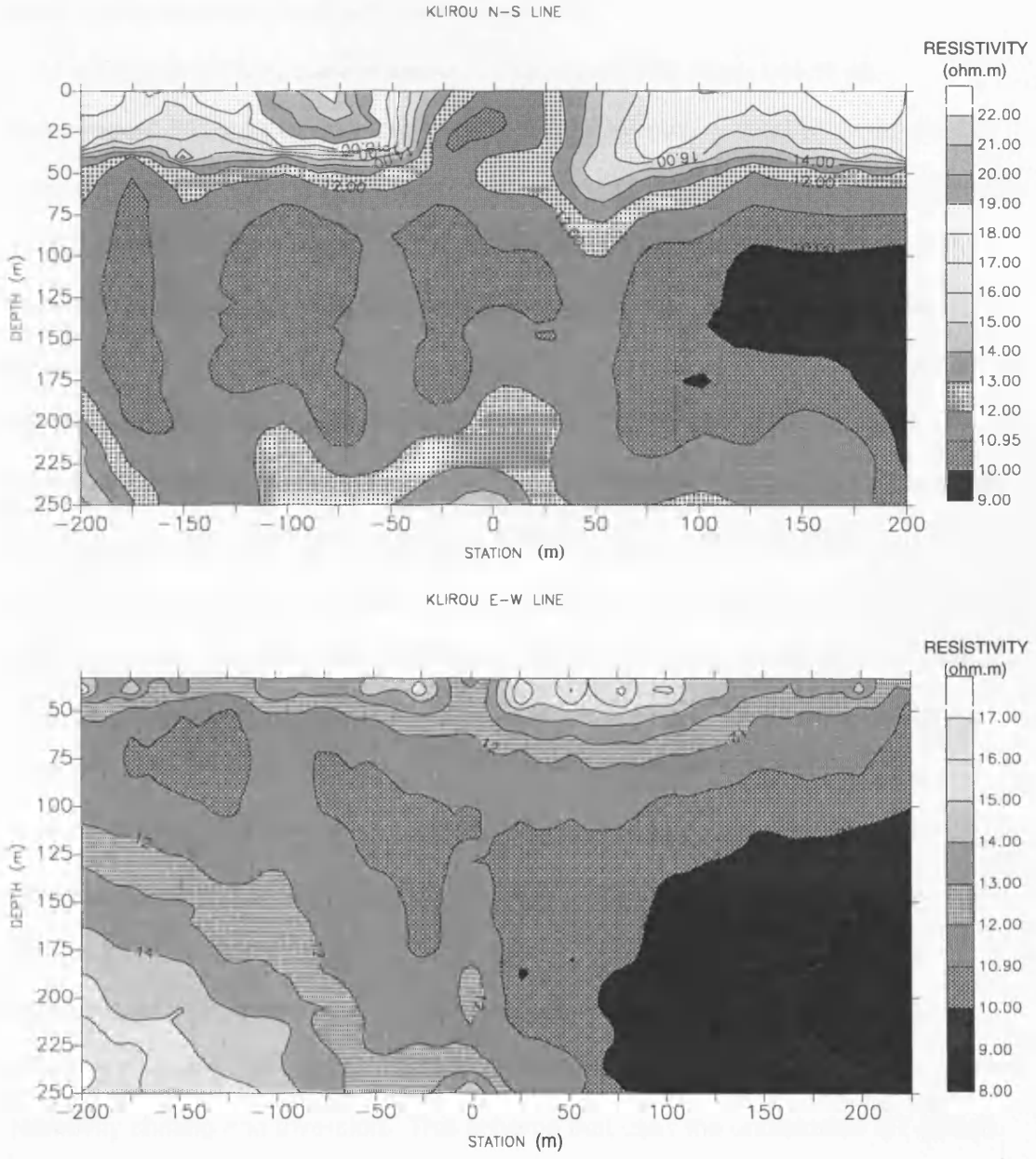

resistivity data from TEM voltage decay curves were then depth converted (Meju, 1992, 1995) yielding data which were plotted as resistivity-depth sections (fig.6.2). Notice the areas of resistivity less than 11ohm-m in the sections. The one ohm.m contour used here was found convenient and does not suggest any level of accuracy of the system employed. These resistivity data were used first to correct the MT data for static shift and then to jointly invert the two data sets to produce the geoelectric model of the subsurface beneath the observational stations.

6.3.2 Joint Inversion for Static Shift remediation

Following the recommendation by Larsen (1977) of the use of an independent EM surface data provided by a complementary induction method that uses only magnetic fields to correct for galvanic distortions in MT apparent resistivity sounding curves, Stenberg et al (1988), Pellerin and Hohman (1990) and others have all shown that the TEM data are well suited for that. This approach was used in the current study where the MT apparent resistivity curves were first shifted along the log apparent resistivity scale to the level of the coincident TEM apparent resisitivty curves mostly where they overlap, and then the two data sets were jointly inverted. The joint MT/TEM inversion scheme by Meju (1996) which is based on Meju (1992) was used to perform these operations. Meju (1996) also showed that the joint inversion of MT-phase and TEM apparent resistivity data is a more versatile extension of the previous work on TEM-based analysis of distorted MT sounding data. In this joint inversion option, no corrections to the distorted MT apparent resistivity curves are necessary. Importantly, no overlap between the MT and TEM data sets is essential for recovering a reliable subsurface resistivity structure, which implies that a simple inexpensive TEM system may be deployed as a logical compliment to MT in routine surveys. This scheme could be regarded as a cost-effective one-stage alternative to the dual-stage interpretational process of apparent resistivity shifting and inversion. This scheme that uses the undistorted MT-phase

and TEM resistivity data was also used in this study and found to be equally effective.

6.4 1-D Models for Klirou site

The Troodos Ophiolite complex can at the least only be described to have the characteristics of a two dimensional environment and would therefore require a minimum of two dimensional forward modelling or inversion to describe its structure. However, workers have shown from two dimensional and three dimensional modelling studies that representative one dimensional sections can be recovered from complex geological environments (Tikhonov and Berdichevsky, 1966; Berdichevsky and Dmitriev, 1976; Raganayaki, 1984; Meju, 1996). Sternberg et al. (1988) has shown that after correction for static shift caused by shallow 2D and 3D inhomogeneities, a 1D inversion is often adequate to represent the resistivity structure. Meju (1996) has indeed shown that the simple data transformation expression developed in his scheme (section 3.8.1) though best suited for horizontally stratified geological environments, provide reliable depth estimates even in multidimensional geological regions. Examples of resulting models for the Klirou area along two N-S and E-W lines (see fig.5.8) are shown in Fig.6.3. Note that in each figure the simple data transformation result and the interpreted 1-D model are shown on the right hand plot and the field data and the response of the constructed model are plotted together on the left hand for comparison. Because the MT TM-mode is more sensitive to surficial and structural changes of the subsurface (Sternberg et al., 1988), only the TM-mode data along with the TEM data were used in this 1D inversion.

Fig. 6.3 1-D model fits for some stations on Klirou N-S and E-W lines. Squares are TEM and crosses MT TM-mode resistivity curves.

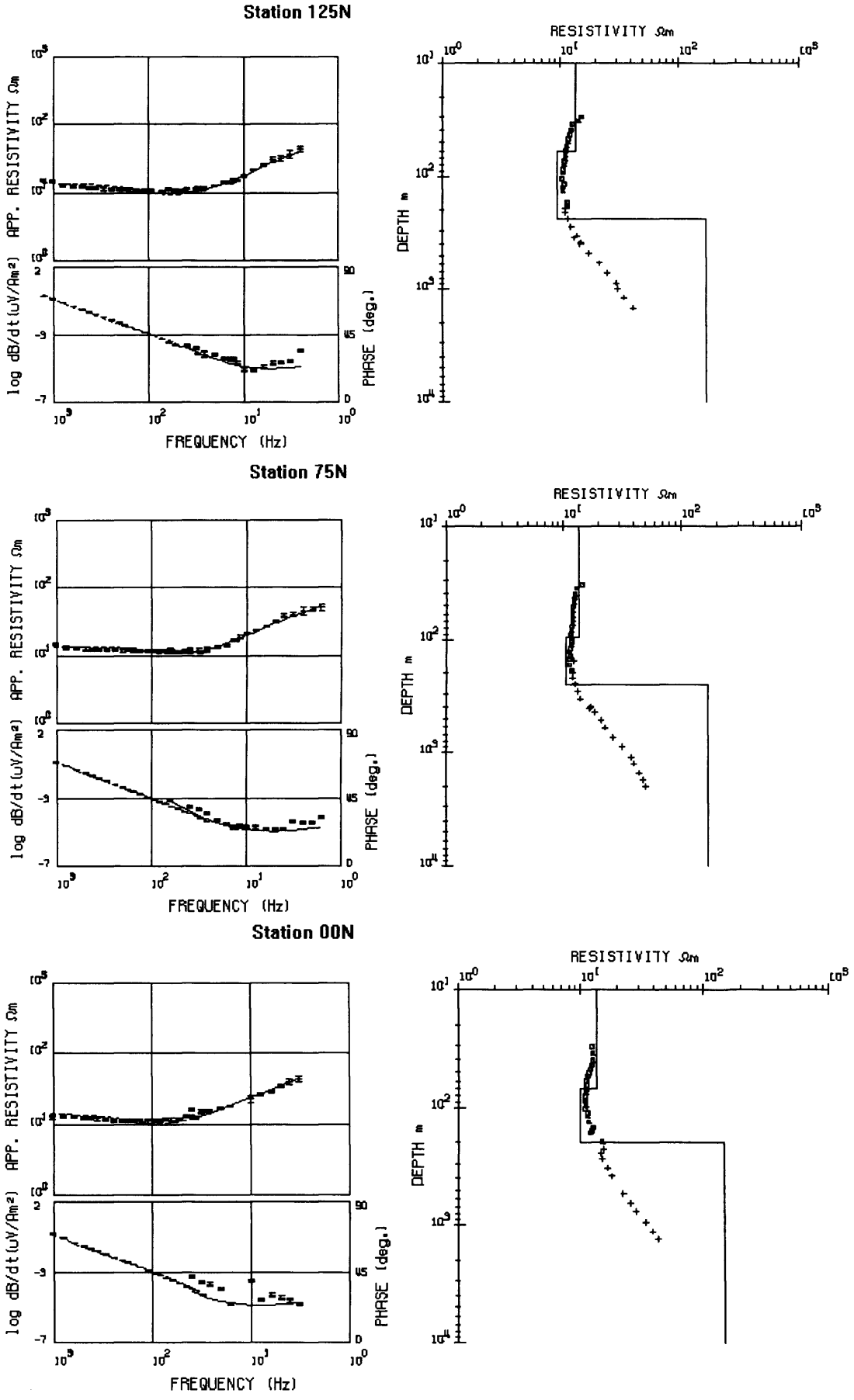

Station 75S

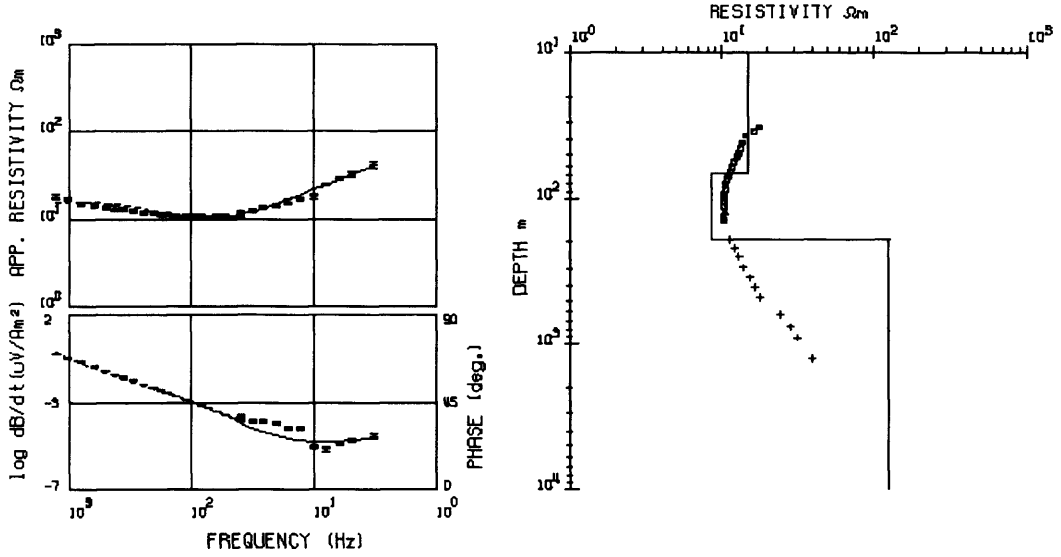

Station 175S

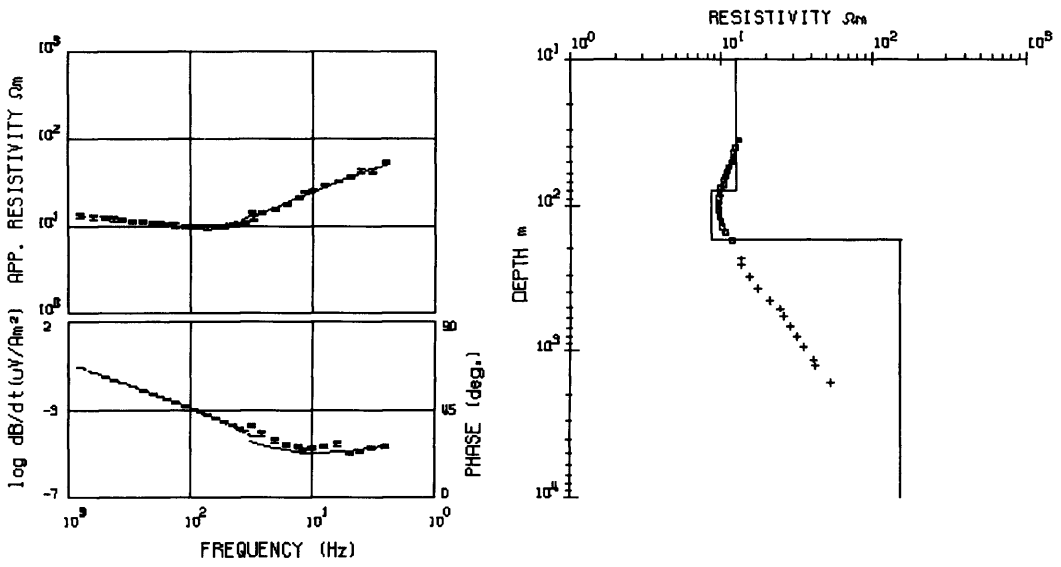

Station 150E

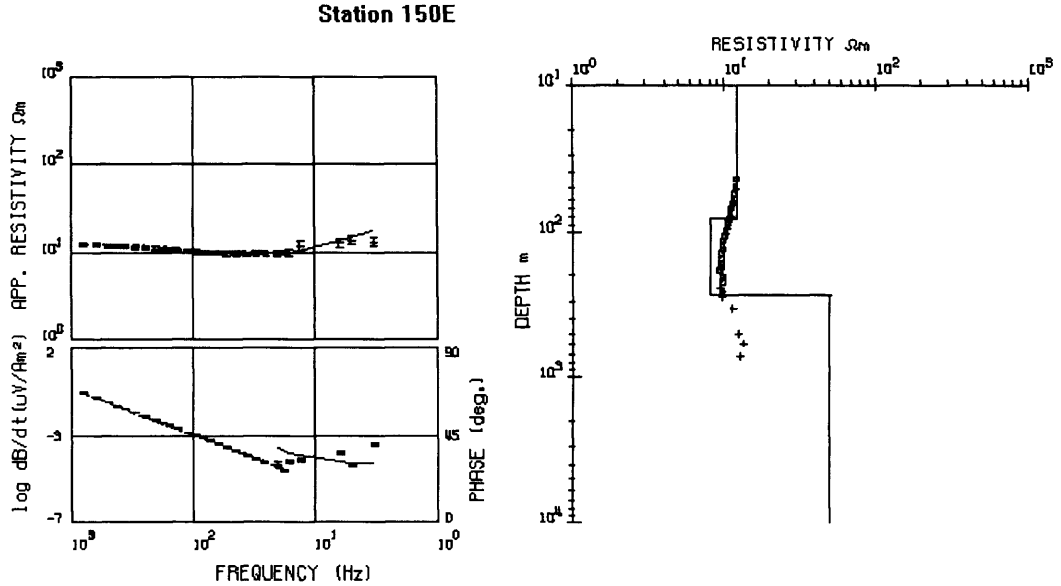

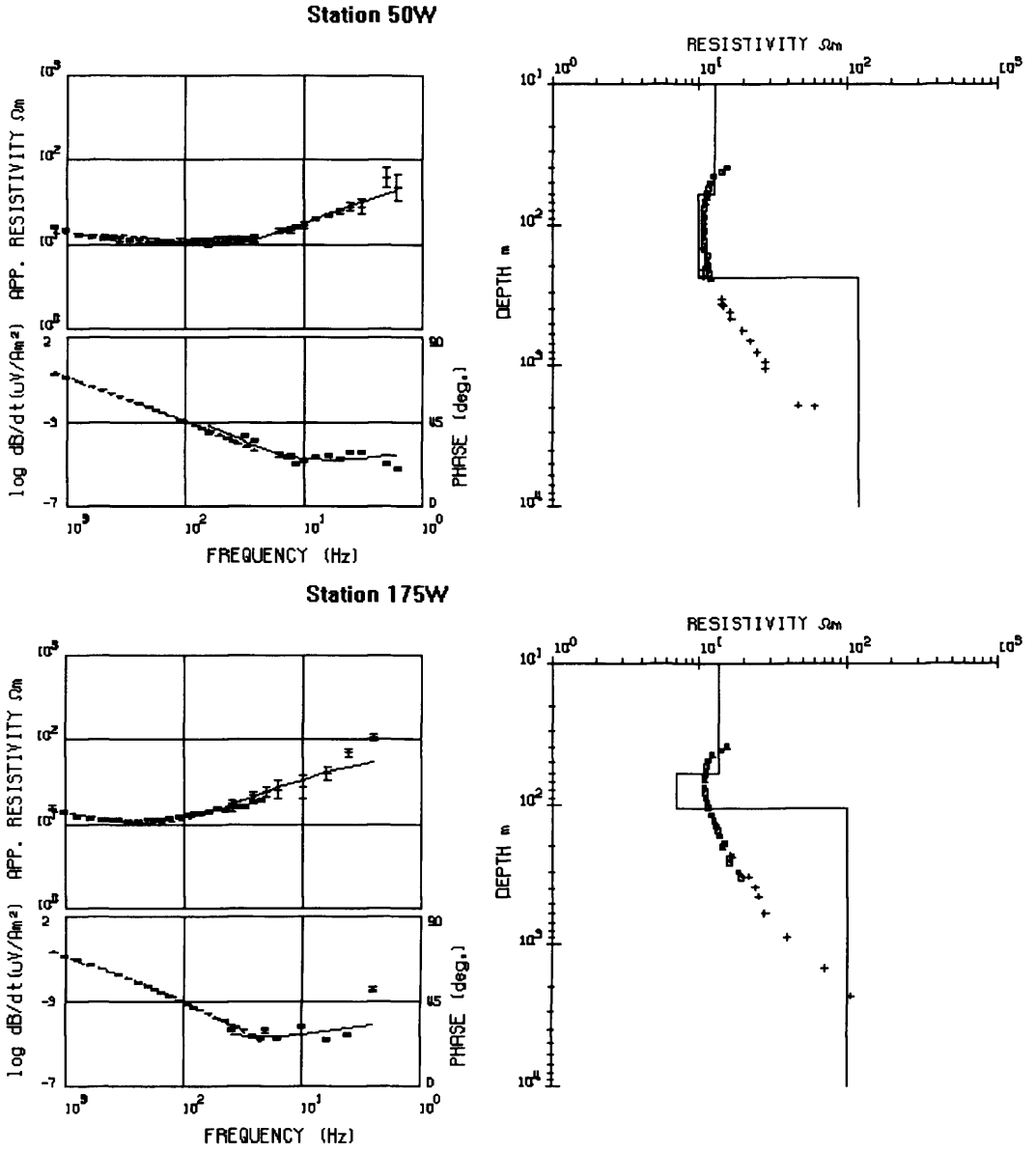

6.4.1 Geoelectrical Sections for Klirou site

The resulting geoelectric sections for the N-S and E-W traverses for Klirou area are shown as figs.6.4a and b. A look at the resistivity-depth sections of the two orthogonal lines shown in the figures indicates a somewhat horizontal to slightly dipping layers to the east and a conductive layer with resistivity of less than 11 ohm-m. The 1-D geoelectric sections show that this conductive zone is a clear

Fig. 6.4a 1D Geoelectric section of the N-S line at Klirou area

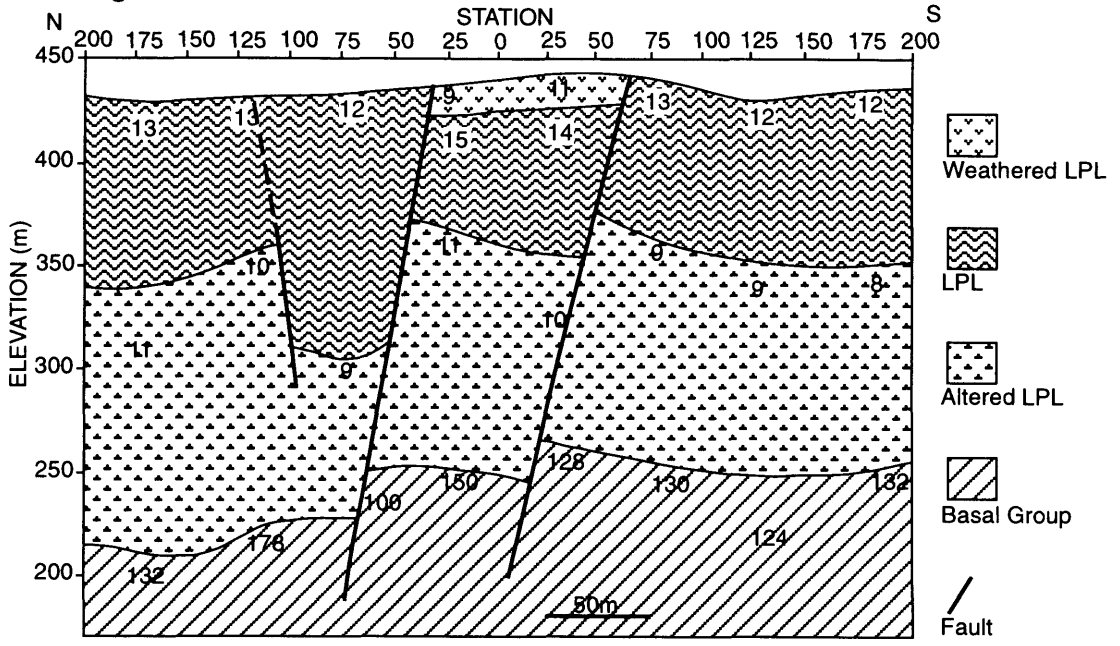

Fig. 6.4b 1D Geoelectric section of the E-W line in Klirou area

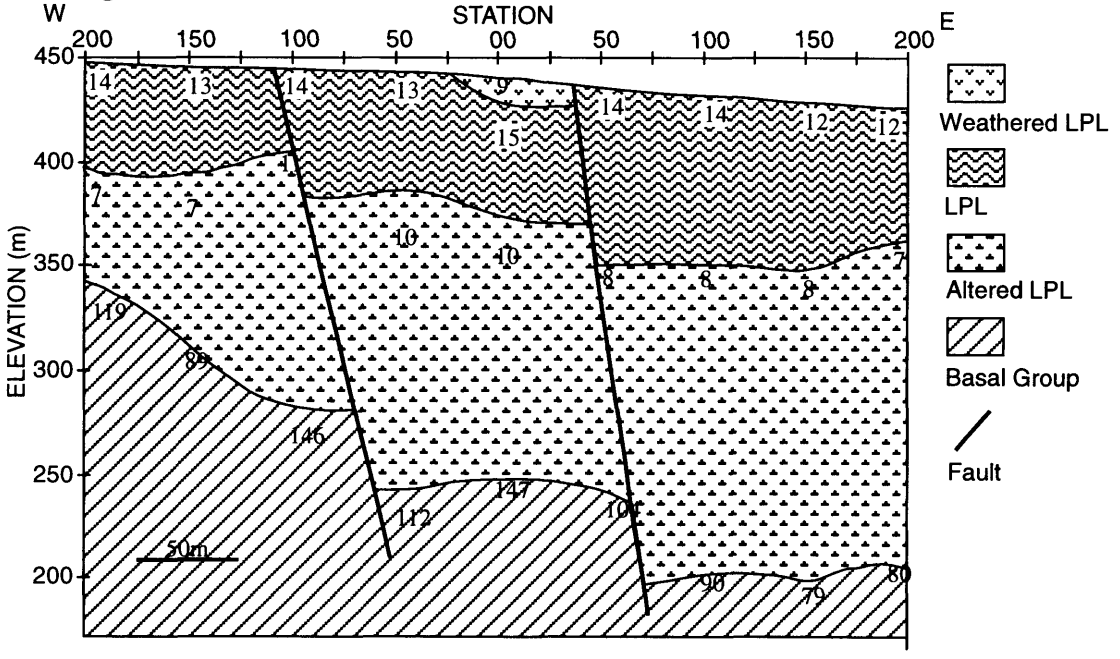

lithological unit and it is known to host the mineralisation in the area. The fault locations are known from geology and borehole data, and they fit in where the interpreted resistivity boundaries show obvious discontinuities. It needs to be stated here that apart from the general knowledge of the geology of the area including structural positions, no other a prori information was used in the production of sections 6.4a and b.

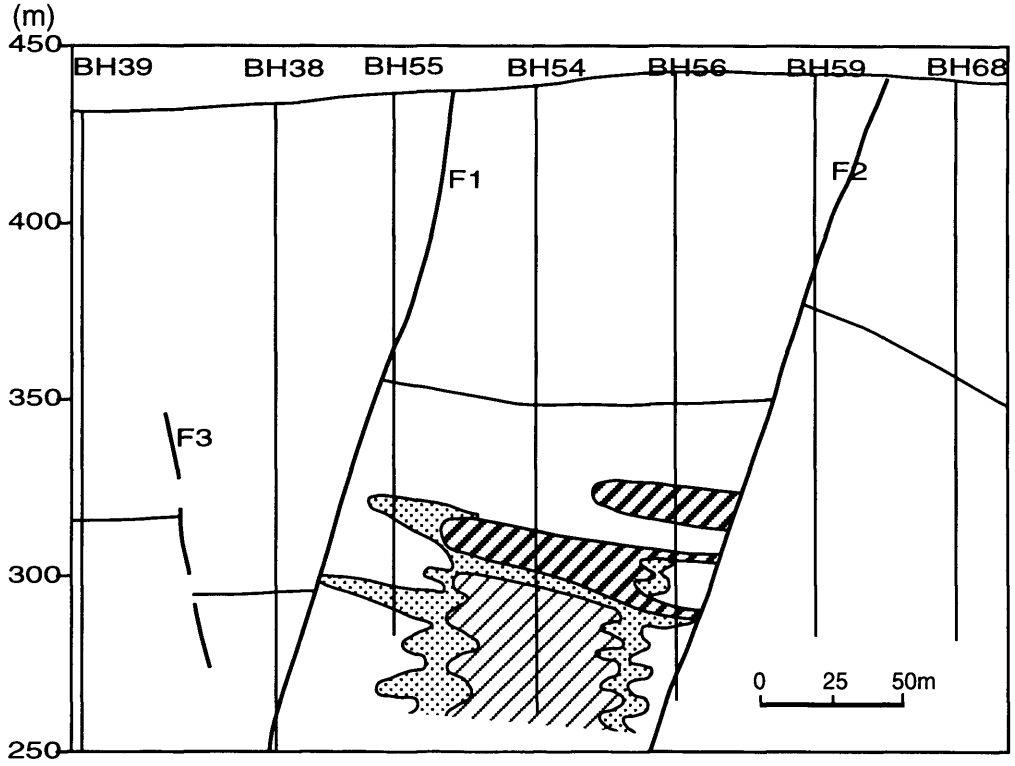

Fig. 6.5a Borehole Section parallel to the N-S Line

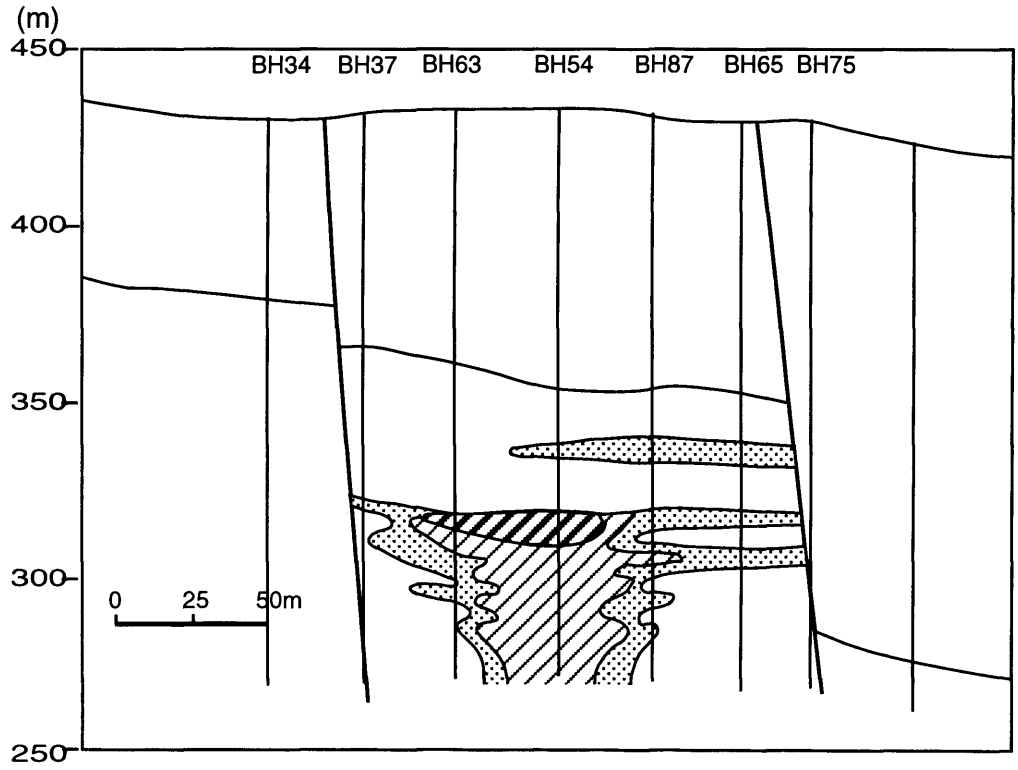

Fig. 6.5b Borehole Section parallel to the E-W Line

6.4.2 Comparison of TEM Resistivity-Depth, Geoelectric and Geological sections, and IP data for Klirou

It is evident that the close agreement between the Resistivity-Depth sections (fig.6.2) and the interpretive geoelectric sections (fig.6.4a and b) cannot be overemphasised. Note the positions of the resistivity blocks observed even in the TEM Resistivity-Depth sections. A comparison of the interpretive geoelectric sections with borehole geological sections (fig.6.5) show that the lithological units and boundaries are in close agreement, and that 1-D inversion depths and fault locations compare very well with those determined from boreholes. The low resistivity unit that hosts the mineralisation is seen clearly in the geoelectric section. The borehole sections reveal that the mineralisation is controlled and bounded by faults which align it in the northwest direction. This type of linear control has been observed around many of the massive sulphide ore deposits of Troodos (Adamides, 1984).

Available IP data from Cyprus Geological Survey (fig.6.6), measured along the E-W line shows good agreement with the results of the TEM/MT data taken along the same line. The IP (metal conduction factor or percent frequency effect) anomaly is right within and constrained by the near vertical faults interpreted in the TEM/MT geoelectrical section. In IP data interpretation, metal conduction factor and percent frequency effect are said to be more diagnostic of the amount of conductive ore present than apparent resistivity (Griffiths and Kings, 1981; Milson, 1989). The metal conduction factor is a measure of the total change in conductivity of a rock given as percent frequency multiplied by the conductivity at zero frequency (DC) and a constant factor $2\pi 10^5$ (Griffiths and Kings, 1981; Milson, 1989). It was based on the IP anomaly that a borehole was drilled which proved the anomaly to be caused by a massive sulphide mineralisation at a depth of about 80-110m. Note the close aggreement between the positions of the interpreted faults in the geoelctrical section and the IP pseudosection, and with the geological section. It is

evident here that a combination of TEM/MT and IP data will go a long way in

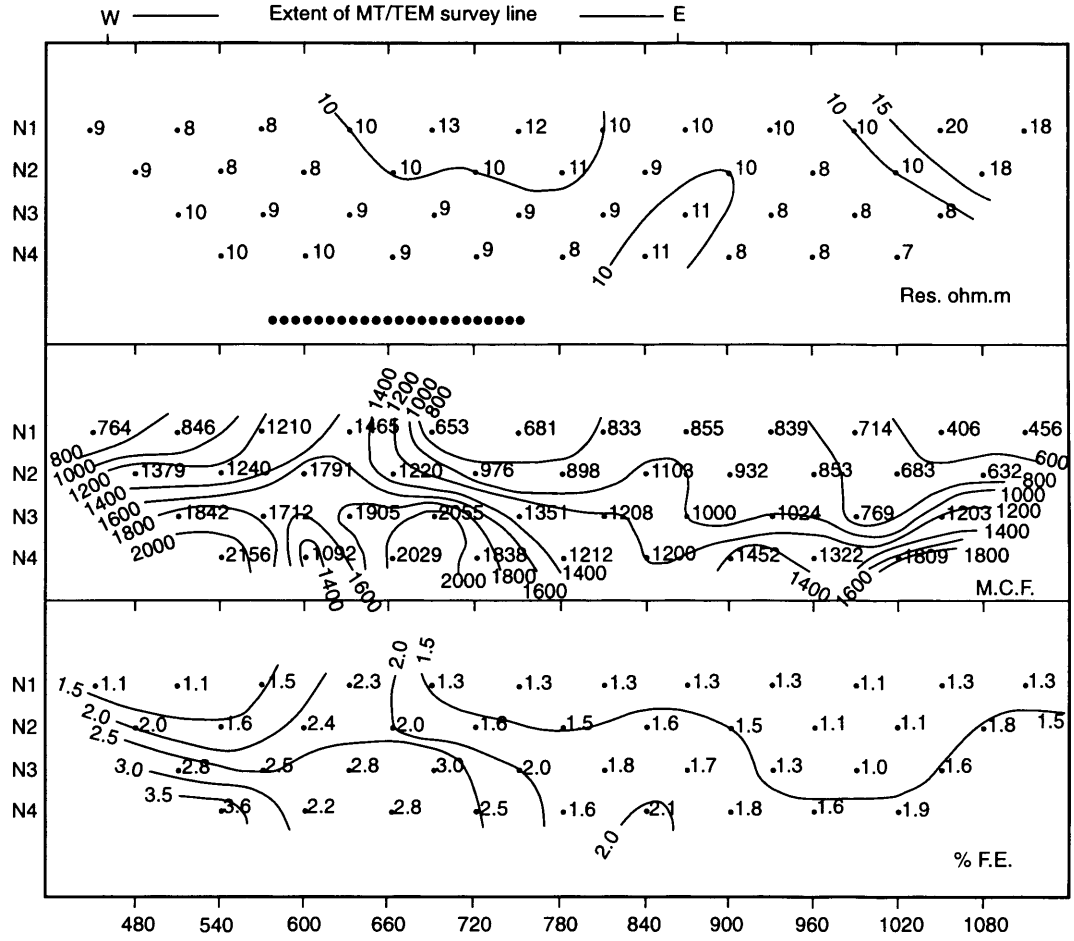

Fig. 6.6 IP pseudosections along the E-W line at Klirou

providing useful information on the location and extent of massive sulphide ore bodies in this type of environment. The 1-D intepretation of combined TEM/MT methods has provided useful and reliable subsurface depth estimates and the position of some structures while distinguishing lithological units from their resistivity variations, while available IP data can furnish the possible location of ore mineralisation in the subsurface. On the basis of the above, one may now speculate on the possible geological meanings of the sections from Ayia Marina area.

6.5 1-D Models for Ayia Marina

Following from the discussion on 1-D models for Klirou site, it can also be argued that the 1-D scheme employed in this study will provide reliable subsurface

depth estimates in the Ayia Marina area. Examples of resulting 1-D models for the Ayia Marina area along Line 9 showing the fit of the data are shown in Fig.6.7. Again the simple data transformation result and the interpreted 1-D model are shown on the right hand plot and the field data and the response of the constructed model are plotted together on the left hand for comparison.

Fig. 6.7 1-D Inversion model fits for some stations on Ayia Marina Line 9. Squares are TEM and crosses MT TM-mode resistivity curves

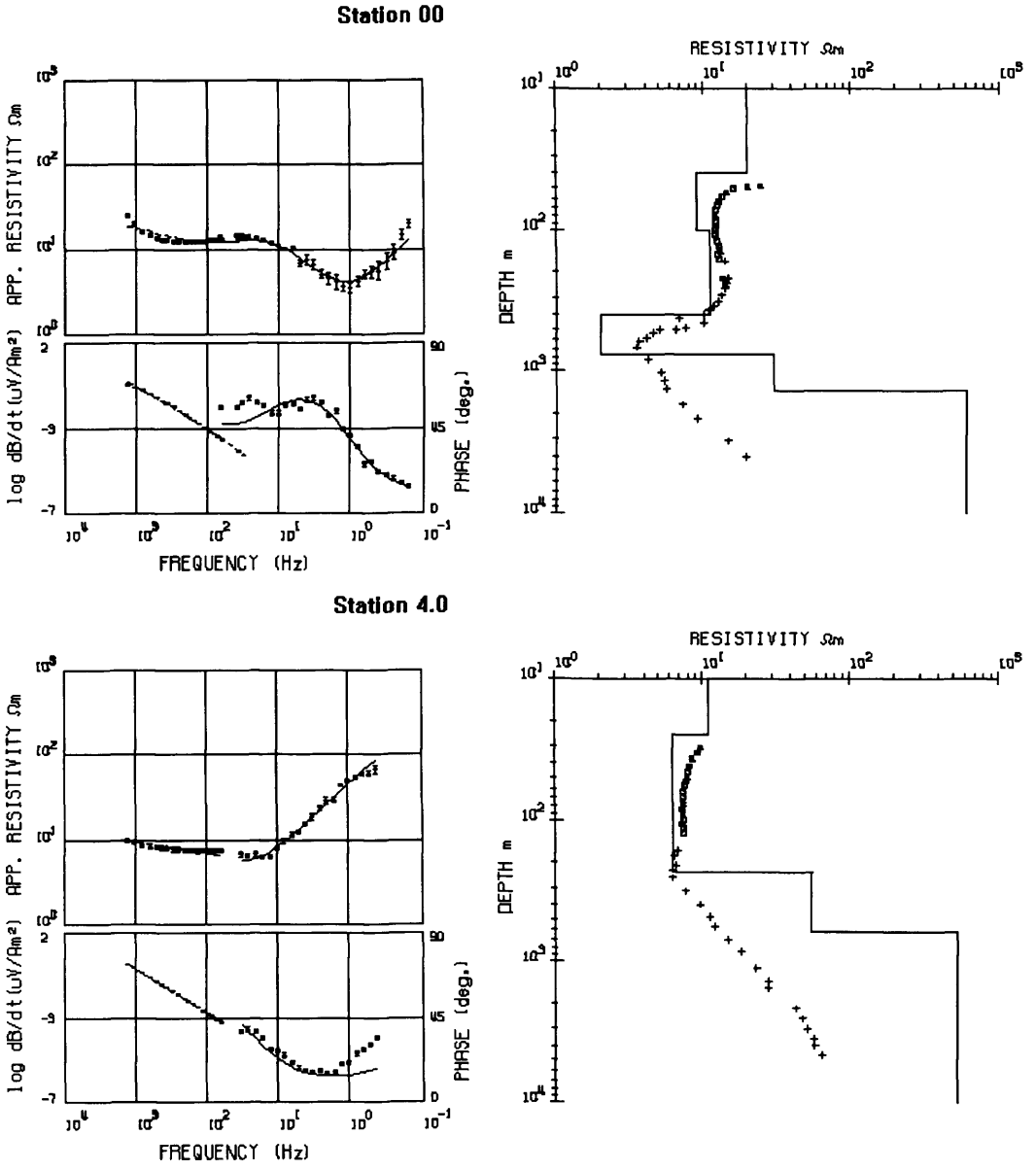

Station 6.0

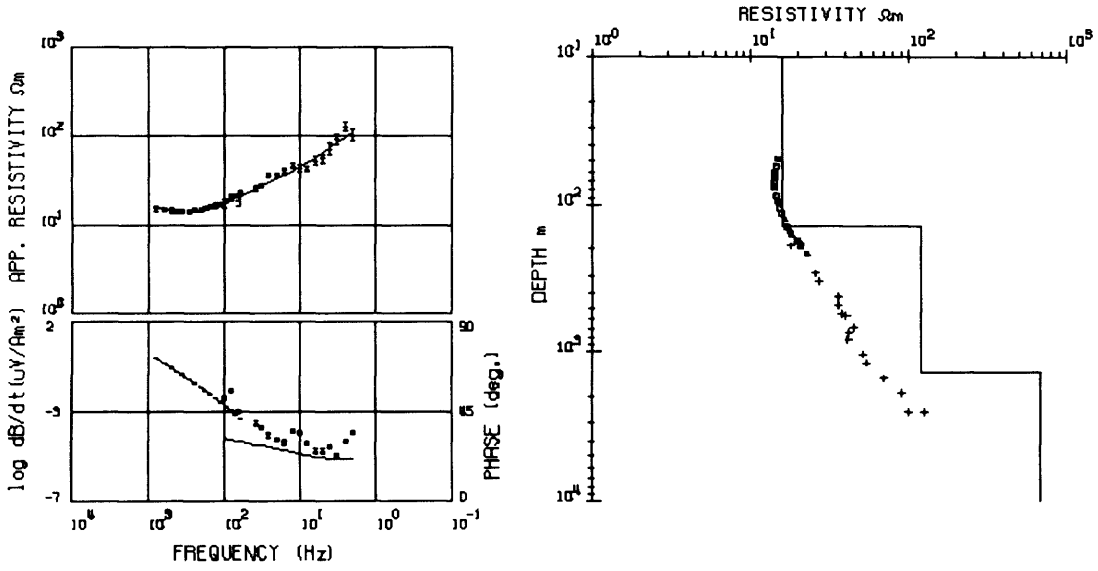

Station 7.5

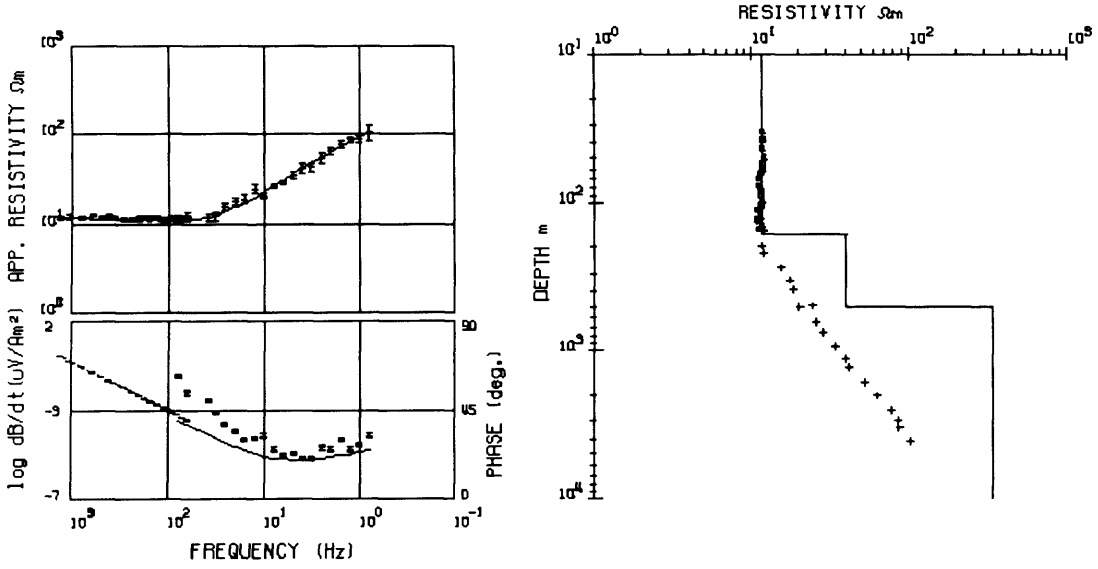

Station 11.0

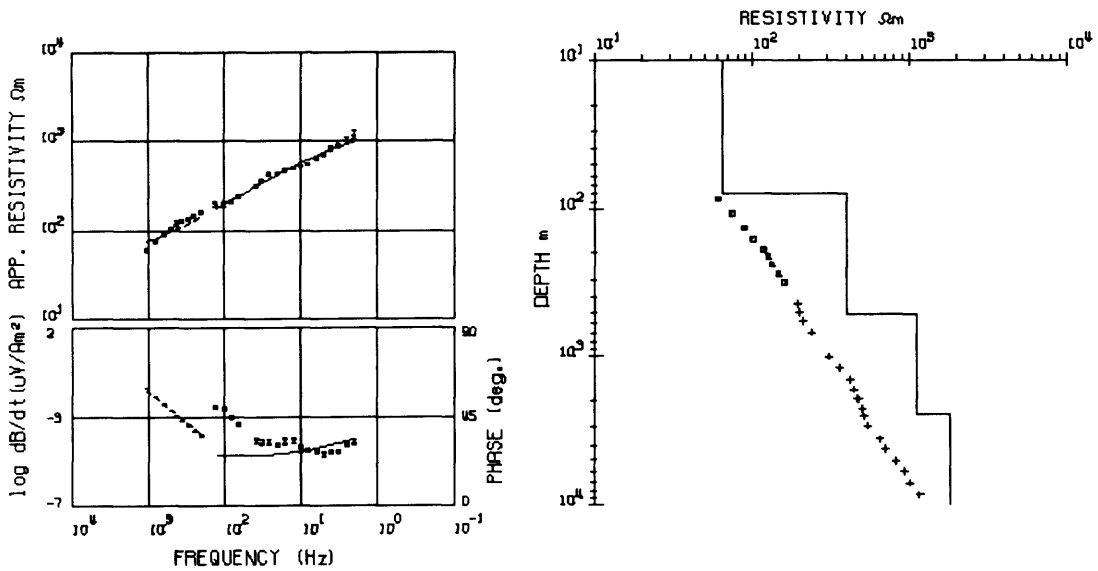

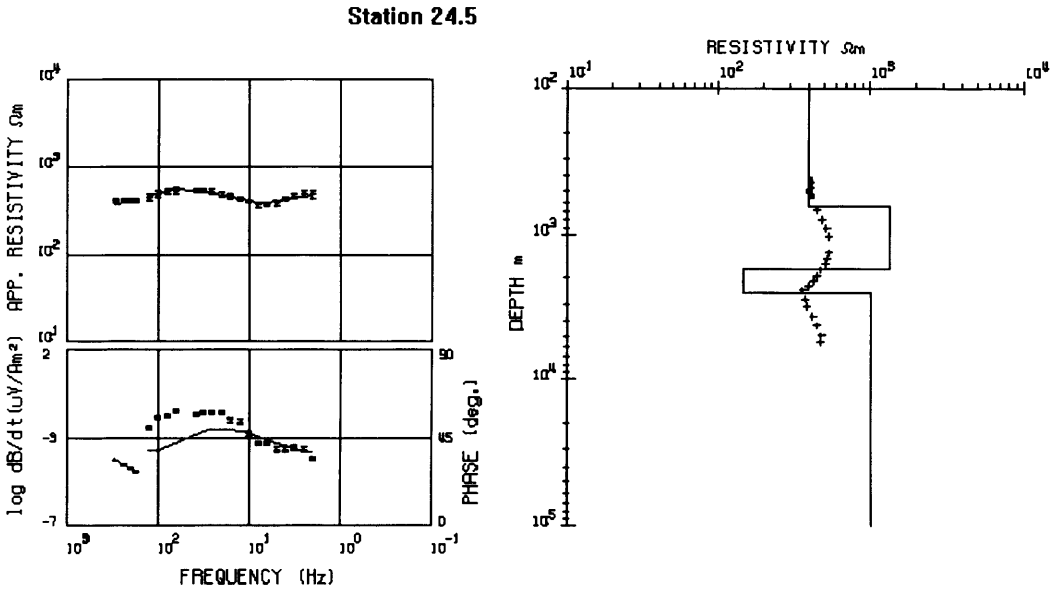

6.5.1 Geoelectric sections for Ayia Marina transects

The interpreted geoelectric sections for the Ayia Marina area from one dimensional modelling and inversion are shown in fig.6.8. Line 9, which is the longest and covers more area, shows a number of geoelectric units and associated interpreted structures. A unit with resistivity of between 26 and 28 ohm.m and an average thickness of about 50 m is observed at the northmost part of the traverse. Below that lies a 60-170 m unit of 9-13 ohm.m resistivity. The next unit has a lower resistivity of 2-6 ohm.m and a thickness of 150-250 m. The following two units in the section have resistivities 30-56 ohm.m and 489-554 ohm.m respectively. The units exhibit a general gentle dip to the north. The southern part of the line shows 400-600 m thick top unit with resistivity of between 145 and 399 ohm.m, followed by a unit of between 1000 and 2000 m thick with a resistivity range of 685-1456 ohm.m. A 400 to 600 m thick unit of 147-204 ohm.m is observed at the southmost part of the line. A 465-1828 ohm.m resistivity unit underlies the whole section. Some faults have been inserted where obvious boundary discontinuities exist and some of them appear to be in accord with some of the lineaments interpreted by Cooper (1993) in the area.

Fig. 6.8 1-D Geoelectric sections for Ayia Marina area

(a) Line 9

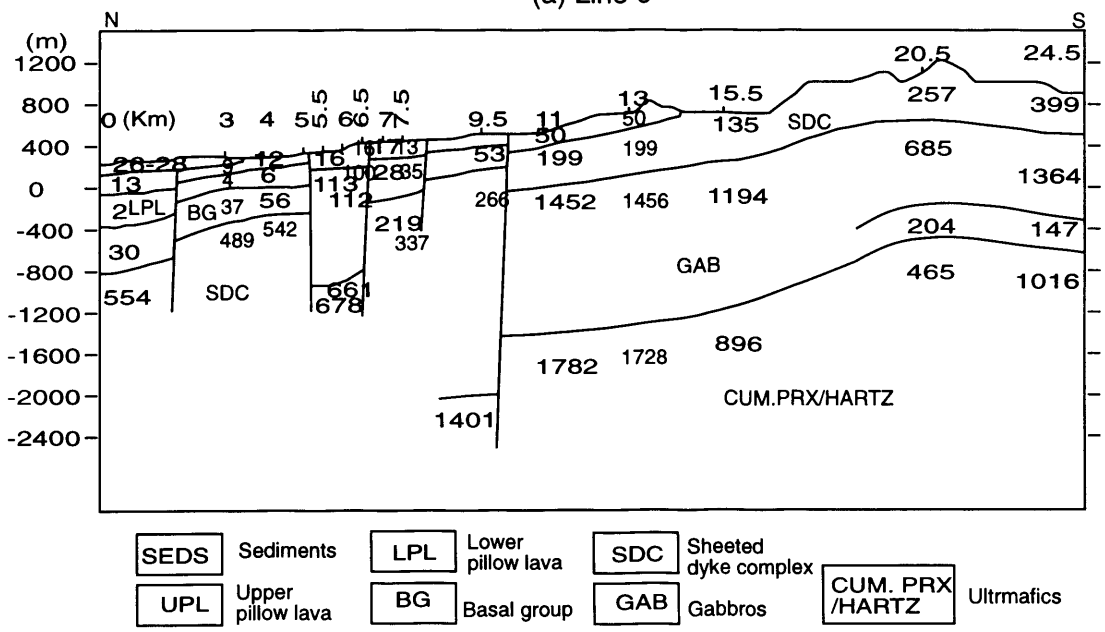

(b) Line 7

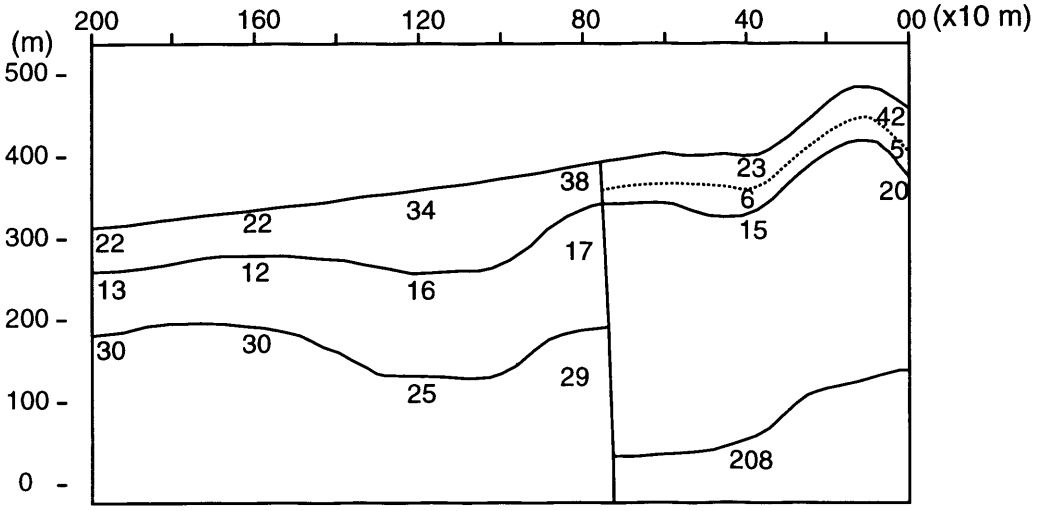

(c) Line 5

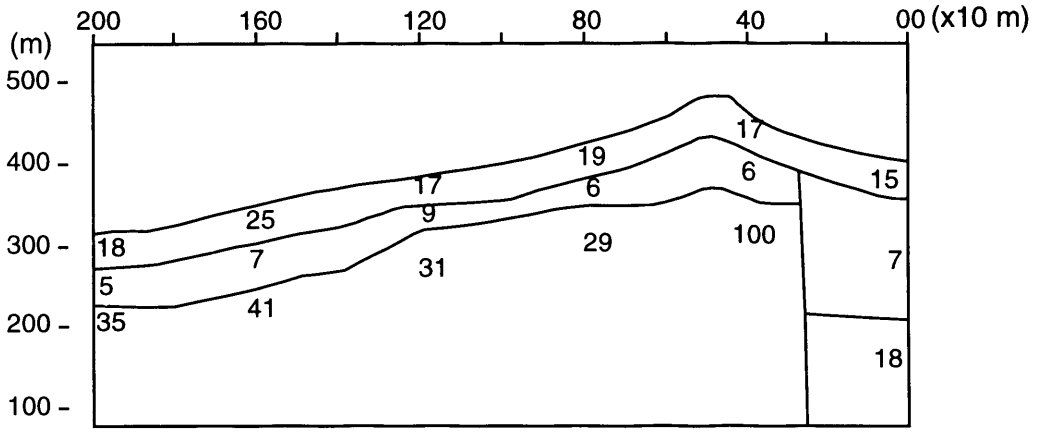

Lines 7 and 5 are very much shorter than Line 9 (2000 m each) and lie 200 and 400 m east of Line 9 respectively. Only the first two bands representing the higher frequency part of the MT system frequency range was used here and hence shallower depth was explored. The two lines show units at depth of more than 100 m with resistivity of 25 ohm.m or more which are thought to correspond to rocks of the diabase. Immediately above that comes a unit with resistivity of 5-9 in Line 5 and 12-17 in Line 7 and this is thought to correspond to the lower part of the LPL in the area. The overlying relatively more resistive layer is thought to represent the weathered portion of the LPL. There appears to be a gradual thinning of the LPL or a general uplift of the diabase as one moves eastwards to Line 5 right from Line 9.

6.5.2 Comparison of Geoelectric, Aeromagnetic and Geological data

The geoelectric sections for Lines 5, 7 and the corresponding portion of Line 9 from Ayia Marina area all show an upper LPL layer underlain by rocks of the BG. They in general agree with the geology of the area. A common fault line is picked up by the three sections which corresponds to one of the structures interpreted in the area from aeromagnetic data by Huntings (1969) and Cooper (1993). The geoelectric section for Line 9 seems to have picked up the various rock types across the area agreeing closely with the surface geology. It has also picked up faults that correspond to 5 of the 8 nearly east-west structures interpreted in the area by Cooper (1993). The 5 fault structures appear to agree more closely with the 5 structures interpreted in the area by Huntings (1969). In general the interpretative sections are in close agreement with the available surface geological information on the area.

CHAPTER SEVEN
TWO DIMENSIONAL MODELLING AND INVERSION OF AYIA MARINA DATA

7.1 Introduction

It has been observed in chapter six that the Troodos ophiolite complex can at the least only be described as a two dimension environment and would therefore require the use of at least two dimensional modeling and inversion for the data acquired from it. This chapter discusses the two dimensional forward modeling and inversion techniques used in the interpretation of data from the longest survey line which starts from the Ayia Marina area. Some of the problems involved in the construction of a two dimensional model and the process of mesh design and the use of *a priori* information are discussed. The fit of the two dimensional models and the agreement of the forward modeling and inversion geoelectric sections with borehole data are then presented.

7.2 Forward Modelling

7.2.1 Model Construction

In the search for a two dimensional interpretative model, the MT response of an initial resistivity model is obtained and compared with the acquired field data for the best possible fit. The construction of a two dimensional model is quite a difficult task and generally the search for an acceptable model can never be exhaustive. This is so because of the reasons given in the case of one dimensional problem. The one dimensional inversion model obtained in the previous chapter was adopted as the initial two dimensional forward model. A finite element forward modeling scheme was employed here with the initial model. An interactive iterative process then ensued during which the parameters of the initial model were progressively adjusted for good fit while the resulting forward models were visually examined for good fit in the light of prior geological and geophysical information. The two

dimensional forward model with the best visual fit was then used as the starting model for two dimensional inversion.

7.2.2 2-D Forward Modeling Program

The finite element program (PW2D) for the solution of magnetotelluric response of two dimensional earth resistivity structure by Wannamaker et al (1985) was employed in this study. The program models two dimensional magnetotelluric problems for both transverse electric (TE) and transverse magnetic (TM) modes of plane wave excitation. The algorithm PW2D is a single program that consolidates a number of routines originally developed at the University of Utah by Rijo (1977). Improvements to the original program include the implementation of a direct solution for the secondary field variations parallel to the strike and the subsequent auxiliary fields thereby circumventing a difficulty with numerical precision at low frequencies observed in total field solutions for the TM mode especially, but also for the TE mode (Wannamaker et al, 1985). An additional innovative modification in the program is the ability to simulate topographic variations. One important result of the topographic modeling facility is that a horizontal placement of the sensors (coils) for H_x and H_y will reduce topographic effects toward low frequencies on apparent resistivity relative to a placement of sensors parallel to the slope (Wannamaker et al, 1985).

Having incorporated the secondary field and topography formulation, and with the additional experience acquired using the program over the years, Wannamaker et al (1985) produced an updated documentation as a modification of that by Stodt (1978). In the algorithm PW2D, the linear interpolation of the unknown field parallel to strike over triangular sub-domains is used in conjunction with Galerkin weighting technique to obtain a system of linear equations which approximate the governing Helmholtz partial differential equation. An estimate of the secondary field values parallel to strike at the nodes of the discritised domain is then given by the solution of this system of linear equations. Care must be taken to

keep the model values of the field parallel to strike within the earth to avoid discontinuities in the derivatives or resistivities (TM mode) associated with the air-earth interface. Auxiliary vertical and transverse fields are derived from a numerical approximation to the differential Maxwell's equations. Boundary conditions are applied at all external grid/mesh boundaries of the discretised domain in solving the magnetotelluric problem. The program PW2D is the result of derivation and

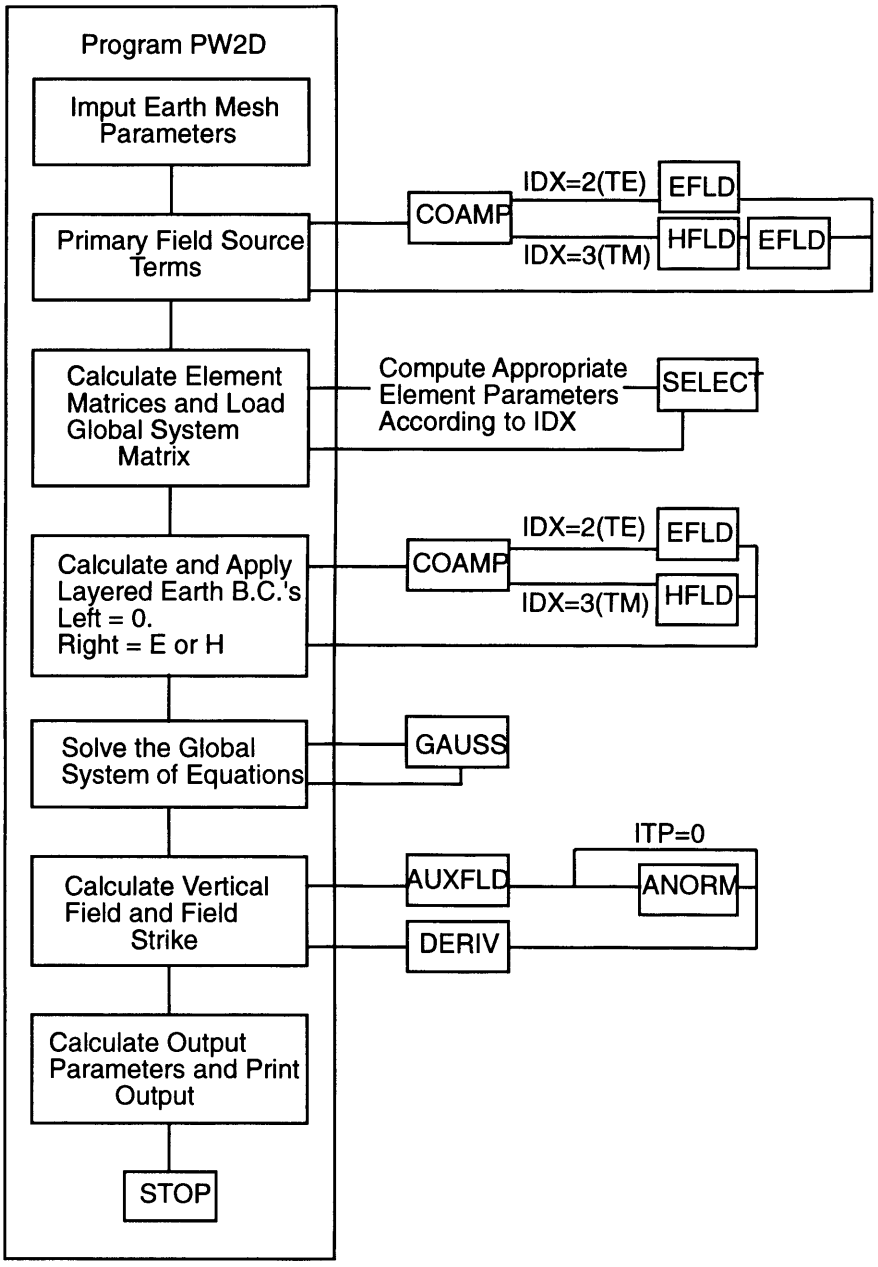

Fig. 7.1 Flow diagram for PW2D execution. Subroutines called are in uppercase in boxes (After Wannamaker et al, 1985).

programming of the elementary equations obtained from the finite element technique in a sufficiently general form so that any physical problem governed by the two dimensional inhomogeneous scalar Helmholtz's equation may be handled with minor modifications to the program. Fig. 7.1 is a flow diagram of the program execution. Finite elements appear to be a flexible and accurate means of computing MT responses of arbitrary 2D sections including topography.

7.2.3 Mesh Design

For meaningful numerical solutions to the two dimensional problem and output from the program, a proper mesh design is very important (Muller and Losecke, 1975; Wannermaker et al, 1985). Proper grid or mesh design is something that is acquired with experience, but some general rules of the thumb concerning element dimensions can be used as a guide line (see Wannermaker et al, 1985).

1) Sizes of adjacent mesh elements should not vary by more than a factor of 3 to 5.

2) Near a conductivity boundary, element dimensions should not exceed a quarter of the skin depth in the medium where the element is situated.

3) A resistivity medium is defined by at least 3 elements horizontally and 2 elements vertically.

4) About 2 to 3 skin depths away from a conductivity boundary, element dimension may be increased up to skin depth of the medium.

5) Because the fields decay exponentially, vertical element dimensions may be increased exponentially downwards from the air-earth interface.

6) Because of the long wavelengths of the field in the air, 7 to 10 element rows increasing upward exponentially are recommended for the air layer in the TE problem.

7) Near the bottom (basement), element dimensions are kept essentially uniform.

The accuracy of the results is checked by modifying the mesh (and the rules with experience) and checking the convergence of the solutions.

7.2.4 Initial Model with a priori Information

The one dimensional inversion model of the Ayia Marina traverse was adopted as the initial model for the two dimensional forward modeling. Previous geophysical aeromagnetic data analysis (Cooper, 1993) has indicated a network of lineaments both cross cutting and parallel to the Ayia Marina traverse. A more dominant E-W structural trend was defined which is perpendicular to the traverse. In addition, previous geological work (Gass, 1980) and geophysical logging (Salisbury et al, 1987) has given the lithological succession of the Troodos ophiolite along with the determined resistivity values. Borehole logs have also provided the depth of the upper lithological units in the Troodos at various locations including the Palekhori borehole which lies at the end of the Ayia Marina line.

The one dimensional geoelectric section for the Ayia Marina traverse showed features that agree with most of the observations above. Additional information included the use of the lithological unit depths observed from the Palekhori borehole (CW-4) and the inclusion of surface topography. The problem was well discretised initially using a mesh size of 145 by 89 elements. A continuous modeling involving a gradual and reasonable modification of model parameters was undertaken to achieve a reasonable fit of the calculated response to the observed field data. When a fairly good fit was obtained, the mesh size was reduced to 48 by 39 elements. This mesh size was more manageable and less time consuming and there was no adverse effect on the shape and accuracy of the result. Interactive modeling continued with necessary parameter adjustments until a reasonable visual fit was obtained for both the TE and TM modes.

The fit of the calculated response curves to the observed field transverse electric and transverse magnetic modes data for the sites is shown in fig. 7.2. The fit in both the amplitude and phase of the electric and magnetic polarisation directions can be said to be reasonably good at most of the sites. The figure shows the field apparent resistivity curves and the calculated response curves for the two polarisation directions and their respective phase responses.

Fig. 7.2a 2-D TE mode MT forward model fits for resistivity and phase (Line 9) Series1 represent field data while Series2 represent the calculated response

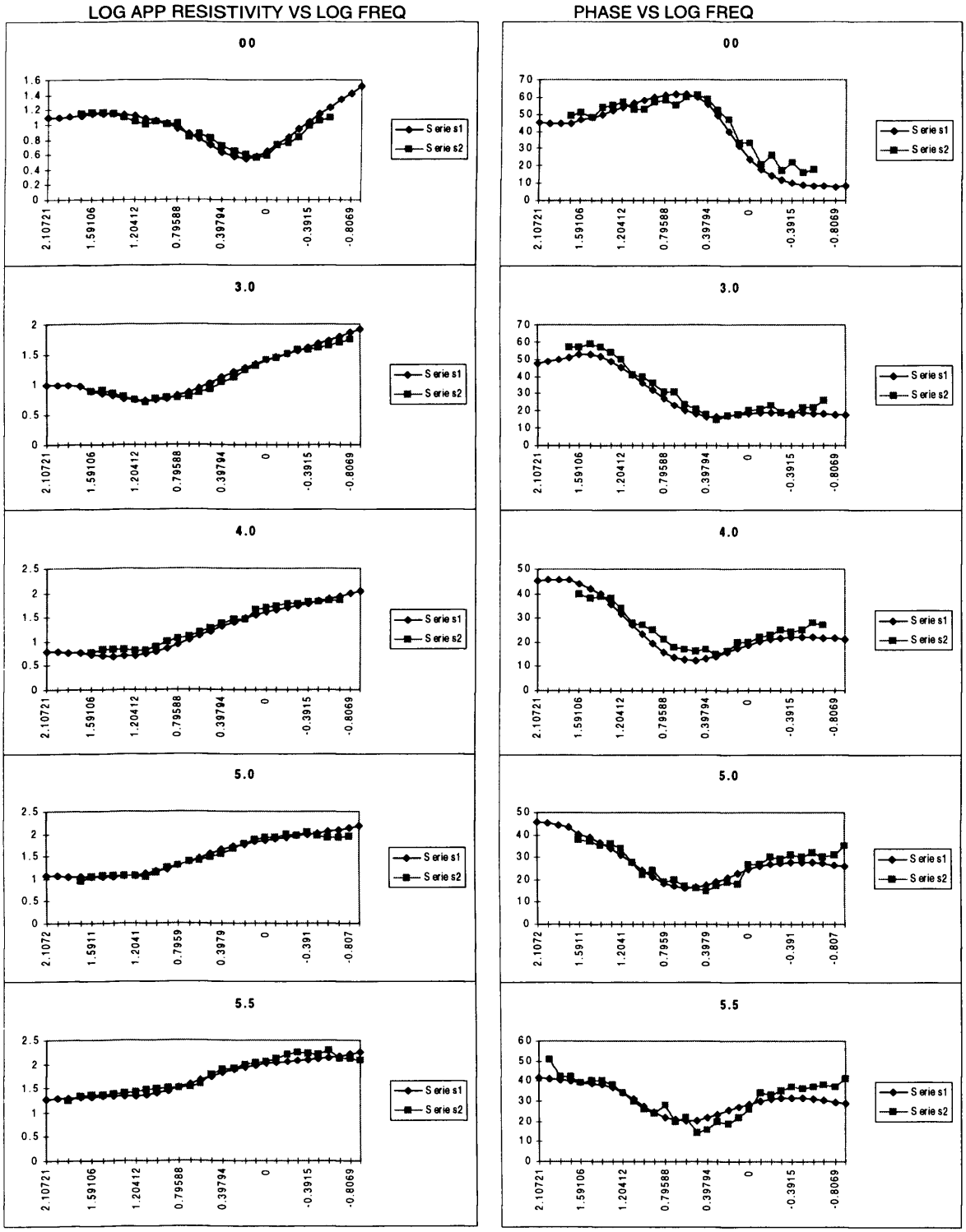

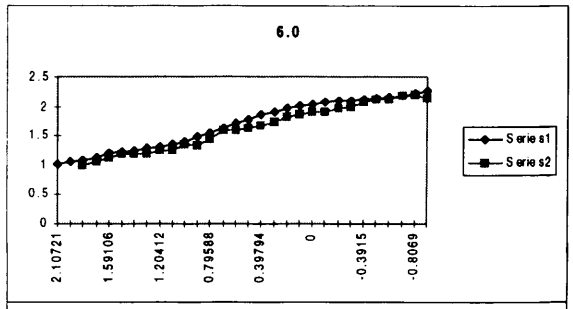
6.0
2.5
2
1.5
1
0.5
0
2.10721
1.59106
1.20412
0.79588
0.39794
0
-0.3915
-0.8069
Series1
Series2

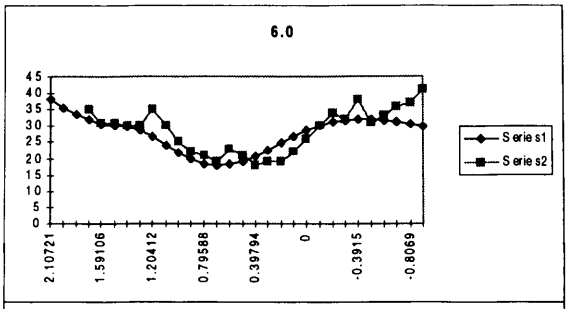
6.0
45
40
35
30
25
20
15
10
5
0
2.10721
1.59106
1.20412
0.79588
0.39794
0
-0.3915
-0.8069
Series1
Series2

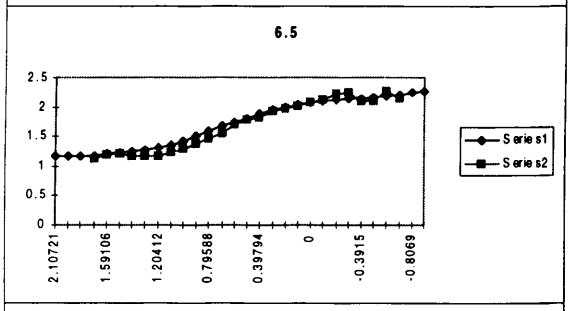
6.5
2.5
2
1.5
1
0.5
0
2.10721
1.59106
1.20412
0.79588
0.39794
0
-0.3915
-0.8069
Series1
Series2

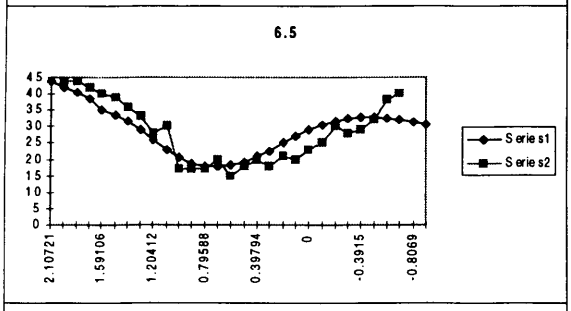
6.5
45
40
35
30
25
20
15
10
5
0
2.10721
1.59106
1.20412
0.79588
0.39794
0
-0.3915
-0.8069
Series1
Series2

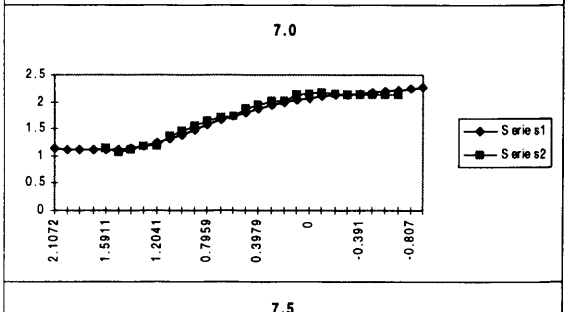
7.0
2.5
2
1.5
1
0.5
0
2.1072
1.5911
1.2041
0.7959
0.3979
0
-0.391
-0.807
Series1
Series2

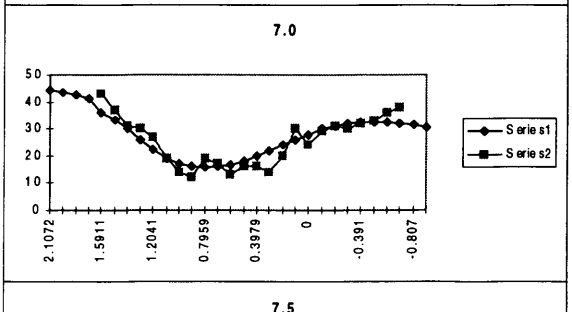
7.0
50
40
30
20
10
0
2.1072
1.5911
1.2041
0.7959
0.3979
0
-0.391
-0.807
Series1
Series2

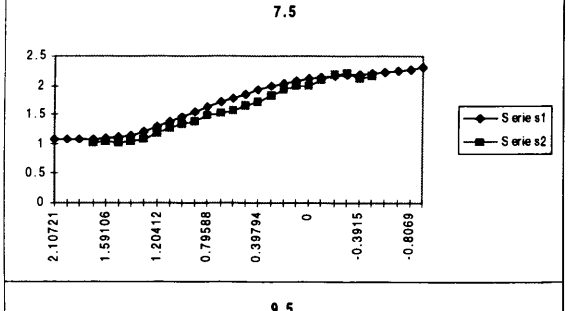
7.5
2.5
2
1.5
1
0.5
0
2.10721
1.59106
1.20412
0.79588
0.39794
0
-0.3915
-0.8069
Series1
Series2

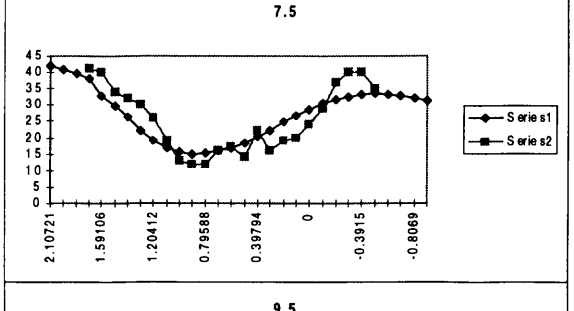
7.5
45
40
35
30
25
20
15
10
5
0
2.10721
1.59106
1.20412
0.79588
0.39794
0
-0.3915
-0.8069
Series1
Series2

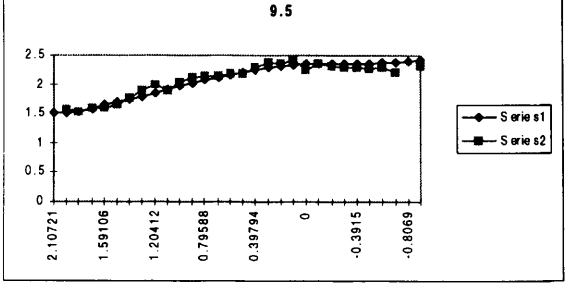
9.5
2.5
2
1.5
1
0.5
0
2.10721
1.59106
1.20412
0.79588
0.39794
0
-0.3915
-0.8069
Series1
Series2

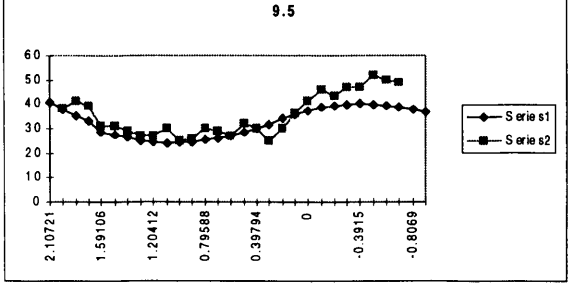
9.5
60
50
40
30
20
10
0
2.10721
1.59106
1.20412
0.79588
0.39794
0
-0.3915
-0.8069
Series1
Series2

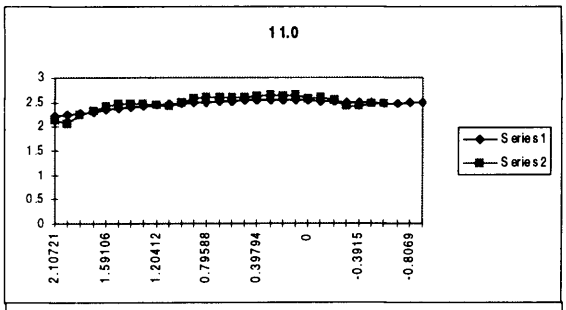
11.0
Series1
Series2

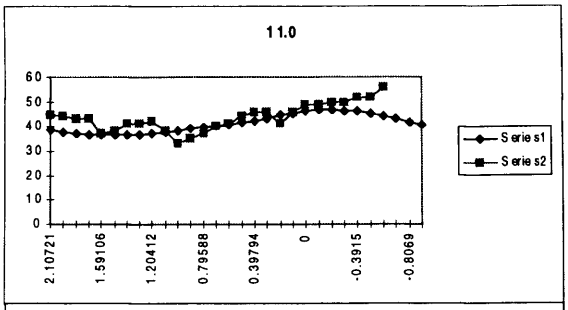
11.0
Series1
Series2

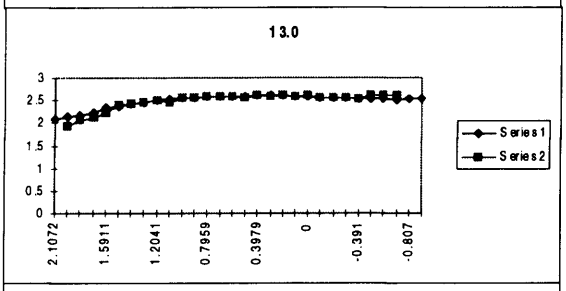
13.0
Series1
Series2

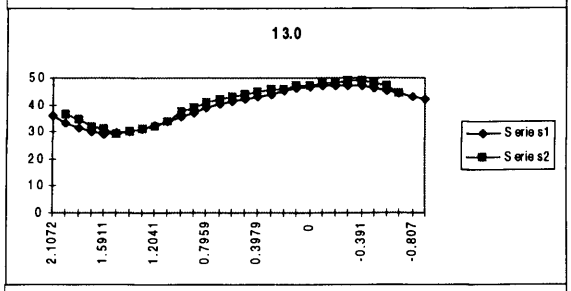
13.0
Series1
Series2

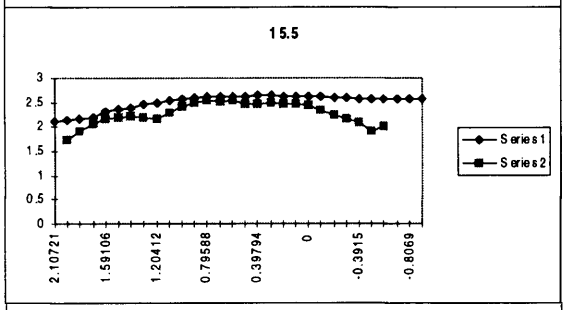
15.5
Series1
Series2

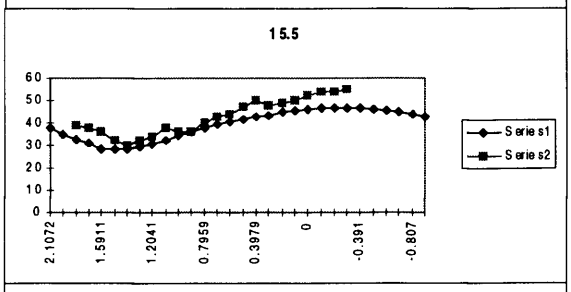
15.5
Series1
Series2

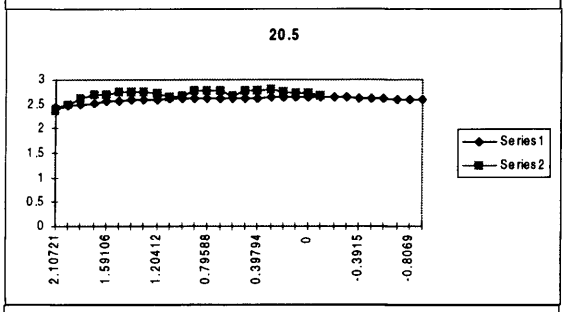
20.5
Series1
Series2

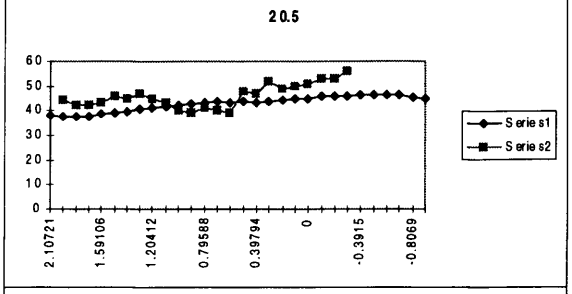
20.5
Series1
Series2

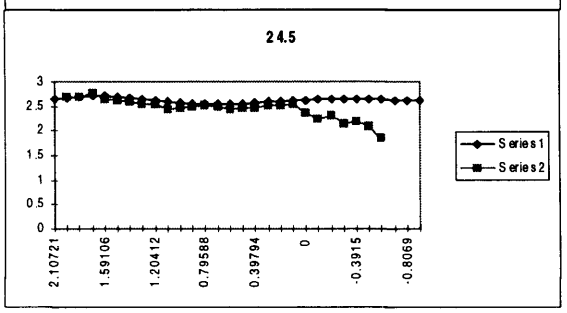
24.5
Series1
Series2

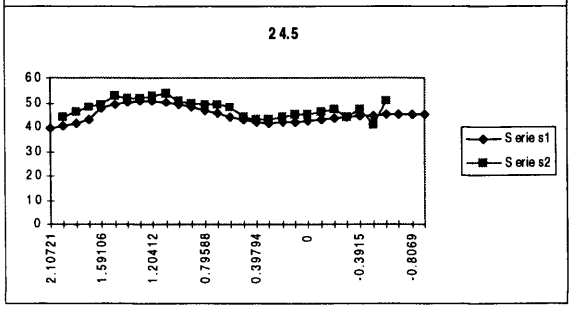
24.5
Series1
Series2

Fig. 7.2b 2-D TM mode MT forward model fits for resistivity and phase (Line 9) Series1 represent field data while Series2 represent the calculated response

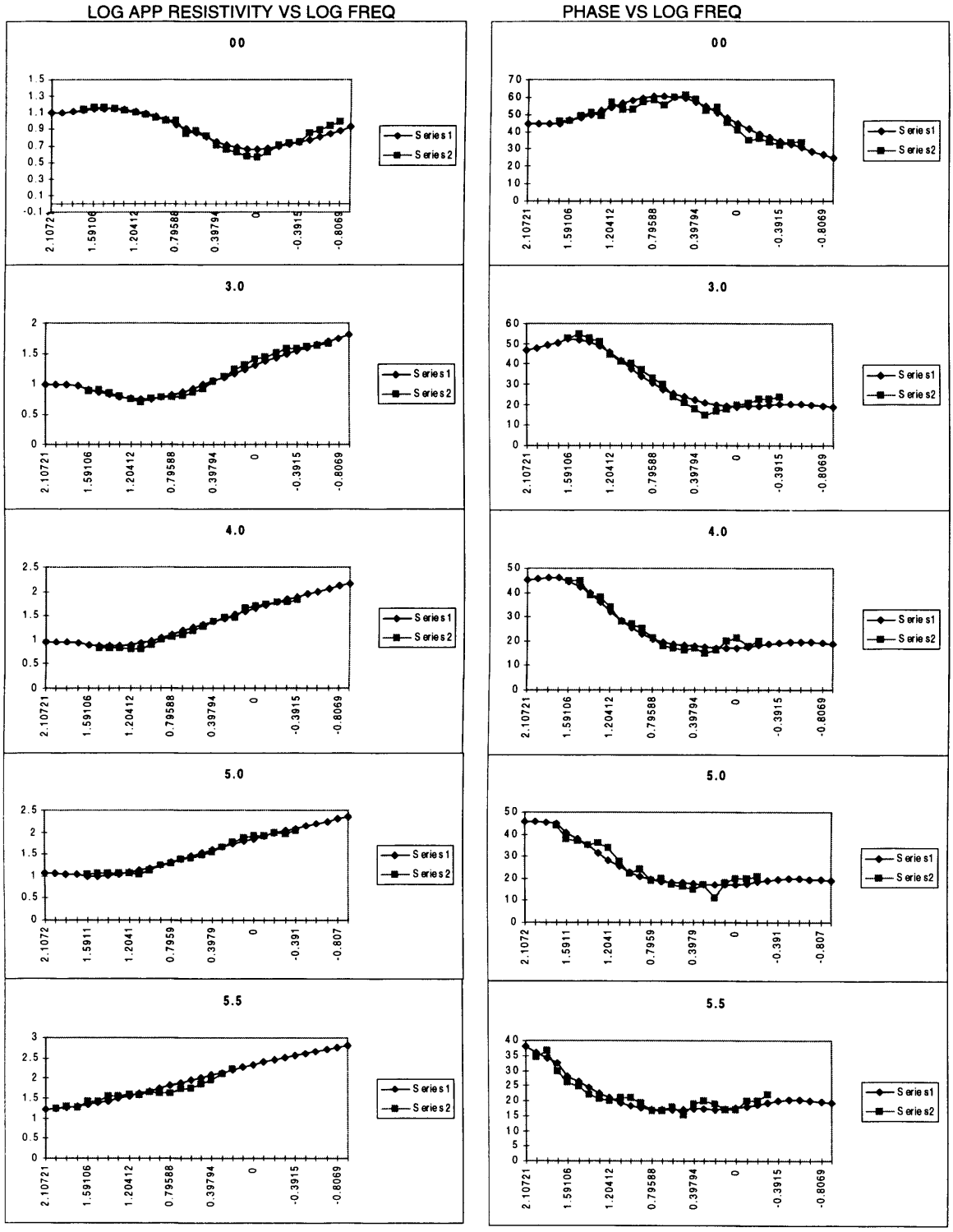

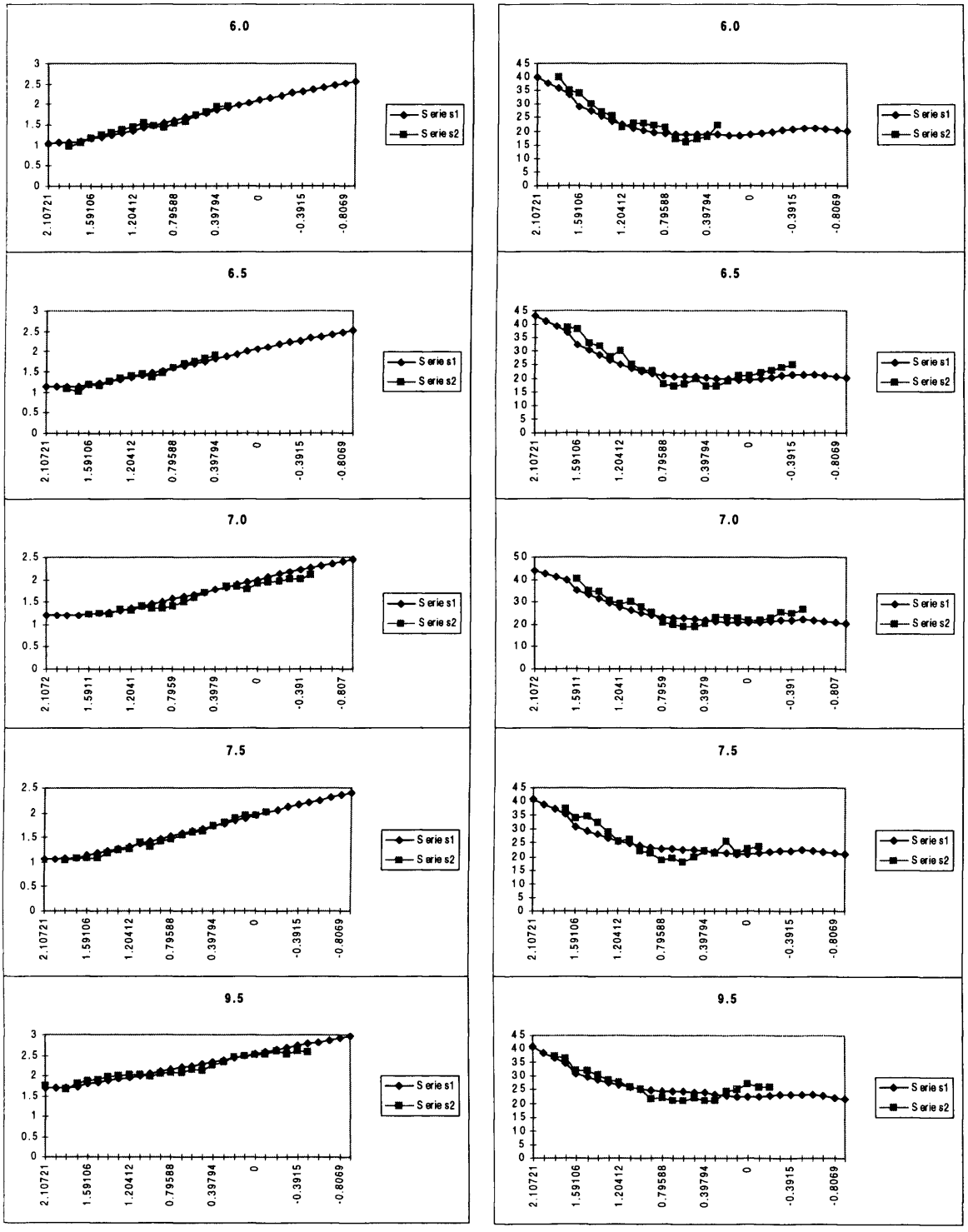
6.0
6.0
6.5
6.5
7.0
7.0
7.5
7.5
9.5
9.5
Serie s1
Serie s2
2.10721
1.59106
1.20412
0.79588
0.39794
0
-0.3915
-0.8069
2.1072
1.5911
1.2041
0.7959
0.3979
-0.391
-0.807

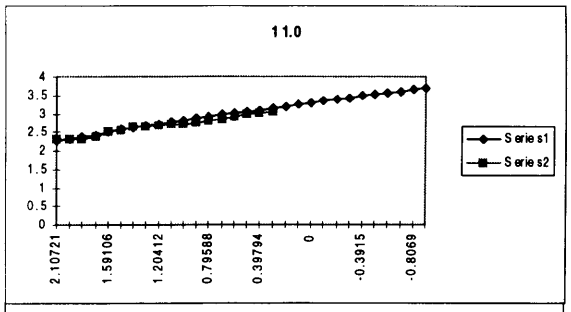
11.0
Series1
Series2
2.10721
1.59106
1.20412
0.79588
0.39794
0
-0.3915
-0.8069

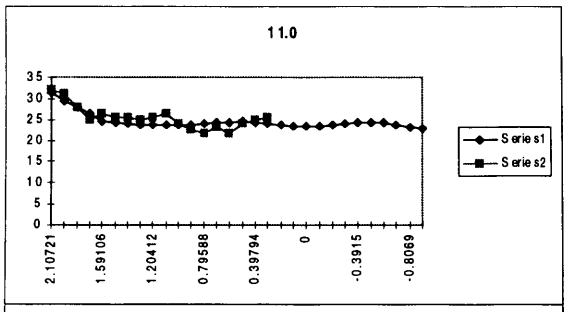
11.0
Series1
Series2
2.10721
1.59106
1.20412
0.79588
0.39794
0
-0.3915
-0.8069

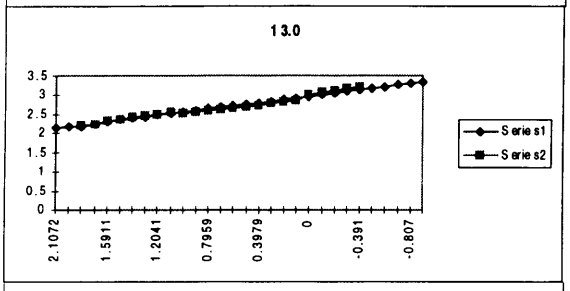
13.0
Series1
Series2
2.1072
1.5911
1.2041
0.7959
0.3979
0
-0.391
-0.807

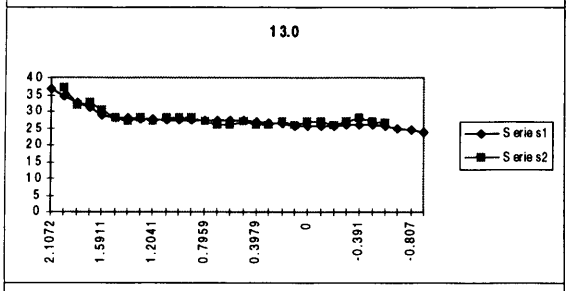
13.0
Series1
Series2
2.1072
1.5911
1.2041
0.7959
0.3979
0
-0.391
-0.807

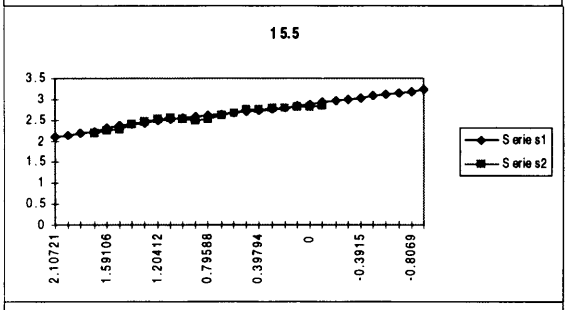
15.5
Series1
Series2
2.10721
1.59106
1.20412
0.79588
0.39794
0
-0.3915
-0.8069

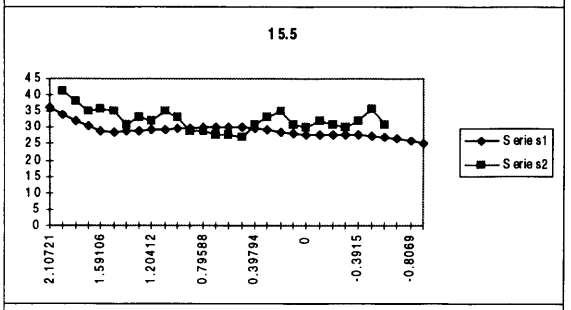
15.5
Series1
Series2
2.10721
1.59106
1.20412
0.79588
0.39794
0
-0.3915
-0.8069

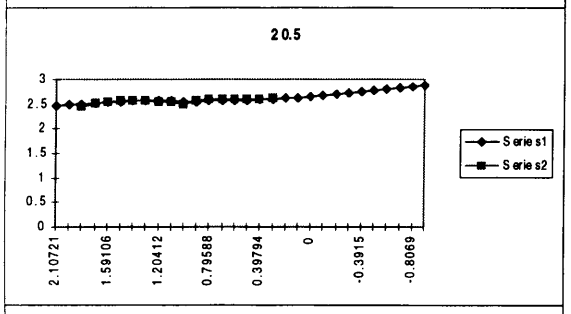
20.5
Series1
Series2
2.10721
1.59106
1.20412
0.79588
0.39794
0
-0.3915
-0.8069

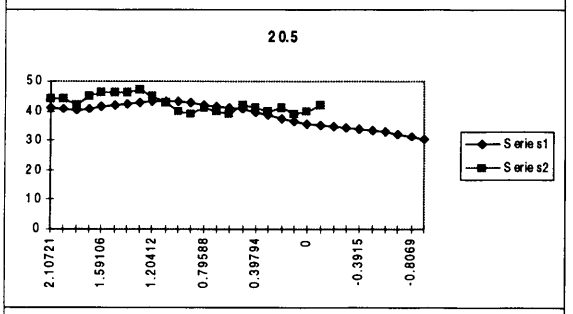
20.5
Series1
Series2
2.10721
1.59106
1.20412
0.79588
0.39794
0
-0.3915
-0.8069

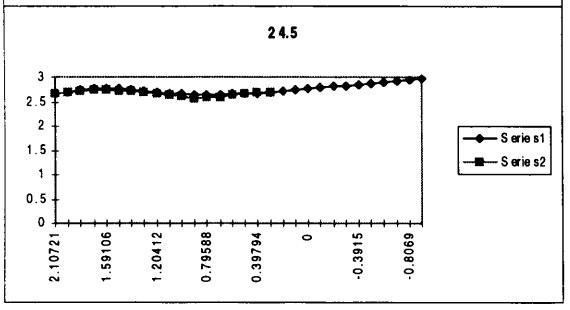
24.5
Series1
Series2
2.10721
1.59106
1.20412
0.79588
0.39794
0
-0.3915
-0.8069

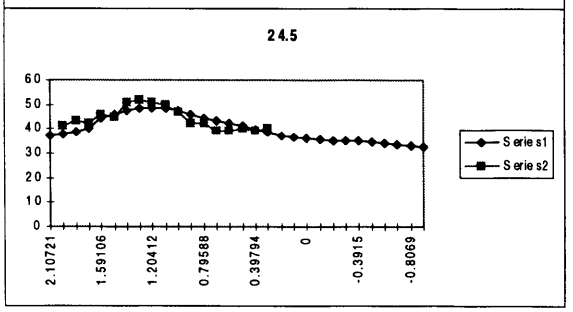
24.5
Series1
Series2
2.10721
1.59106
1.20412
0.79588
0.39794
0
-0.3915
-0.8069

7.2.5 Two Dimensional Geoelecric Model

The resulting 2D geoelectric section from the interactive forward modeling is shown in fig. 7.3. It shows some differences from the original one dimensional model both in terms of resistivity and unit thicknesses. The general structure and orientation of units is however maintained. A general dip to the north is apparent in the model. A unit with resistivity of about 26 ohm.m and thickness of 40-60 m is observed on the surface at the northmost part of the traverse. This unit is underlain

Fig. 7.3 Two dimensional forward modelling geoelectric section for Ayia Marina line 9

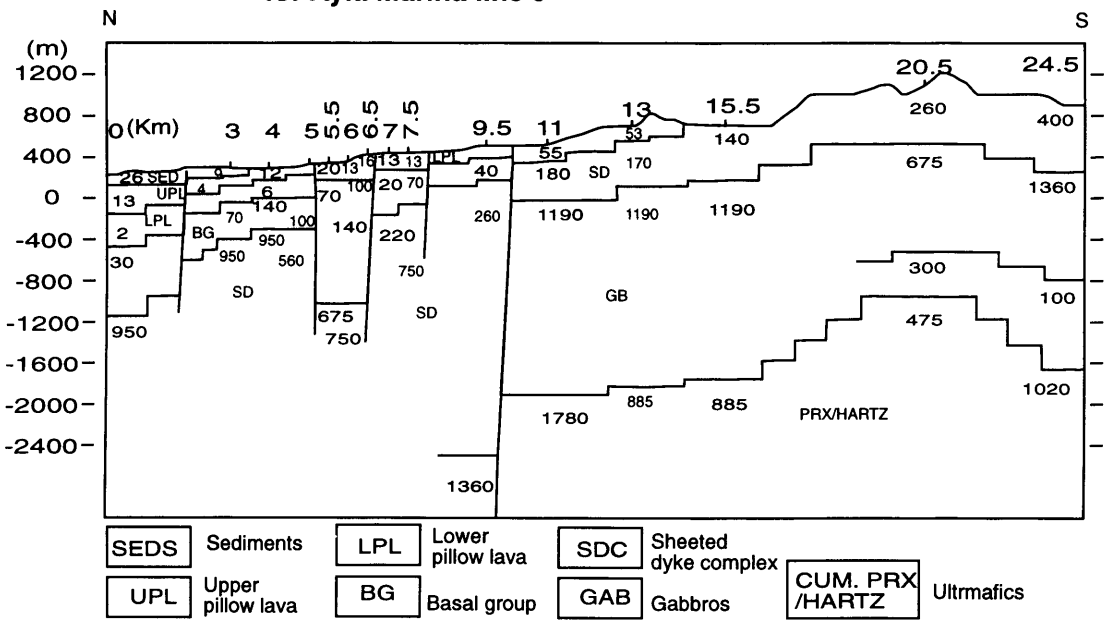

by a 50-200 m unit of a lower resistivity of 9-13 ohm.m. An even lower resistivity unit of 2-6 ohm.m with a thickness of 150-300 m is observed to underlie the 9-13 ohm.m unit. Below these units, the resistivities rise from 20-30 ohm.m to over a thousand ohm.m. As has been observed from 1-D interpretation, the interpreted faults correspond to 5 of the lineaments deciphered by Cooper (1993) (fig.7.4) in Ayia Marina area and agree more with the structures interpreted by Huntings (1969) (fig.7.5). In the southern part of the traverse, the model starts with a 500-600 m thick unit of resistivity between 140-400 ohm.m. This is underlain by a unit of between 1000 and 2000 m thick with a resistivity range of 675-1360 ohm.m. At the

southmost part, a unit of 100-300 ohm.m and 400 to 600 m thick appears next and the whole structure is terminated by a basal unit of 475-1780 ohm.m resistivity.

Fig. 7.4 Structural map of Ayia Marina (after Cooper, 1993)

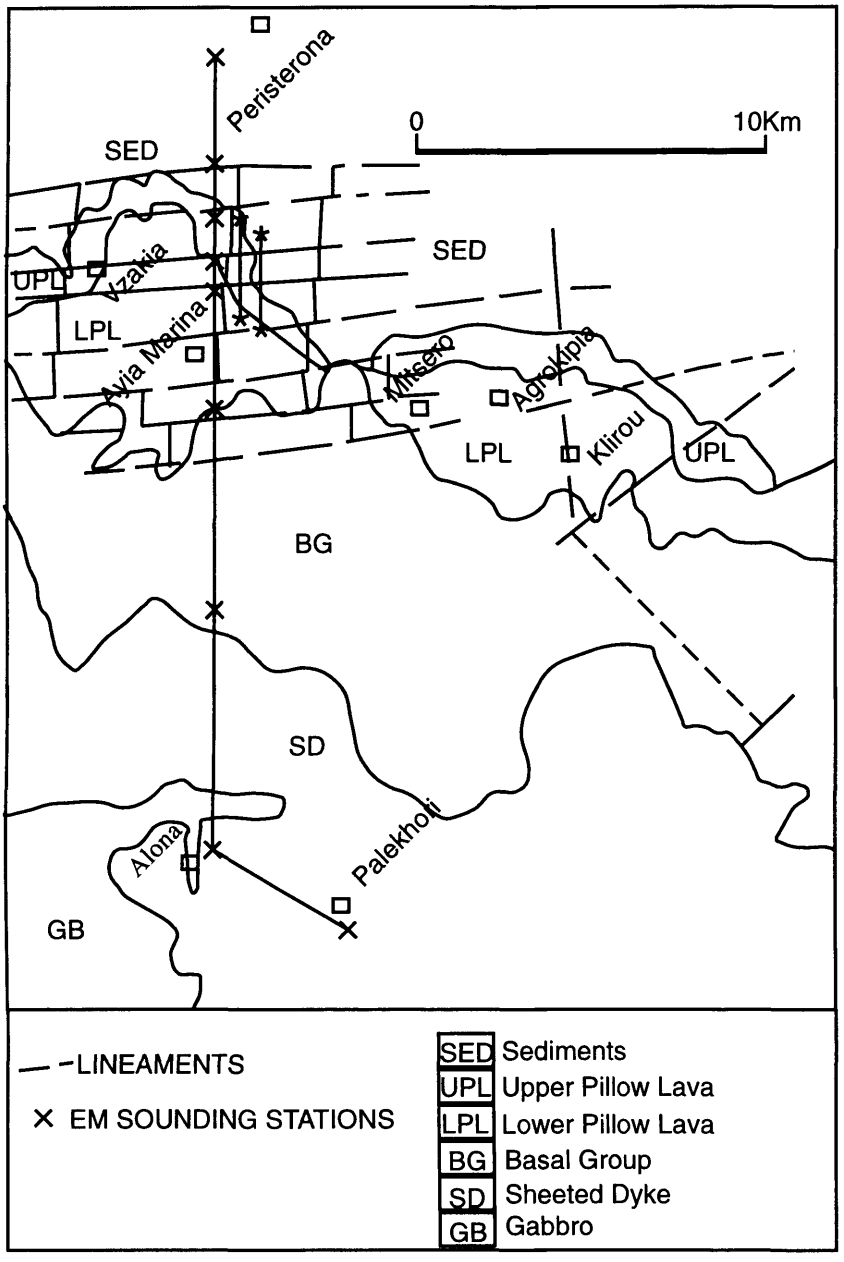

7.3 Two Dimensional Inversion

7.3.1 2-D Inversion Program

The two dimensional inversion program, d2inv-newt, written by Randy Mackie (1994) of M.I.T. was used in this study. The program calculates the maximum likely inverse for a two dimensional magnetotelluric survey using

conjugate gradient relaxation for both the forward and inverse solutions. The network geometry is nodes centred at the top and bottom of each earth block. The program inverts both TM and TE data with the assumption that both have the same frequencies at each

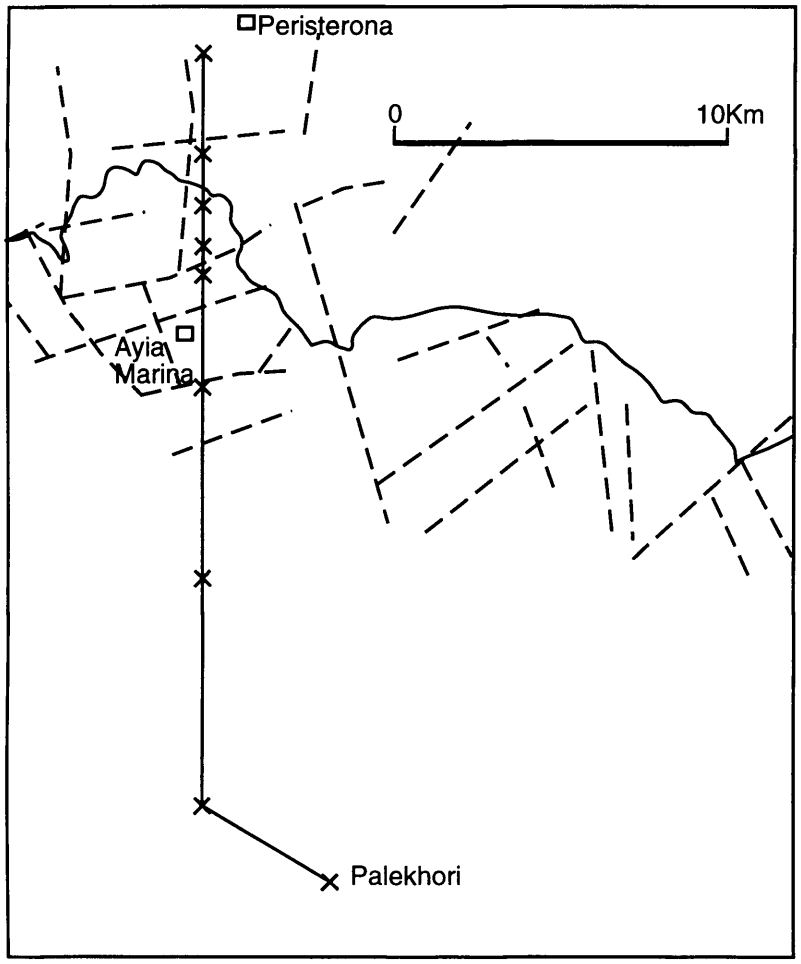

Fig. 7.5 Structural map of Ayia Marina area (after Huntings, 1969)

site. The program is made to allow for and to simulate surface topographic variations. The two dimensional forward geoeletric model shown in fig.7.3 served as the input model for the inversion. The program was then used to derive the optimal resistivity distribution for the region surveyed. The fit of the calculated response curves to the observed field data for both the transverse electric and transverse magnetic modes are shown in fig. 7.6. The quality of fit with minimum

visually achievable error is seen as an indication of the adequacy of the program for this study.

Fig. 7.6a 2-D TE mode MT inversion model fits for resistivity and phase(Line 9) Series1 represent field data while Series2 represent the calculated response

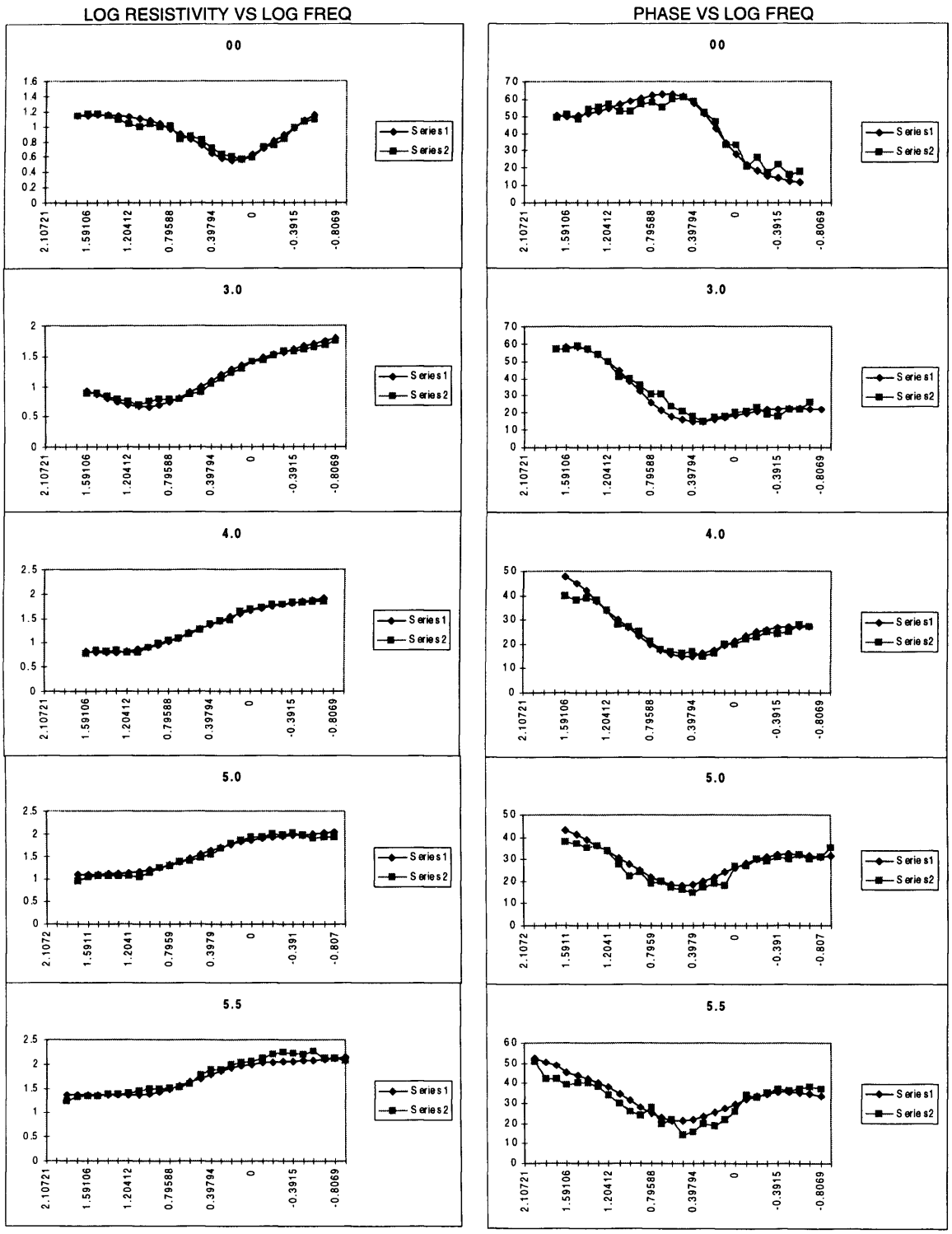

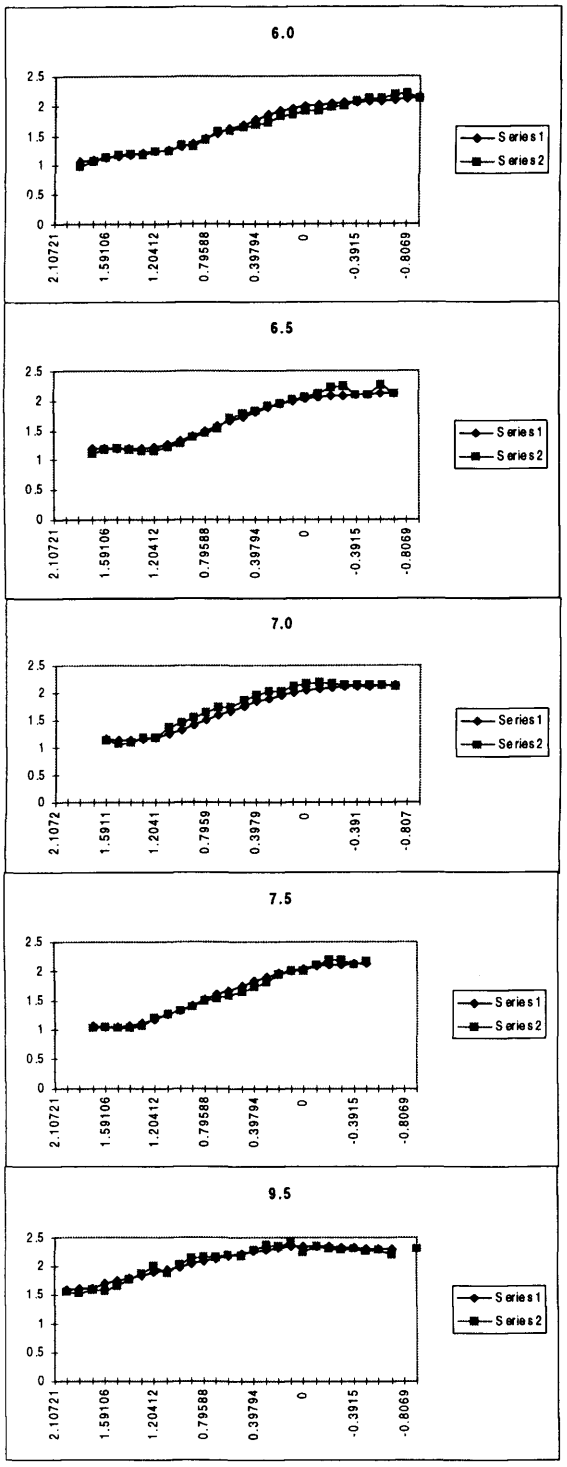
6.0
Series1
Series2
6.5
Series1
Series2
7.0
Series1
Series2
7.5
Series1
Series2
9.5
Series1
Series2

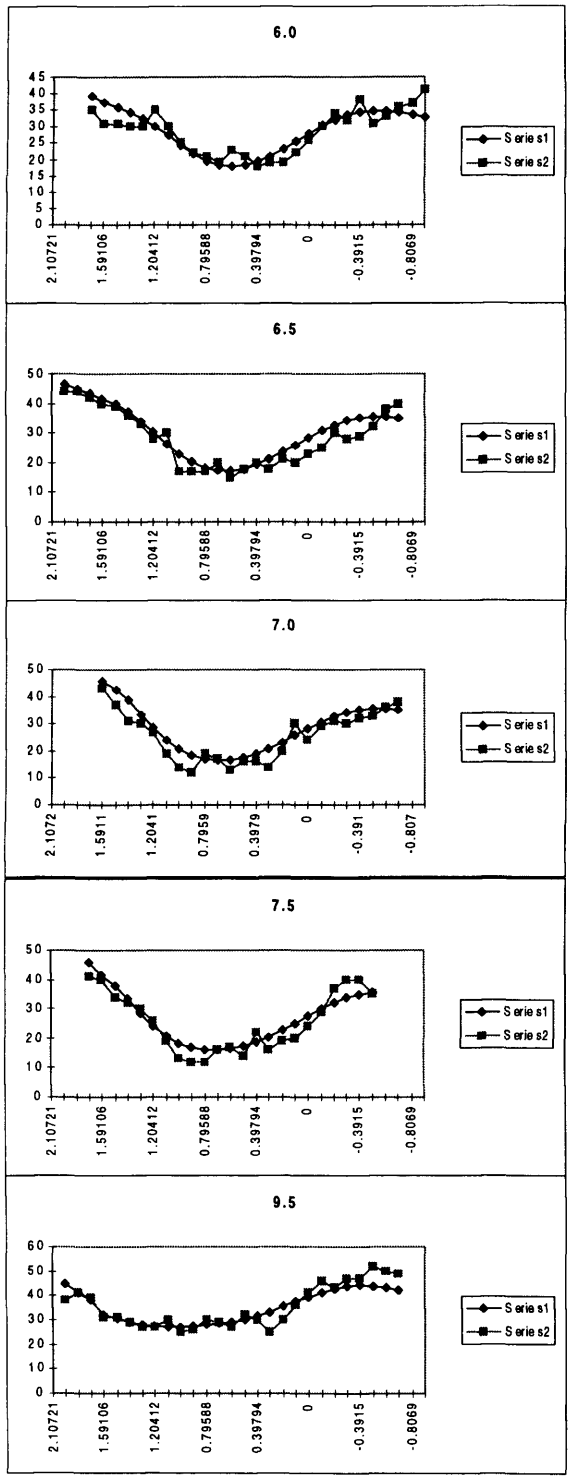
6.0
Serie s1
Serie s2
6.5
Serie s1
Serie s2
7.0
Serie s1
Serie s2
7.5
Serie s1
Serie s2
9.5
Serie s1
Serie s2

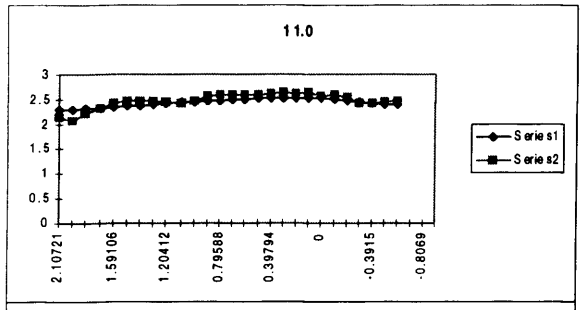
11.0
3
2.5
2
1.5
1
0.5
0
2.10721
1.59106
1.20412
0.79588
0.39794
0
-0.3915
-0.8069
Serie s1
Serie s2

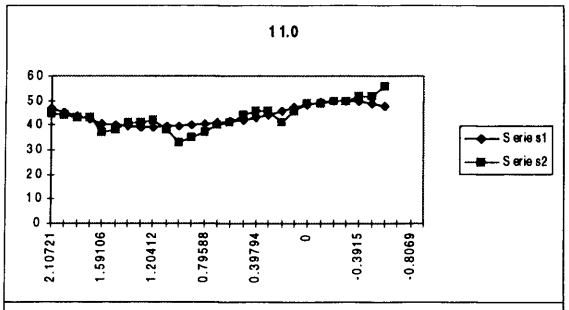
11.0
60
50
40
30
20
10
0
2.10721
1.59106
1.20412
0.79588
0.39794
0
-0.3915
-0.8069
Serie s1
Serie s2

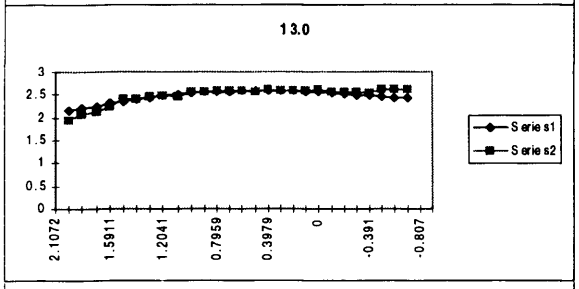
13.0
3
2.5
2
1.5
1
0.5
0
2.1072
1.5911
1.2041
0.7959
0.3979
0
-0.391
-0.807
Serie s1
Serie s2

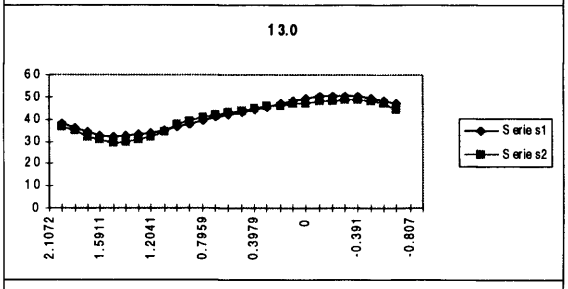
13.0
60
50
40
30
20
10
0
2.1072
1.5911
1.2041
0.7959
0.3979
0
-0.391
-0.807
Serie s1
Serie s2

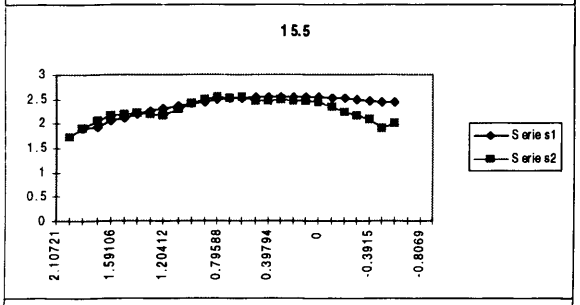
15.5
3
2.5
2
1.5
1
0.5
0
2.10721
1.59106
1.20412
0.79588
0.39794
0
-0.3915
-0.8069
Serie s1
Serie s2

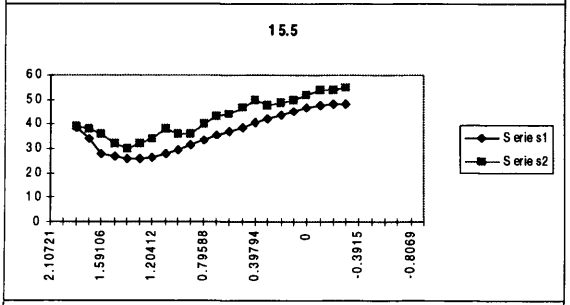
15.5
60
50
40
30
20
10
0
2.10721
1.59106
1.20412
0.79588
0.39794
0
-0.3915
-0.8069
Serie s1
Serie s2

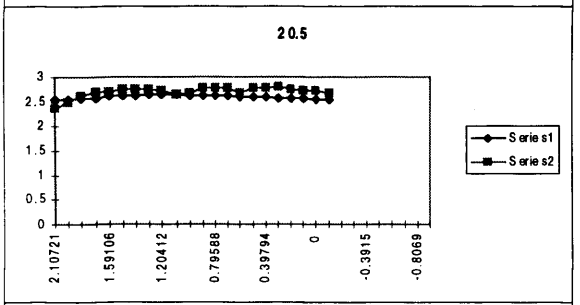
20.5
3
2.5
2
1.5
1
0.5
0
2.10721
1.59106
1.20412
0.79588
0.39794
0
-0.3915
-0.8069
Serie s1
Serie s2

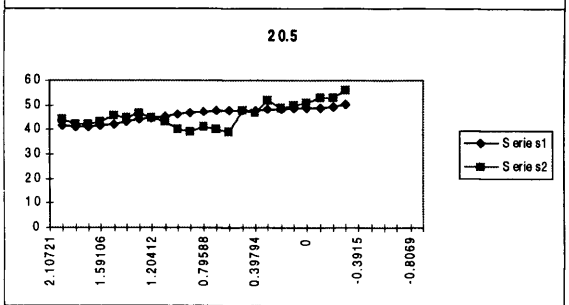
20.5
60
50
40
30
20
10
0
2.10721
1.59106
1.20412
0.79588
0.39794
0
-0.3915
-0.8069
Serie s1
Serie s2

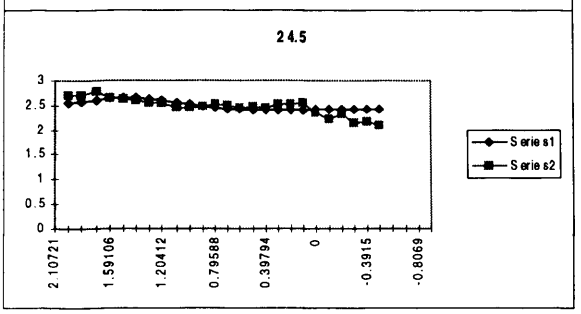
24.5
3
2.5
2
1.5
1
0.5
0
2.10721
1.59106
1.20412
0.79588
0.39794
0
-0.3915
-0.8069
Serie s1
Serie s2

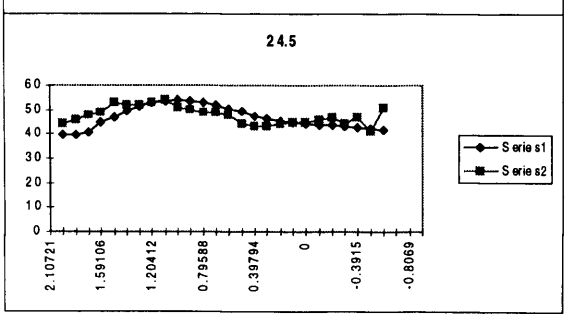
24.5
60
50
40
30
20
10
0
2.10721
1.59106
1.20412
0.79588
0.39794
0
-0.3915
-0.8069
Serie s1
Serie s2

Fig. 7.6b 2-D TM mode MT inversion model fits for resistivity and phase(Line 9) Series1 represent field data while Series2 represent the calculated response

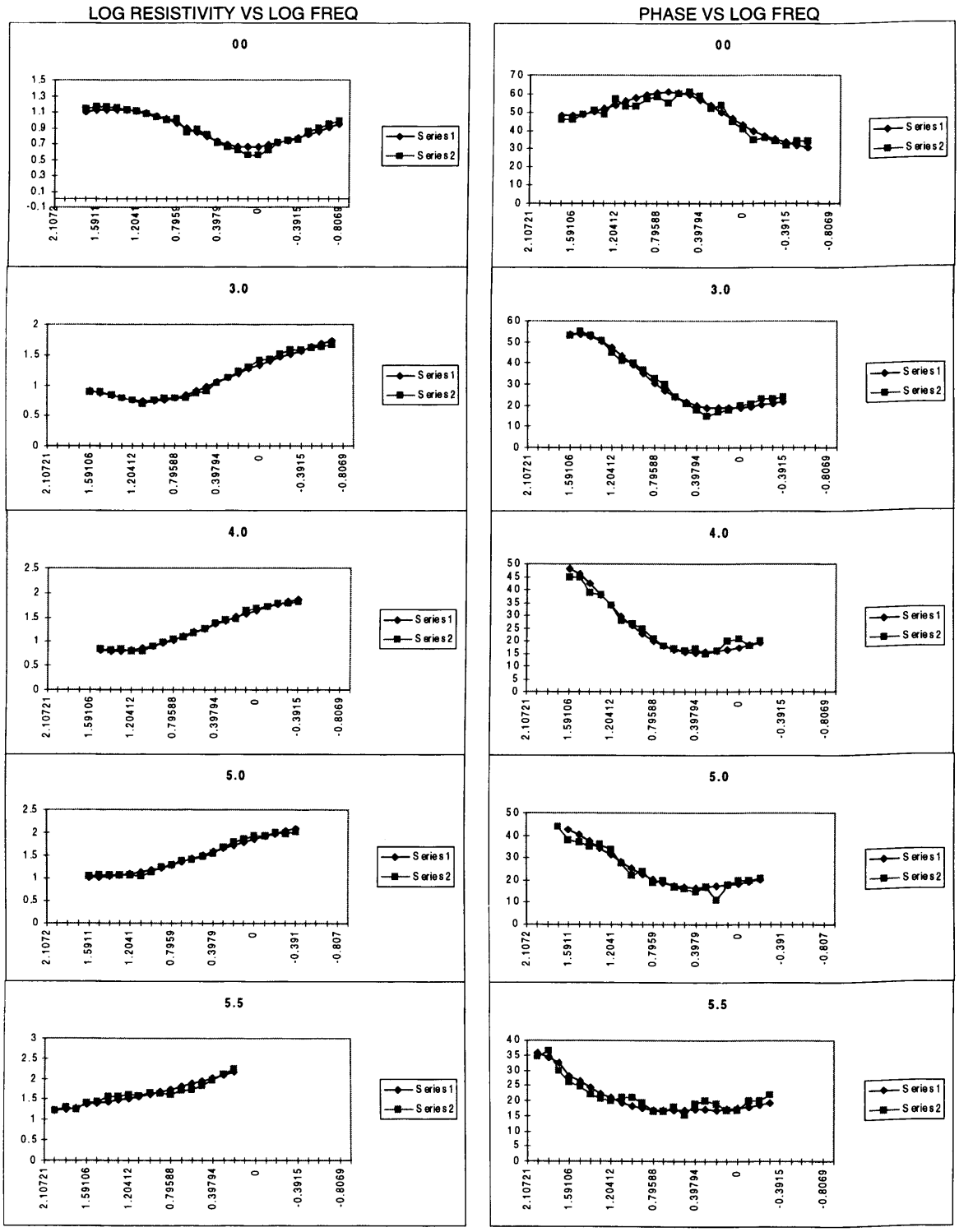

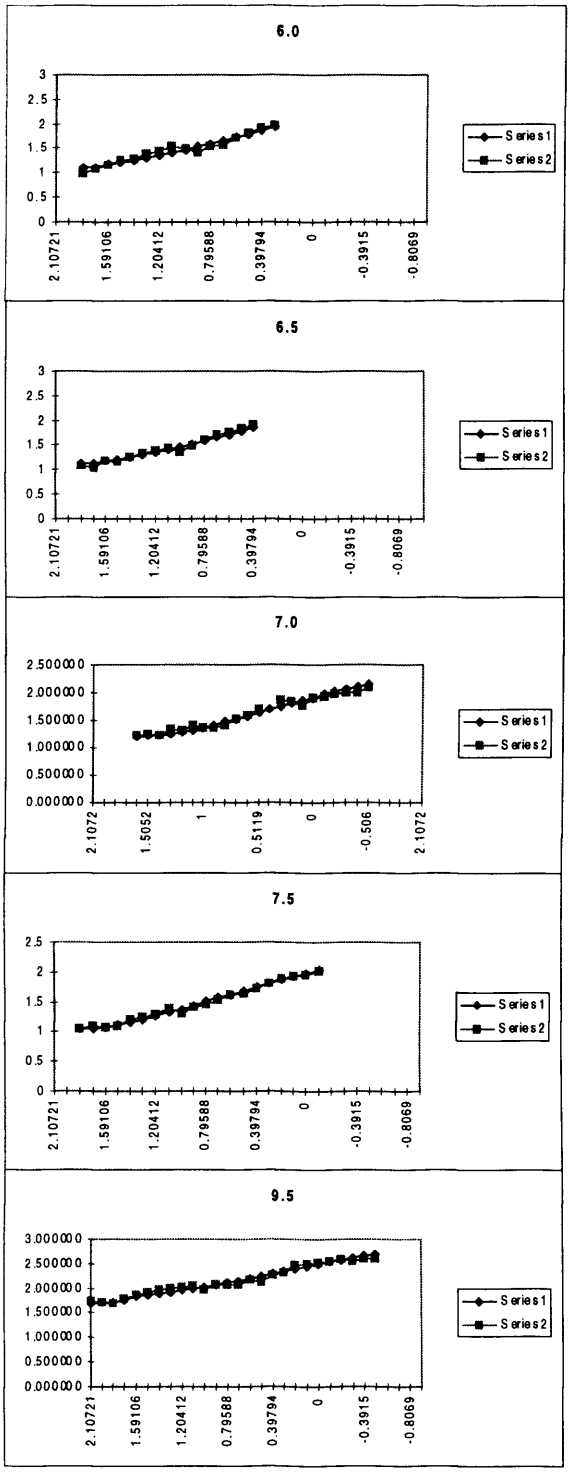
6.0
Series1
Series2
6.5
Series1
Series2
7.0
Series1
Series2
7.5
Series1
Series2
9.5
Series1
Series2

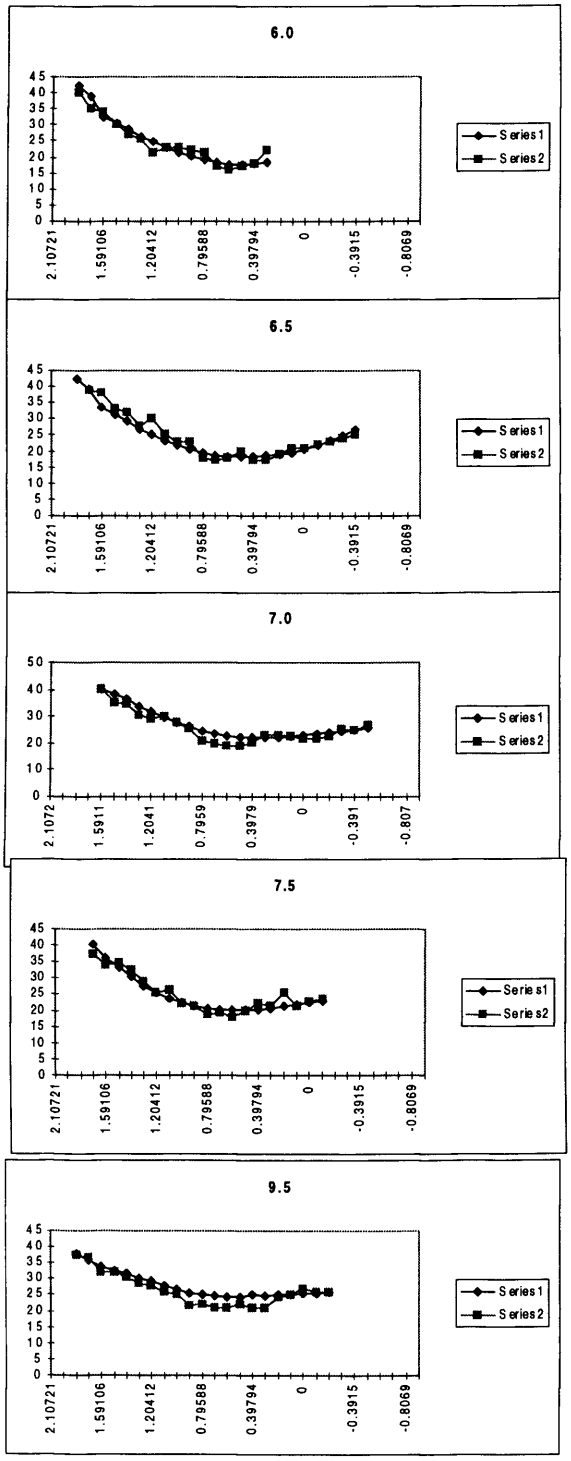
6.0
Series1
Series2
6.5
Series1
Series2
7.0
Series1
Series2
7.5
Series1
Series2
9.5
Series1
Series2

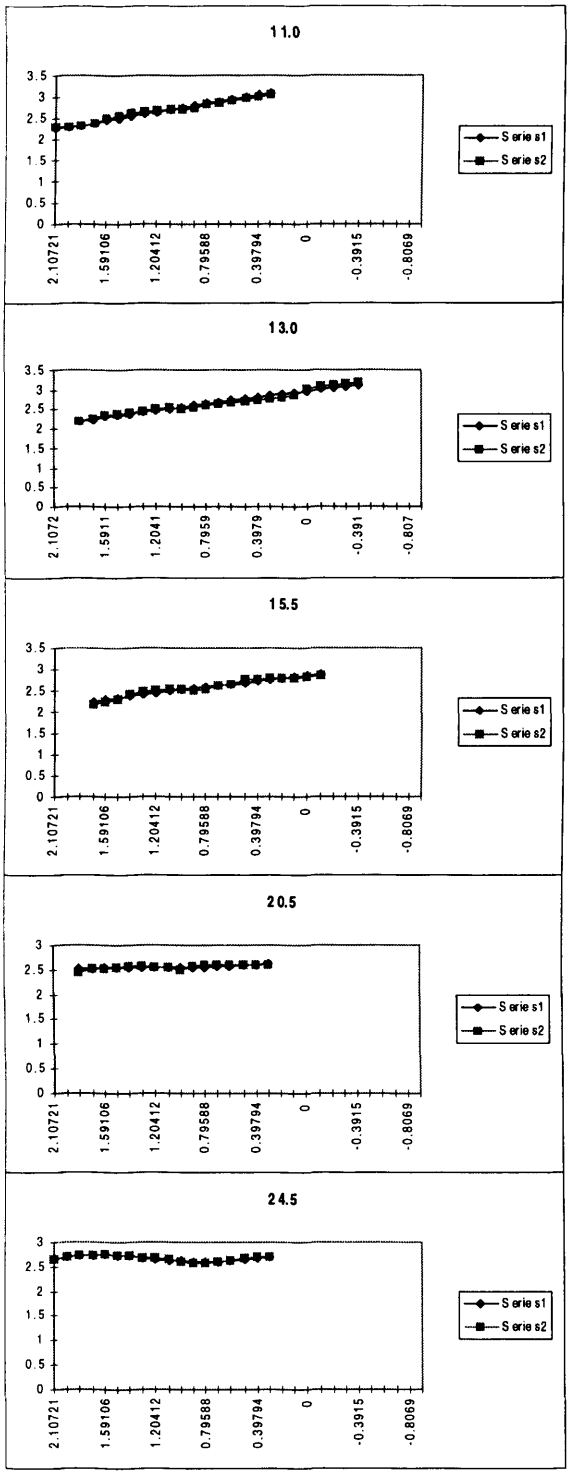
11.0
3.5
3
2.5
2
1.5
1
0.5
0
2.10721
1.59106
1.20412
0.79588
0.39794
0
-0.3915
-0.8069
Series1
Series2

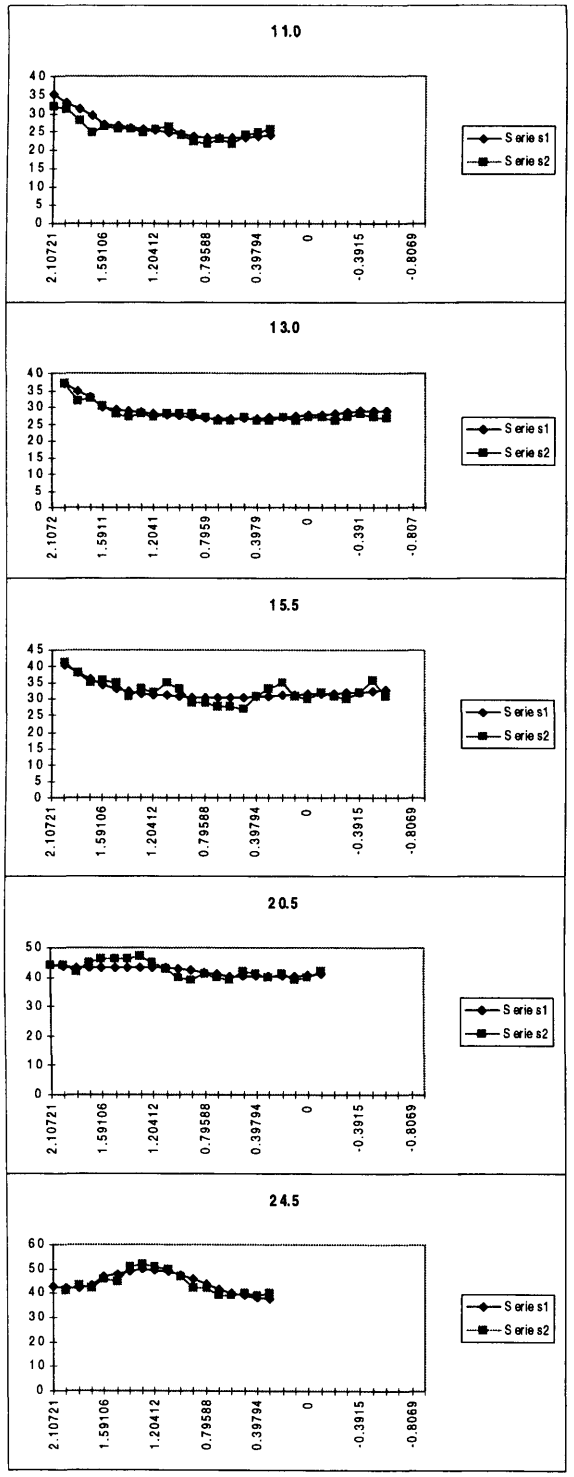
11.0
40
35
30
25
20
15
10
5
0
2.10721
1.59106
1.20412
0.79588
0.39794
0
-0.3915
-0.8069
Series1
Series2

13.0
3.5
3
2.5
2
1.5
1
0.5
0
2.1072
1.5911
1.2041
0.7959
0.3979
0
-0.391
-0.807
Series1
Series2

13.0
40
35
30
25
20
15
10
5
0
2.1072
1.5911
1.2041
0.7959
0.3979
0
-0.391
-0.807
Series1
Series2

15.5
3.5
3
2.5
2
1.5
1
0.5
0
2.10721
1.59106
1.20412
0.79588
0.39794
0
-0.3915
-0.8069
Series1
Series2

15.5
45
40
35
30
25
20
15
10
5
0
2.10721
1.59106
1.20412
0.79588
0.39794
0
-0.3915
-0.8069
Series1
Series2

20.5
3
2.5
2
1.5
1
0.5
0
2.10721
1.59106
1.20412
0.79588
0.39794
0
-0.3915
-0.8069
Series1
Series2

20.5
50
40
30
20
10
0
2.10721
1.59106
1.20412
0.79588
0.39794
0
-0.3915
-0.8069
Series1
Series2

24.5
3
2.5
2
1.5
1
0.5
0
2.10721
1.59106
1.20412
0.79588
0.39794
0
-0.3915
-0.8069
Series1
Series2

24.5
60
50
40
30
20
10
0
2.10721
1.59106
1.20412
0.79588
0.39794
0
-0.3915
-0.8069
Series1
Series2

7.3.2 Two Dimensional Inversion Geoelectric Model

The two dimensional geoelectric section that resulted from the application of the inversion program above is shown in fig 7.7. As can be seen the main structure derived from forward modeling is preserved. The difference is in the modification of some of the resistivity values and slight adjustments to the depths of some of the unit boundaries. For example, the resistivity of the top unit below station 20.5 which was 260 ohm.m in the forward model has been changed to 300 ohm.m in the inverted model while the initial resistivity of 400 ohm.m for the same unit under station 24.5 has been modified to 365 ohm.m in the inversion model. The step-like lower boundary of the second unit beneath stations 5.5, 6 and 6.5 has been adjusted to a straight horizontal boundary in the program's search for an optimal model.

Fig. 7.7 Two dimensional inversion geoelectric section for Ayia Marina Line 9 (Resistivity in ohm.m)

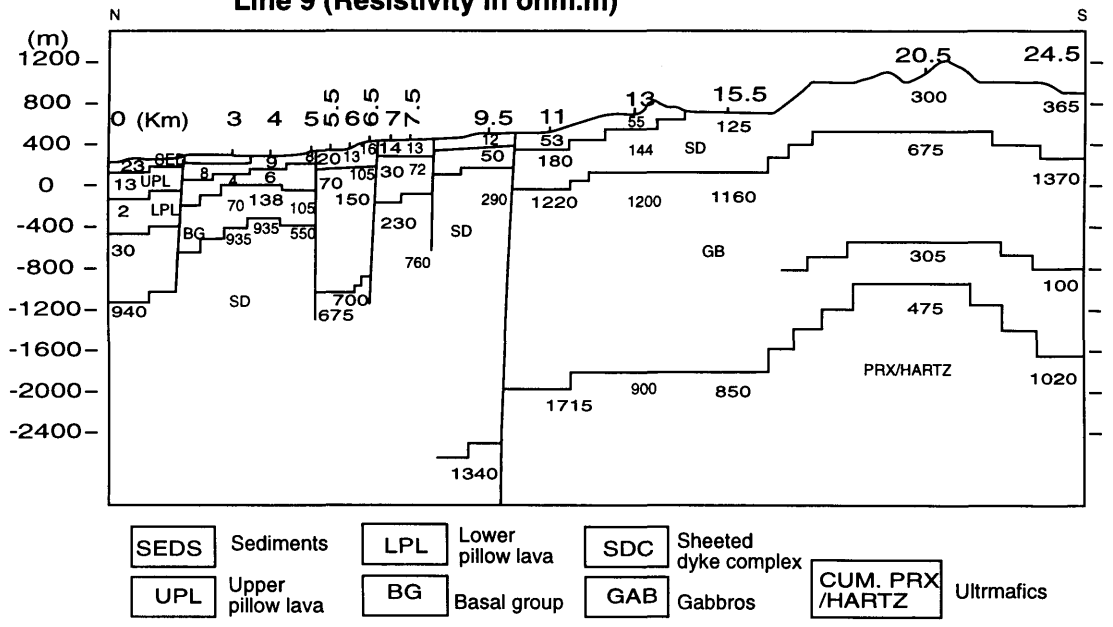

7.3.3 Comparison with 1-D model, Geology and Aeromagnetic data

The two dimensional MT inversion geoelectric section (fig.7.7) compares favourably with the one dimensional joint MT/TEM inversion geoelectric section shown in Fig.6.8. Apart from the depths to the lowermost boundaries at stations 0,

5.5-6.0 Km and the southern part of the section, the structures and unit thicknesses are identical. The only other difference is in the unit resistivity values. This indicates that representative one dimensional geoelectric sections could be obtained from this complex geological environment using the one dimensional joint MT/TEM inversion scheme by Meju (1992, 1996) especially at depths of up to 500 m. This also confirms the observation by some EM workers that representative one dimensional sections can be recovered from complex geological environments like the Ayia Marina area (e.g., Tikhonov and Berdichevsky, 1966; Berdichevsky and Dmitriev, 1976; Raganayaki, 1984; Meju, 1996).

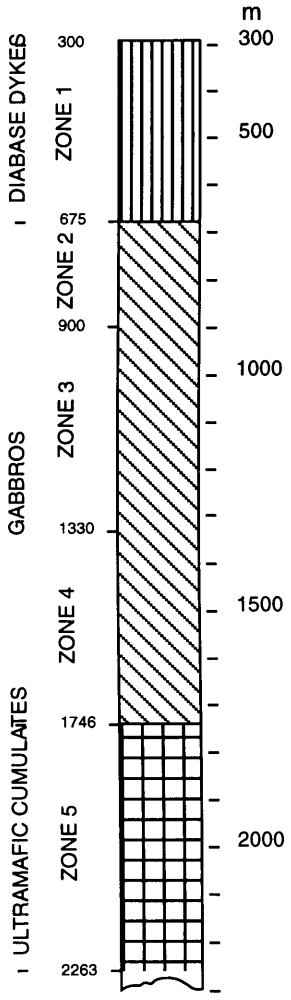

Fig. 7.8 Main lithological units of core from Palekhori borehole (CY-4) (after Malpas et al, 1989; Salisbury et al, 1989)

The lateral resistivity variations along the 2-D MT inversion geoelectric section have enabled the fitting of lateral geological unit boundaries using available geological information and data acquired from field mapping. The variations also enabled the fixing of the five fault structures that closely agree with the five that were interpreted for the area by Huntings (1969) from aeromagnetic data and correspond to five of the eight interpreted by Cooper (1993). At station 24.5 Km (Palekhori) which marks the southern end of Line 9, the 2-D inversion section gives depths of 650 m to the base of the SDC, 1715 m to the base of the gabbros and over 2000 m for the pyroxinite unit which are in close agreement with the values obtained form Palekhori borehole logs (Malpas et al, 1989; Salisbury et al, 1989) as shown in fig.7.8. Based on the structures interpreted from 1-D and 2-D inversion of data from Line 9, their close agreement with aeromagnetic data interpretation by Huntings (1969) and the close correlation of the 1-D geoelectric sections for Lines 5 and 7 with the relevant portion of Line 9 (from stations 5.0 to 7.0), a revised structural map for the Ayia Marina area has been produced and is shown as Fig.7.9.

Fig. 7.9 Modified structural map for Ayia Marina area

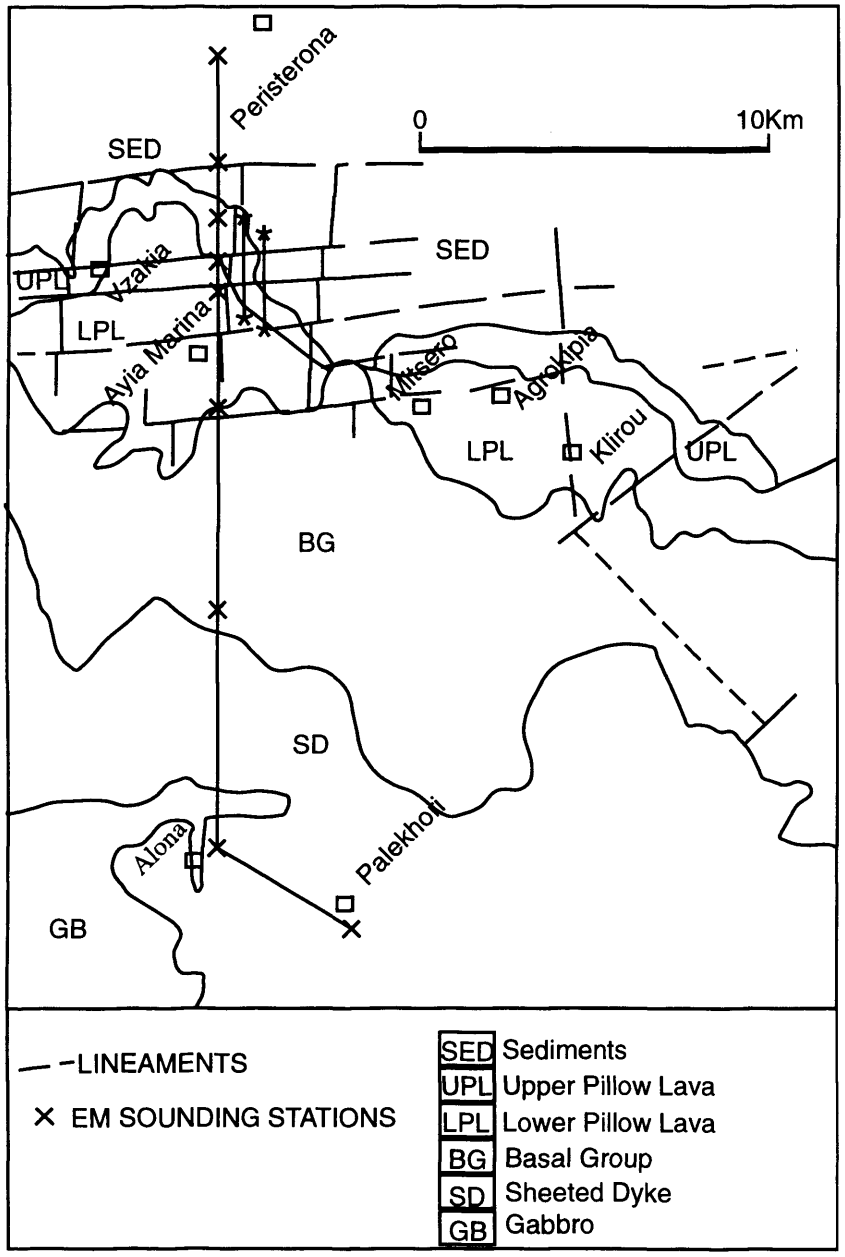

CHAPTER EIGHT

DISCUSSION OF RESULTS AND INTERCORRELATION WITH PRE-EXISTING MODELS

8.1 Introduction

This chapter appraises the resulting interpretative geoelectric sections from the preceding chapters assessing their individual and collective findings, and tries to correlate the results with already existing models from the areas of study. It illustrates how the experience gained from the interpretation of the MT/TEM data from an area of known massive sulphide mineralisation at depth is used in the interpretation of data from an area not yet known to host mineralisation. The regularities of structural control on mineralisation in northeastern Troodos are discussed and the contributions of the results of this study towards a potentially viable electromagnetic massive sulphide exploration model for the Troodos ophiolite environment is illustrated. The general applicability of the MT/TEM methods of exploration to massive sulphide exploration in the Troodos and their inherent constraints are also discussed. The significance of the MT survey in the provision of a 24.5 km geoelectric section across part of north-northeast Troodos is outlined at the end of the chapter.

8.2 Appraisal of Geoelectric Sections

8.2.1 Klirou Test area

The interpretative geoelectric sections for the N-S and E-W lines have been shown as fig.6.4. A quick look at the resistivity-depth sections of the two orthogonal lines shown indicates a somewhat horizontal to slightly dipping

conductive zone (in relation to the other parts) with resistivity of less than 11ohm-m. The 1-D geoelectric sections show that this conductive zone is a clear lithological unit that is known to host the mineralisation in the area. Massive sulphide deposits are usually ideal targets for electromagnetic (EM) methods like the TEM where they are hosted by rocks of contrastingly higher resistivities. In this case, the massive sulphide ore has been silicically altered raising its own resistivity to values similar to those of the lower pillow lava host (Maliotis and Khan, 1980; Kramvis, pers. comm.; Cooper and Swift, 1996). As a result, the TEM/MT methods are not able to detect directly (in isolation) the massive sulphide ore. Spies (1980) has shown that the limits of detection of the TEM method depend to a large extent on the size of the deposit and the conductivity contrast between the deposit and host rock, and that a large body of size 1500 m by 300 m and 150 m thick can be detected at a depth of 350 m if the conductivity contrast between the body and the host is over 50 whereas a smaller deposit with dimensions 900 m by 180 m and 90 m thick requires resistivity contrast of 1000 to be detected at the same depth. He stresses that these results are independent of equipment power or sensitivity, but that in practical exploration such factors as inhomogeneities in the host rock or overburden also need to be taken into account.

However, a comparison of the 1-D Geoelectric sections and borehole sections show that lithological units and boundaries could be clearly deciphered and that 1-D inversion depths and fault locations agree very closely with those determined from boreholes. This is very important. The borehole sections reveal that the faults in the area control the linear extension of the Klirou ore body marking out its limits in essentially all directions and controlling its alignment in the northwest direction. It has been observed that faults control the linear extensions of most of

the massive sulphide ore deposits of the northeastern part of Troodos in two orthogonal directions and this is thought to indicate the relation of ore-forming hydrothermal systems to orthogonal system of faults (Pantazis, 1979; Busby et al, 1983; Adamides, 1984).

Available IP data from Cyprus Geological Survey, measured along the E-W line shows good agreement with the results of the TEM/MT data taken along the same line. Notice the IP anomaly which is right within and constrained by the near vertical faults interpreted in the TEM/MT geoelectrical section. It was based on the IP anomaly that a borehole was drilled which proved to be caused by a massive sulphide ore at a depth of about 80-110m. Note the close agreement between the positions of the interpreted faults in the geoelectrical section and the IP data. It is evident here that a combination of TEM/MT and IP data will go a long way in providing useful information on the location and extent of massive sulphide ore bodies in this type of environment. The combined TEM/MT methods have provided useful and reliable subsurface depth estimates and the position of some structures while distinguishing lithological units from their resistivity variations, and available IP data has furnished the possible location of ore mineralisation in the subsurface.

8.2.2 Ayia Marina Area

The interpretative two dimensional geoelectric section from the 24.5 km Ayia Marina line (fig.7.5) reveals a sequence of rock units that dip gently towards the north. The 23 ohm.m resistivity top unit of 40-80 m thickness in the northern part of the section has been interpreted as part of the sequence of sedimentary rocks that overlie the ophiolite rocks of the northern part of Troodos. An interesting feature is the low persistent resistivity unit (2 ohm.m) observed from the depth of less than 400 m to just over 700 m. The unit coincides with the lower pillow lava rocks which

are known to host most of the massive sulphide deposits in Cyprus. The depth to the low resistivity unit becomes shallower as one moves southwards to depths of about 140 m before outcropping on the surface further south. The unit also shows a gradual increase in resistivity value from the 2 ohm.m to 4-6 ohm.m and to 13-16 ohm.m where it outcrops on the surface. The faults that have been inferred from obvious unit boundary discontinuities are in accord with some of the east-west lineaments that have been described from the interpretation of available aeromagnetic data by Cooper (1993). The faults give the northern part of the section (or area) a step and block faulting (horst and graben) effect that is characteristic of the fossil axial valleys that mark the spreading centres that have been identified in the Troodos (Gass, 1980; Searle and Panayiotou, 1980; Varga and Moores, 1985). A thickened unit of resistivity between 70 and 150 ohm.m, which coincides with the zone of the basal group is thought to represent a downthrown block in the area.

In general the one dimensional model appears to have slightly underestimated the depths to the boundaries of units beyond about 300 m depth. For example, at the southernmost sounding (24.5 km-Palekhori) location on the section, the one dimensional inversion model gave depths of about 500 m to the base of the top unit, interpreted here as the sheeted dyke complex, about 1500 m to the base of the second unit corresponding to the gabbros and about 1850 m to the base of the third unit, thought to represent the pyroxinite/hartzburgite. The two dimensional inversion however gave corresponding depths of around 650 m to the base of the sheeted dyke complex, 1715 m to the base of the gabbros and over 2000 m for the pyroxinite which are very close to the borehole depths for the same units in the area (see fig.7.6). While the TEM data have constrained the shallow depth information and have been very useful in the static correction of the MT data,

the MT data have furnished and constrained the structure at depth. Notice however, that the 100-300 ohm.m unit which coincides with the top of the pyroxinite/hartzburgite unit is not clearly observed north of the 15.5 km location. As a whole, the MT and TEM data sets have together revealed essentially all the lithological units of the Troodos ophiolite and their basic structural relationship at depth in the area worked.

8.3 Regularities, Structures and Controls on Mineralisation

The most obvious regularity in the distribution of massive sulphide deposits in the Troodos in general appears to be their exceptional relationship to the pillow lava series and in particular their location in certain lithostratigraphical levels within the series. So far, only disseminated sulphide mineralisation is known to occur in the rocks of the basal group and the sheeted dyke complex, and none has been reported to the author's knowledge in the lower plutonic complex. Within the pillow lava series, massive sulphide mineralisation is known to occur mostly at two main levels which are the boundaries of the lower pillow lavas with the basal group and the lower pillow lavas with the upper pillow lavas. Analysis of geological maps indicate that while most of the massive sulphide deposits in the Troodos correspond to the levels identified above, some of them like the Skouriotissa deposit, the Sha deposit and the Klirou deposit indicate the presence of a third level of sulphide mineralisation location within the lower pillow lava unit. This intermediate level would be between 40 and 200 m below the contact between the lower pillow lava and the upper pillow lava. Although the main sulphide ores in terms of productivity are located in the first two levels, judging from the Sha deposit, the productivity of the deposits in the intermediate level may include not only small deposits but also medium resource deposits.

The first indication of structural control on the distribution and location of massive sulphide deposits in the Troodos appears to be in the linear extension of about 50% of the deposits in two orthogonal directions which are NW 320°-340° and NE 50°-60° (fig.8.1). This observation emerges clearly from the analysis of the spatial distribution of all manifestations of mineralisation including gossans and umbers. In general all the deposits and prospects, and most of the gossans and umbers show some linear alignment to these directions and most of them appear to be located at the intersections of linear zones aligned in these directions in northeastern part of Troodos (fig.8.2). Practically all identified surface outcrops of sulphide mineralisation are marked by gossans. Umbers, which are metalliferous sediments, appear to have strong genetical and spatial relationship with massive

Fig. 8.1 Rose diagrams of directions of major lineaments in NE Troodos

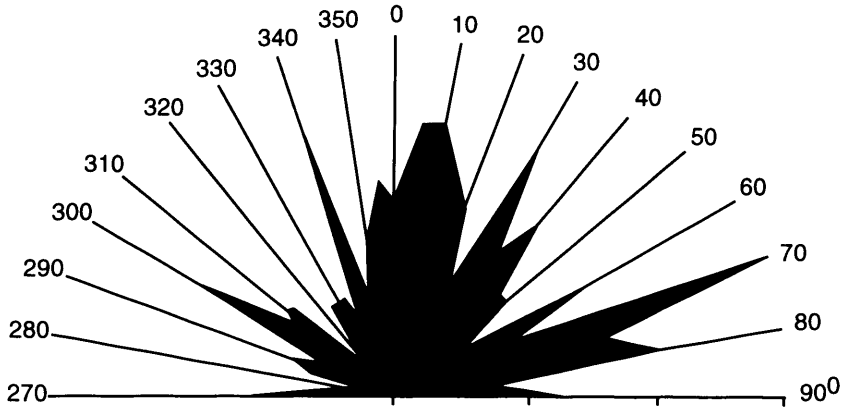

(a) From satelite imagery data

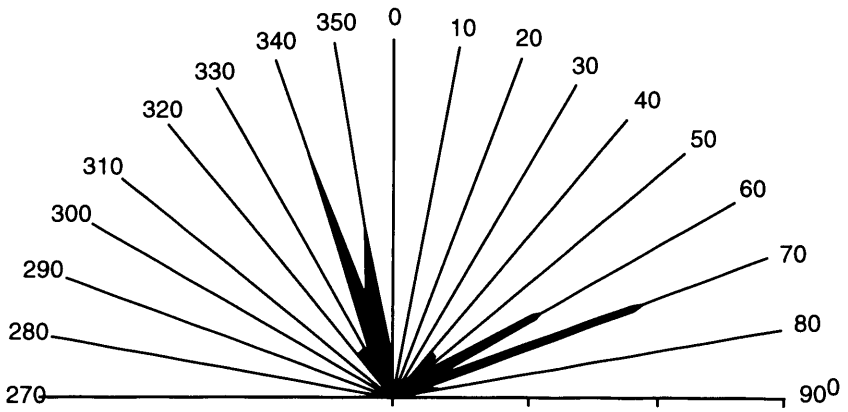

(b) From zones of ore mineralisation

sulphide ores. In Cyprus however, umbers are generally separated from the main sulphide mineralisation location in the lower pillow lava by the upper pillow lava suite and only the Skouriotissa deposit appears to be covered directly by a horizon of umbers.

The location of the sulphide mineralisations in the linear zones determined above and in particular their location at the areas of intersection of these zonessuggest a relationship between the ore-forming hydrothermal systems and the orthogonal system of faults especially their areas of intersection. A comparison of the linear zones of mineralisation location and faults determined from satellite imagery (Mineral exploration in western Cyprus, 1983) and aeromagnetic data interpretation (Huntings,1969; Cooper, 1993) reveals that only faults of direction NW 320°-335° with maximum at about 340° and NE 45°-85° with maximum at about 70° (fig.8.1) actually appear to belong to the ore controlling structures. Note that faults of predominantly NNE 0°-20° and 30°-40° directions do not appear to have any relationship with the sulphide mineralisations, but for example in areas like the Sha

Fig. 8.2 Allignment of orebodies with lineaments in the northeastern part of Troodos (after Huntings, 1969 and Cooper, 1993)

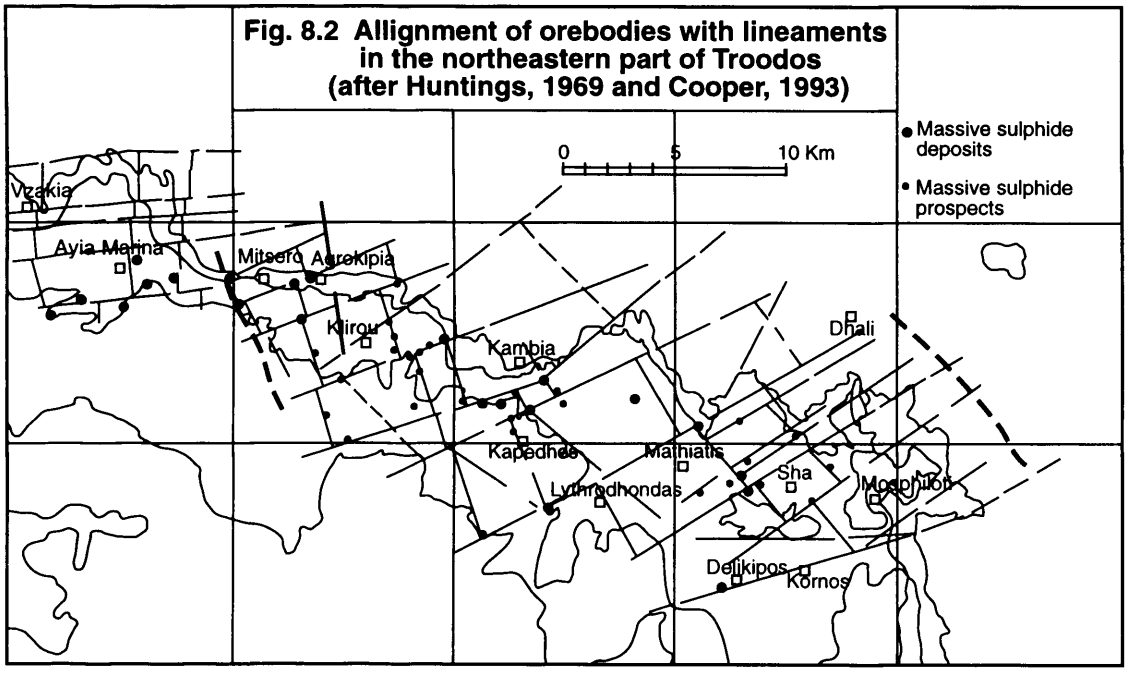

and Klirou they are related to the post mineralisation stage leading to the block structures observed in the areas.

The observation that most of the sulphide deposits and prospects on the Troodos massif occur at areas of intersection of linear NW and NE zones is in accord with information from modern tectonic environments of sulphide mineralisation in rift valleys of ocean basins (Varga and Moores, 1990). This is also in agreement with the proposition that the Troodos ophiolite was produced at a constructive (spreading) margin in a marginal back-arc basin (Gass, 1980) where the NW striking faults are parallel to the spreading axis and the transverse NE striking faults correspond to the transform direction. Indeed work by Richardson et al (1987) and Varga et al (1992) has indicated the existence of zones of pervasive, massive epidosite which strike parallel to the axis of the Solea graben and to the strike of normal extensional faults. They have also observed that evidence from preferential epidotisation in weakly altered areas surrounding massively altered regions suggest that the initial mineralising fluid flow was focused along joints, microfaults and low-angle normal fault zones related to graben formation. The structural location of sulphide mineralisation along longitudinal faults parallel to the spreading axis and transverse faults parallel to transform faults appears to be typical for both modern and ancient peripheral ocean basins. However, the location of mineralisation and by extension their associated mineralising fluids to the areas of intersection of the longitudinal (spreading related) and transverse (transform related) faults seems unique to the Troodos and is yet to be reported for modern spreading centres in the oceans.

8.4 Massive Sulphide Deposit Potentials

Virtually all the surface and near surface sulphide deposits and prospects in Cyprus have been identified as a result of exploratory drilling in the vicinity of ancient slags and over gossans. Even the limited Induced Polarisation (IP) success in locating buried massive sulphide mineralisation has been attributed to exploratory drilling over gossans than to any geophysical methodology. Every known surface expression of massive sulphide mineralisation in the form of gossan or slags has been explored such that every sulphide mineralisation exposed at the current erosional surface is known. In addition almost all the known economical sulphide deposits have been worked out. For any additional sulphide resources therefore, attention has shifted to buried massive sulphide mineralisation not yet seen at the present erosional surface and how they can be located if at all they do exist.

It is believed that many more massive sulphide mineralisations occur buried below the surface. This belief stems from an understanding of the geological environment of the sulphide mineralisations of the Cyprus Troodos ophiolite complex. First of all, the small thicknesses of massive sulphide orebodies indicate that the relatively thick pillow lava series host can hold as many of them as possible if the conditions are right. Secondly, the occurrence of the massive sulphide mineralisations at different levels within a very thick host means that where these potential levels are buried, any sulphide mineralisation they hold will be buried along with them. The fact that the pillow lava series dip gently to the north beneath the sedimentary rocks of the Mesaoria basin implies that a number of massive sulphide orebodies, either initially exposed by weathering and erosion or not, could be buried within the pillow lavas beneath the sedimentary series. Also, from general experience in other parts of the world, economic exploitation of buried small to

medium massive sulphide orebodies does take place at depths of upto 500 m (0.5 km) with the greatest orebodies being mined at maximum depths of between 1 and 1.5 km.

Although the distribution and location of the Troodos massive sulphide deposits is mostly controlled by the intersection of the longitudinal and transverse faults corresponding to the spreading and transform directions respectively, not all these areas of intersection in the region of the pillow lavas currently exposed at the surface have been recognised to host massive sulphide deposits. Those areas of intersection not yet known to host these deposits represent potential ore-bearing zones and perhaps require further investigation. The exploitation of buried massive sulphide deposits would certainly be more complicated and more expensive and as such the deposits at depth must be better enriched in metal content than the surface or near surface deposits if they are to be economically viable.

8.5 Discussions

The lack of new surface or near surface massive sulphide deposits in Cyprus has meant the search for buried deposits in the Troodos ophiolite complex. The lack of appreciable resistivity contrast between the generally low resistivity pillow lava rocks and the variably altered massive sulphide deposits, the relatively small size of the deposits and the lack of vertical and horizontal homogeneity of the host pillow lavas with their associated fractures and dykes have combined to produce complex inconsistent target to host contrasts. This has made the direct detection of buried mineralised bodies a difficult geophysical task in the Troodos. Traditional geophysical methods have only been useful in the evaluation of gossans and the environments of known deposits. To be able to locate buried massive sulphide deposits therefore, other indirect methods of ore location have to be explored. The

Troodos massive sulphide deposits have been shown to have been deposited by exhalative action of hydrothermal solutions into the Cretaceous sea floor within the volcanic zone of the ophiolite (Constantinou and Govett, 1972; Searle, 1972). The hydrothermal fluids and their associated exhalative massive sulphide mineralisations are genetically related to major fracture zones (Pantazis, 1979; Busby et al, 1983; Adamides, 1984) which provided the channel ways for the mineralising fluids. Locating these major fractures and faults that controlled mineralisation is one way of locating the positions of the sulphide ores.

To use fractures and faults in the determination of the location of associated massive sulphide mineralisation, one has to determine the type and group of faults to use and the type of rocks in which to look out for them. This has been done in a previous section (section 8.3) for the northern slopes of the Troodos and have been found to be the NW and NE striking faults, parallel and perpendicular to the spreading axis. The study at the Klirou test site showed that armed with the knowledge of the type of faults that host the mineralisation and the host rock, the use of the joint MT/TEM methods to detect the positions and directions of faults in the area will go a long way in helping to detect the probable location of massive sulphide mineralisation in such an area. Where the selected group of faults are present and constrain coincident IP or geochemical or geological anomaly, a potential massive sulphide mineralisation may have been located in the area.

The group of NNW and ENE trending structures that have been interpreted from aeromagnetic data for the Ayia Marina seem to correspond to the location of the western flank of the Mitsero graben. The model section resulting from the Ayia Marina line 9 traverse has picked up in its northern part fault structures that correspond to these structures. It is envisaged that the extrusion of the Troodos massive sulphide lavas took place at the flanks of the spreading axes (Adamides,

1984). Also, this northern part of the interpretative geoelectric section reveals clearly a very low resistivity zone below the surface with resistivity values of 2-4-6 ohm.m. Constantinou and Govett (1972) concluded that virgin concealed deposits should be sought for only beneath olivine basalts and that because ochre is spatially and genetically associated only with sulphide mineralisation, its identification would lead to virgin sulphide deposits. North of Ayia Marina town in the faulted area mentioned occurs olivine-bearing volcanic rocks, also about 2 km north-northwest of Ayia Marina is a site for the extrusion of upper pillow lava where an andesite plug in two parts covering eight acres occur (see Carr and Bear, 1960). A combination of all the factors enumerated above tend to suggest that the very low resistivity zone observed in the northern part of the model may correspond to an area of volcanic and subsequent hydrothermal activity and therefore a prospective zone for the location of buried massive sulphide mineralisation. This is an example of the integration of all available geological, geochemical and geophysical information in the interpretation of an anomaly.

Active hydrothermal systems generally cause significant physical changes to their host rocks and the resultant anomalies, once the system has cooled down, are amenable to detection and delineation by geophysical methods (Allis, 1990). However, the resistivity values would have increased due to these changes, and varying erosion, weathering, or tectonic deformation may have caused additional changes to the resistivity pattern. Many of the resultant anomalies may be one or two orders of magnitude larger in area than the target zone of precious metal or sulphide ore mineralisation. In the absence of other information indicating probable mineralisation zones, the recognition of these large scale anomalies is a prerequisite for identifying areas of potential mineralisation. Clearly, each epithermal prospect has its own unique combination of hydrothermal and geological

histories which determine the large scale resistivity patterns of fossil geothermal systems (Allis, 1990). Generally, where the resistivity of the host rock is more than 50 ohm.m, then resistivity mapping is capable of delineating the extent of both active and fossil hydrothermal systems. In the Troodos ophiolite complex, the low resistivity of the host rock and the lack of appreciable resistivity contrast between the host rock and the fossil hydrothermal alteration or mineralisation zones makes the detection of the zones difficult. The variability and subtlety of the geological, geochemical and geophysical signatures of epithermal systems usually means that no one exploration method can be relied on, and an integration of all types of data is essential.

Often post mineralisation alteration, such as that caused by late stage acidic fluids, or by deep weathering, is sufficient to cause the bulk resistivity of silicified rock to be lowered. In addition, current channeling in low resistivity zones tends to make electrical prospecting methods insensitive to local high resistivity zones (Allis, 1990). In IP surveys of massive sulphide deposits in epithermal systems, clay and zeolites which form one source of noise in such surveys, may be the dominant source of IP anomalies. However, the coincidence of IP anomalies with low resistivity can be a useful indicator of hydrothermal argillic or propylitic alteration zones (Allis, 1990; Izawa et al, 1990) as shown in the case of Klirou sulphide mineralisation.

8.6 Significance of MT Survey in the Troodos

This study has for the first time revealed the geoelectrical section of part of the Troodos ophiolite complex at such a scale. The long Ayia Marina-Palekhori section shows the general distribution of subsurface resistivity and lithological unit depths along the line of section in the region of study. The MT method has given

the resistivity distribution at such low frequencies that reflect deeper subsurface structure, which can not be obtained by other electrical and electromagnetic surveys. The TEM survey has furnished the resistivity distribution of the shallower subsurface structure providing the information at shallower depth that would otherwise not be revealed by the MT method of exploration. The resulting geoelectric section shows that the different resistivity units revealed by the MT/TEM survey correspond to specific lithological units confirming the usefulness of the methods in subsurface lithological and structural mapping especially in areas with rocks of contrasting resistivities. This survey has shown that using the right field system and the right measurement frequencies, the deep geoelectric structure of the Troodos ophiolite can be revealed. This is very important in the study and understanding of the electrical structure and characteristics of the Troodos ophiolite at depth. The complementary roles of the MT and TEM methods where the TEM data constrains the shallow depth information and helps in the correction of static shift in MT data, and where the MT method constrains the information at depth, have been demonstrated.

CHAPTER NINE

CONCLUSIONS AND RECOMMENDATIONS

9.1 Introduction

In this chapter, the salient points emanating from the results of the preceding chapters are brought together in the form of concluding remarks. The results illustrate the contributions of the different methods and techniques used in this study and highlight the importance of the integration of all available geological, geochemical, borehole and geophysical information in the interpretation of anomalies in geologically complex environments like the Troodos. The effectiveness of the joint MT/TEM methods in structural and lithological mapping yielding reliable depth estimates and their limitations in the Troodos environment, are also demonstrated. Recommendations for future massive sulphide exploration programmes in the Troodos are given at the end.

9.2 Conclusions

The main importance of the study of fault control on massive sulphide mineralisation location in the metallogenesis of the Troodos ophiolite complex will be the establishment of limits for the massive sulphide mineralisation zones. In this respect, the ability to remotely determine reliable depth estimates, lithological units and structural position using fairly cheap TEM/MT sounding data in comparison to more expensive drilling could be seen as a useful cost saving measure in this environment. Where the deciphered lithological units and structures closely match those known to host massive ores, and where the geological, geochemical and other relevant available information match those known to occur in recognised massive sulphide environments, further work could then be undertaken in the area.

In conclusion, a number of observations are made from this study:
The joint MT/TEM methods of exploration have been very useful in providing geoelectric sections along short and fairly long traverses showing the subsurface resistivity distribution across the areas studied. They have also enabled the retrieval of reliable estimates of depth to resistivity boundaries which are comparable to depths measured in boreholes. The resistivity units correspond directly to the subsurface lithological units known to occur in the region. This is very important as it confirms the usefulness of the methods in subsurface lithological mapping in this type of area and especially in areas where the lithological units have contrasting resistivities.

MT/TEM sounding data are useful in the determination of the locations of fault structures in this type of environment particularly where varying resistivity units occur on adjacent sides of the fault. The use of small station interval provides closely spaced or denser data and thereby denser subsurface information leading to better constrained subsurface unit resistivity interpretation and more reliable interpretive geoelectric section. This goes further to affirm the effectiveness of the methods in general structural mapping.

Although the joint MT/TEM methods could not directly detect the subsurface massive sulphide mineralisation because of their size, the variable hydrothermal alteration effects and the associated dykes and structures of the host pillow lava, and hence the absence of distinct resistivity contrast between the orebodies and the host rocks, they were able to furnish useful information on the host rocks and the structures that control the mineralisation in the area of Troodos studied leading to a potentially viable exploration model. In this model, when the structural and lithological information thus recovered is combined with available geological, geochemical and any relevant geophysical data (especially IP), the locations of

potential massive sulphide deposits may then be determined. Where Induced Polarisation (IP) data is available, it helps in the determination of probable subsurface massive sulphide mineralisation location from the observed IP high metal conduction factor or percent frequency effect anomaly.

For depths of less than 300 to 400 m, one dimensional modelling and inversion of MT/TEM sounding data appears capable of providing representative geoelectric sections with useful and reliable depth information even in geologically complex environments like the Troodos ophiolite. In general, there was a slight underestimation of depths by the one dimensional modelling and inversion, especially for depths of more than 400 m. The close agreement between subsurface parameters obtained from two dimensional modelling and inversion and measurements in boreholes even at depths of more than 2 km, suggest that the region studied could be approximated to a two dimensional environment. This suggests that although the Troodos ophiolite is a complex geological environment, it appears to be a fairly simple geoelectric environment at least in the areas surveyed.

The novel one dimensional modelling and inversion scheme by Meju (1992, 1996) employed in the interpretation enables the retrieval of useful subsurface parameters from field data both in the field and at base. In the field, it enables the adjustment or adaptation of survey parameters where necessary to acquire good or better quality field data and to achieve the desired objectives of the survey.

This study has again demonstrated the usefulness of TEM data in the static shift correction of MT data in areas like the Troodos. The effectiveness of the joint inversion of undistorted MT phase data and TEM data proposed by Meju (1996) as against the dual correction of static shift before inversion, has also been demonstrated. This study has also demonstrated the effectiveness of the use of the joint methods in the study of the geoelectric sections across areas like the Troodos

environment where TEM data provides shallow depth control and MT data furnishes constraints on the deep structure.

It can be seen that with a reasonably large body, sufficient resistivity contrast between the massive sulphide deposit and the host rocks, and in the absence of structures that distort the response of the orebody (that is, in an ideal environment with sufficient resistivity contrast between orebody and host rock), the MT/TEM methods could determine the locations of the orebodies directly as in some other parts of the world.

9.3 Recommendations

Based on previous work, it is believed that the Cyprus massive sulphide deposits are genetically and spatially related to fractures which served as channels for the transportation and localisation of the mineralising fluids that deposited the massive sulphides. Mapping of fractures in the volcanic rocks, in association with the evidence of mineralisation will, therefore, assist in the delineation of potential targets. A necessary pre-requisite here would be a knowledge of the stratigraphic horizon of the mineralisation. Studies of topographic maps, aeromagnetic and satellite data have revealed that these structures are spreading related oriented in the NNW and ENE directions, parallel (longitudinal) to and perpendicular (transcurrent) to the spreading axes. Initial high resolution aeromagnetic survey to help pinpoint the locations of the structures sought for prior to ground EM survey should be very helpful here.

The TEM method has been shown to be an effective tool for relatively shallow structural mapping in the Troodos-type environment while the MT method constrains the features/structures at depth. A deployment of the MT/TEM methods to a reasonable number of the known structurally controlled massive sulphide

orebodies and unmineralised structures that belong to the group of potentially mineralised structures (i.e., NNW and ENE trending) in northeastern Troodos, for detailed geophysical surveys and subsequent data analysis, may establish a pattern and shed some light on the difference between barren and mineralised structures. Where a clear difference exists, the characteristic pattern determined for the mineralised structures should help in the design of a proper exploration model for the massive sulphides in the Troodos environment.

Meju and Fontes (1993) in their work on static shift in MT data have demonstrated that, for a large scale survey in an excellent practical setting like the Parnaiba basin, the patterns of MT static shift can be classified and used to demarcate different geological environments. Although the Troodos environment is geologically complex with inconsistent response resulting from the variability in the alteration of the massive sulphide deposits and the inhomogeneity of the host pillow lavas along with their associated structures and dykes, the suggested study above may still show a general static shift pattern for the mineralised structures and another for the unmineralised ones. Where an identifiable difference exists between the two patterns, that could be used as a guide in the search for the massive sulphide deposits in the Troodos environment.

It has been observed that massive sulphide ore localisation may, in the absence of influencing tectonic structures, take place at an intermediate level within the pillow lava pile. It is thought that deposits resulting in this way may characteristically be of low grade resulting from the extensive interaction of the mineralising fluids with the wall rock and the absence of strong temperature and pressure gradients. However, lithological factors like the existence of glassy horizons within the lavas may cause the precipitation of richer mineralisation by replacement, in exceptional circumstances. Under normal circumstances, the

physical changes and resultant anomalies caused by the interaction of the mineralising fluids and the host rocks are usually amenable to detection by geophysical methods. However, varying erosion, weathering and tectonic deformation may cause changes to the resistivity pattern leading to anomalies that are much larger than the target zone such that in the absence of any other information indicating probable mineralisation zones, the recognition of these large scale zones becomes a pre-requisite for identifying areas of potential mineralisation. In a complex geological environment like the Troodos, the identification of such zones will require meticulous planning and grid setup, and the use of highly sensitive MT and TEM instrumentation.

APPENDIX

The processing of MT data essentially involves the conversion of recorded time series for the five electric and magnetic field components to reliable earth response functions that are necessary for qualitative and quantitative (computer modelling and inversion) analysis. On return from fieldwork and prior to procedures for actual processing of the recorded data, the field data which were stored on cartridges (TU58 for SPAM Mk IIa) were first transferred onto floppy discs useable on computers. The program by Swift based on Swift (1967) was used for general processing and retrieval of the unrotated response functions while the program by Groom and Bailey based on their formulation (Groom and Bailey, 1989) was used for the rotation of the data.

The main steps involved in the processing procedure include the scaling of the time series by the recording gains and then the data are tapered with the cosine bell function before being Fourier transformed. The data in the frequency domain are now corrected for the effect of the instrument's (induction coils and telluric signal preamplifier) response functions. The auto- and cross-spectral estimates of the calibrated Fourier coefficients are computed for every channel and averaged over 8 bands per decade to reduce the variance of the estimates. The response functions are then calculated by stacking the smoothed spectra from many time segments. These steps are executed for every recorded window for all the runs in each of the measurement frequency bands in turn. At the end it is the most consistent runs that are stacked to yield the required earth response functions.

Great care was taken in the field to orient the telluric cables and magnetic coils in the regional structural direction. As a result there was little or no difference between the rotated and unrotated resistivity/phase data retrieved from the field data as shown in the examples in figs. A1 and A2. The field apparent resistivity data were therefore directly corrected for static shift using the coincident TEM apparent resistivity data (Sternberg et al., 1988; Pellerin and Hohman, 1990; Meju, 1996) since both the rotated and unrotated apparent resistivity data yielded the same results after the rigorous computer modelling and inversion that followed.

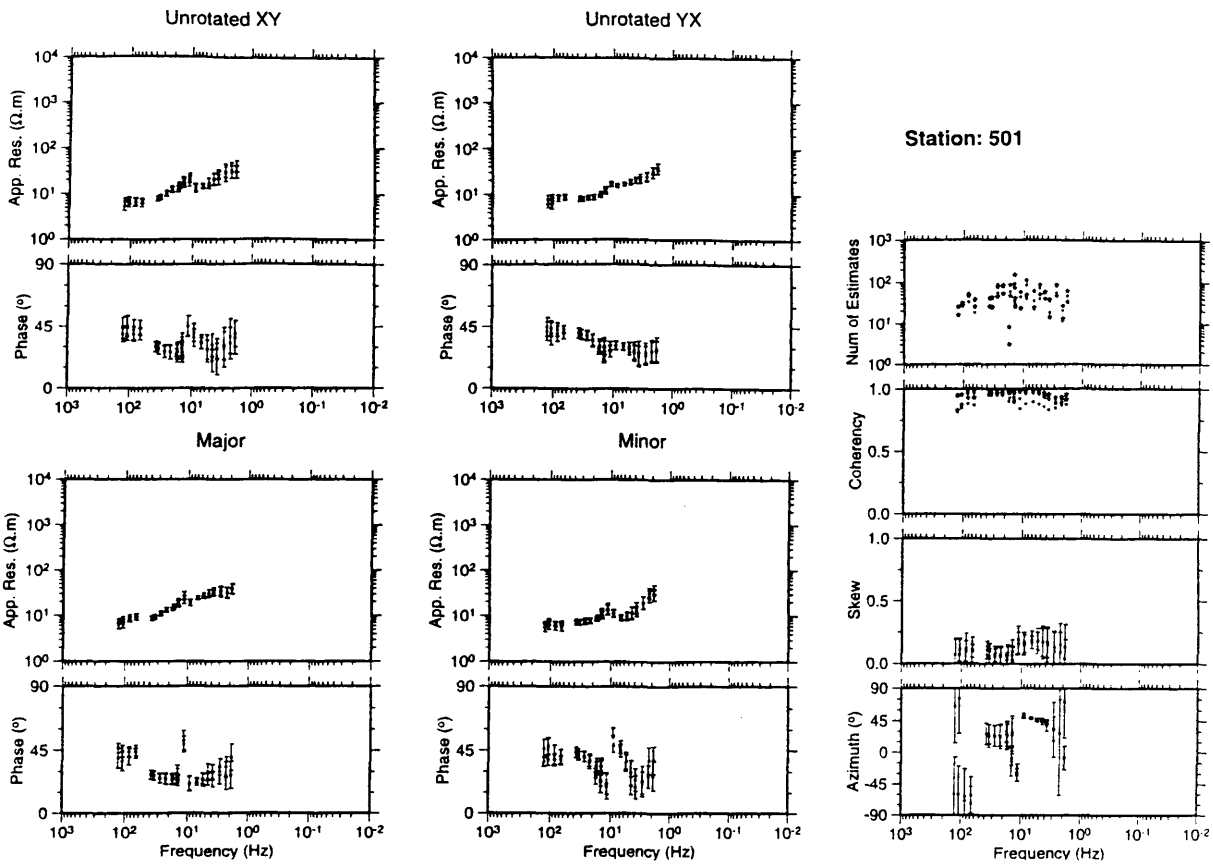

Fig. A1 Unrotated apparent resistivity and phase data

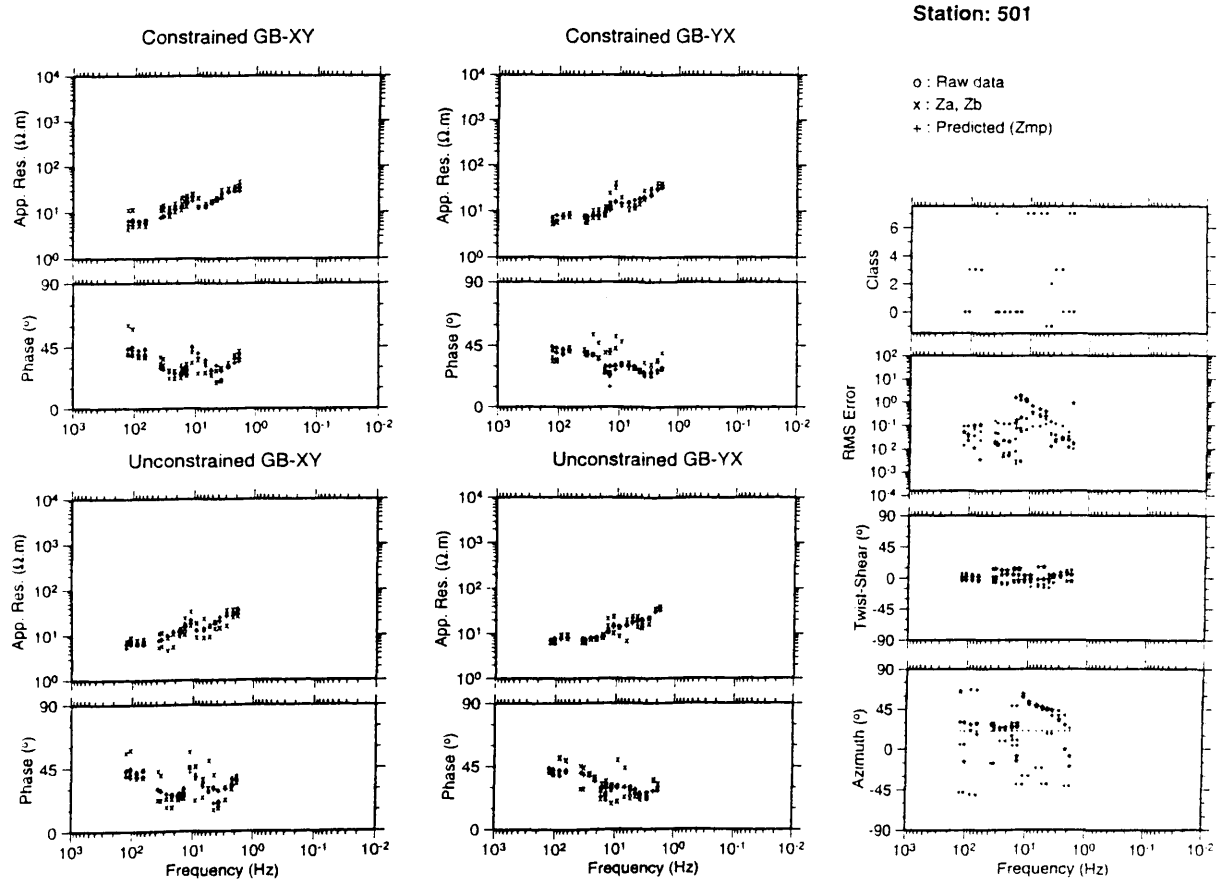

Fig. A2 Rotated apparent resistivity and phase data

REFERENCES

Adamides, N., 1980: The Form and Environment of Formation of the Kalavassos Ore Deposit, Cyprus. Proc.Int.Ophio.Symp.(Panayiotou, A., ed), Cyp.Geol.Surv. Dept., p.117-127.

Adamides, N., 1984: The Cyprus Volcanogenic Sulphide Deposits: Ph.D Thesis, Univ. of Leicester, U.K.

Adamides, N., 1990: Hydrothermal Circulation and Ore Deposition in the Troodos Ophiolite, Cyprus. In "Ophiolites, Oceanic Analogues" (Malpas, J. et.al., eds.), Proc.Symp."Troodos 1987", Cyp.Geol.Surv.Dept., p.685-704.

Allerton, S., 1989: Fault Block Rotations in Ophiolites: Results of Palaeomagnetic studies in the Troodos Complex, Cyprus. In "Palaeomagnetic Rotations and Continental Deformation" (Kissel, C. and Laj, C., eds.), NATO ARI series C, vol.254, p.393-410.

Allerton, S. and Vine, F.J., 1987: Spreading Structure of the Troodos Ophiolite, Cyprus: Some Paleomagnetic Constraints, Geology, vol.15, p.593-597.

Allerton, S. and Vine, F.J., 1990: Palaeomagnetic and Structural studies of the southeastern part of the Troodos complex. In "Ophiolites, Oceanic Crustal Analogues" (Malpas, J. et al, eds.), Proc.Symp."Troodos 1987", Cyp.Geol.Surv. Dept., p.99-111.

Allerton, S. and Vine, F.J., 1991: Spreading Evolution of the Troodos Ophiolite, Cyprus. Geology, vol.19, no.6, p.637-640.

Allis, R.G., 1990: Geophysical anomalies over Epithermal Systems. J.Geochem.Expl., vol.36, p.339-374.

Anderson, W.L., 1982: Nonlinear Least-Squares Inversion of Transient Soundings for a Central Induction Loop System (Program NLSTCI). U.S.G.S. Open File Rep.

82-1129, 85p.

Archie, G.E., 1942:The Electrical Resistivity Log as an aid in Determining some Reservoir Characteristics. Trans.AIME, Petrol.Br., vol.146, p.54-62.

Archie, G.E., 1947: Electrical Resistivity an aid in Core Analysis Interpretation. Bull.Am.Assoc.Petrol.Geologists, vol.31, no.2.

Baroz, F., 1980: Volcanism and Continent Island arc Collisoin in the Pendactylos Range, Cyprus. In "Ophiolites" (Panayiotou, A. ed.), Proc.Inter.Symp.Cyprus 1979,Cyp.Eco.Surv.Dept., p.73-86.

Barringer, A.R., 1962: A New Approach to Exploration - The INPUT Airbourne Electical Pulse Prospecting Systems: Min. Congress Journ. 48, 49-52.
Bates and Jackson, 1987:

Bear, L.M., 1960: The Geology and Mineral Resources of the Akaki-Lythrodonda Area. Cyprus Geol.Surv.Dept., Ministry of Agriculture & Mineral Resources, Memoir 3, p.1-122.

Bear, L.M., 1963: The Mineral Resources and Mining Industry of Cyprus. Cyp.Geol. Surv.Dept.Bull. no.1 208p.

Becher, W.D. and Sharpe, C.B., 1969: A Synthesis Approach to Magnetotelluric Exploration. Radio Sci., vol.4, p.1089-1094.

Bechon, F. and Rocci, G., 1982: Fault Chronology in the Arakapas Zone, Cyprus: Their Incidence in Lava Flows. C.R.Acad.Sc. Paris. Serie 2 249 16, p.999-1002.

Ben-Avraham, Z., 1978: The Structure and Tectonic Setting of the Levant Continental Margin, Eastern Mediterranean. Tectonnophysics, vol.46, p.313-331.

Berdichevsky, M.N. and Dmitriev, V.I., 1976: Distortion of Magnetic and Electric Fields by Near Surface Lateral Inhomogeneities. Acta Geodaet.Geophys.Montanist. Acad.Sci.Hung., vol.11, p.447-483.

Bettison-Varga, L., Varga, R.J. and Schiffman, P., 1992: Relation Between Ore Forming Hydrothermal Systems and Extensional Deformation in the Solea Graben Spreading Center, Troodos Ophiolite, Cyprus. Geology, vol.20, p.987-990.

Bloomer, S.H. and Hawkins, J.W., 1987: Petrology and Geochemistry of Boninite Series Volcanic Rocks from the Mariana Trench. Contib.Mineral.Petrol., vol.98, p.361-377.

Boldly, J., 1981: Prospecting for Deep Volcanogenic Ore. Can.Inst.Min. vol.74, no.834 55-65.

Bostick, F.X., 1977: A Simple Almost Exact Method of MT Analysis. Presented at the Workshop on Electrical Methods in Geothermal Exploration, U.S.Geol.Surv., Contract 14080001-8-359.

Boyle, J.F. and Robertson, A.H.F., 1984: Evolving Metallogenesis at the Troodos Spreading Axis. In "Ophiolites and Oceanic Lithosphere" (Gass, I.G. et.al. eds.) Geol.Soc.Lond.Spec.Pub. vol.13, p.169-181.

Busby, J., Khan, M.A. and Maliolitis, G., 1983: IP Applied to Mineral Exploration in Cyprus. Trans.Inst.Min.Metall. vol.92, p.B201-208.

Buselli, G., 1981: The Effect of Near Surface Superparamagnetic Material on Electromagnetic Measurements. Geophysics, vol.47, p.1315-1324.

Buselli, G. and O'Neill, B., 1977: A New Portable Instrument for Multichannel TEM Measurements. Expl.Geophys. vol.8, p.82-87.

Buselli, G., McCracken, K.G. and Rutter, H., 1985: Manual for SIROTEM Field Procedures and Data Interpretation. C.S.I.R.O., Inst.Earth.Res., Div.Min.Phys. and Mineralogy.

Cagniard, L., 1953: Basic Theory of the Magnetotelluric Method of Geophysical Prospecting, Geophysics, vol.18, p.605-635.

Cantwell, T., 1960: Detection and Analysis of Low Frequency Magnetotelluric Signals. Ph.D. Thesis, M.I.T., Cambidge, Mass. U.S.A.

Carr, J.M. and Bear, L.M., 1960: The Geology and Mineral Resources of the Peristerona-Lagoudhera Area. Geol.Surv.Dept.Cyp., mem. no.2.

Clube, T.M.M. and Robertson, A.H.F., 1986: The Palaeorotation of the Troodos Microplate, Cyprus, in thLate Mesozoic-early Cenozoic Plate Tectonic Framework of the Eastern Mediterranean. Surv.Geophys., vol.8, p.375-437.

Constable, S.C., Parker, R.L.. and Constable, C.G., 1987: Occam's Inversion: a Practical Algorithm for generating Smooth Models From Electromagnetic Sounding Data. Geophysics, vol.52 no.3, p.289-300.

Constantinou, G., 1979: Massive Sulphide Deposits and Umbers. In "Field Excursion Guidebook", Cyp.Geol.Surv.Dept., p.19-27.

Constantinou, G. and Govett, G.J.S., 1972: Genesis of Sulphide Deposits, Ochre and Umber of Cyprus. Trans.Inst.Min.Metall., vol.81, B34-46.

Constantinou, G. and Govett, G.J.S., 1973: Geology, Geochemistry and Genesis of Cyprus Sulphide Deposits. Econ.Geol., vol.68, p.843-854.

Cooper, N.J., 1993: Integrated Geophysical Exploration of the North East Troodos Ophiolite, Cyprus. Ph.D. Thesis, Univ.Leicester, U.K.

Cooper, N.J. and Swift, R., 1996: The Application of TEM to Cyprus-type Massive Sulphide exploration in Cyprus. Geophysics, vol.59, no.2, p.202-214.

Crawford, A.J., Beccaluva, L. and Serri, G., 1981: Tectonomagmatic Evolution of the West Philippine-Mariana Region and the Origin of Boninites. Earth Planet.Sci. Lett., vol.54, p.346-356.

Crone, B.N., 1977: Ground Pulse EM - Examples of Survey Results in the Search

for Massive Sulphides and New Equipment Development. Expl.Geophys., vol.8, p.38-42.

Dawes, G.J.K., 1984: Short Period Automatic MT (SPAM) System. In "A Broadband Tensorial MT Study in the Travale-Radicondoli Geothermal Field", by Hutton,V.R.S., Dawes, G.J.K., Devlin, T. and Roberts, R.

Dewey, J.F., Pitman III, W.C., Ryan, W.B.F. and Bonnin, J., 1973: Plate Tectonics and the Evolution of the Alpine System, Geol.Soc.Am.Bull., vol.84, p.3137-3180.

Dilek, Y. and Eddy, C.A., 1992: Ophiolites as structural models. Tectonics, vol.11, no.4, p.916-923.

Dilek, Y. and Eddy, C.A., 1992: The Troodos (Cyprus) and Kizildag (S. Turkey) Ophiolite Models for Slow-Spreading Ridge Segments. Journ.Geol., vol.100, p.305-32.

Dilek, Y. and Moores, E.M., 1990: Regional Tectonics of the Eastern Mediterranean Ophiolites. In "Ophiolites, Oceanic Analogues" (Malpas, J., et al eds.), p.295-309.

Dilek, Y., Thy, P., Moores, E.M. and Ramsden, T.W., 1990: Tectonic evolution of the Troodos ophiolite within the Tethyan framework. Tectonics, vol.9, no.4, p.811-823.

Dilek, Y., Thy, P., Moores, E.M. and Ramsden, T.W., 1992: Reply (to Macleod et al., 1992), Tectonics, vol.11, no.4, p.916-923.

Eaton, P.A. and Hohmann, G.W., 1989: An Evaluation of Electromagnetic Methods in the Presence of Geologic Noise. Geophys., vol.52, no.8, p.1106-1126.

Eddy, C.A., and Moores, E.M., 1992: A Fossilised Caldera and Seamount with Associated Massive Sulfide Mineralization in the Troodos Ophiolite, Cyprus. Eos vol.71, p.629.

Fullagar, P.K., 1989: Generation of Conductivity Depth Pseudosection from

Coincident Loop and In-Loop TEM Data. Expl.Geophys., vol.20, p.43-45.

Fullagar, P.K. and Reid, J.E., 1992: Conductivity-Depth Transformations of Fixed Loop TEM Data. Expl.Geophys., vol.23, p.515-520.

Gamble, T.D., Goubau, W.M. and Clarke, J., 1978: Magnetotellurics with a Remote Magnetic Reference. Geophysics, vol.44, p.53-68.

Gamble, T.D., Goubau, W.M. and Clarke, J., 1979: Error Analysis for Remote Reference Magnetotellurics. Geophysics, vol.44, p.959-968.

Gass, I.G., 1960: The Geology and Mineral Resources of the Dhali Area. Cyprus Geol.Surv.Dept. Memoir 4, 116pp.

Gass, I.G., 1968: Is the Troodos Complex, Cyprus formed by Sea Floor-Spreading? Nature, vol.22, p.39-42.

Gass, I.G., 1980: The Troodos Massif: Its Role in the Unravelling of the Ophiolite Problem and Its Significance in the Understanding of Constructive Plate Margin Process. In "Proc.Int.Ophio.Symp." (Panayiotou, A., ed.), Cyp.Geol.Surv.Dept., p.23-35.

Gass, I.G. and Smewing, J.D., 1973: Intrusion, Extrusion and Metamorphism at Constructive Margins: Evidence from the Troodos Massif, Cyprus. Nature, vol.242, p.26-29.

Gass, I.G. and Masson-Smith, D., 1963: The Geology and Gravity Anomalies of the Troodos Massif, Cyprus. Phil.Trans.Roy.Soc.Lon. A255, p.417-467.

Goldberg, S. and Rotstein, Y., 1982: A Simple form of Presentstion of Magnetotelluric Data using the Bostick Transform. Geophysical Prospecting, vol.30, p.211-216.

Grant, F.S. and West, G.F., 1965: Interpretation Theory in Applied Geophysics. McGraw-Hill "Int. Series in the Earth Sciences" 210-222, 306-354.

Griffiths, D.H. and King, R.F., 1981: Applied Geophysics for Geologists and Engineers, Second Edition, Pergamon Press, Oxford.

Groom, R.W. and Bailey, R.C., 1989: Decomposition of Magnetotelluric Impedance Tensor in the Presence of Local Three-Dimensional Galvanic Distortion. J.Geophys. Research, vol.94, no.B2, p.1913-1925.

Hermance, J.F., 1973: Processing of Magnetotelluric Data. Phys.Earth Plan.Int., vol.7, p.349-364.

Hickey, R.J. and Frey, F.A., 1982: Geochemical Characteristics of Boninite Series Volcanics: Implications for their Source. Geochim.Cosmochim.Acta., vol.46, p.2099-2115.

Hobbs, B.A., 1982: Automatic Model Finding for the One Dimensional Magnetotelluric Problem. Geophys.J.R.Astr.Soc., vol.68, p.253-264.

Hoversten, G.M. and Morrison, H.F., 1982: Transient Fields of a current Loop Source above a Layered Earth. Geophysics, vol.47, p.1068-1077.

Hunting Geology and Geophysics Ltd., 1969: An Airborne Magnetic and Electromagnetic Survey in Cyprus. Cyp.Geol.Surv.Dept., Bull. no.3.

Hurst S.D., Karson, J.A., and Verosub, K.L., 1994: Structural and geophysical expression of the Solea graben, Troodos Ophiolite, Cyprus. Tectonics, vol.13, no.1, p.139-156.

Hutchinson, R.W., 1965: Genesis of Canadian Massive Sulphides Reconsidered by Comparison to Cyprus Deposits. Trans.Can.Inst.Min.Metall., vol.68, p.286-300.

Hutchinson, R.W. and Searle, D.L., 1971: Stratabound Pyrite Deposits in Cyprus and Relations to other Sulphide Ores. In "Proc.Symp.Stratabound Sulph.Ore.Deps., IMA-IAGOD meetings '70", IAGOD vol. (Soc.Min.Geol.Japan, Tokyo), p.198-205.

Hutton, V.R.S., Dawes, G.J.K., Devlin, T. and Roberts, R., 1984: A Broadband Tensorial Magnetotelluric Study in the Travale-Radicondoli Geothermal Field. EEC Report Series. Contract no. EG-A2-031-UK. Final Report.

Innocenti, F., Mazzuoli, R., Pasquare, G., Radicati di Brozolo, F. and Villari, L., 1976: The Neogene Calcalkaline Volcanism of Central Anatolia: Geochronological Data on Kayseri-Nigde area. Geol.Mag., vol.112, p.349-360.

Izawa, E., Urashima, Y., Ibaraki, K., Suzuki, R., Yokoyama, T, Kawasaki, K., Koga, A. and Taguchi, S., 1990: The Hishikari Gold Deposit: High-Frade Epithermal veins in Quaternary Volcanics of Southern Kyushu, Japan. In "Epithermal Gold Mineralisation of the Circum-Pacific: Geology, Geochemistry, Origin and Exploration, II. J.Geochem. Explor., vol.36, p.1-56.

Jackson, D.D., 1979: The Use of A Priori Data to Resolve Non-Uniqueness in Linear Inversion. Geophys.J.Astr.Soc., vol.57, p.137-157.

Jannisen, K., 1988: Investigation of Decripitation-Activity, Fluid Inclusions and Alteration Minerals in the Alestos Sulphise, Troodos Ophiolite, Cyprus. M.Sc. Thesis Technische Hochschule Aachen, FRD.

Jones, A.G., 1983: On the Equivalence of the 'Niblet' and 'Bostick' Transformations in the Magnetotelluric Method. J.Geophys., vol.53, p.72-73

Jones, A.G. and Hutton, V.R.S., 1979: A Multi-Station Magnetotelluric Study in Southern Scotland-II. Monte-Carlo Inversion of the Data and its Geophysical and Tectonic Implications. Geophys.J.R.Astr.Soc., vol.56, p.351-368.

Jupp, D.L.B. and Vozoff, K., 1975: Stable Iterative Methods for Inversion of Geophysical Data. Geophys.J.R.Astr.Soc., vol.42, p.957-976.

Kato, Y. and Kikuchi, T., 1950: On the Phase Diference of Earth Currents Induced by Changes of the Earth's Magnetic Field, Parts I and II. Sci.Rep. Tohoku Univ., Ser.V., Geophysics, vol.2, p.139-145.

Kaufman, A.A. and Keller, G.V., 1983: Frequency and Transient Soundings. Methods in Geochemistry and Geophysics, vol.16, Elsevier Publ.Co.

Keller, G.V. and Frischknecht, F.C., 1966: Electrical Methods in Geophysical Prospecting. Pergamon Press, New York.

Khan, M.A., Summers, C., Bamford, S.A.D., Chroston, P.N., Poster, C.K. and Vine, F.J., 1972: Reversed Seismic Refraction Line on Troodos Massif, Cyprus. Nature Phys.Sci., vol.238, no.87, p.134-136.

Knight, J.H. and Raiche, A.P., 1982: Transient Electromagnetic Calculations using the Gaver-Stehfest Inverse Laplace Transform method. Geophysics, vol.47, no.1, p.47-50.

Laird, C.E. and Bostick, F.X., Jn., 1970: One Dimensional Magnetotelluric Inversion Techniques. Electr.Geophys.Res.Lab., University of Texas, Tech.Rep.no.101.

Lajoie, J.J. and West, G.F., 1976: Electromagnetic Response of a Conductive Inhomogeneity in a Layered Earth. Geophysics, vol.41, p.1133-1156.

Lakanen, M.E., 1986: A Successful Application of the Transient Method. In "Electrical Prospecting for Ore Deposits in the Basaltic Shield (Hjelt, S.E. and Fokin, A.F., eds.), Issue 2, EM Methods: Rep. of Invest.Geol.Surv.Finland.

Lamontagne, Y.L., 1975: Application of Wideband, Time-Domain EM Measurements in Mineral Exploration. Ph.D. Thesis, Univ. of Toronto.

Lanczos, C., 1961: Linear Differential Operators. D. Van Nostrand Co. London.

Larsen, J.C., 1977: Removal of Local Surface Conductivity Effects from Low Frequency Mantle Response Curves: Acta Geodaet. Geophys. et. Montanist. Acad. Sci. Hung., vol.12, p.183-186.

Larsen, J.C., 1981: A New Technique for Layered Earth Magnetotelluric Inversion.

Geophysics, vol.46, no.9, p.1247-1257.

Lee, T., 1984: The Effect of Superparamagnetic Layer on the Transient Electromagnetic Response of a Ground. Geophys.Prosp., vol.32, p.480-496.

Leith, W., 1982: Rock Assemblages in Central Asia and the Evolution of the Southern Asian Margin. Tectonics, vol.1, p.303-318.

Lippard, S.J., Shelton, A.W. and Gass, I.G., 1986: The Ophiolite of Northern Oman. Geol.Soc., London Memoir.

Lowrie, W. and West, G.F., 1965: The Effect of a Conducting Overburden on EM Prospecting Measurements. Geophysics, vol.30, p.624-632.

Lyden, J.W., 1983: Comparison of a Volcanogenic Massive Sulphide of Cyprus with one of Canadian Achean Green Belt. Geol.Assoc.Can., 8 44.

Lyden, J.W. and Galley, A.G., 1988: The Chemical and Mineralogical Zonation of the Mathiati Alteration Pipe, Cyprus and Its Genetic Significance. In "Metallogeny of Basic and Igneous Rocks" (Lyden et. al. eds.), p.1-20.

Mace, C., 1939: Gravity Measurements in Cyprus. Roy.Astr.Soc.(Geophys.Suppl.) vol.4, no.7, p.473-480.

Mackie, R.L., 1994: d2inv-newt, a 2D Inversion Program. Massachusetts Institute of Technology Earth Resources Laboratory Report, Cambridge, Massachusetts.

Macleod, C.J., Allerton, S., Gass, I.G., and Xenophontos, C., 1990: Structure of a Fossil Ridge-Transform Intersection in the Troodos Ophiolite. Nature, vol.348, p.717-720.

Macleod, C.J., Robertson, A.H.F., Allerton, S., Browning, P., Gass, I.G., Taylor, R.N., Vine, F.J. and Xenophontos, C., 1992: Comment on "Tectonic evolution of the Troodos ophiolite within the Tethyan framework" by Y. Dilek, P. Thy, E. M. Moores, and T. W. Ramsden. Tectonics, vol.11, no.4, p.910-915.

Maliotis, G., 1978: The Applicability and Limitations of the IP Method in Sulphide Exploration in Cyprus. Ph.D. Thesis, Univ.Leicester, U.K.

Maliotis, G. and Khan, M.A., 1980: The Applicability of the IP Method of Geophysical Investigation in the Search for Sulphide Mineralisation within the Troodos Ophiolite Complex of Cyprus. In "Proc.Int.Oph.Symp. Cyprus 1979" (Panayiotou, A. ed.), Cyprus Geol.Surv.Dept., p.129-138.

Malpas, J., 1990: Crustal Accretinary Process in the Troodos Ophiolite, Cyprus. In "Ophiolites, Oceanic Crustal Analogues" (Malpas, J. et. al. eds.) Cyprus Geol.Surv. Dept. 65-74.

Malpas, J., Robinson, P.T. and Salisbury, M., 1989: Geology and Geophysics of Borehole CY-4 of Cyprus Crustal Study Project: Summary. In "Cyprus Crustal Study Project: Initial Report Hole CY-4" (Gibson, I.L., et.al., eds.). Geol.Surv.Can. 88-9, 381-393.

McCracken, K.G., Hohman, G.W. and Oristaglio, M.L., 1980: Why Time Domain? Bull.Austrl.Soc.Explor.Geophys., vol.11, p.318-321.

McNeill, J.D., 1980: EM37 Ground TEM System. Tech. Note 10, Geonics Ltd, Ontario, Canada.

Meju, M.A., 1988: The Deep Electrical Structure of the Great Glen Fault, Scotland. Ph.D. Thesis, Univ.Edinburgh, U.K.

Meju, M.A., 1992a: Biased Estimation: An Effective Ridge Regression Procedure for Resistivity Data Inversion. Computers & Geosciences, vol.18, p.99-118.

Meju, M.A., 1992b: FEM2D: A Multi-Method 2D Finite-Element Modelling Program for Electromagnetic Survey Data. Environmental and Industrial Geophysics Research Report 92/1, Univ.Leicester.

Meju, M.A., 1994a: Geophysical Data Analysis: Understanding Inverse Problem

Theory and Practice. Soc.Expl.Geophys., SEG Course Notes Series, vol.6, Tulsa, Oklahoma.

Meju, M.A., 1994b: Joint TEM and AMT Surveys: Cost-Effective Exploration in Frontier Basin Regions. Proc.10th Petr.Congr.Exhib. Ankara, Turkey,Apr. 11-15, 1994, Geophys. vol., 157-176.

Meju, M.A., 1994c: A Simple Framework for Inversion and Uncertainty Analysis with Prior Information. Geophys.Journ.Int. 62281.

Meju, M.A., 1995: Simple Effective Resistivity-Depth Transformations for Infield or Real-Time Data Processing. Computers and Geosciences, vol.21, p.985-992.

Meju, M.A., 1996: Joint Inversion of TEM and Distorted MT Data: Some Effective Practical Considerations. Geophysics vol.61, p.56-65.

Meju, M.A., 1997: A Simple Method of Transient Electromagnetic Data Analysis. (Geophysics accepted).

Meju, M.A. and Fontes, S.L., 1993: An Investigation of Static Shifts in MT Data from Parnaiba Basin using Central Loop TEM Data. 3rd Internat.Congr.Brazil. Geophys.Soc., Expanded Abstracts, p.1474-1479.

Meyer, C. and Hemley, J.J., 1967: Wall Rock Alteration. In "Geochemistry of Hydrothermal Ore Deposits" (Barnes, H.L., ed.). Holt, Rinehart and Winston, p.166-235.

Miller, E.L., Gans, P.B. and Garing, J., 1983: The Snake Range Decollement: An Exhumed Mid-Tertiary Ductile-Brittle Transition. Tectonics, vol.2, p.239-263.

Milson, J., 1989: Field Geophysics. Geological Society of London Handbook, John Willey and Sons, Chichester.

Moores, E.M. and Vine, F.G., 1971: The Troodos Massif, Cyprus and other Ophiolites as Oceanic Crust: Evaluation and Implications. Phil.Trans.Roy.Soc.Lond.

A268, p.443-466.

Moores, E.M., Varga, R.J. & Verosub, K.L., 1987: Regional Structure, Troodos Sheeted Complex, Cyprus. Abs.Symp. Troodos'87, Ophiolites & Oceanic Lithosphere, Nicosia, Cyprus Geol.Surv.Dept. 26.

Morrison, H.F., Phillips, R.J. and O'Brien, D.P., 1969: Quantitative Interpretation of Transient EM Fields over a Layered Half Space. Geophys.Prosp., vol.17, p.82-101.

Muller, W. and Losecke, W., 1975: Accelerating Convergence Techniques and Grid Spacing Problems in Two-Dimensional Magnetotelluric Modelling. Geophys. J.R.Astr.Soc., vol.41, p.185-191.

Nabetani, S. and Rankin, D., 1969: An Inverse Method of Magnetotelluric Analysis for a Multi-Layered Earth. Geophysics, vol.34, no.1, p.75-86.

Nabighian, M.N., 1979: Quasi-Static Transient Response of a Conductive-Half-Space: An Approximate Representation. Geophys. vol.44, no.10, p.1700-1705.

Nabighian, M.N. and Macnae, J.C., 1991: Time Domain EM Prospecting Methods. In "EM Methods in Applied Geophysics" (Nabighian, M.N. ed.), vol.2, Invest. Geophys.Soc.Expl.Geophys.

Nekut, A.G., 1987: Direct Inversion of Time-Domain Electromagnetic Data. Geophysics, vol.52, p.1431-1435.

Niblett, E.R. and Sayn-Wittgenstein, C., 1960: Variation of Electrical Conductivity with Depth by the Magnetotelluric Method. Geophysics, vol.25, p.998-1008.

O'Brien, D.P. and Morrison, H.F., 1967: EM Fields in an n-Layer Anisotropic Half-Space. Geophys., vol.32, p.668-677.

Oldenburg, D.W., 1979: One-Dimensional Inversion of Natural Source Magnetotelluric Observations. Geophysics, vol.44 no.7, p.1218-1244.

Oldenburg, D.W., 1983: Funnel Functions in Linear and Nonlinear Appraisal. J.Geophys.Res., vol.88, B9, p.7387-7398.

Oldenburg, D.W., Whittal, K.P. and Parker, R.L., 1984: Inversion of Ocean Bottom Magnetotelluric Data Revisited. J.Geophys.Res., vol.89, B3, p.1829-1833.

Orange, A.S., 1989: MT Exploration for Hydrocarbons. Proc.IEEE vol.77, no.2, p.287-317.

Panayiotou, A., 1979: An overview of the geology of Cyprus. In "Field Excursion Guidebook", Cyp.Geol.Surv.Dept., p.1-18.

Pantazis, T.M., 1979: General Features of the Geology and Mineralisation of Cyprus. In Field Excursion Guidebook, Cyp.Geol.Surv.Dept., p.1-18.

Park, S.K., Orange, A.S. and Madden, T.R., 1983: Effects of Three-Dimensional Structure on Magnetotelluric Sounding Curves. Geophysics, vol.48, no.10, p.1402-1405.

Parker, R.L., 1970: The Inverse Problem of Electrical Conductivity in the Mantle. Geophys.J.R.Astr.Soc., vol.22, p.121-138.

Parker, R.L., 1977: Understanding Inverse Theory. Ann.Rev.Earth Plan.Sci., vol.5, p.35-64.

Parker, R.L., 1980: The Inverse Problem of Electromagnetic Induction: Existence and Construction of Solutions Based on Incomplete Data. J.Geophys.Res., vol.85, B8 p.4421-4428.

Parker, R.L. and Whaler, K., 1981: Numerical Methods for Establishing Solutions to the Inverse Problem of Electromagnetic Induction. J.Geophys.Res., vol.86, p.9574-9584.

Parkhomenko, E.I., 1967: Electrical Properties of Rocks. Plenum Press, New York

NY, p.276-278.

Pearce, J.A., Lippard, S.J. and Roberts, S., 1984: Characteristics and Tectonic Significance of Suprasubduction Zone Ophiolites. In "Marginal Basin Geology, Volcanic and Associated Sedimentary and Tectonic Processes in Modern and Ancient Marginal Basins" (Kokelaar, B.P. and Howells, M.F., eds.), Geol. Soc.Lond.Spec.Publ., vol.16, p.77-94.

Pellerin, L. and Hohmann, G.W., 1990: TEM Inversion: A Remedy for MT Static Shift. Geophys. vol.55, p.1242-1250.

Raiche, A.P., 1984: The Effect of Ramp Function Turnoff on TEM Response of a Layered Ground. Explor.Geophys., vol.15, p.37-41.

Ranganayaki, R.P., 1984: An Interpretive Analysis of Magnetotelluric Data. Geophysics, vol.49, p.1730-1748.

Ranganayaki, R.L. and Madden, T.R., 1980: Generalized Thin Sheet Analysis in Magnetotellurics: An Extension of Price's Analysis. Geophys.J.R.Astr.Sco., vol.60, p.445-457.

Richardson, C.J., Cann, J.R., Richards, H.G. & Cowan, J.G., 1987: Metal-Depleted Root Zones of the Troodos Ore-Forming Hydrothermal Systems, Cyprus. Earth & Plan.Sci.Letts. 84 243-253.

Rijo, L., 1977: Modelling of Electric and Electromagnetic Data. Ph.D. Thesis, University of Utah.

Robertson, A.H.F. and Dixon, J.E., 1984: Introduction: Aspects of the Geological Evolution of the Eastern Mediterranean. In "The Geological Evolution of the Eastern Mediterranean" (Dixon, J.E. and Robertson, A.H.F., eds.), Geol.Soc. London, Special Publ., vol.17.

Robertson, A.H.F. and Woodcock, N.H., 1980: Tectonic Setting of the Troodos Massif in the East Mediterranean. In "Ophiolites" (Panayiotou, A., ed.),

Proc.Internat. Symp. Cyprus 1979, Cyp.Geol.Surv.Dept., p.261-272.

Robertson, A.H.F. and Woodcock, N.H., 1986: The Geological Evolution of the Kyrenia Range: A Critical Lineament in the Eastern Mediterranean. In "Major Crustal Lineaments and their Influence on the Geological History of the Continental Lithosphere" (Reading, H.G., eds.), Phil.Trans.R.Soc. London, A317, p.141-171.

Robertson, A.H.F. and Xenphontos, C., 1993: Development of concepts concerning the Troodos ophiolite and adjacent units in Cyprus. In Magmatic Processes and Plate Tectonics, eds. Prichard, H. M., Alabaster, T., Harris, N. B.,and Neary, C. R., Geological Society Special Publication, vol.76, p.85-119.

Robertson, A.H.F., Clift, P.D, Degnam, P.J. and Jones, G., 1991: Palaeoceanographic and Palaeotectonic Evolution of the Eastern Mediterranean Neotethys. Palaeogeography, Palaeoclimatology, Palaeoecology, vol.87, p.289-343.

Robinson, P.T., Gibson, I.L. and Panayiotou, A., (eds.) 1987: Cyprus Crustal Study Project Initial Report Holes CY-2 and 2a. Geol.Surv. Canada Special Paper 85-29.

Robinson, P.T. and Malpas, J., 1987: The Troodos ophiolite of Cyprus: new perspectives on its origin and emplacement. In: "Ophiolites, Oceanic Analogues" (Malpas, J., et al, eds.), p.13-36.

Salisbury, M.H., Christensen, N.I., Vine, F.J., Smith, G.C. and Eleftheriou, S., 1989: Geophysical structure of the Troodos ophiolite from downhole logging. In: Cyprus Crustal Study Project: Initial Report, Hole CY-4, eds.Gibson, I.L., Malpas, J., Robinson, P.T. & Xenophontos; Geological Survey of Canada, vol.88, no.9, p.331-349.

Sandberg, S.K. and Hohmann, G.W., 1982: Controlled Source Audiomagnetotellurics in Geothermal Exploration. Geophysics, vol.47, p.100-116.

Schminke, H.U. & Bednarz, U., 1990: Pillow, Sheet Flow and Breccia Flow

Volcanoes and Volcano-Tectonic Hydrothermal Cycles in Extrusive Series of Northeastern Troodos Ophiolite, Cyprus. In "Ophiolites, Oceanic Analogues" (Malpas, J. et. al. eds.), Cyp.Geol.Surv.Dept. p.185-206.

Searle, D.L., 1972: Mode of Occurrence of the Cupriferous Pyrite Deposits of Cyprus. Inst.Min.Metall. B81 B189-B197.

Searle, D.L. and Panayiotou, A., 1980: Structural Implications in the Evolution of the Troodos Massif, Cyprus. In "Ophiolites" (Panayiotou, A., ed.), Proc.Internat. Symp. Cyprus 1979, Cyp.Geol.Surv.Dept., p.50-60.

Sengor, A.M.C., Yilmaz, Y. and Sungurlu, O., 1984: Tectonics of the Western Mediterranean Cimmerides: Nature and Evolution of the Termination of Palaeo-Tethys. In "The Geological Evolution of the Eastern Mediterranean" (Dixon, J.E. and Robertson, A.H.F., eds.), Geol.Soc. London Special Publ., vol.17, p.77-112.

Sharashkin, A.Y., Bogdanov. N.A. and Zakarizade, G.S., 1981: Geochemistry and Timing of the Marginal Basin and Arc Magmatism in the Philippine Sea. Philos. Trans.R.Soc. London, Ser. A., 300, p.287-297.

Shelton, A.W. and Gass, I.G., 1980: Rotation of the Cyprus Microplate. In "Ophiolites" (Panayiotou, A. ed.), Proc.Int.Ophio.Symp., Cyprus 1979, Nicosia, Cyprus Geol. Surv. Dept. p. 61-65.

Sheriff, R.E., 1991: Encyclopedic Dictionary of Exploration Geophysics. Publ. Soc.Expl.Geophys., Tulsa, Oklahoma, USA.

Sims, W.E. and Bostick, F.X. (Jr.), 1969: Methods of Magnetotelluric Analysis. Techn.Rep.No.58, 1-86, Electrical Geophys.Res.Lab., Univ. Texas.

Sims, W.E., Bostick, F.X. (Jr.) and Smith, H.J.W., 1971: The Estimation of Magnetotelluric Impedance Tensor Elements from Measured Data. Geophysics, vol.36, p.938-942.

Silberman, M.L. & Berger, B.R., 1985: Relationship of Trace Element Patterns to

Alteration and Morphology in Epithermal Precious-Metal Deposits: Geology & Geochemistry of Epithermal Systems, Reviews in Economic Geology, v, 2 Soc. Econ. Geologists.

Smith, R.S. and West, G.F., 1988: An Explanation of Abnormal TEM Responses: Coicident-Loop Negatives and Loop Effect. Expl.Geophys., vol.19, p.435-446.

Smith, R.S., Edwards, R.N. and Buselli, G., 1994: An Automatic Technique for Presentation of Coincident-Loop, Impulse-Response, Transient Electromagnetic Data. Geophysics, vol.59, p.872-888.

Spies, B.R., 1980: Interpretation and Design of Time Domain EM Surveys in areas of Conductive Overburden. Bull.Austrl.Soc.Explor.Geophys., vol.11 no.4 p.272-281.

Spies, B.R., 1989: Depth of Investigation in Electromagnetic Sounding Methods. Geophysics, vol.54, no.7, p.872-888.

Spooner, E.T.C., 1977: Hydrothermal Model for the Origin of the Ophhiolitic Pyrite Deposits of Cyorus. Geol.Soc. London Spec.Publ. no.7, p.58-71.

Srivastava, S.P., 1967: Magnetotelluric Two- and Three-Layer Master Curves. Publ. Dominion Obs., Ottawa, 35(7).

Sternberg, B.K., Washburne, J.C. & Pellirin, L.., 1988: Correction of Static Shift in MT Using TEM Soundings. Geophys. v. 53 p. 1459-1468.

Stodt, J.A., 1978: Documentation of a Finite Element Program for Solution of Geophysical Problems Governed by the Inhomogeneous 2D Scalar Helmholtz Equation. NSF Program Listing and Documentation, Univ. of Utah, 66p.

Swarbrick, R.E., 1980: The Mamonia Complex of SW Cyprus and its Relationship with the Troodos Complex. In "Ophiolites" (Panayiotou, A. ed.), Proc.Int.Ophio. Symp., Cyprus 1979, Nicosia, Cyprus Geol. Surv. Dept. p. 86-92.

Swift, C.M., 1967: A Magnetotelluric Investigation of an Electrical Conductivity

Anomaly in the Southwestern United States. In "Magnetotelluric Methods", Soc.Expl. Geophys. (Vozoff, K., ed.), ser. No.5, p.156-166.

Swift, R., 1990: Transient Electromagnetic Soundings in Complex Geological Environments. Ph.D Thesis, Univ. Leicester, U.K.

Telford,W.M., Geldart, L.P., Sheriff, R.E. and Keys, D.A., 1990: Applied Geophysics 2nd Edition. Cambridge University Press.

Thomas, E.G. and Meadows, A.J., 1985: Maxwell's Equations and their Applications. Students Monograph in Physics Series, Adam Higler Ltd.

Tikhonov, A.N., 1950: Determination of the Electrical Characteristics of the Deep Strata of the Earth's Crust. Dokl.Akad.Nauk., U.S.S.R., vol.73, p.295-297.

Tikhonov, A.N. and Berdichevsky, M.N., 1966: Experience in the use of Magnetotelluric Methods to Study the Geologic Structure of Sedimentary Basins. Bull.Izv.Acad.Sci., U.S.S.R., Geophys.Ser., vol.2, p.93-97.

Thy, P. and Moores, E.M., 1988: Crustal Accretion and Tectonic Setting of the Troodos Ophiolite, Cyprus. Tectonophysics 147 221-145.

Varga, R.J., 1991: Modes of Extension at Oceanic Spreading Centres: Evidence from the Solea Graben, Troodos Ophiolite, Cyprus. Journ.Struc.Geol. 13 517-537.

Varga, R.J. and Moores, E.M., 1985: Spreading Structure of the Troodos Ophiolite, Cyprus. Geology 13 846-850.

Varga, R.J. and Moores, E.M., 1990: Intermittent Magmatic Spreading and Tectonic Extension in the Troodos Ophiolite: Implications for Exploration for Black Smoker-Type Ore Deposits. In "Ophiolites, Oceanic Crustal Analogues" (Malpas et al, eds.), Cyp.Geol.Surv.Dept., p.53-64.

Verosub, K.L. and Moores, E.M., 1981: Tectonic rotations in extensional regimes and their paleomagnetic consequences for oceanic basalts. Journal of Geophysical

Research, **86**, 6335-6349.

Vine, F.J. & Mathews, D.H., 1963: Magnetic Anomalies over Oceanic Ridges. Nature 199 947-949.

Vine, F.J. & Moores, E.M., 1969: Palaeomagnetic Results for the Troodos Ophiolite Massif, Cyprus. Trans.Am.Geophys.Union. EOS 50 131.

Vine, F.J., Poster, C.K. & Gass, I.G., 1973: Aeromagnetic Survey of the Troodos Massif, Cyprus. Nature 244 133 34-38.

Vozoff, K., 1972: The MT Method in the Exploration of Sedimentary Basins. Geophys. 37 98-141.

Wait, J.R., 1951: A Conducting Sphere in a Time Varying Magnetic Field. Geophys. vol.16 p.666-672.

Wait, J.R., 1962: Theory of Magnetotelluric Fields. J.Geophys.Res., NBS 66D, 509-541.

Wannamaker, P.E., Stodt, J.A. and Rijo, L., 1985: PW2D - Finite Element Program for Solution of Two-Dimensional Earth Resistivity Structure. User Documentation, Univ. of Utah Res.Inst.Rep. ESL-158.

Ward, S.H. and Fraser, D.C., 1987: Conduction of Electricity in Rocks: In "Soc.Expl.Geophys., Mining Geophysics, vol.II Theory" (Hansen, D.A., et.al., eds.). Publ.Soc.Expl.Geophys., Tulsa, Oklahoma, p.197-224.

Weaver, J.T., 1970: The General Theory of EM Induction in a Conducting Half-Space. Geophys.Journ.Roy.Astr.Soc. 22 83-100.

Wight, D.E. and Bostick, F.X., 1980: Cascade Decimation - A Technique for Real Time Estimation of Power Spectra. In "Proc. IEEE Internat.Conf. on Acoustic Speech and Signal Processing (Apr. 9-11, 1980, Denver, CO), p.626-629.

Wilson, R.A.M., 1959: The Geology of the Xeros-Troodos Area. Cyp.Geol.Surv. Dept. Mem. 1 135pp.

Wood, D.A., Joron, J.L., Marsh, N.G., Tarney, J. and Treuil, M., 1980: Major and Trace Element Variations in Basalts from the North Philippine Sea Drilled During Deep Sea Drilling Project LEG 58: A Comparative Study of Back-arc Basin Basalts with Lava Seriesfrom Japan and Mid-Ocean Ridges. Initial Reports, D.S.D.P., 58, p.873-894.

Wu, F.T., 1968: The Inverse Problem of Magnetotelluric Sounding. Geophysics, vol.33, no.6, p.972-979.

Yungul, S.H., 1961: Magnetotelluric Sounding Three Layer Interpretation Curves. Geophysics, vol.26, no.4, p.465-473.

Yungul, S.H., 1996: Electrical methods in Geophysical Exploration of Deep Sedimentary Basins. Publ. Chapman and Hall, London.